All Possible Lightest Supersymmetric Particles in Proton Hexality Violating Minimal Supergravity Models and their Signals at Hadron Colliders

Dissertation
zur
Erlangung des Doktorgrades (Dr. rer. nat.)
der
Mathematisch-Naturwissenschaftlichen Fakultät
der
Rheinischen Friedrich-Wilhelms-Universität
zu Bonn

vorgelegt von

Sebastian Grab

geb. in
Altenkirchen

Bonn 2009

Angefertigt mit Genehmigung der Mathematisch-Naturwissenschaftlichen Fakultät der Universität Bonn.

Referent: Prof. Herbert Dreiner
Korreferent: Prof. Manuel Drees

Tag der Promotion: 02.Juli 2009

Diese Dissertation ist auf dem Hochschulschriftenserver der ULB Bonn `http://hss.ulb.uni-bonn.de/diss_online` elektronisch publiziert.
Erscheinungsjahr: 2009

To Christine

Acknowledgements

I would like to thank several people and institutions. Without their experience and support, this thesis would not have been possible.

First of all, I would like to thank my supervisor Herbi Dreiner for his excellent support. It has been a pleasure to work with him and to benefit from his expertise.

I would like to thank the *Bonn-Cologne Graduate School of Physics and Astronomy* and especially the *Deutsche Telekom Stiftung* for financial support. Without their assistance many fruitful visits to summer schools, workshops, conferences etc. would not have been possible.

I also would like to express my gratitude to my collaborators Ben Allanach, Markus Bernhardt, Siba Prasad Das, Klaus Desch, Sebastian Fleischmann, Steve Kom, Daniel Koschade, Michael Krämer, Ulrich Langenfeld, Ben O'Leary, Peter Richardson, and Maike Trenkel. I hope that we will continue our good collaboration in the future.

I would also like to mention my working group who made working, studying and partying a lot of fun. Thank you Alessandro Barri, Markus Bernhardt, Marja Hanussek, Jong Soo "Zong" Kim, Olaf Kittel, Ulrich Langenfeld, Christoph Luhn, Anja Marold, Branislav Poletanovic, Marc Thormeier and Karina Williams. I especially enjoyed many profound discussions with Zong.

In addition, I benefited a lot from discussions with various other people including Sascha Bornhauser, Volker Büscher, Manuel Drees, Gudrun Hillert, Sushita Kulkarni, Nicolas Moeser, Tilman Plehn, Jan Schumacher, and the TASI08 people. I also would like to thank the theory groups of Fermilab National Accelerator, Argonne National Laboratory, UC Santa Cruz, IPPP Durham, University of Karlsruhe, and Cambridge University for helpful discussions and warm hospitality.

I am grateful to our secretaries, Dagmar Fassbender, Patricia Zündorf, and Sandra Heidbrink, who helped me to survive at our institute.

I also would like to thank Ina Eisenschneider, Jong Soo Kim, Olaf Kittel, and Karina Williams for reading parts of my thesis.

After my PhD, I will start to work in the excellent theory group of UC Santa Cruz. I am therefore deeply grateful to my referees Herbi Dreiner, Michael Krämer, and Peter Richardson, who wrote letters of recommendation for my postdoc application.

Finally none of this would have been possible without the support of my family and my lovely girlfriend Christine. Thank you!

Abstract

The most widely studied supersymmetric scenario is the minimal supersymmetric standard model (MSSM) with more than a hundred free parameters. However for detailed phenomenological studies, the minimal supergravity (mSUGRA) model, a restricted and well-motivated framework for the MSSM, is more convenient. In this model, lepton- and baryon-number violating interactions are suppressed by a discrete symmetry, R-parity or proton-hexality, to keep the proton stable. However, it is sufficient to forbid only lepton- or baryon-number violation. We thus extend mSUGRA models by adding a proton-hexality violating operator at the grand unification scale.

This can change the supersymmetric spectrum leading on the one hand to a sneutrino, smuon or squark as the lightest supersymmetric particle (LSP). On the other hand, a wide parameter region is reopened, where the scalar tau (stau) is the LSP. We investigate in detail the conditions leading to non-neutralino LSP scenarios. We take into account the restrictions from neutrino masses, the muon anomalous magnetic moment, $b \to s\gamma$, and other precision measurements. We furthermore investigate existing restrictions from direct searches at LEP, the Tevatron, and the CERN $p\bar{p}$ collider.

It is vital to know the nature of the LSP, since supersymmetric particles normally cascade decay down to the LSP at collider experiments. We present typical LHC signatures for sneutrino LSP scenarios. Promising signatures are high-p_T muons and jets, like-sign muon events and detached vertices from long lived taus. We also classify the stau LSP decays and describe their dependence on the mSUGRA parameters. We then exploit our results for resonant single slepton production at the LHC. We find novel signatures with like-sign muon and three- and four-muon final states. Finally, we perform a detailed analysis for single slepton production in association with a single top quark. We show that the signal can be distinguished from the background at the LHC.

Contents

1. Introduction

1.1. Motivation

The Standard Model (SM) of particle physics [1, 2] provides an extremely successful and precise description of nearly all known phenomena [3][1]. It was developed over the last decades by an effective interplay between theory and experiment. On the experimental side, especially particle accelerators lead to continuous progress. Only the Higgs particle has not been discovered yet.

However, several issues remain open. Among those, the "hierarchy problem" is one of the most problematic [8, 9, 10, 11, 12]. The Higgs mass parameter m_H in the SM is very sensitive to nearly all new physics. For example, even if a new fermion with mass m_F couples only indirectly to the Higgs field via gauge interactions, m_H^2 receives the radiative corrections [13]

$$\Delta m_H^2 \propto m_F^2 + \dots . \tag{1.1}$$

We expect at the Planck scale, $M_{Pl} = \mathcal{O}(10^{19}\,\text{GeV})$, new physics including fermions which couples somehow to the Higgs. Therefore, m_H^2 receives corrections of $\mathcal{O}(M_{Pl}^2)$. In contrast, the SM predicts the physical Higgs mass to be $\lesssim 1\,\text{TeV}$ to preserve unitarity [14, 15, 16]. We thus need to unphysically fine-tune counterterms to cancel corrections like Eq. (1.1) on the one side and to obtain the correct physical Higgs mass on the other side.

Supersymmetry (SUSY), a symmetry between bosons and fermions, solves the hierarchy problem in an elegant way. Each particle has now an additional *superpartner* with its spin differing by 1/2. All quadratic contributions to the Higgs mass squared cancel now. This is true even if SUSY is (softly) broken. In this case, to avoid fine-tuning, the superpartners of the SM fields need to have masses of $\lesssim \mathcal{O}(1\,\text{TeV})$; see for example the discussion in Refs. [8, 13].

There are further theoretical as well as experimental facts that point to SUSY and especially to a supersymmetric extension of the SM (SSM) with minimal particle content:

- Supersymmetry is the only allowed spacetime symmetry besides Lorentz invariance [17, 18].
- Local gauge invariance requires the introduction of a gauge boson. Similarly, local SUSY requires the introduction of a massless spin-2 field, the graviton (and its spin-3/2 superpartner, the gravitino) which mediates gravitational interactions. We have thus a connection to general relativity [19, 20, 21, 22, 23, 24, 25].

[1] Probably the most important discrepancy between an SM prediction and electroweak precision measurements has been found for the anomalous magnetic moment of the muon [4, 5, 6, 7]. Here, a deviation of more than 3σ has been established.

- Supersymmetry is needed for the construction of realistic string models, although this does not necessarily imply weak-scale SUSY; see for example Refs. [26, 27, 28, 29, 30] and references therein.
- Although many theories exist which predict a unification of the gauge interactions, the gauge couplings due not unify within the SM. However, the gauge couplings will meet at a scale of $\mathcal{O}(10^{16}\,\mathrm{GeV})$ in the SSM as long as the SUSY particle masses are of $\mathcal{O}(100\,\mathrm{GeV} - 10\,\mathrm{TeV})$ [31, 32, 33, 34, 35].
- Within the SSM, a positive Higgs mass parameter squared of $\mathcal{O}(100^2\,\mathrm{GeV}^2)$ at a scale of $\mathcal{O}(10^{16}\,\mathrm{GeV})$ can run to a negative value at the electroweak scale, M_Z. This mechanism thus provides a natural explanation for the origin of electroweak symmetry breaking and the large difference between M_{Pl} and M_Z. It is called radiative electroweak symmetry breaking (REWSB) [36]. The superpartners of the SM fields are then required to be not heavier than a few TeV.
- Precision fits to electroweak data show that the physical (SM) Higgs mass needs to be < 191 GeV at 95% C.L. [37]. In addition, a SM Higgs with a mass between 160 GeV and 170 GeV has recently been excluded at the Tevatron at 95% C.L. [38]. The SSM predicts the lightest CP-even Higgs mass to be not larger than roughly 140 GeV [39, 40].
- The SSM contributions to the anomalous magnetic moment of the muon can explain the more than 3σ discrepancy between the SM prediction and experimental observations [4, 5, 6, 7]. For this, at least parts of the SSM mass spectrum must be $\lesssim 1\,\mathrm{TeV}$.
- If lepton- and baryon-number violating interactions are prohibited, the SSM contains a good cold dark matter candidate, the neutralino [41][2].
- The SSM possesses an elegant mechanism to generate neutrino masses if lepton number is violated [45, 46, 47, 48, 49][3].

It is remarkable that several arguments for SUSY point to superpartners of the SM fields with masses of $\mathcal{O}(\lesssim 1\mathrm{TeV})$. Therefore, SUSY should be immently testable at the Tevatron [55] and the Large Hadron Collider (LHC) [56, 57], which will start collecting data this year.

1.2. Goals of the Thesis

In the collider search for SUSY at colliders, it is essential to know the nature of the lightest supersymmetric particle (LSP), because SUSY particles, if produced, normally cascade decay down to the LSP within the detector. The LSP is thus a central ingredient of almost all SUSY signatures. It is the purpose of this thesis to investigate the possible candidates for the LSP and its phenomenology at hadron colliders. We will focus on the proton-hexality,

[2] There are also other dark matter candidates which are valid, even if lepton- or baryon-number are violated. One example is the axino, the supersymmetric partner of the axion, which is also a suitable candidate for dark matter [42, 43, 44].

[3] If we extend the SSM by right-handed neutrinos, we can also generate neutrino masses via the seesaw mechanism [50, 51, 52, 53, 54]. However, this introduces an additional scale in our theory, namely the Majorana mass of the right handed neutrinos.

P_6, violating minimal supergravity (mSUGRA) model [58] and its low-energy SSM spectrum. We give for the first time a complete list of all possible LSP candidates within this model.

Lepton- and baryon-number are conserved in the SM. But this is only an accidental consequence of gauge invariance and the SM particle content. In contrast, renormalizable lepton- and baryon-number violating interactions are possible in the SSM. In the upcoming years, the LHC will probably decide if and which version of SUSY is realized in nature. To provide some guidance on what might be expected at the LHC, we will present novel collider signatures which are unique to the lepton-number violating SSM.

1.3. Organization of the Thesis

This thesis is organized as follows. In Sect. 2, we give a short introduction to the relevant parts of the SSM and the mSUGRA model with and without P_6. We point out distinguishing features between the P_6 conserving and violating SSM which can have a strong impact on collider phenomenology. We especially focus on the renormalization group running of sparticle masses from the grand unification scale to the electroweak scale. In Sect. 3, we consider all possible LSPs within P_6 violating mSUGRA. We first investigate the mechanism leading to new LSP candidates. We then show the respective mSUGRA parameter space. In Sect. 4, we concentrate on the sneutrino LSP. We analyze the allowed sneutrino LSP parameter space and give examples for characteristic signatures at the LHC. We present new signatures which can help to discover SUSY as well as to distinguish P_6 conserving from P_6 violating mSUGRA. In Sect. 5, we investigate the scalar tau (stau) as the LSP. We classify its decay modes (2- and 4-body decays) as a function of mSUGRA parameters. We then exploit our results for single slepton production at the LHC. We show novel collider signatures with like-sign dimuons and three and four muons in the final state. Finally, in Sect. 6, we consider single slepton production in association with a single top quark. We compute event rates for the Tevatron and LHC and show that the signal can be distinguished from the background. We summarize and conclude in Sect. 7.

In Appendix A, we give the low energy spectrum of mSUGRA models relevant for this work. In Appendix B we calculate for the first time the three-body slepton decay $\tilde{\ell}_i^- \to W^- \bar{b} d_k$. In Appendix C, we give branching ratios and production cross sections relevant for Sect. 5.

1.4. Publications

Most of the results contained in this thesis have already been published. In Ref. [59], we investigate all possible LSP candidates in P_6 violating mSUGRA models. In Refs. [60, 61], we focus on the sneutrino LSP and show characteristic LHC signatures. The work on stau LSP decays as a function of mSUGRA parameters and its impact on single slepton production has been published in Ref. [62]. Finally, in Ref. [63] we investigate single slepton production in association with a top quark.

2. The Model

A very detailed introduction to supersymmetry (SUSY) and the supersymmetric standard model (SSM) can be found in several textbooks, review articles and lecture notes. See, for example, Refs. [8, 13, 28, 64, 65, 66, 67, 68, 69, 70, 71, 72]. We briefly describe in this section our notation and the SUSY models relevant for this work.

In Sect. 2.1, we shortly introduce global SUSY. In Sect. 2.2, we introduce the SSM. Then, in Sect. 2.3, we present the superpotential of the SSM. We introduce possible discrete symmetries, like proton-hexality, P_6, to avoid proton decay. We also point out the differences between the P_6 conserving and violating SSM. Finally, in Sect. 2.4, we introduce the minimal supergravity (mSUGRA) model with and without P_6. Here, we will focus on the renormalization group running of the SUSY particle masses.

2.1. Global Supersymmetry

A SUSY transformation changes a bosonic state into a fermionic one and vice versa:

$$Q\,|\text{boson}\rangle = |\text{fermion}\rangle\,, \quad Q\,|\text{fermion}\rangle = |\text{boson}\rangle\ . \tag{2.1}$$

Here, Q is the generator of the SUSY transformation. Q must transform as a spinor, because it changes the spin of a field by 1/2. The SUSY generators satisfy the following algebra of anticommutation and commutation relations[1]

$$\begin{aligned} &\{Q_\alpha, \bar{Q}_{\dot{\beta}}\} = 2\sigma^\mu_{\alpha\dot{\beta}} P_\mu, \quad \{Q_\alpha, Q_\beta\} = 0, \quad \{Q_{\dot{\alpha}}, \bar{Q}_{\dot{\beta}}\} = 0, \\ &[Q_\alpha, P^\mu] = 0, \quad [\bar{Q}_{\dot{\alpha}}, P^\mu] = 0, \end{aligned} \tag{2.2}$$

where Q ($\bar{Q}$) is a left-handed (right-handed) two-component Weyl spinor with $\alpha, \beta\,(\dot{\alpha}, \dot{\beta}) = 1, 2$. We have $\sigma^\mu = \{\mathbb{1}, \vec{\sigma}\}$ with $\mathbb{1}$ the identity matrix and $\vec{\sigma}$ the Pauli matrices. P^μ is the momentum operator, *i.e.* the generator of spacetime translations. In principle it is possible to have more than only one SUSY generator Q. However, these models are phenomenological excluded for a four dimensional field theory, although (N=1/N=2) hybrid models with an interesting phenomenology are possible; see, for example, Refs. [73, 74, 75, 76]

Each SM particle belongs to an irreducible representation of the SUSY algebra, the so-called supermultiplets, and has a superpartner with its spin differing by 1/2. The superpartners of the SM fields must have the same gauge quantum numbers, because Q commutes with the generators of gauge interactions. As can be seen from Eq. (2.2), Q also commutes with $P^2 = M^2$. All fields in a supermultiplet thus posses the same mass. Therefore, if SUSY

[1] We do not show the commutators involving rotation generators, because they play no role in our discussion.

SM (SUSY) particles	superfield	spin 0	spin 1/2	spin 1	$SU(3)_C$, $SU(2)$, $U(1)_Y$
quarks (squarks)	Q_i $\bar{U}_i$ $\bar{D}_i$	$(\tilde{u}_{Li},\, \tilde{d}_{Li})$ $\tilde{u}^c_{Ri}$ $\tilde{d}^c_{Ri}$	$(u_{Li},\, d_{Li})$ u^c_{Ri} d^c_{Ri}		$(\mathbf{3},\, \mathbf{2},\, +1/6)$ $(\bar{\mathbf{3}},\, \mathbf{1},\, -2/3)$ $(\bar{\mathbf{3}},\, \mathbf{1},\, +1/3)$
leptons (sleptons)	L_i $\bar{E}_i$	$(\tilde{\nu}_i,\, \tilde{\ell}_{Li})$ $\tilde{\ell}^c_{Ri}$	$(\nu_i,\, \ell_{Li})$ ℓ^c_{Ri}		$(\mathbf{1},\, \mathbf{2},\, -1/2)$ $(\mathbf{1},\, \mathbf{1},\, +1)$
gauge bosons (gauginos)	V_1 V_2 V_3		$\tilde{B}^0$ $\tilde{W}^{\pm},\, \tilde{W}^0$ $\tilde{g}_a$	B^0 $W^{\pm},\, W^0$ g_a	$(\mathbf{1},\, \mathbf{1},\, 0)$ $(\mathbf{1},\, \mathbf{3},\, 0)$ $(\mathbf{8},\, \mathbf{1},\, 0)$
Higgs (Higgsinos)	H_u H_d	$(H^+_u,\, H^0_u)$ $(H^0_d,\, H^-_d)$	$(\tilde{H}^+_u,\, \tilde{H}^0_u)$ $(\tilde{H}^0_d,\, \tilde{H}^-_d)$		$(\mathbf{1},\, \mathbf{2},\, +1/2)$ $(\mathbf{1},\, \mathbf{2},\, -1/2)$

Table 2.1.: Fields (with their gauge representation) of the SSM. $i = 1, 2, 3$ are generation indices.

exists in nature, it must be broken, because no superpartners of the SM particles were observed so far [3]. One can also show, by using Eq. (2.2), that the number of bosonic degrees of freedom in a supermultiplet are equal to the number of fermionic degrees of freedom; see *e.g.* Ref. [13].

Relevant for the construction of a minimal supersymmetric extension of the SM are two kinds of supermultiplets: A *chiral* supermultiplet, which contains a single two-component Weyl fermion (spin 1/2) and a complex scalar field (spin 0); a *vector* supermultiplet with a massless vector boson (spin 1) and a two-component Weyl fermion. For gravity to be included, we need an additional supermultiplet with the graviton (spin 2) and its superpartner the gravitino (spin 3/2).

In addition, each supermultiplet contains an auxiliary field, which allows the SUSY algebra, Eq. (2.2), to close off-shell (when the classical equations of motion are not satisfied). These fields can be expressed in terms of the physical fields with the help of the equations of motion.

The supermultiplets can be written in a compact form using the so-called superfield formalism. A superfield is made up of the bosonic, fermionic and auxiliary fields. The superfield formalism is especially helpful for the systematic development of supersymmetric theories. A more detailed description of this formalism can be found, for example, in the references given at the beginning of Sect. 2.

2.2. The Supersymmetric Standard Model

In order to extend the SM to a supersymmetric theory, we need at least the fields shown in Table 2.1. This model is known as the supersymmetric SM (SSM) with minimal particle content.

The left- and right-handed SM fermions belong to different chiral supermultiplets and have therefore different superpartners called sfermions. We have three generations, $i = 1, 2, 3$, of

left-handed (right-handed) squarks, $\tilde{u}_{Li}$, $\tilde{d}_{Li}$ ($\tilde{u}_{Ri}$, $\tilde{d}_{Ri}$), which are the spin-0 superpartners of the left-handed (right-handed) up- and down-type quarks, respectively; the left-handed (right-handed) charged sleptons, $\tilde{\ell}_{Li}$ ($\tilde{\ell}_{Ri}$), which are the superpartners of the left-handed (right-handed) charged leptons; and the superpartners of the neutrinos, the so-called sneutrinos, $\tilde{\nu}_i$. Following the convention in the standard literature (see references given at the beginning of Sect. 2), all SM fermions are described by left-handed Weyl spinors. We thus show the conjugates of the right-handed quarks and leptons in Tab. 2.1, which are left-handed spinors.

Each gauge boson belongs to a vector supermultiplet. The superpartners are called gauginos. In Table 2.1 we have the bino, $\tilde{B}^0$, the superpartner of the $U(1)_Y$ gauge boson; the neutral and charged winos, $\tilde{W}^0, \tilde{W}^\pm$, the superpartners of the $SU(2)$ gauge bosons; and the gluinos, $\tilde{g}_a$, $a = 1..8$, the superpartners of the $SU(3)_C$ gauge bosons.

In Table 2.1, we also observe that we need at least two Higgs doublets and their superpartners to embed the SM into a supersymmetric theory. On the one hand, the fermionic partner of a single Higgs doublet would lead to a gauge anomaly of the electroweak symmetry [72]. With two Higgs doublets with opposite $U(1)_Y$ charge, *cf.* Table 2.1, the contributions to the anomaly cancel. On the other hand, SUSY requires the superpotential to be a holomorphic function of the chiral superfields. We thus need two Higgs doublets to be able to give mass to the up- and down-type quarks via the Higgs-mechanism.

As argued in the last section, if SUSY exists, it must be broken. SUSY is broken explicitly when we add the following interactions to the supersymmetrized SM Lagrangian [58]

$$\begin{aligned} -\mathcal{L}_{\text{soft}} \;=\; & \left(\frac{1}{2}M_1\tilde{B}\tilde{B} + \frac{1}{2}M_2\tilde{W}\tilde{W} + \frac{1}{2}M_3\tilde{g}\tilde{g} + h.c.\right) + m_{H_d}^2 H_d^\dagger H_d + m_{H_u}^2 H_u^\dagger H_u \\ & + \tilde{L}_i^\dagger (\mathbf{m}_{\tilde{\mathbf{L}}}{}^2)_{ij}\tilde{L}_j + \tilde{\bar{E}}_i(\mathbf{m}_{\tilde{\mathbf{E}}}{}^2)_{ij}\tilde{\bar{E}}_j^\dagger + \tilde{Q}_i^\dagger(\mathbf{m}_{\tilde{\mathbf{Q}}}{}^2)_{ij}\tilde{Q}_j + \tilde{\bar{U}}_i(\mathbf{m}_{\tilde{\mathbf{U}}}{}^2)_{ij}\tilde{\bar{U}}_j^\dagger + \tilde{\bar{D}}_i(\mathbf{m}_{\tilde{\mathbf{D}}}{}^2)_{ij}\tilde{\bar{D}}_j^\dagger \\ & + \Big[-\tilde{B}H_dH_u + (\mathbf{h}_E)_{ij}\tilde{L}_iH_d\tilde{\bar{E}}_j + (\mathbf{h}_D)_{ij}\tilde{Q}_iH_d\tilde{\bar{D}}_j + (\mathbf{h}_U)_{ij}\tilde{Q}_iH_u\tilde{\bar{U}}_j + h.c.\Big]. \end{aligned} \tag{2.3}$$

We sum over repeated indices and keep the gauge indices implicit.

The first three terms give mass to the gauginos; the mass M_1 to the bino, the mass M_2 to the three winos, and the mass M_3 to the eight gluinos. The other two terms in the first row of Eq. (2.3) are the mass terms for the Higgs scalars.

In the second row of Eq. (2.3), we introduce the 3×3 mass matrices of the left-handed sleptons, $\mathbf{m}_{\tilde{\mathbf{L}}}$, the right-handed sleptons, $\mathbf{m}_{\tilde{\mathbf{E}}}$, the left-handed squarks, $\mathbf{m}_{\tilde{\mathbf{Q}}}$, the right-handed down squarks, $\mathbf{m}_{\tilde{\mathbf{D}}}$, and the right-handed up squarks, $\mathbf{m}_{\tilde{\mathbf{U}}}$. The slepton and squark fields (*cf.* Table 2.1) are expressed in terms of 3-vectors in generation space, *e.g.* $\tilde{\bar{E}} = (\tilde{\ell}^c_{R1}, \tilde{\ell}^c_{R2}, \tilde{\ell}^c_{R3})$ and $\tilde{L} = [(\tilde{\nu}_1, \tilde{\ell}_{L1}), (\tilde{\nu}_2, \tilde{\ell}_{L2}), (\tilde{\nu}_3, \tilde{\ell}_{L3})]$.

Finally, in the third row, we show the scalar interactions that correspond to the superpotential, Eq. (2.5). The first (bilinear) interaction contributes to the Higgs masses. The three trilinear scalar interaction terms will contribute, among other things, to the slepton and squark masses. They mix the left- and right-handed sleptons and squarks after electroweak symmetry breaking (EWSB). The trilinear scalar interactions are 3×3 matrices

in generation space. Note that we can also add lepton- and baryon-number violating (but gauge invariant) interactions to $\mathcal{L}_{\text{soft}}$; see next section for details.

The supersymmetrization of the SM (aside from the extended Higgs sector) introduces no additional new parameters. $\mathcal{L}_{\text{soft}}$ however, leads to more than 100 new, *a priori* unknown parameters [77]. It is very difficult to do detailed phenomenological studies in this extensive parameter space. We therefore need a guiding principle. We will address this topic in Sect. 2.4.

It is clear by taking a look at Eq. (2.1) that the soft breaking Lagrangian, Eq (2.3), breaks SUSY, because $\mathcal{L}_{\text{soft}}$ involves only fields without their superpartners. It was shown in Ref. [78] that a Lagrangian like Eq. (2.3) is free of quadratic divergencies from quantum corrections to scalar masses and thus called *soft*. The hierarchy problem can therefore still be solved. However, logarithmic divergencies arise. To avoid fine-tuning, the mass parameters in Eq. (2.1) are restricted to be no larger than $\mathcal{O}(1\,\text{TeV})$, *cf.* Sect. 1.1.

After EWSB, some of the fields in Table 2.1 will have the same quantum numbers. Thus, they can mix. If lepton-number is conserved, the resulting mass eigenstates are [65, 79, 80]

- The neutralinos, $\tilde{\chi}^0_n$, with $n = 1, 2, 3, 4$. The neutralinos are admixtures of the bino, the neutral wino and the neutral Higgsinos.
- The charginos, $\tilde{\chi}^+_l$, with $l = 1, 2$. The charginos are admixtures of the charged winos and the charged Higgsinos.
- Sleptons and squarks. The squark and slepton fields in Table 2.1 are given in the flavor basis. They can mix on the one hand between different generations and on the other hand between different "helicities", *i.e.* left- and right-handed fields will mix. For example, the up- and down-type squarks each posses a 6×6 mass matrix. However, mixing between different generations of sleptons and squarks is highly restricted due to the non-observation of large flavor changing neutral currents (FCNCs) [81, 82]. In addition, the (squared) mass terms which mix left- and right-handed states within one generation are normally assumed to be proportional to the respective SM fermion mass (see Sect. 2.4.1). We therefore consider in the following only L-R mixing for the third generation of sleptons and squarks.

We see in Table 2.1 that the lepton and Higgs superfields have the same gauge quantum numbers after EWSB. Note that lepton number is only conserved accidentally in the SM, *i.e.* lepton-number conservation is only a consequence of gauge invariance and the SM particle content. The lepton and Higgs superfields can mix if we assume that lepton number is violated. We then have [58]

- Mixing between neutralinos and neutrinos. We now have a 7×7 mass matrix.
- Mixing between charginos and charged leptons. The respective mass matrix is thus a 5×5 matrix.
- Mixing between charged sleptons and charged Higgs bosons resulting in a 8×8 mass matrix. One mass eigenstate is zero. This field is a Goldstone boson from EWSB.
- Mixing between sneutrinos and neutral Higgs scalars. If CP is conserved, we have two 5×5 mass matrices: One matrix mixes the CP-even part of the sneutrino fields with the CP-even Higgs fields and one matrix mixes the CP-odd sneutrinos with the

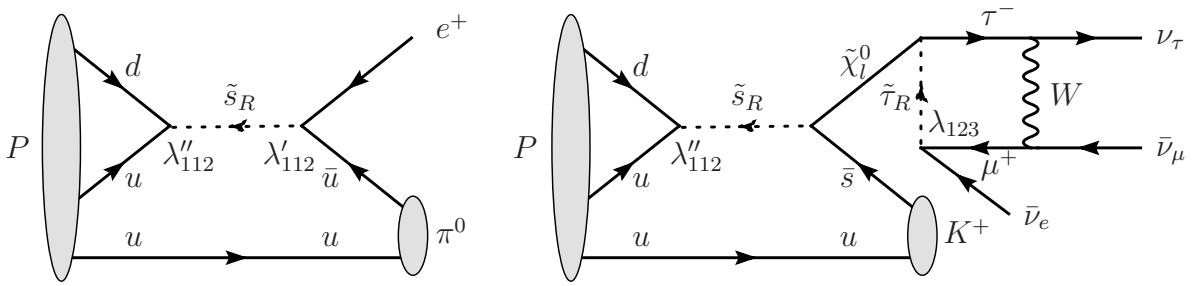

Figure 2.1.: Proton decay $P \to \pi^0 e^+$ via non-vanishing couplings $\lambda'_{112} \times \lambda''_{112}$ (left figure) and $P \to K^+ \nu_\tau \bar{\nu}_e \bar{\nu}_\mu$ via non-vanishing couplings $\lambda_{123} \times \lambda''_{112}$ (right figure).

CP-odd Higgs fields. The latter mass matrix again has a zero mass eigenstate, due to the presence of a Goldstone boson. The CP-even sneutrinos can also develop non-vanishing vacuum expectation values (vevs) after EWSB. However, these vevs must be small to avoid unphysically large neutrino masses [58].

In the following, we can neglect the additional mixing due to lepton number violation. All terms in the SSM Lagrangian, which mix (at tree-level) components of the Higgs superfields with components of the lepton superfields are either proportional to the sneutrino vevs or proportional to the parameters κ_i, $\tilde{D}_i$ or $\mathbf{m}^2_{\tilde{L}_i H_d}$; see next section for more details. The vevs and κ_i, $\tilde{D}_i$, and $\mathbf{m}^2_{\tilde{L}_i H_d}$ must be small to be consistent with small neutrino masses [46, 47, 58]. We will therefore only check that neutrino-neutralino mixing does not introduce too large neutrino masses.

2.3. Superpotential and Discrete Symmetries

With the fields given in Table 2.1 we can write down many possible interactions. The Yukawa interactions, for example, can be described with the help of the so-called superpotential. The most general gauge invariant and renormalizable superpotential of the SSM is [83, 84]

$$W_{\rm SSM} = W_{\rm P_6} + W_{\not{\rm P}_6}\,, \tag{2.4}$$

$$W_{\rm P_6} = \epsilon_{ab}\left[(\mathbf{Y}_E)_{ij} L_i^a H_d^b \bar{E}_j + (\mathbf{Y}_D)_{ij} Q_i^{ax} H_d^b \bar{D}_{jx} + (\mathbf{Y}_U)_{ij} Q_i^{ax} H_u^b \bar{U}_{jx} + \mu H_d^a H_u^b\right], \tag{2.5}$$

$$W_{\not{\rm P}_6} = \epsilon_{ab}\left[\frac{1}{2}\lambda_{ijk} L_i^a L_j^b \bar{E}_k + \lambda'_{ijk} L_i^a Q_j^{bx} \bar{D}_{kx} + \kappa_i L_i^a H_u^b\right] + \frac{1}{2}\epsilon_{xyz}\lambda''_{ijk} \bar{U}_i^x \bar{D}_j^y \bar{D}_k^z\,. \tag{2.6}$$

where $i, j, k = 1, 2, 3$ are generation indices. We have employed the standard notation of Ref. [85].

The superpotential, Eq. (2.4), consists of two different parts. $W_{\rm P_6}$ involves the lepton, $\mathbf{Y}_E$, down-quark, $\mathbf{Y}_D$, and up-quark, $\mathbf{Y}_U$, 3×3 Yukawa matrices, which give mass to the leptons and quarks after EWSB. A more detailed description of the structure of Yukawa matrices is given in Appendix A.1. μ is the Higgs mixing parameter, which contributes, among other things, to the Higgs masses.

$W_{\not{\rm P}_6}$ consists of lepton- and baryon-number violating operators, which together can lead to rapid proton decay in contradiction to experimental observations [86, 87, 88, 89, 90]. In

Fig. 2.1 we show two examples. In the left figure (right figure), proton decay is mediated via a non-vanishing product $\lambda'_{112} \times \lambda''_{112}$ ($\lambda_{123} \times \lambda''_{112}$). The resulting bounds from non-observation of proton decay are [89]

$$\lambda'_{112} \times \lambda''_{112} \lesssim \mathcal{O}(10^{-25}), \quad \lambda_{123} \times \lambda''_{112} \lesssim \mathcal{O}(10^{-14}), \tag{2.7}$$

assuming an universal SUSY particle (sparticle) mass of 1 TeV. Thus, even if the decay is loop suppressed (*e.g.* right process in Fig. 2.1), proton decay puts an extreme upper bound on (all) products of lepton- and baryon-number violating couplings [89].

To keep the proton stable, one needs to suppress either the lepton- or the baryon-number violating operators in Eq. (2.6). This can be achieved with the help of a discrete symmetry. It was shown in Refs. [91, 92, 93, 94], that there are three discrete symmetries which are consistent with an underlying anomaly-free $U(1)$ gauge theory[2] and which allow a Majorana neutrino mass term LH_uLH_u: R-parity (R_p), baryon-triality (B_3), and proton-hexality (P_6). The most widely assumed symmetry is the $\boldsymbol{Z}_2$-symmetry R_p (or equivalently matter-parity)[3]

$$(L_i, \bar{E}_i, Q_i, \bar{U}_i, \bar{D}_i) \to -(L_i, \bar{E}_i, Q_i, \bar{U}_i, \bar{D}_i), \qquad (H_d, H_u) \to (H_d, H_u), \tag{2.8}$$

where the superfields are given in Table 2.1. R_p thus prohibits $W_{\not P_6}$. However, R_p allows dangerous dimension-five proton decay operators such as $QQQL$ [86]. A second possibility is B_3 (or equivalently baryon-parity)

$$(Q_i, \bar{U}_i, \bar{D}_i) \to -(Q_i, \bar{U}_i, \bar{D}_i), \qquad (L_i, \bar{E}_i, H_d, H_u) \to (L_i, \bar{E}_i, H_d, H_u). \tag{2.9}$$

B_3 is a $\boldsymbol{Z}_3$-symmetry which prohibits only the $\bar{U}\bar{D}\bar{D}$ operators in Eq. (2.6) but also the dangerous dimension five operators. Finally, we have P_6, a $\boldsymbol{Z}_6 = \boldsymbol{Z}_2 \times \boldsymbol{Z}_3$-symmetry. It only allows for interactions which are consistent with Eq. (2.8) and Eq. (2.9) at the same time. P_6 has therefore the same effect on the renormalizable interactions as R_p but forbids, in addition, the dangerous dimension-five operators. It is thus preferred in comparison to R_p. The SSM with conserved R_p or P_6 is conventionally denoted the minimal supersymmetric standard model (MSSM).

We also obtain a stable proton, if we only allow for the baryon number violating $\bar{U}\bar{D}\bar{D}$ interactions[4]. This can be achieved by the discrete symmetry lepton-parity [94]:

$$(L_i, \bar{E}_i) \to -(L_i, \bar{E}_i), \qquad (Q_i, \bar{U}_i, \bar{D}_i, H_d, H_u) \to (Q_i, \bar{U}_i, \bar{D}_i, H_d, H_u). \tag{2.10}$$

However, lepton parity cannot be written as a remnant of a broken anomaly-free gauge symmetry [91, 92, 93]. One therefore expects that quantum gravity effects violate lepton-parity [95, 96]. As pointed out above, B_3 can be written as the remnant of an anomaly free $U(1)$ gauge symmetry. Lepton-number violation within the SSM is thus, from a theoretical point of view, better motivated then baryon-number violation. We will therefore mainly concentrate on B_3 SUSY models in the following.

[2] Note that anomalies can also be canceled by introducing additional fields.

[3] R-parity is often defined as $R_p = (-1)^{2S+3B+L}$. Here S denotes the spin, B the baryon-number, and L the lepton-number of a particle.

[4] In addition, the LSP should be heavier than the proton. For example, the baryon number violating part of the right diagram in Fig. 2.1 will lead to proton decay if $m_{\tilde{\chi}^0_1} < m_P - m_K$.

The P_6 violating SSM has some distinguishing features compared to the MSSM, which can have a strong impact on (hadron) collider phenomenology [89, 94, 97, 98]:

- The renormalization group equations (RGEs) receive additional contributions [58, 99, 100, 101, 102, 103, 104, 105]. This can alter the sparticle mass spectrum and the SUSY couplings at the electroweak scale M_Z [58, 101, 106].
- Neutrino masses can be generated as experimentally observed [45, 48, 107, 108, 109, 110].
- The LSP can decay into SM particles via the P_6 violating couplings. In principle, any sparticle can now be the LSP, because the cosmological bound on stable LSPs no longer holds [41].
- Sparticles may be produced singly, possibly on resonance; see *e.g.* Refs. [89, 111, 112, 113, 114] and Sect. 4.3.3, Sect. 5, and Sect. 6.
- The decay patterns of the sparticles can change due to changes in the mass spectrum and the additional P_6 violating interactions; see Ref. [106], and Sect. 4.3.1, and Appendix C for explicit examples.

We will address all of these aspects in the following sections.

If we allow for lepton- and baryon-number violation, we also need to add additional bilinear and trilinear interactions to the soft breaking Lagrangian, Eq. (2.3), [58]

$$\begin{aligned} -\mathcal{L}_{\text{soft}}^{\not{P}_6} &= \left[-\tilde{D}_i \tilde{L}_i H_u + (\mathbf{h}_{E^k})_{ij} \tilde{L}_i \tilde{L}_j \tilde{\bar{E}}_k + (\mathbf{h}_{D^k})_{ij} \tilde{L}_i \tilde{Q}_j \tilde{\bar{D}}_k + (\mathbf{h}_{U^i})_{jk} \tilde{\bar{U}}_i \tilde{\bar{D}}_j \tilde{\bar{D}}_k + h.c.\right] \\ &\quad + \tilde{L}_i^\dagger (\mathbf{m}^2_{\tilde{L}_i H_d}) H_d + H_d^\dagger (\mathbf{m}^2_{H_d \tilde{L}_i}) \tilde{L}_i \,. \end{aligned} \tag{2.11}$$

We sum over repeated indices again and keep the gauge indices implicit. The scalar fields are described in Sect. 2.2. The mass dimension one [two] trilinear [bilinear] couplings $(\mathbf{h}_{E^k})_{ij}$, $(\mathbf{h}_{D^k})_{ij}$, $(\mathbf{h}_{U^i})_{jk}$ $[\tilde{D}_i]$ are the soft breaking analogue to the trilinear [bilinear] couplings λ_{ijk}, λ'_{ijk}, λ''_{ijk} $[\kappa_i]$ of the superpotential, Eq. (2.4). The terms in the second row of Eq. (2.11) are mass terms, which contribute to the slepton Higgs mass matrices.

The P_6 violating part of the superpotential, Eq. (2.6), and of the soft breaking Lagrangian, Eq. (2.11), introduces roughly 100 new unknown parameters in addition to the more than 100 unknown P_6 conserving soft breaking interactions, Eq. (2.3)! It is almost impossible to do detailed phenomenological studies in this huge parameter space. We thus urgently need a guiding principle, which reduces the number of free parameters. We will address this issue in the following section.

2.4. mSUGRA with and without Proton Hexality P_6

2.4.1. Motivation

The slepton and squark mass matrices in the soft breaking Lagrangian, Eq. (2.3), need to be hermitian in order to have a real Lagrangian. One might generically assume that the generational diagonal and off-diagonal matrix elements in Eq. (2.3) have the same order of magnitude. However, in this case, the SSM (and MSSM) is phenomenological excluded if

one assumes that the SUSY breaking scale is $\lesssim \mathcal{O}(1\,\text{TeV})$[5]. Large generational off-diagonal matrix elements would lead to large FCNCs in contrast to experimental observations [81, 82]. For example, the non-observation of the process $\mu \to e\gamma$ puts strong constraints on matrix-elements which couple the scalar muon (smuon), $\tilde{\mu}$, to the scalar electron (selectron), $\tilde{e}$ [81, 115, 116]. In the squark sector, experimental constraints from meson-antimeson mixing like K^0–$\bar{K}^0$, D^0–$\bar{D}^0$, B^0–$\bar{B}^0$ mixing and from processes like $b \to s\gamma$ strongly restrict the magnitude of the generational off-diagonal masses [81, 117, 118, 119, 120]. Note that bounds involving fields of the third generation are in general less restrictive than those involving only the first and second generation.

If we assume in Eq. (2.3) that

$$\mathbf{m}_{\tilde{\mathbf{L}}} = m_{\tilde{L}} \times \mathbb{1},\ \mathbf{m}_{\tilde{\mathbf{E}}} = m_{\tilde{E}} \times \mathbb{1},\ \mathbf{m}_{\tilde{\mathbf{Q}}} = m_{\tilde{Q}} \times \mathbb{1},\ \mathbf{m}_{\tilde{\mathbf{U}}} = m_{\tilde{U}} \times \mathbb{1},\ \mathbf{m}_{\tilde{\mathbf{D}}} = m_{\tilde{D}} \times \mathbb{1}, \quad (2.12)$$

i.e proportional to the identity matrix at M_Z, we avoid dangerous FCNCs. Note that also other solutions exist [121, 122, 123, 124, 125, 126].

The trilinear couplings $\mathbf{h}_E, \mathbf{h}_D, \mathbf{h}_U$ in Eq. (2.3) will, after EWSB, also contribute to the slepton and squark mass matrices. They couple left- and right-handed fields to each other. To avoid large FCNCs, one can make the ansatz

$$\mathbf{h}_E = A_E \times \mathbf{Y}_E,\ \mathbf{h}_D = A_D \times \mathbf{Y}_D,\ \mathbf{h}_U = A_U \times \mathbf{Y}_U, \quad (2.13)$$

i.e. assume that the trilinear couplings are proportional to the respective Yukawa matrices at M_Z. Their contribution is thus only significant for the third generation.

As pointed out in Sect. 1.1, a strong motivation for SUSY is the unification of gauge couplings at a scale of $\mathcal{O}(10^{16}\,\text{GeV})$. If we assume that the SSM is embedded into a grand unified theory (GUT), we can naturally have a common gaugino mass, *cf.* Eq. (2.3), at the GUT scale M_{GUT}. This is the case because the gauginos all live in the same representation of the unified gauge group [11, 127, 128, 129, 130]. We thus have

$$M_1 = M_2 = M_3 \equiv M_{1/2} \quad \text{at } M_{\text{GUT}}\,. \quad (2.14)$$

Then it also seems natural to assume the boundary conditions, Eq. (2.12) and Eq. (2.13), at M_{GUT}. We can further simplify our model by assuming an universal soft breaking scalar mass, M_0, for all the sfermions and Higgs fields and an universal trilinear interaction, A_0, *i.e.*

$$m_{\tilde{L}} = m_{\tilde{E}} = m_{\tilde{Q}} = m_{\tilde{D}} = m_{\tilde{U}} = m_{H_d} = m_{H_u} \equiv M_0 \quad \text{at } M_{\text{GUT}}\,, \quad (2.15)$$

$$A_E = A_D = A_U \equiv A_0 \quad \text{at } M_{\text{GUT}}\,. \quad (2.16)$$

We now need only two additional parameters to be able to determine the complete spectrum of the MSSM at M_Z via the RGEs[6]. A convenient choice for these parameters is $\tan\beta$

[5] The Higgs mass needs to be fine-tuned, if the soft breaking masses are $\gtrsim \mathcal{O}(10\,\text{TeV})$, *cf.* Sect. 1.1.

[6] Note that in general there is no universal scalar mass and trilinear interaction at M_Z. This can lead to FCNCs. However these are small and consistent with experimental observation as long as P_6 is conserved [131]. If P_6 is violated, we need to make sure that we do not produce too large FCNCs. This will be checked throughout this thesis.

and $\mathrm{sgn}(\mu)$. $\tan\beta = \langle H_u \rangle / \langle H_d \rangle$ is the ratio of the vevs of the two Higgs doublets. $\mathrm{sgn}(\mu)$ is the sign of the Higgs mixing parameter μ, *cf.* Eq. (2.5). The magnitude of μ (and the corresponding soft breaking coupling $\tilde{B}$) at M_Z can then be derived from EWSB, *i.e.* from minimizing the scalar potential [132]. This well-motivated and strongly restricted model for the MSSM is known as the minimal supergravity (mSUGRA) model.

We have not introduced new CP-phases in addition to the one in the SM. However, the MSSM offers in principle 40 additional physical phases [133]. But these are strongly restricted by experimental observations [3, 81, 118, 120, 134, 135, 136, 137, 138, 139, 140]. Our ansatz is thus well motivated.

SUSY is a local symmetry in so-called *supergravity* models [19, 20, 21, 22, 23, 24, 25]. This allows gravity to be taken into account. By making certain simplifying assumptions about the supergravity Lagrangian, we obtain the minimal supergravity model [141, 142, 143, 144][7]. Our assumptions from phenomenological considerations can therefore also be motivated from a purely theoretical side.

Up to now, we have only discussed the MSSM. The more general case of the SSM with P_6 violating interactions and its incorporation in the mSUGRA framework will be addressed in Sect. 2.4.3.

2.4.2. Mass Spectrum of P_6 mSUGRA Models

The P_6 conserving mSUGRA model reduces the more than 100 free parameters of the MSSM to only five:

$$M_0, M_{1/2}, A_0, \tan\beta, \mathrm{sgn}(\mu)\,, \tag{2.17}$$

where M_0, $M_{1/2}$ and A_0 are defined at M_{GUT}, *cf.* Eqs. (2.14)-(2.16). We obtain the (experimentally accessible) spectrum at M_Z with the help of the RGEs. One can derive approximate expressions for the sparticle masses in terms of the mSUGRA parameters, Eq. (2.17). The masses relevant for this work are given in Appendix A.2

Fig. 2.2 shows the running of the slepton (blue lines), squark (red lines) and gaugino soft breaking masses (black lines) from M_{GUT} to M_Z. Note that the soft breaking masses give the dominant contribution to the (physical) sparticle masses. In addition, we show the running of the quantities $(\mu^2 + m_{H_d}^2)^{1/2}$ and $(\mu^2 + m_{H_u}^2)^{1/2}$ (green lines) which appear in the Higgs potential. The dashed lines correspond to third generation masses. The input parameters are $M_0 = 80$ GeV, $M_{1/2} = 250$ GeV, $A_0 = -500$ GeV, $\tan\beta = 10$ and $\mathrm{sgn}(\mu) = +1$. Fig. 2.2 is from Ref. [13].

In Fig 2.2 we observe that the squarks at M_Z are much heavier than the sleptons although they have equal masses at M_{GUT}. This can easily be understood by taking a look at the dominant one-loop contributions to the RGEs for the squared slepton and squark soft breaking

[7] In principle, we should use the boundary conditions, Eqs. (2.14), (2.15) and (2.16), at M_{Pl}, where SUSY is broken, instead of M_{GUT}. However, we know little about the RGEs between M_{GUT} and M_{Pl}. It is thus popular to assume all boundary conditions at M_{GUT}. Furthermore, the resulting error should only be a loop factor times $\ln(M_{\mathrm{Pl}}/M_{\mathrm{GUT}})$ which is expected to be small.

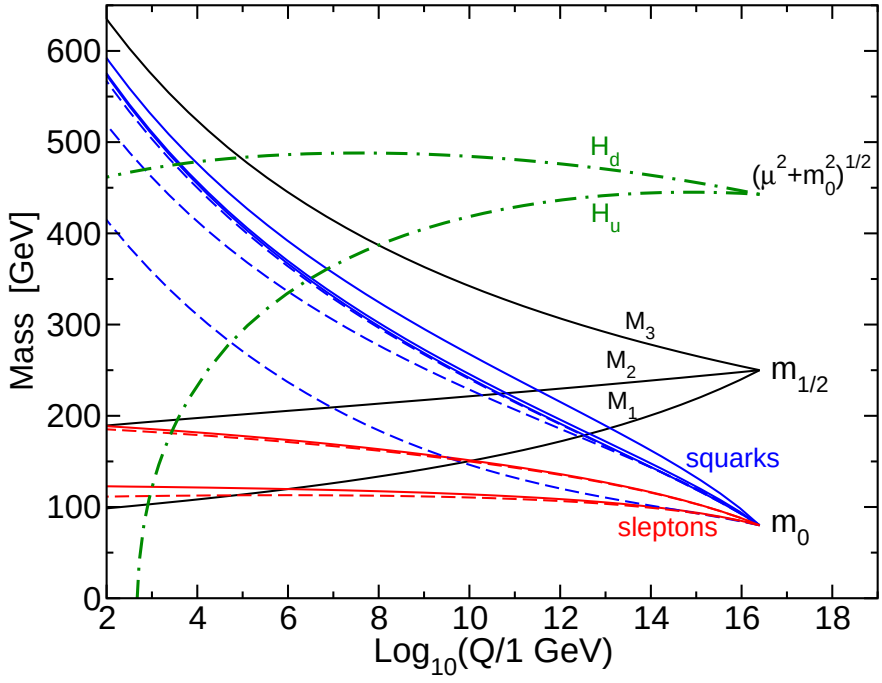

Figure 2.2.: Running of slepton (red lines), squark (blue lines) and gaugino (black lines) soft breaking masses from $M_{\rm GUT}$ to M_Z. We also show the running of the quantities $(\mu^2+m_{H_d}^2)^{1/2}$ and $(\mu^2+m_{H_u}^2)^{1/2}$ (green lines). Third generation masses correspond to dashed lines. This figure has been taken from Ref. [13].

masses, *cf.* Eq. (2.3), of the first two generations ($i=1,2$) [58]

$$16\pi^2\frac{d(\mathbf{m}_{\tilde{\mathbf{E}}}{}^2)_{ii}}{dt} = -\left(\frac{24}{5}g_1^2|M_1|^2-\frac{6}{5}g_1^2\mathcal{S}\right), \tag{2.18}$$

$$16\pi^2\frac{d(\mathbf{m}_{\tilde{\mathbf{L}}}{}^2)_{ii}}{dt} = -\left(\frac{6}{5}g_1^2|M_1|^2+6g_2^2|M_2|^2+\frac{3}{5}g_1^2\mathcal{S}\right), \tag{2.19}$$

$$16\pi^2\frac{d(\mathbf{m}_{\tilde{\mathbf{U}}}{}^2)_{ii}}{dt} = -\left(\frac{32}{15}g_1^2|M_1|^2+\frac{32}{3}g_3^2|M_3|^2+\frac{4}{5}g_1^2\mathcal{S}\right), \tag{2.20}$$

$$16\pi^2\frac{d(\mathbf{m}_{\tilde{\mathbf{D}}}{}^2)_{ii}}{dt} = -\left(\frac{8}{15}g_1^2|M_1|^2+\frac{32}{3}g_3^2|M_3|^2-\frac{2}{5}g_1^2\mathcal{S}\right), \tag{2.21}$$

$$16\pi^2\frac{d(\mathbf{m}_{\tilde{\mathbf{Q}}}{}^2)_{ii}}{dt} = -\left(\frac{2}{15}g_1^2|M_1|^2+6g_2^2|M_2|^2+\frac{32}{3}g_3^2|M_3|^2-\frac{1}{5}g_1^2\mathcal{S}\right), \tag{2.22}$$

with

$$\mathcal{S} \equiv \mathrm{Tr}[\mathbf{m}_{\tilde{\mathbf{Q}}}{}^2-\mathbf{m}_{\tilde{\mathbf{L}}}{}^2-2\mathbf{m}_{\tilde{\mathbf{U}}}{}^2+\mathbf{m}_{\tilde{\mathbf{D}}}{}^2+\mathbf{m}_{\tilde{\mathbf{E}}}{}^2]+m_{H_u}^2-m_{H_d}^2\,. \tag{2.23}$$

Here g_1, g_2 and g_3 are the $U(1)_Y$, $SU(2)$ and $SU(3)_C$ gauge couplings, respectively. $t=\ln Q$ with Q the renormalization scale. Note that the main contributions come from the terms proportional to the gaugino masses squared, M_1^2, M_2^2 and M_3^2, because $\mathcal{S}$, which can be negative, is identical to zero at $M_{\rm GUT}$ for universal scalar masses. In addition, the coefficients

of the M_1^2, M_2^2 and M_3^2, terms are larger compared to the $\mathcal{S}$ term. The right hand side of Eqs. (2.18) - (2.22) is therefore negative at every scale.

A negative slope in the RGEs leads to an increase of the slepton and squark masses running from $M_{\rm GUT}$ down to M_Z. This can be seen in Fig. 2.2. The various magnitudes of the slopes are mainly due to the different gauge charges. They are largest for the strongly interacting sparticles. This explains why the squarks are so much heavier then the sleptons. A similar effect leads to a mass splitting between the left- and right-handed sleptons, which is also observable in Fig. 2.2. The right-handed sleptons couple only via their $U(1)_Y$ gauge charges whereas the left-handed sleptons couple also via their $SU(2)$ charges and thus get larger contributions from the gaugino masses.

Fig. 2.2 also implies for the mass ordering of the gauginos $M_1 < M_2 < M_3$ at M_Z. This can easily be understood by noting that the coefficients b_i, which describe the running of the gaugino masses and the gauge couplings, are the same [99]

$$16\pi^2 \frac{dM_i}{dt} = 2 b_i g_i^2 M_i \,, \tag{2.24}$$

with $b_i = \{33/5, 1, -3\}$ for $i = 1, 2, 3$; *cf.* also Eq. (5.14). As for the gauge coupling g_3, the mass of the $SU(3)_C$ gaugino, M_3, increases when going from $M_{\rm GUT}$ to M_Z. The masses of the bino, M_1, and winos, M_2, decrease. We find at every scale (up to small two-loop effects) the following ratios [99]

$$\frac{M_1}{g_1^2} = \frac{M_2}{g_2^2} = \frac{M_3}{g_3^2} = \frac{M_{1/2}}{g_{\rm GUT}^2} \,, \tag{2.25}$$

with $g_{\rm GUT} \simeq 0.71$ the universal gauge coupling at $M_{\rm GUT}$. It directly follows that $M_3 : M_2 : M_1 \simeq 7 : 2 : 1$ at M_Z.

The masses of the sleptons and squarks of the third generation are generally lighter then the first and second generation masses, *cf.* dashed lines in Fig. 2.2. On the one hand, this is due to the Higgs-Yukawa interactions. For the third generation, they are roughly as strong as the gauge interactions. For example, the dominant contribution to the RGE of the right-handed (soft breaking) stop mass squared is [58]

$$\begin{aligned} 16\pi^2 \frac{d(\mathbf{m}_{\tilde{\mathbf{U}}}{}^2)_{33}}{dt} &= -\left(\frac{32}{15} g_1^2 |M_1|^2 + \frac{32}{3} g_3^2 |M_3|^2 + \frac{4}{5} g_1^2 \mathcal{S}\right) \\ &\quad + (\mathbf{Y}_U)_{33}^2 \left[4(\mathbf{m}_{\tilde{\mathbf{U}}}{}^2)_{33} + 4(\mathbf{m}_{\tilde{\mathbf{Q}}}{}^2)_{33} + 4 m_{H_u}^2\right] + 4(\mathbf{h}_U)_{33}^2, \end{aligned} \tag{2.26}$$

with $(\mathbf{h}_U)_{33} = (\mathbf{Y}_U)_{33} \times A_0$ at $M_{\rm GUT}$. Compared with Eq. (2.20), the running of the right-handed stop mass is now additionally affected by the the large top-Yukawa coupling, $(\mathbf{Y}_U)_{33}$, and the corresponding trilinear scalar interaction, $(\mathbf{h}_U)_{33}$. These new terms in Eq. (2.26) are always positive and therefore tend to decrease the stop mass going from M_{GUT} to M_Z. We thus expect the third generation sfermions to be the lightest generation. We will see, in the next sections, that additional lepton- and baryon-number violating Yukawa couplings, and the corresponding trilinear scalar couplings, can affect the running in a significant way, such that we even get new candidates for the LSP. On the other hand, we can have large L-R mixing for the third generation which additionally decreases the mass of the lighter mass eigenstate.

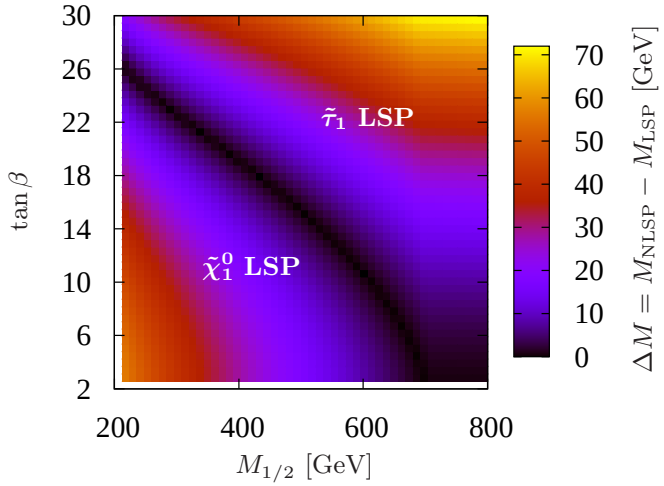

Figure 2.3.: Mass difference, ΔM, between the NLSP and LSP. The LSP candidates are explicitly mentioned. The other mSUGRA parameter are those of SPS1a [146]. The black contour corresponds to $m_{\tilde{\chi}_1^0} = m_{\tilde{\tau}_1}$.

The up-type Higgs also directly couples to the top-Yukawa operator. This leads to a large decrease of the up-type Higgs mass, m_{H_u}, *cf.* Fig. 2.2. The quantity $(\mu^2 + m_{H_u}^2)$ even runs to negative values. This effect leads to radiative electroweak symmetry breaking (REWSB) [36][8]. Having fixed $\tan\beta$, Eq. (2.17), we can derive the magnitude of the Higgs mixing parameter μ and the corresponding soft breaking coupling $\tilde{B}$ from the minimization of the scalar Higgs potential [132][9]. As pointed out in Sect. 1.1, the dynamical breaking of the electroweak symmetry is one strong motivation for SUSY.

We finally expect from Fig. 2.2 that the LSP must be a bino-like neutralino, $\tilde{\chi}_1^0$. For the mSUGRA parameters of Fig. 2.2 we obtain $M_1 = 95$ GeV, $M_2 = 190$ GeV and $\mu = 440$ GeV at M_Z. Mixing of the bino with the wino and the Higgsinos is thus small [79, 80]. The next-to-lightest LSP (NLSP) is a slepton. According to the discussion above, this slepton must be the lighter (mainly right-handed) scalar tau (stau), $\tilde{\tau}_1$, due the rather large tau Yukawa coupling and due to L-R mixing, *cf.* Eq. (A.16). One can now imagine from Fig. 2.2 that increasing $M_{1/2}$ will at some point lead to a spectrum in which the $\tilde{\tau}_1$ becomes the LSP instead of the $\tilde{\chi}_1^0$. This is indeed the case, as can be seen in Fig. 2.3.

We show, in Fig. 2.3, the LSP content in the $M_{1/2}$–$\tan\beta$ plane. The black contour separates the areas with a $\tilde{\chi}_1^0$ LSP and a $\tilde{\tau}_1$ LSP. The other mSUGRA parameters are those of SPS1a [146]. We employed `SOFTSUSY2.0.10` [145, 147] to calculate the masses at M_Z. We indeed observe that the $\tilde{\tau}_1$ becomes the LSP instead of the $\tilde{\chi}_1^0$ when we increase $M_{1/2}$. Increasing $M_{1/2}$ increases the mass of the (bino-like) $\tilde{\chi}_1^0$ faster than the mass of the (mainly right-handed) $\tilde{\tau}_1$, *cf.* Eq. (A.17) and Eq. (A.15), respectively. Apart from that, we can also get a $\tilde{\tau}_1$ LSP by increasing $\tan\beta$. Increasing $\tan\beta$ increases on the one hand the magnitude of the

[8] A negative value of $(\mu^2 + m_{H_u}^2)$ will help, but is not strictly necessary for EWSB; see for example Ref. [13, 66].

[9] To calculate μ and $\tilde{B}$ (numerically) at $M_{\rm GUT}$, we can, for example, employ an iterative procedure, as it is done in the program `SOFTSUSY` [145].

tau Yukawa coupling, $(\mathbf{Y}_E)_{33}$. This increases the (negative) effect of $(\mathbf{Y}_E)_{33}$ on the running of the $\tilde{\tau}$ mass; *cf.* the discussion after Eq. (2.26). On the other hand, $\tan\beta$ increases the mixing between $\tilde{\tau}_L$ and $\tilde{\tau}_R$; see Appendix A.2 for details.

2.4.3. The P_6 violating mSUGRA model

In Sect. 2.4.1 and Sect. 2.4.2 we discussed the mSUGRA model and its MSSM mass spectrum at M_Z. We now want to extend our discussion to the more general SSM with additional lepton- or baryon number violating-interactions, Eq. (2.6) and Eq. (2.11). For that purpose the P_6 violating ($\not{\mathrm{P}}_6$) mSUGRA model[10] was proposed in Ref. [58]. We now have the six parameters

$$M_0, M_{1/2}, A_0, \tan\beta, \mathrm{sgn}(\mu), \mathbf{\Lambda}\,, \tag{2.27}$$

with

$$\mathbf{\Lambda} \in \{\lambda_{ijk}, \lambda'_{ijk}, \lambda''_{ijk}\} \quad \text{at } M_{\mathrm{GUT}}\,, \tag{2.28}$$

i.e. we assume one additional (real) trilinear coupling at M_{GUT}. According to Ref. [58] it is natural that the bilinear $\not{\mathrm{P}}_6$ operators can be rotated away at M_{GUT}. However this is no longer possible at lower scales due to different running of κ_i and $\tilde{D}_i$ [58]; *cf.* Sect. 4.1.1. Analogous to Eq. (2.13) and Eq. (2.16), we have, at M_{GUT}, also one non-vanishing $\not{\mathrm{P}}_6$ term in the soft breaking Lagrangian, Eq. (2.11), namely $\mathbf{h_\Lambda} = A_0 \times \mathbf{\Lambda}$. We have thus reduced the more than 200 free parameters of the $\not{\mathrm{P}}_6$ SSM to only six. The $\not{\mathrm{P}}_6$ mSUGRA model is therefore well suited for detailed phenomenological studies. Note that B_3 (and P_6) is incompatible with a GUT gauge symmetry, since the quark and lepton superfields are treated differently, *cf.* Eq. (2.9). However, B_3 operators can be generated after the GUT symmetry is broken, see Ref. [58] for details.

From a phenomenological point of view, a single dominating $\mathbf{\Lambda}$ coupling is well motivated. Bounds on products of two different $\not{\mathrm{P}}_6$ couplings are in general stronger than bounds on single couplings [89, 148]. However, one $\not{\mathrm{P}}_6$ coupling at M_{GUT} will generate additional $\not{\mathrm{P}}_6$ couplings at M_Z [58, 85, 100, 102, 103, 104, 105]. We will take this effect into account in this thesis. Note that also the SM offers an extreme hierarchy between different Yukawa couplings.

As pointed out in Sect. 2.3, an important difference between $\not{\mathrm{P}}_6$ mSUGRA compared to P_6 mSUGRA is that every sparticle is allowed to be the LSP, because it will decay. A $\tilde{\tau}_1$ LSP in $\not{\mathrm{P}}_6$ mSUGRA is therefore as well motivated as a $\tilde{\chi}_1^0$ LSP; see Fig. 2.3 and Ref. [58, 106]. In addition, the RGEs get new $\not{\mathrm{P}}_6$ contributions which can effect the running of the sparticle masses in a significant way.

For example, the RGE of the soft breaking sneutrino (and left-handed charged slepton) mass, Eq. (2.19), receives additional one-loop contributions in the presence of $\lambda'_{ijk}|_{\mathrm{GUT}} \neq 0$

[10] We also refer to the P_6 violating mSUGRA model as the B_3 mSUGRA model, if only lepton-number is violated, *cf.* Sect. 2.3.

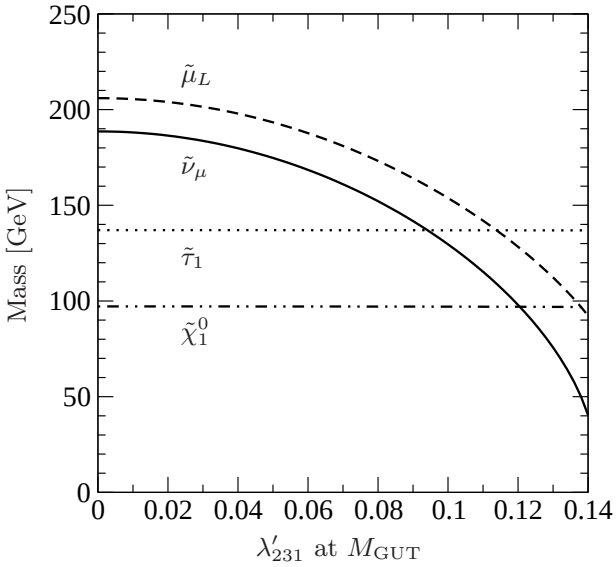

Figure 2.4.: Masses of $\tilde{\chi}_1^0$, $\tilde{\tau}_1$, $\tilde{\nu}_\mu$ and $\tilde{\mu}_L$ at M_Z as a function of $\lambda'_{231}|_{\rm GUT}$. The other mSUGRA parameters are that of SPS1a [146]. We assume up-mixing, *cf.* Appendix A.1.

[58][11]:

$$16\pi^2 \frac{d(\mathbf{m}_{\tilde{\mathbf{L}}}{}^2)_{ii}}{dt} = -\frac{6}{5}g_1^2 M_1^2 - 6g_2^2 M_2^2 - \frac{3}{5}g_1^2 \mathcal{S} + 6\lambda'^2_{ijk}\left[(\mathbf{m}_{\tilde{\mathbf{L}}})^2_{ii} + (\mathbf{m}_{\tilde{\mathbf{Q}}})^2_{jj} + (\mathbf{m}_{\tilde{\mathbf{D}}})^2_{kk}\right] + 6(\mathbf{h}_{\mathbf{D^k}})^2_{ij} \qquad (2.29)$$

with

$$(\mathbf{h}_{\mathbf{D^k}})_{ij} \equiv \lambda'_{ijk} \times A_0, \qquad \text{at } M_{\rm GUT}\,. \qquad (2.30)$$

Here $(\mathbf{h}_{D^k})_{ij}$ is the soft breaking coupling corresponding to λ'_{ijk}, *cf.* Eq. (2.11). There is no summation over repeated indices in Eq. (2.29).

The running of $(\mathbf{m}_{\tilde{\mathbf{L}}}{}^2)_{ii}$ is governed by two different sets of terms. The first three terms in Eq. (2.29) are proportional to the gauge couplings squared. We found in the last section that the sum of these three terms is negative at every scale. They therefore lead to an increase in $(\mathbf{m}_{\tilde{\mathbf{L}}}{}^2)_{ii}$, going from $M_{\rm GUT}$ to M_Z.

The remaining contributions are proportional to λ'^2_{ijk} and $(\mathbf{h}_{D^k})^2_{ij}$; the latter is also proportional to λ'^2_{ijk} at $M_{\rm GUT}$, *cf.* Eq. (2.30). These terms are positive and will therefore reduce $(\mathbf{m}_{\tilde{\mathbf{L}}}{}^2)_{ii}$, going from $M_{\rm GUT}$ to M_Z. They are also new to the $\not{P}_6$ mSUGRA model compared to minimal mSUGRA. The influence of these new contributions on $(\mathbf{m}_{\tilde{\mathbf{L}}}{}^2)_{ii}$ depends on the magnitude of $\not{P}_6$ λ'_{ijk} and also on the other mSUGRA parameters, Eq. (2.27), especially on A_0, as we will show in Sect. 4.2.1.

In Fig. 2.4, we demonstrate the impact of a non-vanishing $\lambda'_{231}|_{\rm GUT}$ on the running of the sneutrino mass. The other mSUGRA parameters are that of SPS1a [146]. In the P_6

[11] For $i = 3$, we can also have significant terms proportional to $(\mathbf{Y}_E)^2_{33}$, *i.e.* proportional to the tau Yukawa coupling squared.

conserving case, the $\tilde{\chi}_1^0$ is the LSP and the $\tilde{\tau}_1$ is the NLSP. See also Ref. [106] for the case of $\lambda'_{331}|_{\rm GUT}$. The mass of the muon sneutrino, $\tilde{\nu}_\mu$, decreases for increasing $\lambda'_{231}|_{\rm GUT}$, as described by Eq. (2.29). Furthermore, the mass of the left-handed smuon, $\tilde{\mu}_L$, decreases, as it belongs to the same $SU(2)$ doublet. The running of the $\tilde{\mu}_L$ mass squared is also described by Eq. (2.29). But note that the mass difference between $\tilde{\nu}_\mu$ and $\tilde{\mu}_L$, is not the same at all values of $\lambda'_{231}|_{\rm GUT}$, as can be seen in Fig. 2.4. This is due to the different D-term contributions to $m_{\tilde{\nu}_\mu}$ and $m_{\tilde{\mu}_L}$, *cf.* Eq. (A.11), for different $\lambda'_{231}|_{\rm GUT}$. The mass difference is approximately 20 GeV (50 GeV) for $\lambda'_{231}|_{\rm GUT} = 0.0$ (0.14). The $\tilde{\mu}_L$ is also always heavier than the $\tilde{\nu}_\mu$, as long as $\tan\beta > 1$. We calculated the sparticle masses in Fig. 2.4 with a $\not{R}_6$ version of `SOFTSUSY` [149, 150, 147].

At one-loop order, the masses of the $\tilde{\chi}_1^0$ and the $\tilde{\tau}_1$ are not changed, as can be seen in Fig. 2.4. They do not directly couple to the $L_2 Q_3 \bar{D}_1$ operator, in contrast to $\tilde{\nu}_\mu$, $\tilde{\mu}_L$, *cf.* Eq. (2.29). The RGEs of the $\tilde{\chi}_1^0$ and the $\tilde{\tau}_1$ mass get thus no contributions (at one-loop) which depend on λ'_{231}. We therefore obtain for the parameter set SPS1a with $\lambda'_{231}|_{\rm GUT} > 0.12$ a new candidate for the LSP, namely the sneutrino! In Sect. 4, we systematically investigate the conditions which lead to a $\tilde{\nu}_i$ LSP in $\not{R}_6$ mSUGRA models. From Eq. (2.29) it is clear that we need a coupling $\lambda'_{ijk}|_{\rm GUT} \neq 0$. The smallest $\lambda'_{ijk}|_{\rm GUT}$ coupling which we found leading to a $\tilde{\nu}_i$ LSP is $\lambda'_{ijk}|_{\rm GUT} = 0.054$. Otherwise, the new contributions in the RGE, Eq. (2.29), are not large enough to reduce the $\tilde{\nu}_i$ mass significantly.

A non-vanishing $\lambda'_{ijk}|_{\rm GUT}$ also reduces the left-handed squark masses of generation j, and the right-handed down-squark masses of generation k, because these squarks couple directly to the $L_i Q_j \bar{D}_k$ operator [58, 106]. One might worry that this effect leads to unwanted FCNCs when we rotate the quarks and squarks from the flavor-basis to their mass-basis. But, for example for SPS1a with $\lambda'_{231}|_{\rm GUT} = 0.13$, the respective squark masses are reduced by less than 4%, thus avoiding FCNCs which are in contradiction with experiment [81, 82].

3. All Possible LSP Candidates in P_6 Violating mSUGRA Models

As pointed out in Sect. 2.3, the LSP is no longer stable if lepton- or baryon-number violating interactions, Eq. (2.6), are present. The LSP is then also not restricted to be the lightest neutralino, $\tilde{\chi}_1^0$, and can in principle be any SUSY particle

$$\tilde{\chi}_1^0,\ \tilde{\chi}_1^\pm,\ \tilde{\ell}_{L/Ri}^\pm,\ \tilde{\tau}_1,\ \tilde{\nu}_i,\ \tilde{q}_{L/Rj},\ \tilde{b}_1,\ \tilde{t}_1,\ \tilde{g}_a\,; \tag{3.1}$$

see Sect. 2.2 and Table 2.1. We have separately listed the lightest stau, $\tilde{\tau}_1$, sbottom, $\tilde{b}_1$, and stop, $\tilde{t}_1$, as they are promising LSP candidates.

In the collider search for supersymmetry at colliders, it is essential to know the nature of the LSP, because SUSY particles, if produced, normally cascade decay down to the LSP within the detector. The LSP is thus a central ingredient of almost all SUSY signatures.

In Eq. (3.1), we have a bewildering array of potential LSPs. We thus need a guiding principle. A well motivated restricted framework for detailed studies is the proton-hexality, P_6, violating mSUGRA model; see Sect. 2.4.3. We thus have a simple well-motivated framework, in which we can systematically investigate the nature of the LSP. In Ref. [58, 106] it was shown that in such models there are two different LSP candidates if the $\not{P}_6$ coupling $\mathbf{\Lambda}$, Eq. (2.28), is $\lesssim \mathcal{O}(10^{-2})$: the $\tilde{\chi}_1^0$ and the $\tilde{\tau}_1$; see also Fig. 2.3. However, as we saw in Fig. 2.4 for the example of a sneutrino, $\tilde{\nu}_i$, LSP, $\mathbf{\Lambda} \gtrsim \mathcal{O}(10^{-1})$ can significantly alter the renormalization group running such that we obtain a non-$\tilde{\chi}_1^0$ and non-$\tilde{\tau}_1$ LSP. It is the purpose of this section to determine all possible LSPs in the $\not{P}_6$ mSUGRA model. This is very important for SUSY searches at the LHC.

We describe in Sect. 3.1 the mechanism which produces non-$\tilde{\chi}_1^0$ and non-$\tilde{\tau}_1$ LSPs. We also give a complete list of all LSP candidates in $\not{P}_6$ mSUGRA. In Sect. 3.2 (Sect. 3.3) we discuss the LSPs which can be obtained via a non-vanishing $L_iL_j\bar{E}_k$ ($\bar{U}_i\bar{U}_j\bar{D}_k$) operator, *cf.* Eq. (2.6). In Sect. 3.4 we conclude.

coupling $\mathbf{\Lambda}$	LSP	coupling $\mathbf{\Lambda}$	LSP
λ_{132}	$\tilde{\mu}_R$	λ_{121},λ_{131},λ_{231}	$\tilde{e}_R$
λ'_{ijk}	$\tilde{\nu}_i$	λ''_{212}	$\tilde{s}_R/\tilde{d}_R$
$\lambda''_{123}, \lambda''_{213}, \lambda''_{223}$	$\tilde{b}_1$	λ''_{323}	$\tilde{t}_1$

Table 3.1.: All possible non-$\tilde{\chi}_1^0$ (and non-$\tilde{\tau}_1$) LSP candidates in $\not{P}_6$ mSUGRA via a non-vanishing $\mathbf{\Lambda} = \mathcal{O}(10^{-1})$, consistent with the experimental bounds, *cf.* Refs. [85, 89, 94, 148].

3.1. Non-$\tilde{\chi}_1^0$ LSP Parameter Space

If a sparticle directly couples to $\mathbf{\Lambda}$, the dominant contributions to the RGE of the running sparticle mass $\tilde{m}$ are [58][1]:

$$16\pi^2 \frac{d(\tilde{m}^2)}{dt} = -a_i g_i^2 M_i^2 - b g_1^2 \mathcal{S} + \mathbf{\Lambda}^2 \mathcal{F} + c\, \mathbf{h}_{\mathbf{\Lambda}}^2 \,, \tag{3.2}$$

$$\mathbf{h}_{\mathbf{\Lambda}} \equiv \mathbf{\Lambda} \times A_0 \qquad \text{at } M_{\rm GUT}\,. \tag{3.3}$$

Here we sum over repeated indices. $\mathcal{S}$ and $\mathcal{F}$ are linear functions of products of two soft breaking scalar masses and a_i, b, c are constants of $\mathcal{O}(10^{-1} - 10^{1})$ [58]; see Eq. (2.29) for an explicit example.

The sum of the first two P_6 terms in Eq. (3.2) is negative and thus *increases* $\tilde{m}$ when running from $M_{\rm GUT}$ to M_Z. In contrast, the last two $\not{P}_6$ terms proportional to $\mathbf{\Lambda}^2$, $\mathbf{h}_{\mathbf{\Lambda}}^2$, are always positive and therefore *decrease* $\tilde{m}$. We thus expect new LSP candidates beyond $\tilde{\chi}_1^0$ and $\tilde{\tau}_1$ if these latter terms contribute substantially. This is the case if $\mathbf{\Lambda} = \mathcal{O}(10^{-1})$, *i.e.* $\mathbf{\Lambda} = \mathcal{O}(g_i)$; see Fig. 2.4. We can strengthen the (negative) contribution of $\mathbf{h}_{\mathbf{\Lambda}}^2$, by choosing a negative A_0 with a large magnitude; for moderate positive A_0 there is a cancellation in the RGE evolution of $\mathbf{h}_{\mathbf{\Lambda}}$. We will discuss this effect in detail in Sect. 4.2.1. The other terms are not significantly affected by A_0. Note that we also need $M_{1/2}$ ($\tan\beta$) large (small) enough to avoid a $\tilde{\chi}_1^0$ ($\tilde{\tau}_1$) LSP, *cf.* Fig. 3.2. In Ref. [58, 106] it was shown that $\lambda'_{ijk}|_{\rm GUT} = \mathcal{O}(10^{-1})$ can lead to a $\tilde{\nu}_i$ LSP. Ref. [58, 101] gives the example of a $\tilde{e}_R$ LSP via $\lambda_{231}|_{\rm GUT} = \mathcal{O}(10^{-1})$.

Here we investigate all possible LSP candidates in $\not{P}_6$ mSUGRA via a non-vanishing coupling $\mathbf{\Lambda} = \mathcal{O}(10^{-1})$. Our results are shown in Table 3.1 and are explained in the following. We only consider couplings for which $\mathbf{\Lambda} = \mathcal{O}(10^{-1})$ is consistent with existing bounds [85, 89, 94, 148]. We argue that Table 3.1 gives a complete list of all possible non-$\tilde{\chi}_1^0$ (and non-$\tilde{\tau}_1$) LSP candidates in $\not{P}_6$ mSUGRA. We refer to Sect. 4 for a very detailed discussion of the $\tilde{\nu}_i$ LSP via $\lambda'_{ijk}|_{\rm GUT} \neq 0$.

We now investigate the non-$\tilde{\chi}_1^0$ (and non-$\tilde{\tau}_1$) LSP parameter space of $\not{P}_6$ mSUGRA. We calculate the sparticle mass spectra with a $\not{P}_6$ version of `SOFTSUSY` [149, 150, 147]. In the figures, we show (green) contour lines corresponding to the 2σ windows for BR($b \to s\gamma$) [151],

$$2.74 \times 10^{-4} < \text{BR}(b \to s\gamma) < 4.30 \times 10^{-4}\,, \tag{3.4}$$

[1] For third generation sparticles we also need to take into account the contributions from the Higgs-Yukawa interactions. Their effect is similar compared to $\mathbf{\Lambda}$ and $\mathbf{h}_{\mathbf{\Lambda}}$ in Eq. (3.2); *cf.* the discussion after Eq. (2.26)

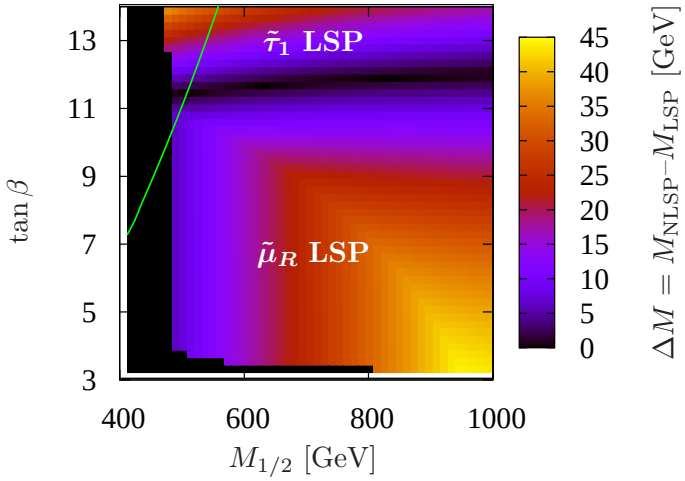

Figure 3.1.: Mass difference, ΔM, between the NLSP and LSP. The LSP candidates are explicitly mentioned. The blackened out region on the left and bottom corresponds to parameter points, which posses a tachyon or which violate other constraints as described in the text. The green contour line is described in the text. The other mSUGRA parameter are $\lambda_{132}|_{\rm GUT} = 0.09$, $M_0 = 170$ GeV, $A_0 = -1500$ GeV and $\mathrm{sgn}(\mu) = +1$.

and for the SUSY contributions to the anomalous magnetic moment of the muon [4, 5, 6]

$$11.9 \times 10^{-10} < \delta a_\mu^{\rm SUSY} < 47.1 \times 10^{-10} \,. \tag{3.5}$$

See Sect. 4.2 for more details. We employ the LEP exclusion bound on the light Higgs mass [152], $m_h > 114.4$ GeV, which we reduce by 3 GeV to account for numerical uncertainties of `SOFTSUSY` [40, 106, 153, 154].

3.2. Non-$\tilde{\chi}_1^0$ LSPs via LLE

The least constrained couplings of the $L_i L_j \bar{E}_k$ operator, Eq. (2.6), are [85, 89, 94, 148]

$$\begin{aligned} &\lambda_{121}, \lambda_{131} \;< 0.15, \qquad \lambda_{123} < 0.05 \times (m_{\tilde{\tau}_R}/100\,\mathrm{GeV}) \,, \\ &\lambda_{132}(\lambda_{231}) < 0.07 \times (m_{\tilde{\mu}_R, \tilde{e}_R}/100\,\mathrm{GeV}) \,, \end{aligned} \tag{3.6}$$

where the bounds apply at M_Z. Note, that λ_{ijk} is reduced by roughly a factor of 1.5 when running from M_Z to $M_{\rm GUT}$ [85].

We give in Fig. 3.1 the $\tilde{\mu}_R$ LSP region in the $M_{1/2}$–$\tan\beta$ plane for a λ_{132}-coupling. We show the mass difference, ΔM, between the NLSP and LSP. We have employed a lower bound of 190 GeV on the $\tilde{\mu}_R$ mass to fulfill the strong bound on λ_{132}. The remaining SUSY particles are then so heavy within $\not{R}_6$ mSUGRA, that other collider constraints from LEP and the Tevatron are automatically fulfilled.

We see that the $\tilde{\mu}_R$ LSP exists in an extended region of $\not{R}_6$ mSUGRA. We find a $\tilde{\mu}_R$ LSP for all $M_{1/2} > 480$ GeV, because $M_{1/2}$ increases the mass of the (bino-like) $\tilde{\chi}_1^0$ faster than

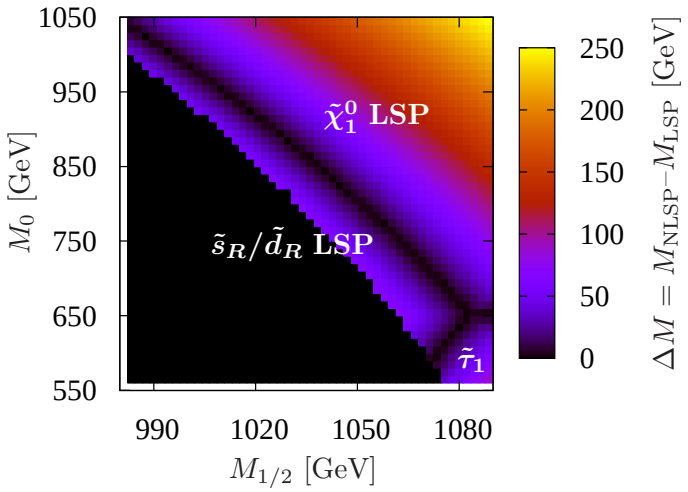

Figure 3.2.: Same as Fig. 3.1, but with $\lambda''_{212}|_{\rm GUT} = 0.5$, $A_0 = -3700$ GeV, $\tan\beta = 19$ and $\mathrm{sgn}(\mu) = +1$.

the mass of the $\tilde{\mu}_R$, *cf.* Eq. (A.11) and Eq. (A.17). The complete $\tilde{\mu}_R$ LSP region in Fig. 3.1 agrees with BR($b \to s\gamma$) at 2σ. But only a tiny region is consistent with $\delta a_\mu^{\rm SUSY}$ at 2σ, *i.e.* lies above the green line. The mass spectra are rather heavy and thus $\delta a_\mu^{\rm SUSY}$ is suppressed [7, 155].

If we use λ_{231}, λ_{121} or λ_{131} instead of λ_{132} in our parameter scans, we obtain a $\tilde{e}_R$ as the LSP. We can not obtain a $\tilde{\ell}_L$ as the LSP in $\not{P}_6$ mSUGRA with $\lambda|_{\rm GUT} \neq 0$. On the one hand, the P_6 contributions to the RGEs of $m^2_{\tilde{\ell}_L}$ have a larger magnitude compared to $m^2_{\tilde{\ell}_R}$. On the other hand, the (negative) $\not{P}_6$ contributions to $m^2_{\tilde{\ell}_L}$ are smaller in magnitude compared to those for $m^2_{\tilde{\ell}_R}$ [58].

3.3. Non-$\tilde{\chi}_1^0$ LSPs via UDD

The following baryon-number violating couplings, λ''_{ijk}, are only constrained by perturbativity [85, 89, 94, 148]

$$\lambda''_{212}\,, \lambda''_{123}\,, \lambda''_{213}\,, \lambda''_{223}\,, \lambda''_{323} \lesssim \mathcal{O}(1)\,. \tag{3.7}$$

We can obtain right-handed squark, $\tilde{q}_R$, LSPs via these λ''_{ijk} couplings.

We assume that the weak- and mass-eigenstates of *right*-handed quarks are the same. With this assumption we avoid the RGE generation of additional couplings λ''_{lmn} at M_Z out of $\lambda''_{ijk}|_{\rm GUT}$, which might be in contradiction with experiment [85, 89, 94, 148]. We also avoid large FCNCs [81, 82]. Note that we only have experimental information about mixing in the left-handed quark sector; see Sect A.1.

We show in Fig. 3.2 the $\tilde{d}_R/\tilde{s}_R$ LSP region via $\lambda''_{212}|_{\rm GUT} = 0.5$ in the $M_{1/2}$–M_0 plane. The $\tilde{d}_R$ and $\tilde{s}_R$ are degenerate in mass, because both sparticles interact the same via the gauge interactions and via λ''_{212} [58]. We impose a lower bound of 380 GeV on the $\tilde{d}_R/\tilde{s}_R$ mass,

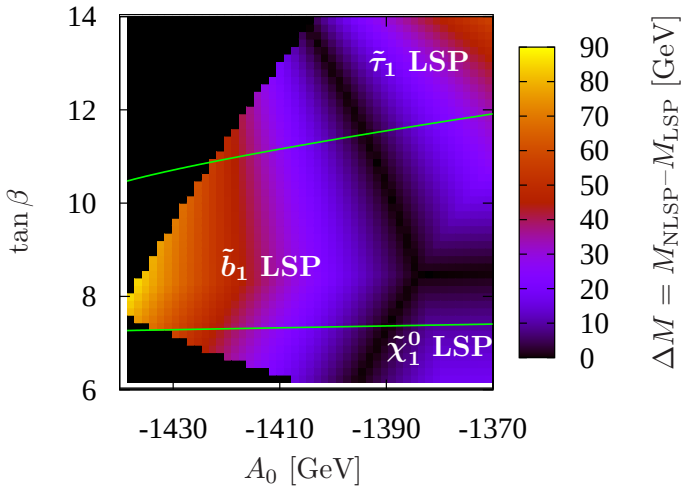

Figure 3.3.: Same as Fig. 3.1, but with $\lambda''_{223}|_{\rm GUT} = 0.5$, $M_0 = 120$ GeV, $M_{1/2} = 400$ GeV and $\mathrm{sgn}(\mu) = +1$.

consistent with the non-observation of the $\tilde{d}_R/\tilde{s}_R$ in resonance searches in the dijet channel at the Tevatron [156][2].

We can not get a $\tilde{c}_R$ LSP via $\lambda''_{212}|_{\rm GUT} \neq 0$. The $\not{P}_6$ contributions to the RGEs of the $\tilde{d}_R$, $\tilde{s}_R$ and $\tilde{c}_R$ mass are the same [58]. But the $\tilde{c}_R$ couples stronger to the $U(1)_Y$ gaugino than the $\tilde{d}_R$ and $\tilde{s}_R$ and is therefore always heavier than $\tilde{d}_R$ and $\tilde{s}_R$[3], *cf.* Eq. (A.12). For example, the $\tilde{c}_R$ in Fig. 3.2 is roughly 60 GeV heavier than the $\tilde{d}_R/\tilde{s}_R$.

Due to $m_{\tilde{d}_R/\tilde{s}_R} > 380$ GeV, we need $M_{1/2} = \mathcal{O}(1\,\mathrm{TeV})$, as can be seen in Fig. 3.2, to obtain also a heavy $\tilde{\chi}_1^0$. This results in such a heavy mass spectrum that $\delta a_\mu^{\rm SUSY}$ lies beyond the experimental 2σ window. However the complete $\tilde{d}_R/\tilde{s}_R$ LSP region in Fig. 3.2 is consistent with $\mathrm{BR}(b \to s\gamma)$ at 1σ.

Only small $M_{1/2}$ intervals are allowed in Fig. 3.2, because $m_{\tilde{d}_R/\tilde{s}_R}$ at M_Z increases very rapidly with increasing $M_{1/2}$, *cf.* Eq. (A.12). The dependence on M_0 is weaker, *i.e.* M_0 intervals up to 100 GeV (for constant $M_{1/2}$) are allowed in Fig. 3.2. These are general features of most of the squark LSP regions. We thus concentrate on A_0 and $\tan\beta$ in what follows. $\tan\beta$ is important, because increasing $\tan\beta$ increases [decreases] $\delta a_\mu^{\rm SUSY}$ [$\mathrm{BR}(b \to s\gamma)$], *cf.* Ref [106].

We give in Fig. 3.3 the $\tilde{b}_1$ LSP region via $\lambda''_{223}|_{\rm GUT} = 0.5$ in the A_0–$\tan\beta$ plane. The $\tilde{b}_1$ LSP mass lies between 77 GeV and 180 GeV. The lower value corresponds to the strongest LEP bound [157]. Note, that there is no bound on the $\tilde{b}_1$ LSP mass from Tevatron searches. The single $\tilde{b}_1$ production cross section via $\lambda''_{223}|_{\rm GUT} = 0.5$ lies below the exclusion limits for a dijet resonance, *cf.* Ref. [156], due to the small incoming parton luminosity.

[2] It is not clear if Ref. [156] can exclude $m_{\tilde{d}_R/\tilde{s}_R} < 380$ GeV. They did not search for single squark resonances. A more detailed analysis is required, including NLO corrections to single $\tilde{d}_R/\tilde{s}_R$ production.

[3] The $\tilde{c}_R$ can in principle be lighter than the $\tilde{d}_R$ and $\tilde{s}_R$ if $M_{1/2} \lesssim 200$ GeV due to different D-term contributions, see Eq. (A.12) for details. However, the $\tilde{c}_R$ LSP parameter space is in that case excluded by constraints from LEP [157, 152].

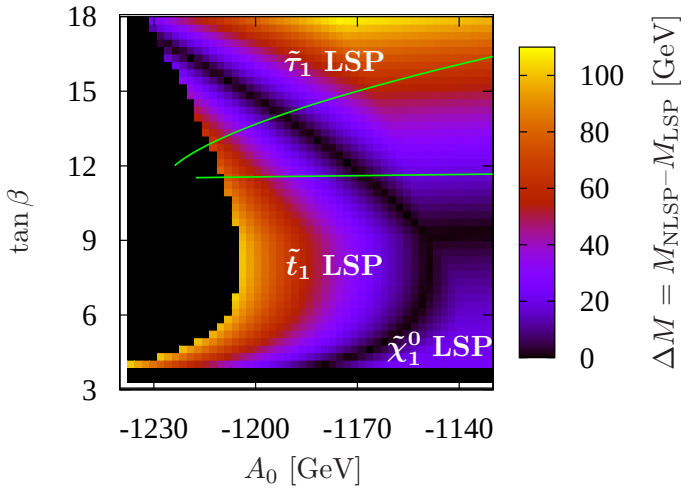

Figure 3.4.: Same as Fig. 3.1, but with $\lambda''_{323}|_{\rm GUT} = 0.35$, $M_0 = 120$ GeV, $M_{1/2} = 480$ GeV and $\mathrm{sgn}(\mu) = +1$.

Most of the $\tilde{b}_1$ LSP region in Fig. 3.3 is also consistent with BR($b \to s\gamma$) (below upper green line) and $\delta a_\mu^{\rm SUSY}$ (above lower green line) at the 2σ level. We observe that $A_0 = \mathcal{O}(-1\,\mathrm{TeV})$ is vital to obtain a $\tilde{b}_1$ LSP. Increasing A_0 reduces the (negative) effect of $\lambda''_{223}|_{\rm GUT}$ on the running of the $\tilde{b}_1$ mass and we re-obtain the $\tilde{\chi}_1^0$ or $\tilde{\tau}_1$ LSP, see Sect. 4.2.1.

We can also obtain a $\tilde{b}_1$ LSP, if we use $\lambda''_{123}|_{\rm GUT}$, $\lambda''_{213}|_{\rm GUT} \neq 0$. But now there are additional constraints from the Tevatron on dijet resonances [156]. The couplings λ''_{123} and λ''_{213} unlike λ''_{223} allow for single $\tilde{b}_1$ production via a valence quark or antiquark, which enhances the hadronic cross section. Note, that these three couplings can only lead to a $\tilde{b}_1$ LSP, because the $\tilde{b}_1$ mass (compared to the $\tilde{q}_R$ masses of the first two generations) is further reduced by the large bottom Yukawa coupling and by larger left-right mixing.

For $\lambda''_{323}|_{\rm GUT} = 0.35$, we obtain a $\tilde{t}_1$ LSP as shown in Fig. 3.4 for the A_0–$\tan\beta$ plane. The $\tilde{t}_1$ LSP mass ranges from 94 GeV to 200 GeV. The lower bound corresponds to the LEP bound on $m_{\tilde{t}_1}$ [157][4]. The $\tilde{t}_1$ LSP region between the upper and lower green line is also consistent with BR($b \to s\gamma$) and $\delta a_\mu^{\rm SUSY}$ at 2σ.

We need in general a smaller coupling $\lambda''_{ijk}|_{\rm GUT}$ to obtain a $\tilde{t}_1$ LSP than $\tilde{b}_1$ LSP, because the $\tilde{t}_1$ mass is further reduced by the large top Yukawa coupling; see discussion after Eq. (2.26). This effect is enhanced by a negative A_0 with a large magnitude, see Sect. 4.2.1. $A_0 = \mathcal{O}(-1\,\mathrm{TeV})$ also leads to large left-right mixing, which further reduces the $\tilde{t}_1$ mass. For the same reasons we can not obtain another squark LSP than the $\tilde{t}_1$ via $\lambda''_{323}|_{\rm GUT} \neq 0$.

The complete $\tilde{t}_1$ LSP region in Fig. 3.4 should be testable at the Tevatron [158]. The authors found that $\tilde{t}_1$ masses up to 190 GeV (210 GeV) can be explored at the Tevatron for an integrated luminosity of 2 fb^{-1} (8 fb^{-1}). However, this analysis has not yet been performed by the Tevatron collaborations.

[4] Unlike the b_1 LSP, the $\tilde{t}_1$ LSP has a large left-handed component due to left-right mixing. As a conservative approach, we take the (stronger) mass bounds from Ref. [157] for purely left-handed up-type squarks.

3.4. Conclusion of Section 3

We have investigated for the first time all possible non-$\tilde{\chi}_1^0$ (and non-$\tilde{\tau}_1$) LSPs in P_6 violating mSUGRA models; see Table 3.1. We have found that a non-vanishing $L_iL_j\bar{E}_k$ operator at the GUT scale can lead to a $\tilde{e}_R$ ($i = 1$) or $\tilde{\mu}_R$ ($i = 2$) LSP; *cf.* Fig. 3.1. A non-vanishing $L_iQ_j\bar{D}_k$ operator can lead to a $\tilde{\nu}_i$ LSP. We can also obtain squark LSPs, namely the $\tilde{s}_R$, $\tilde{d}_R$, $\tilde{b}_1$ and $\tilde{t}_1$ via a non-vanishing $\bar{U}_i\bar{D}_j\bar{D}_k$ operator; see Fig. 3.2, Fig. 3.3 and Fig. 3.4, respectively. We have found $\tilde{\mu}_R$, $\tilde{\nu}_i$, $\tilde{b}_1$ and $\tilde{t}_1$ LSP scenarios consistent with the observed anomalous magnetic moment of the muon and $b \to s\gamma$ as well as consistent with collider constraints from LEP and the Tevatron. According to Ref. [158], $\tilde{t}_1$ LSPs up to a mass of 190 GeV can be tested at the Tevatron with 2 fb^{-1} of data. We therefore want to encourage the Tevatron collaborations to investigate the $\tilde{t}_1$ LSP parameter space of P_6 violating mSUGRA, as well as to look for squark LSP resonances in dijet events.

4. Sneutrino LSPs in B_3 mSUGRA Models and Signals at the LHC

We have shown in Sect. 2.4.3 that a non-vanishing coupling λ'_{ijk} at the grand unification scale, $M_{\rm GUT}$, can affect the supersymmetric spectrum at the electroweak scale, M_Z, such that a sneutrino, $\tilde{\nu}_i$, is the LSP. This requires $\lambda'_{ijk} \gtrsim 0.05$ at $M_{\rm GUT}$ corresponding to $\lambda'_{ijk} \gtrsim 0.15$ at M_Z. In this section we consider in detail the case of a $\tilde{\nu}_i$ LSP within baryon-triality, B_3, mSUGRA[1], *cf.* Sect. 2.3 and Sect. 2.4.3. In Ref. [106] only one example scenario with a $\tilde{\nu}_\tau$ LSP was presented. We go beyond this work and systematically investigate the B_3 mSUGRA parameter space with a $\tilde{\nu}_i$ LSP.

In Sect. 4.1, we analyze the experimental bounds, especially on the $L_iQ_j\bar{D}_k$ operator, Eq. (2.6), which restrict the $\tilde{\nu}_i$ LSP parameter space. We then investigate in Sect. 4.2 in detail the conditions at $M_{\rm GUT}$ leading to a $\tilde{\nu}_i$ LSP. Finally, in Sect. 4.3, we simulate SUSY events at the LHC within one $\tilde{\nu}_\mu$ LSP scenario. We focus on signatures, which are special for $\tilde{\nu}_i$ LSP scenarios. We conclude in Sect. 4.4.

4.1. Experimental Bounds on Sneutrino LSP Models

We now investigate for which couplings $\lambda'_{ijk}|_{\rm GUT}$ the upper bounds are sufficiently weak such that a $\tilde{\nu}_i$ LSP can be generated. For the bounds, we first take into account the generation of tree level neutrino masses. Then we review other indirect bounds on these couplings. Finally we discuss the restrictions from direct searches for supersymmetric particles at LEP, at the Tevatron and the CERN $p\bar{p}$ collider.

4.1.1. Bounds from Tree Level Neutrino Masses

If $\lambda'_{ijk}|_{\rm GUT} \neq 0$ and the bilinear coupling $\kappa_i|_{\rm GUT} = 0$, *cf.* Eq. (2.6), $\kappa_i|_{\rm M_Z} \neq 0$ will be generated via the RGEs [58, 100, 102, 103, 104, 105]

$$16\pi^2 \frac{d\kappa_i}{dt} = -3\mu\lambda'_{ijk}(\mathbf{Y}_D)_{jk} + \dots \,. \tag{4.1}$$

Furthermore, $\lambda'_{ijk}|_{\rm GUT}$ will generate the corresponding soft breaking term of κ_i, namely $\tilde{D}_i$, Eq. (2.11), via [58, 100, 102, 103, 104, 105]

$$16\pi^2 \frac{d\tilde{D}_i}{dt} = -3\left[2\mu(\mathbf{h}_{D^k})_{ij} + \tilde{B}\lambda'_{ijk}\right](\mathbf{Y}_D)_{jk} + \dots \,. \tag{4.2}$$

[1] We also refer to the P_6 violating mSUGRA model as the B_3 mSUGRA model, if only lepton-number is violated.

Here, $\tilde{B}$ is the soft breaking coupling corresponding to μ and is determined by REWSB [36, 58], *cf.* Eq. (2.3). Since the RGEs are different for κ_i and $\tilde{D}_i$, they are not aligned at the weak scale and can not be rotated away through a field redefinition.

The sneutrino of generation i will develop a vacuum expectation value v_i due to the non-vanishing couplings κ_i and $\tilde{D}_i$. The vacuum expectation value v_i, and the κ_i operator will mix the neutralino fields with the neutrino fields which generates one massive neutrino, m_{ν_i}, for non-vanishing $\lambda'_{ijk}|_{\rm GUT}$ at tree-level [45, 58, 105, 159, 160].

Demanding that this neutrino mass is smaller than the cosmological bound on the sum of neutrino masses, determined by the combination of the WMAP data [161] and the 2dFGRS data [162],

$$\sum_i m_{\nu_i} < 0.71\,\text{eV}\,, \tag{4.3}$$

results in upper bounds on $\lambda'_{ijk}|_{\rm GUT}$, which were calculated in Ref. [58] for the parameter point SPS1a [146].

It was found in Ref. [58], assuming quark mixing solely in the down-sector, Eq. (A.5), and assuming no accidental cancellations, that the bounds on $\lambda'_{ijk}|_{\rm GUT}$ are of the order of $\mathcal{O}(10^{-3} - 10^{-6})$. However, if quark mixing is solely in the up-sector, Eq. (A.4), than $(\mathbf{Y}_D)_{jk}$ vanishes at M_Z for $j \neq k$. This suppresses the right hand side of Eq. (4.1) and Eq. (4.2). The neutrino masses and therefore the bounds on $\lambda'_{ijk}|_{\rm GUT}$ are significantly softened. Taking also two loop effects into account, we summarize in Table 4.1 the λ'_{ijk} couplings, which are unrestricted by the neutrino mass bound, Eq. (4.3), as long as quark mixing is dominantly in the up-sector, *cf.* Eq. (A.4). We also include the strictest experimental bound, which we discuss in the following subsection.

4.1.2. Indirect Bounds on λ'_{ijk}

In this section, we review the relevant indirect bounds on the couplings λ'_{ijk} from electroweak precision measurements. In Table 4.1, we present the strongest bounds on the single λ'_{ijk} couplings at the 2σ level [85, 89, 94, 148, 163]. The bounds apply to the couplings at M_Z. To obtain the respective bound at $M_{\rm GUT}$ one has to divide the corresponding bound in Table 4.1 by roughly a factor of three, *cf.* Sect. 5.2. For each coupling the bound depends linearly on the sfermion mass of the virtual particle exchanged in the relevant process. In the right column, we show which sneutrino can become the LSP. We see that an electron sneutrino LSP, $\tilde{\nu}_e$, is disfavored due to the strong bounds on the couplings λ'_{1jk}, which stem from atomic parity violation measurements and pion decays [89]. We have found that only in a small range of mSUGRA parameter space a $\tilde{\nu}_e$ LSP is found, although large squark masses weaken the bounds. In the following we will thus concentrate on muon sneutrinos, $\tilde{\nu}_\mu$, and tau sneutrinos, $\tilde{\nu}_\tau$, as LSP candidates.

One non-vanishing $\lambda'_{ijk}|_{\rm GUT}$ will also generate additional (*$LQ\bar{D}$ and $LL\bar{E}$*) B_3 operators, Eq. (2.6), at M_Z, which violate the same lepton number; see Sect. 5.2. For example, for one $\lambda'_{2jk}|_{\rm GUT} \neq 0$, we will generate all other muon number violating operators at M_Z via one and two loop effects. Since bounds on products of two different B_3 couplings are often much stronger than on only one B_3 coupling [85, 89, 94, 148, 163], we have also checked that

coupling	upper bounds at M_Z	LSP
λ'_{121}	$0.03 \times (m_{\tilde{c}_L}/100\,\text{GeV})$	$\tilde{\nu}_e$
λ'_{131}	$0.02 \times (m_{\tilde{t}_L}/100\,\text{GeV})$	$\tilde{\nu}_e$
λ'_{112}	$0.02 \times (m_{\tilde{s}_R}/100\,\text{GeV})$	$\tilde{\nu}_e$
λ'_{221}	$0.18 \times (m_{\tilde{s}_L}/100\,\text{GeV})$	$\tilde{\nu}_\mu$
λ'_{231}	$0.18 \times (m_{\tilde{b}_L}/100\,\text{GeV})$	$\tilde{\nu}_\mu$
λ'_{212}	$0.06 \times (m_{\tilde{s}_R}/100\,\text{GeV})$	$\tilde{\nu}_\mu$
λ'_{321}	$0.52 \times (m_{\tilde{d}_R}/100\,\text{GeV})$	$\tilde{\nu}_\tau$
λ'_{331}	$0.32 \times (m_{\tilde{d}_R}/100\,\text{GeV})$	$\tilde{\nu}_\tau$
λ'_{312}	$0.11 \times (m_{\tilde{s}_R}/100\,\text{GeV})$	$\tilde{\nu}_\tau$

Table 4.1.: Upper bounds on single couplings λ'_{ijk} from electroweak precision measurements. Only couplings are shown, which are consistent with the cosmological bound on neutrino masses, Eq. (4.3); see also Ref. [58]. The bounds depend strongly on the masses of the relevant squarks, $m_{\tilde{q}}$. The third column shows the $\tilde{\nu}_i$ LSP, which can be generated via the respective $\lambda'_{ijk}|_{\text{GUT}}$ coupling.

all generated products of the dominant λ'_{ijk} coupling with a generated coupling satisfy the bounds. All products lie at least one order of magnitude below the strongest upper bounds if $\lambda'_{ijk}|_{\text{GUT}} = 0.1$.

After REWSB, the single coupling scheme, which was assumed in deriving the bounds in Table 4.1, cannot be realized in the quark mass eigenbasis [164]. In Sect. 4.1.1, we stated that quark mixing must be dominantly in the up-sector, Eq. (A.4), to fulfill the cosmological bound on the sum of neutrino masses, Eq. (4.3). Therefore, in the quark mass basis we will generate the following B_3 couplings

$$\tilde{\lambda}'_{imk} = (\mathbf{V}^*_{CKM})_{mj} \lambda'_{ijk}\,. \tag{4.4}$$

$\tilde{\lambda}'_{imk}$ with $m = 1, 2, 3$ couples an up-quark superfield of generation m (in the mass basis) to a lepton and down-quark superfield of generation i and k, respectively. These effective couplings can give rise to D_0–$\bar{D}_0$ mixing if $m = 1, 2$ [164, 165, 166]. D_0 oscillations were investigated by the BABAR [167, 168], Belle [169, 170] and CDF [171] collaborations. The Heavy Flavor Averaging Group combined all experimental results and obtained windows for the allowed mass difference and the allowed lifetime difference of the D_0–$\bar{D}_0$ system [172].

Ref. [166] employed the experimental 2σ errors on the D_0–$\bar{D}_0$ mass difference to obtain the following bounds on λ'_{ijk}

$$|\tilde{\lambda}'_{i21}\,\tilde{\lambda}'_{i11}| = |\lambda_W\,\lambda'^2_{i21}| \leq 0.0029 \left[\left(\frac{100\,\text{GeV}}{m_{\tilde{\ell}_{Li}}} \right)^2 + \left(\frac{100\,\text{GeV}}{m_{\tilde{d}_R}} \right)^2 \right]^{-1/2}, \tag{4.5}$$

where $\lambda_W = 0.23$ is the Wolfenstein parameter [173, 174] and $i = 1, 2, 3$. For the evaluation of Eq. (4.5), Ref. [166] assumed that the mass splitting arises solely from B_3 contributions. Note that the first equality of Eq. (4.5) only holds if quark mixing is solely in the up-sector, Eq. (A.4). The corresponding upper bound on $|\lambda_W\,\lambda'^2_{i12}|$ can be obtained from Eq. (4.5) by replacing $m_{\tilde{d}_R}$ with $m_{\tilde{s}_R}$.

The experimentally allowed range for the difference in lifetime of the D_0–$\bar{D}_0$ system was used in Ref. [165] to obtain the bounds

$$|\tilde{\lambda}'_{i21}\,\tilde{\lambda}'_{i11}| = |\lambda_W\,\lambda'^2_{i21}| \leq 0.082\left(\frac{m_{\tilde{\ell}_{Li}}}{100\text{GeV}}\right)^2. \tag{4.6}$$

These are valid for $i = 1, 2$. Unlike Ref. [166], Ref. [165] also took (destructive) interference between the B_3 and SM contributions into account. The bound on $|\lambda_W\,\lambda'^2_{i12}|$ is the same.

If we assume a $\tilde{\ell}_{Li}$ with a mass of 200 GeV and squarks with a mass of 500 GeV, we obtain the upper bounds $\lambda'_{i21}, \lambda'_{i12} \leq 0.15$ at M_Z from the D_0–$\bar{D}_0$ mass difference, Eq. (4.5), and $\lambda'_{i21}, \lambda'_{i12} \leq 1.2$ at M_Z from the D_0–$\bar{D}_0$ lifetime difference, Eq. (4.6). Thus the $\tilde{\nu}_i$ LSP parameter space is strongly restricted by the D_0–$\bar{D}_0$ mass difference. However it was pointed out in Ref. [165] that destructive interference, for example between P_6 violating and P_6 conserving contributions, may significantly weaken the bounds of Eq. (4.5), as in the case of the D_0–$\bar{D}_0$ lifetime difference.

In the following, we mainly focus on the couplings λ'_{231} and λ'_{331} leading to a $\tilde{\nu}_\mu$ and $\tilde{\nu}_\tau$ LSP, respectively. These couplings are not restricted by D_0–$\bar{D}_0$ mixing, because the relevant CKM matrix elements to generate $\tilde{\lambda}'_{i21}$ and $\tilde{\lambda}'_{i11}$ out of λ'_{i31} are too small, *cf.* Eq. (4.4).

4.1.3. Collider Constraints

4.1.3.1. Constraints from LEP

We now determine bounds on the $\tilde{\nu}_i$ LSP mass from LEP. For the case of a non-vanishing λ'_{ijk} coupling the $\tilde{\nu}_i$ LSP will dominantly decay into two jets:

$$\tilde{\nu}_i \;\rightarrow\; \bar{d}_j d_k. \tag{4.7}$$

Here, d_k ($\bar{d}_j$) is a (anti) down quark of generation k (j). This decay will occur instantaneously in the detector, *i.e.* with no detached vertex, since in our model λ'_{ijk} is bounded from below by the requirement of a $\tilde{\nu}_i$ LSP. $\tilde{\nu}_i$ pair production followed by the decay, Eq. (4.7), would lead to four jet events at LEP.

Bounds on the total $\tilde{\nu}_i$ pair production cross section, with the $\tilde{\nu}_i$ decaying via λ'_{ijk} were obtained by the OPAL collaboration [175] and also by the ALEPH collaboration [157]. From these we can obtain lower bounds on the mass of the $\tilde{\nu}_i$ LSP. We calculated the pair production cross section using the formulas given in Ref. [176], with the fine structure constant equal to its value at M_Z, *i.e.* $\alpha = 1/128$. We show in Table 4.2 the strongest lower bounds on the $\tilde{\nu}_i$ LSP masses for different lepton flavors i.

The $\tilde{\nu}_i$ LSP mass bounds for the second and third generation ($i = 2, 3$) are universal. The $\tilde{\nu}_e$ mass bound, in contrast, depends also on the chargino parameters. The chargino parameters enter through t-channel diagrams to the sneutrino pair production cross section. We calculated the different bounds on the electron sneutrino mass by assuming, that the lightest chargino is wino-like. This is the case for most mSUGRA scenarios. We then varied its mass between 120 GeV and 1000 GeV to obtain the numbers in Table 4.2.

	$m_{\tilde{\nu}_e}$	$m_{\tilde{\nu}_\mu}$	$m_{\tilde{\nu}_\tau}$
OPAL	$> 68 - 89$ GeV	> 74 GeV	> 74 GeV
ALEPH	$> 75 - 95$ GeV	> 79 GeV	> 79 GeV

Table 4.2.: Lower bounds on the $\tilde{\nu}_i$ LSP masses from direct $\tilde{\nu}_i$ decay via λ'_{ijk}. The bounds were obtained from the OPAL [175] and ALEPH [157] analyses, respectively. The $\tilde{\nu}_\mu$ and $\tilde{\nu}_\tau$ mass bounds are universal. The $\tilde{\nu}_e$ mass bound depends on the chargino parameters due to potential interference effects.

In the following, we investigate the $\tilde{\nu}_\mu$ LSP and $\tilde{\nu}_\tau$ LSP parameter space in detail. A $\tilde{\nu}_e$ LSP is less favored due to the stronger bounds on the λ'_{1jk} couplings, *cf.* Table 4.1. We employ a lower mass bound of 78 GeV. This corresponds to the bound obtained by the ALEPH collaboration, see Table 4.2, reduced by 1 GeV to account for numerical uncertainties in `SOFTSUSY` [153].

Only the mass bounds of the directly decaying $\tilde{\nu}_i$ LSP need to be considered, because all the other bounds from LEP on direct and indirect decays of heavier sparticles (compared to the $\tilde{\nu}_i$ LSP) are automatically fulfilled. In addition, the LEP exclusion bound on the light Higgs, h, is $m_h > 114.4$ GeV at 95% confidence level [152]. Anticipating a numerical error of 3 GeV of `SOFTSUSY`s prediction of m_h [40, 106, 153, 154], we have imposed a lower bound of 111.4 GeV.

4.1.3.2. Constraints from the Tevatron

At the Tevatron, a non-vanishing λ'_{ijk} coupling allows for resonant single $\tilde{\ell}^-_{Li}$ and $\tilde{\nu}_i$ production leading to dijet events

$$\bar{u}_j d_k \;\to \tilde{\ell}^-_{Li} \;\to \bar{u}_j d_k \,, \tag{4.8}$$

$$\bar{d}_j d_k \;\to \tilde{\nu}_i \;\to \bar{d}_j d_k \,. \tag{4.9}$$

The expected reach for the slepton resonance search at the Tevatron in the dijet channel is estimated in Ref. [177] as a function of the hadronic cross section for the processes in Eq. (4.8) and Eq. (4.9) and the slepton mass. In Ref. [177], the discovery potential for slepton masses between 200 GeV and 1200 GeV is given assuming an integrated luminosity of 2 fb^{-1} and 30 fb^{-1}. We have checked that all the couplings shown in Table 4.1, assuming $\lambda'_{ijk}|_{\rm GUT} = 0.1$, lead to production cross sections which lie at least one order of magnitude below the expected discovery region for 2 fb^{-1} given in Ref. [177]. We have employed the QCD and SUSY-QCD next-to-leading order (NLO) cross section [114].

Tevatron searches for new resonances in the dijet channel have indeed been performed by the D0 collaboration [178] and the CDF collaboration [156, 179, 180]. Although B_3 models were not considered, bounds on the production cross section of additional vector bosons, W' and Z', which decay into two jets, were obtained. These processes are very similar to the B_3 processes, Eq. (4.8) and Eq. (4.9). W' and Z' masses between 180 GeV and 1400 GeV were probed. In this mass region, the production cross section for a single $\tilde{\ell}^-_{Li}$ and $\tilde{\nu}_i$ with

process	cross section [pb]	
$PP \to W(Z) \to q\bar{q}$	2.7×10^4	(7.9×10^3)
$P\bar{P} \to \tilde{\mu}_L \to q\bar{q}$	9.2×10^2	(5.7×10^2)
$P\bar{P} \to \tilde{\nu}_\mu \to q\bar{q}$	1.3×10^3	(8.0×10^2)

Table 4.3.: Hadronic cross section for dijet production via an on shell W (Z) boson in comparison to B_3 violating dijet production via $\tilde{\mu}_L$, Eq. (4.8) and $\tilde{\nu}_\mu$, Eq. (4.9), with a mass equal to the W (Z) mass. We assumed $\lambda'_{221}|_{\rm GUT} = 0.1$. The charge conjugated processes are also taken into account.

subsequent decay into two jets, lies at least one order of magnitude below the experimental limits on W' and Z' production. We assumed $\lambda'_{ijk}|_{\rm GUT} = 0.1$ and one coupling of Table 4.1.

We now estimate if the Tevatron has a chance to observe dijet pair production for $\tilde{\ell}^-_{Li}$ and $\tilde{\nu}_i$ masses *below* 180 GeV. We show in Table 4.3 the hadronic cross sections for dijet production via an on-shell W (Z) boson [181, 182]. We also give the NLO production cross section for a $\tilde{\ell}^-_{Li}$ and $\tilde{\nu}_i$ with a mass equal to the Z and W mass [114], assuming $\lambda'_{221}|_{\rm GUT} = 0.1$. We see that the B_3 cross sections are roughly one order of magnitude smaller than the SM cross sections. We conclude that the processes, Eq. (4.8) and Eq. (4.9), for slepton masses below 180 GeV can not be seen at the Tevatron because the Z and the W have not been observed at the Tevatron in the dijet channel so far.

Singly produced charged sleptons, Eq. (4.8), may also cascade decay into a lepton ℓ_i, two jets and missing energy:

$$\begin{aligned} \tilde{\ell}^-_{Li} \to & \tilde{\chi}^0_1 \ell^-_i \\ & \hookrightarrow \tilde{\nu}_i \bar{\nu}_i \\ & \quad \hookrightarrow \bar{d}_j d_k \,. \end{aligned} \tag{4.10}$$

In principle, this signature could be more easily distinguished from the (QCD) background than pure dijet events, due to the additional isolated lepton in the final state. However the cascade decay, Eq. (4.10), is kinematically forbidden in most regions of the $\tilde{\nu}_i$ LSP parameter space, as we show in Sect. 4.2. In that case one might think about the 3-body decay, $\tilde{\ell}^-_{Li} \to \ell^-_i \bar{\nu}_i \tilde{\nu}_i$, via a virtual neutralino. However, this process can only occur at a significant rate, if the 2-body decay mode into two jets, Eq. (4.8), is forbidden or kinematically suppressed. This is the case for $j = 3$, *i.e.* a top quark in the final state. But the $\tilde{\ell}^-_{Li}$ can then not be produced as a single resonance, because we also need a top quark in the initial state, see Eq. (4.8). Furthermore the 3-body decay, $\tilde{\ell}^-_{Li} \to \ell^-_i \bar{\nu}_i \tilde{\nu}_i$, is heavily suppressed compared to the 3-body decay via a virtual top-quark, as we will see in Sect. 4.3.1.

A non-vanishing λ'_{i31} coupling can lead to B_3 top-quark decay at the Tevatron [164, 183, 184, 185, 186, 187]. For example $t \to d\,\tilde{\ell}_{Li}$ if $m_{\tilde{\ell}i} < m_t$. However, the Tevatron can only test couplings λ'_{i31} via top decay, which lie at their upper bounds [187], see Table 4.1. We use smaller λ'_{i31} couplings in the following.

A non-vanishing λ'_{i31} coupling contributes also to top-pair production, see Refs. [187, 188, 189]. The top quarks in the $t\bar{t}$ events are polarized, since the B_3 operator couples only to

left-handed top quarks. It is shown in Refs. [187, 188, 189], that the Tevatron at the end of Run II can only test couplings λ'_{i31}, which lie near their current upper bounds, *cf.* Table 4.1. The LHC will be able to probe couplings λ'_{i31} down to $\lambda'_{i31} = 0.2$ via top polarization [189].

4.1.3.3. Constraints from the CERN $p\bar{p}$ Collider

Unlike D0 and CDF, the UA2 collaboration at the CERN $p\bar{p}$ collider was able to measure the hadronic decay mode of the Z and W [190]. They also searched for a W' and Z' decaying into two jets. They found no excess over the SM background and therefore set exclusion limits for W' and Z' production with masses between 80 GeV and 320 GeV [190, 191].

We compared the exclusion limits with our NLO cross section predictions for single slepton, Eq. (4.8), and sneutrino, Eq. (4.9), production assuming again $\lambda'_{ijk}|_{\rm GUT} = 0.1$ and one of the couplings shown in Table 4.1 [114]. Our cross section prediction is at least one order of magnitude smaller than the exclusion limits in the relevant mass range.

4.2. Sneutrino LSP Parameter Space

We have shown in Sect. 2.4.3, that one non-vanishing coupling $\lambda'_{ijk}|_{\rm GUT} = \mathcal{O}(10^{-1})$ may lead to a $\tilde{\nu}_i$ LSP in B_3 mSUGRA models, *cf.* Fig 2.4. We also presented the λ'_{ijk} couplings, which have sufficiently weak upper bounds to allow for a $\tilde{\nu}_i$ LSP, see Table 4.1. All lepton flavors are possible, although a $\tilde{\nu}_e$ LSP is disfavored due to the stronger bounds on the λ'_{1jk}. Thus we concentrate on $\tilde{\nu}_\mu$ and $\tilde{\nu}_\tau$ LSPs in the following.

In this section, we investigate in detail the dependence of the $\tilde{\nu}_i$ LSP parameter space on the mSUGRA parameters M_0, $M_{1/2}$, A_0 and $\tan\beta$. We explore 2-dimensional parameter spaces, where our scans are centered around the following points

$$\begin{aligned} \textbf{Point I:}\ & M_0 = 50\,\text{GeV},\ M_{1/2} = 500\,\text{GeV}, \\ & A_0 = -600\,\text{GeV},\ \tan\beta = 10, \\ & \text{sgn}(\mu) = +1,\ \lambda'_{231}|_{\rm GUT} = 0.11, \\ \textbf{Point II:}\ & M_0 = 200\,\text{GeV},\ M_{1/2} = 290\,\text{GeV}, \\ & A_0 = -550\,\text{GeV},\ \tan\beta = 12, \\ & \text{sgn}(\mu) = +1,\ \lambda'_{331}|_{\rm GUT} = 0.12. \end{aligned} \tag{4.11}$$

We perform our parameter scans with a B_3 version of `SOFTSUSY` [149, 150, 147].

Point I results in a $\tilde{\nu}_\mu$ LSP with a mass of 130 GeV. The next-to-LSP (NLSP) is the left-handed smuon, $\tilde{\mu}_L$, with a mass of 159 GeV. Note that the $\tilde{\mu}_L$ mass is also reduced due to $\lambda'_{231}|_{\rm GUT} \neq 0$, and the $\tilde{\mu}_L$ is always heavier than the $\tilde{\nu}_\mu$ for $\tan\beta > 1$, see Eq. (A.11) and Fig. 2.4. The masses of the other LSP candidates, namely the $\tilde{\tau}_1$ and the $\tilde{\chi}^0_1$, are 186 GeV and 205 GeV, respectively. Due to the rather large mass difference between the $\tilde{\nu}_\mu$ LSP on the one side, and $\tilde{\tau}_1$ and $\tilde{\chi}^0_1$ on the other, we expect an extended $\tilde{\nu}_\mu$ LSP parameter space. This is indeed the case, as shown in the following.

Point II results in a $\tilde{\nu}_\tau$ LSP with a mass of 107 GeV. The NLSP is the $\tilde{\chi}_1^0$ with a mass of 116 GeV. The next-to-NLSP (NNLSP) is the $\tilde{\tau}_1$, which has a large left-handed component here, because the soft breaking mass $(\mathbf{m}_{\tilde{\mathbf{L}}})_{33}$, Eq. (2.3), is also reduced via the non-vanishing $\lambda'_{331}|_{\rm GUT}$ coupling, *cf.* Eq. (2.29). In contrast, $(\mathbf{m}_{\tilde{\mathbf{E}}})_{33}$ is not affected. The $\tilde{\tau}_1$ mass is 120 GeV.

The mass difference between the $\tilde{\nu}_\tau$ LSP and the $\tilde{\tau}_1$ is smaller for Point II than Point I, because $\lambda'_{331}|_{\rm GUT}$ also reduces the mass of the $\tilde{\tau}_1$, which is an admixture of $\tilde{\tau}_L$ and $\tilde{\tau}_R$. This competes with the $\tilde{\nu}_\tau$ to be the LSP; *cf.* Ref. [106]. In contrast, $\lambda'_{231}|_{\rm GUT} \neq 0$ reduces the mass of the $\tilde{\mu}_L$. But the $\tilde{\mu}_L$ is always heavier than the $\tilde{\nu}_\mu$. We therefore expect a smaller $\tilde{\nu}_\tau$ LSP parameter space around Point II than the $\tilde{\nu}_\mu$ LSP parameter space around Point I.

It is worth mentioning, that Point I leads to a heavier sparticle mass spectrum than Point II. This stems from the fact, that we have chosen our central scan points, such that the SUSY contributions to the anomalous magnetic moment of the muon, $\delta a_\mu^{\rm SUSY}$, can explain the observed discrepancy, δa_μ, between experiment, $a_\mu^{\rm exp}$, and the SM prediction, $a_\mu^{\rm SM}$,

$$\delta a_\mu = a_\mu^{\rm exp} - a_\mu^{\rm SM} = (29.5 \pm 8.8) \times 10^{-10}\,, \tag{4.12}$$

which corresponds to a 3.4σ deviation [4, 5, 6]. In the following, we show in our parameter scans in Figs. 4.2 –4.5 contour lines, where the SUSY contributions, $\delta a_\mu^{\rm SUSY}$, correspond to the

$$\begin{aligned}
&\text{central value}: \delta a_\mu^{\rm SUSY} = 29.5 \times 10^{-10} \\
&\qquad\qquad \Leftrightarrow \text{yellow line, labeled with “0”}\,, \\
&\text{central value} \pm 1\sigma: \delta a_\mu^{\rm SUSY} = (29.5 \pm 8.8) \times 10^{-10} \\
&\qquad\qquad \Leftrightarrow \text{blue line, labeled with “}\pm 1\text{”}\,, \\
&\text{central value} \pm 2\sigma: \delta a_\mu^{\rm SUSY} = (29.5 \pm 17.6) \times 10^{-10} \\
&\qquad\qquad \Leftrightarrow \text{green line, labeled with “}\pm 2\text{”}\,, \\
&\text{central value} \pm 3\sigma: \delta a_\mu^{\rm SUSY} = (29.5 \pm 26.4) \times 10^{-10} \\
&\qquad\qquad \Leftrightarrow \text{magenta line, labeled with “}\pm 3\text{”}\,.
\end{aligned} \tag{4.13}$$

Yellow (labeled with “0”), green (labeled with “$\pm$ 1”), blue (labeled with “$\pm$ 2”) and magenta (labeled with “$\pm$3”) are the colors of the contour lines in the plots, which we show in the following sections.

The SUSY contributions to the anomalous magnetic moment of the muon, $\delta a_\mu^{\rm SUSY}$, enter starting at the one loop level, see for example Refs. [7, 155], and involve the $\tilde{\mu}_L$ and $\tilde{\nu}_\mu$. Thus, they are enhanced if the $\tilde{\mu}_L$ and $\tilde{\nu}_\mu$ are light. As a consequence, $\delta a_\mu^{\rm SUSY}$ increases if we switch on $\lambda'_{231}|_{\rm GUT}$, because the mass of the $\tilde{\mu}_L$ and $\tilde{\nu}_\mu$ decrease. In contrast, $\lambda'_{331}|_{\rm GUT}$ does not affect $\delta a_\mu^{\rm SUSY}$. Note, that we have not included B_3 contributions to $\delta a_\mu^{\rm SUSY}$, because they are at most at the percent level and can therefore be neglected [192].

We also consider the constraints from the BR($b \to s\gamma$). The current experimental value is [151]

$$\text{BR}(b \to s\gamma) = (3.52 \pm 0.25) \times 10^{-4}\,. \tag{4.14}$$

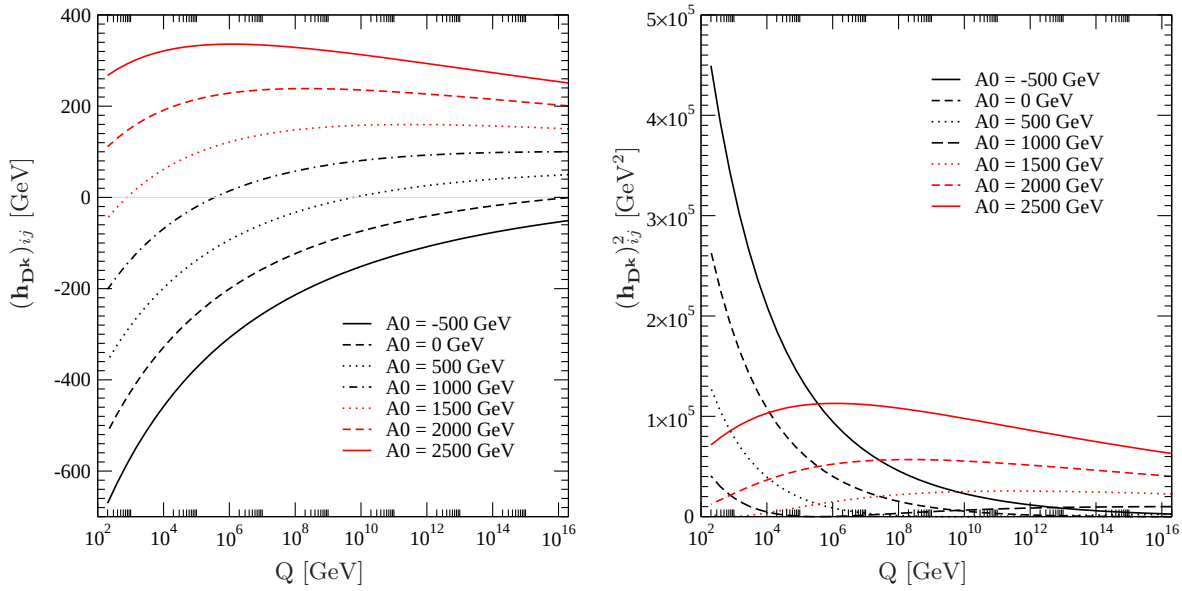

Figure 4.1.: Running of $(\mathbf{h_{D^k}})_{ij}$ (left figure) and $(\mathbf{h_{D^k}})^2_{ij}$ (right figure) from $M_{\rm GUT}$ to M_Z for different values of A_0. At $M_{\rm GUT}$, we choose $M_{1/2} = 500$ GeV and $\lambda'_{ijk} = 0.1$.

Here we have added the statistical and systematic errors in quadrature [151]. If we also include the combined theoretical error of 0.3×10^{-4} [193, 194] we obtain the 2σ window

$$2.74 \times 10^{-4} < \mathrm{BR}(b \to s\gamma) < 4.30 \times 10^{-4}\,, \tag{4.15}$$

where we have now added theoretical and experimental errors in quadrature.

The complete $\tilde{\nu}_\mu$ LSP parameter space, which we will show in the following, *i.e.* Figs. 4.2, 4.4(a), 4.5(a), is consistent with $\mathrm{BR}(b \to s\gamma)$ at the 2σ level, Eq. (4.15). The $\tilde{\nu}_\tau$ LSP parameter space in the A_0–$\tan\beta$ [$M_{1/2}$–M_0] plane, Fig. 4.4(b) [Fig. 4.5(b)], is consistent with $\mathrm{BR}(b \to s\gamma)$ at 2σ, Eq. (4.15), for $\tan\beta \lesssim 11$ [$M_{1/2} \gtrsim 290$ GeV] corresponding to the dashed black line in Fig. 4.4(b) [Fig. 4.5(b)]. We will show mainly contour lines for $\delta a_\mu^{\rm SUSY}$ in the following, *cf.* Eq. (4.13), because the experimental value of a_μ is in general more restrictive on the $\tilde{\nu}_i$ LSP parameter space than $\mathrm{BR}(b \to s\gamma)$.

We finally want to point out that the complete $\tilde{\nu}_\mu$ and $\tilde{\nu}_\tau$ LSP parameter space, which we will show in the next three sections posses a branching ratio for $B_s \to \mu^+\mu^-$, which lies at least one order of magnitude below the current experimental upper bound [151],

$$\mathrm{BR}(B_s \to \mu^+\mu^-) < 4.7 \times 10^{8}\,. \tag{4.16}$$

We have employed `micrOMEGAs1.3.7` [195] to calculate $\delta a_\mu^{\rm SUSY}$, $\mathrm{BR}(b \to s\gamma)$ and $\mathrm{BR}(B_s \to \mu^+\mu^-)$. According to Ref. [106], B_3 contributions to $\mathrm{BR}(b \to s\gamma)$ and $\mathrm{BR}(B_s \to \mu^+\mu^-)$ can also be neglected for only one dominant $\lambda'_{ijk}|_{\rm GUT}$.

4.2.1. A_0 Dependence

We have chosen two scenarios, Point I and Point II, Eq. (4.11), which we use as central values for 2-dimensional mSUGRA parameter scans. For both points $A_0 < 0$, with a magnitude of

a few hundred GeV. We now show that this choice of A_0 enhances the negative contribution to the $\tilde{\nu}_i$ mass, which originates from a non-vanishing $\lambda'_{ijk}|_{\rm GUT}$ coupling, *cf.* Eq. (2.29).

According to Eq. (2.29) and Eq. (2.30), A_0 enters the running of $m_{\tilde{\nu}_i}$ via the B_3 soft-breaking, trilinear scalar coupling $(\mathbf{h_{D^k}})_{ij}$, Eq. (2.11). Thus $(\mathbf{h_{D^k}})_{ij}$ gives a negative contribution to $m^2_{\tilde{\nu}_i}$, as t is decreased. It is proportional to the integral of $(\mathbf{h_{D^k}})^2_{ij}$ over t, from $t_{\rm min} = \ln(M_Z)$ to $t_{\rm max} = \ln(M_{\rm GUT})$.

We show in Fig. 4.1 (left figure) the running of the trilinear scalar coupling $(\mathbf{h_{D^k}})_{ij}$. We assume one non-vanishing coupling $\lambda'_{ijk}|_{\rm GUT}= 0.1$ and a universal gaugino mass $M_{1/2} = 500$ GeV. Different lines correspond to different values of A_0. We have employed the one-loop contributions from gauge interactions [58], as well as the B_3 leading interaction

$$\begin{aligned} 16\pi^2 \frac{d(\mathbf{h_{D^k}})_{ij}}{dt} &= -(\mathbf{h_{D^k}})_{ij}\left(\frac{7}{15}g_1^2 + 3g_2^2 + \frac{16}{3}g_3^2\right) \\ &\quad +\lambda'_{ijk}\left(\frac{14}{15}g_1^2 M_1 + 6g_2^2 M_2 + \frac{32}{3}g_3^2 M_3\right) . \end{aligned} \tag{4.17}$$

The running of $(\mathbf{h_{D^k}})_{ij}$ is dominated by the strong interaction, *i.e.* by the strong coupling g_3 and the gluino mass M_3. The running is governed by two terms with opposite sign in Eq. (4.17), one proportional to λ'_{ijk} and one proportional to $(\mathbf{h_{D^k}})_{ij}$.

The term proportional to λ'_{ijk} is always positive and thus decreases $(\mathbf{h_{D^k}})_{ij}$ when we go from $M_{\rm GUT}$ to M_Z. Note, that we assume λ'_{ijk} is positive. Furthermore, the gluino mass M_3 will increase by a factor of roughly 2.5 and also λ'_{ijk} will increase by roughly a factor of 3 when we run from $M_{\rm GUT}$ to M_Z. Therefore this term gets relatively more important towards lower scales.

The sign of the term proportional to $(\mathbf{h_{D^k}})_{ij}$ depends on the sign of A_0, according to Eq. (2.30). At $M_{\rm GUT}$, this term is positive (negative) for negative (positive) A_0. Therefore, for positive A_0, the term proportional to $(\mathbf{h_{D^k}})_{ij}$ increase $(\mathbf{h_{D^k}})_{ij}$ when we run from $M_{\rm GUT}$ to M_Z.

We can now understand the running of $(\mathbf{h_{D^k}})_{ij}$ in Fig. 4.1. Looking at the solid red line, $A_0 = 2500$ GeV, we see that $(\mathbf{h_{D^k}})_{ij}$ first increases when we go from $M_{\rm GUT}$ to smaller scales. Due to the large A_0 at $M_{\rm GUT}$, the negative term proportional to $(\mathbf{h_{D^k}})_{ij}$ dominates and increases $(\mathbf{h_{D^k}})_{ij}$. Going to lower scales the positive term proportional to λ'_{ijk} grows faster and starts to dominate at $Q \approx 10^6$ GeV. From this scale on, $(\mathbf{h_{D^k}})_{ij}$ decreases. In contrast, if we start with negative A_0 (solid black line), both terms give negative contributions to the running of $(\mathbf{h_{D^k}})_{ij}$. Then, $(\mathbf{h_{D^k}})_{ij}$ decreases with a large slope.

The resulting running of $(\mathbf{h_{D^k}})^2_{ij}$ is shown in Fig. 4.1 (right figure). Recall Eq. (2.29), $m^2_{\tilde{\nu}_i}$ is reduced proportional to the integral of $(\mathbf{h_{D^k}})^2_{ij}$ over t. A negative value of A_0 therefore leads to a smaller $m_{\tilde{\nu}_i}$ compared to a positive value of A_0 with the same magnitude. We expect from Fig. 4.1, that a $\tilde{\nu}_i$ LSP in B_3 mSUGRA is preferred for negative values of A_0 with a large magnitude. We also expect, that $m_{\tilde{\nu}_i}$ in the A_0 direction has a maximum at $A_0 = 1000$ GeV, if $M_{1/2} = 500$ GeV. In general, there should be a line in the $M_{1/2}$–A_0 plane, where $m_{\tilde{\nu}_i}$ is "maximal", falling to either side.

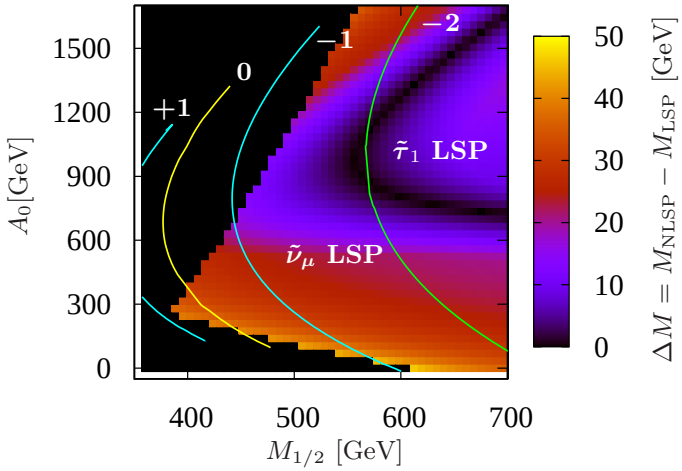

Figure 4.2.: Mass difference in GeV between the NLSP and the LSP as a function of $M_{1/2}$ and A_0. The other mSUGRA parameters are $M_0 = 0$ GeV, $\tan\beta = 10$, $\mathrm{sgn}(\mu) = +1$ and $\lambda'_{231}|_{\rm GUT} = 0.16$. We observe a $\tilde{\nu}_\mu$ LSP and a $\tilde{\tau}_1$ LSP region. The contour lines correspond to different SUSY contributions to the anomalous magnetic moment of the muon, *cf.* Eq. (4.13). The blackened out region is excluded due to tachyons or the LEP $\tilde{\nu}_\mu$, h mass bounds, see Sect. 4.1.3.1.

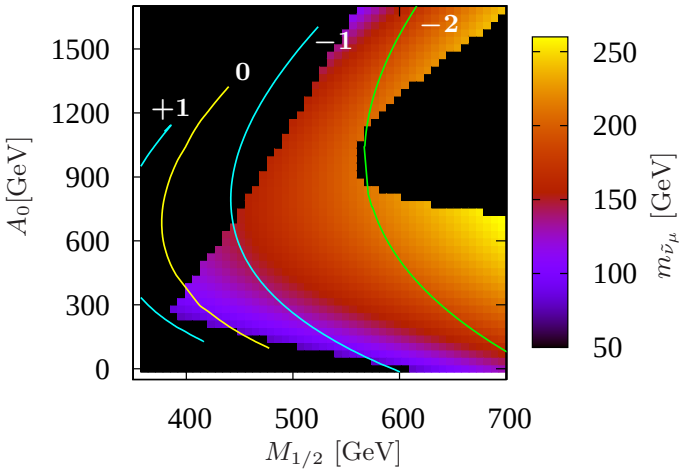

Figure 4.3.: Mass of the $\tilde{\nu}_\mu$ in GeV for the $\tilde{\nu}_\mu$ LSP region shown in Fig. 4.2.

We show in Fig. 4.2 the mass difference in GeV between the NLSP and the LSP as a function of $M_{1/2}$ and A_0. The other mSUGRA parameters are $M_0 = 0$ GeV, $\tan\beta = 10$, $\mathrm{sgn}(\mu) = +1$ and $\lambda'_{231}|_{\rm GUT} = 0.16$. The yellow (labelled with "0"), blue (labeled with "± 1") and green (labeled with "± 2") line indicate the SUSY contributions to the anomalous magnetic moment of the muon as described in Eq. (4.13). The blackened out region corresponds to mSUGRA points, which lead to tachyons or where $m_{\tilde{\nu}_\mu}$ or m_h lies below the LEP bound, see Sect. 4.1.3.1. In Fig. 4.3, we give the mass of the $\tilde{\nu}_\mu$ in GeV for the $\tilde{\nu}_\mu$ LSP region shown in Fig. 4.2.

We see in Fig. 4.2 a region with a $\tilde{\nu}_\mu$ LSP and a region with a $\tilde{\tau}_1$ LSP. The cross over region

is marked in black. We get a $\tilde{\nu}_\mu$ LSP for small and very large values of A_0, as expected from Fig. 4.1. We also see in Fig. 4.3 that $m_{\tilde{\nu}_\mu}$ is maximal for $M_{1/2} = 500$ GeV and $A_0 \approx 1000$ GeV in the A_0 direction. The region of negative A_0 is not shown in Figs. 4.2 and Fig. 4.3, because the influence of $\lambda'_{ijk}|_{\rm GUT}$ on $m_{\tilde{\nu}_\mu}$ is so enhanced, that we violate the mass bound of 78 GeV or even obtain a tachyonic $\tilde{\nu}_\mu$ in large regions of $A_0 < 0$ GeV. In the following, we choose smaller values of $\lambda'_{ijk}|_{\rm GUT}$.

4.2.2. A_0–$\tan\beta$ Plane

We investigate in this section the sneutrino LSP parameter space in the A_0–$\tan\beta$ plane. As central values for our 2-dimensional scans, we choose the points given in Eq. (4.11).

We show in Fig. 4.4(a) [Fig. 4.4(b)] the $\tilde{\nu}_\mu$ LSP [$\tilde{\nu}_\tau$ LSP] parameter space in the A_0–$\tan\beta$ plane. We have chosen $\lambda'_{231}|_{\rm GUT} = 0.11$ [$\lambda'_{331}|_{\rm GUT} = 0.12$]. Both figures show the mass difference between the NLSP and the LSP in GeV. The solid contour lines correspond to different SUSY contributions to the anomalous magnetic moment of the muon, $\delta a_\mu^{\rm SUSY}$, as described in Eq. (4.13). The dashed black line in Fig. 4.4(b) corresponds to $\mathrm{BR}(b \to s\gamma) = 2.74 \times 10^{-4}$, Eq. (4.15), *i.e.* the parameter space below that line is consistent with $b \to s\gamma$ at 2σ. The blackened out region is excluded due to the presence of tachyons or by the LEP $\tilde{\nu}_{\mu/\tau}$ and Higgs mass bound, see Sect. 4.1.3.1.

We observe that the $\tilde{\nu}_\mu$ LSP lives in an extended region of B_3 mSUGRA parameter space. For $\tan\beta = 6$, we find a $\tilde{\nu}_\mu$ LSP between $A_0 = -750$ GeV and $A_0 = -300$ GeV. For $A_0 = -700$ GeV, we find a $\tilde{\nu}_\mu$ LSP between $\tan\beta = 4$ and $\tan\beta = 21$. We also observe that most of the $\tilde{\nu}_\mu$ LSP region is consistent with the observed anomalous magnetic moment of the muon at the 1σ (blue lines) and 2σ (green lines) level, *cf.* Eq. (4.13). Recall, that the complete $\tilde{\nu}_\mu$ LSP region in Fig. 4.4(a) is also consistent with $\mathrm{BR}(b \to s\gamma)$ at 2σ, Eq. (4.15). The large region of $\tilde{\nu}_\mu$ LSP parameter space is a consequence of the choice of our central scan point, *i.e.* Point I of Eq. (4.11). Here, the mass difference between the $\tilde{\nu}_\mu$ LSP and the $\tilde{\tau}_1$ ($\tilde{\chi}_1^0$), *i.e.* the other LSP candidates, is rather large, namely 56 GeV (75 GeV).

We see in Fig. 4.4(a) that we obtain a $\tilde{\tau}_1$ LSP if we increase A_0. We explained this in the last section. A large magnitude and negative value of A_0 enhances the (negative) effect of $\lambda'_{231}|_{\rm GUT}$ on the $\tilde{\nu}_\mu$ mass via the soft breaking trilinear coupling $(\mathbf{h_{D^1}})_{23}$. The $\tilde{\tau}_1$ mass on the other hand, depends only weakly on A_0. The dependence is via the tau Yukawa-coupling, Eq. (A.15), and due to left-right-mixing, Eq. (A.13). According to the last section, there should also be a $\tilde{\nu}_\mu$ LSP for large values of A_0. But in this case the Higgs mass lies below the LEP bound.

We also obtain a $\tilde{\tau}_1$ LSP, when we increase $\tan\beta$. $\tan\beta$ hardly affects the mass of the $\tilde{\nu}_\mu$ but affects the $\tilde{\tau}_1$ mass in two ways. First, increasing $\tan\beta$ increases the tau Yukawa coupling, which reduces the $\tilde{\tau}_1$ mass going from $M_{\rm GUT}$ to M_Z. This is parametrized by Eq. (A.15). Second, increasing $\tan\beta$ increases the absolute value of the off diagonal elements of the stau mass matrix, Eq. (A.13). This leads to larger left-right mixing and thus also reduces the $\tilde{\tau}_1$ mass.

Fig. 4.4(a) shows no region with a $\tilde{\chi}_1^0$ LSP. The entire allowed A_0–$\tan\beta$ plane in Fig. 4.4(a) has a $\tilde{\tau}_1$ LSP for vanishing λ'_{231} because $M_{1/2} \gg M_0$.

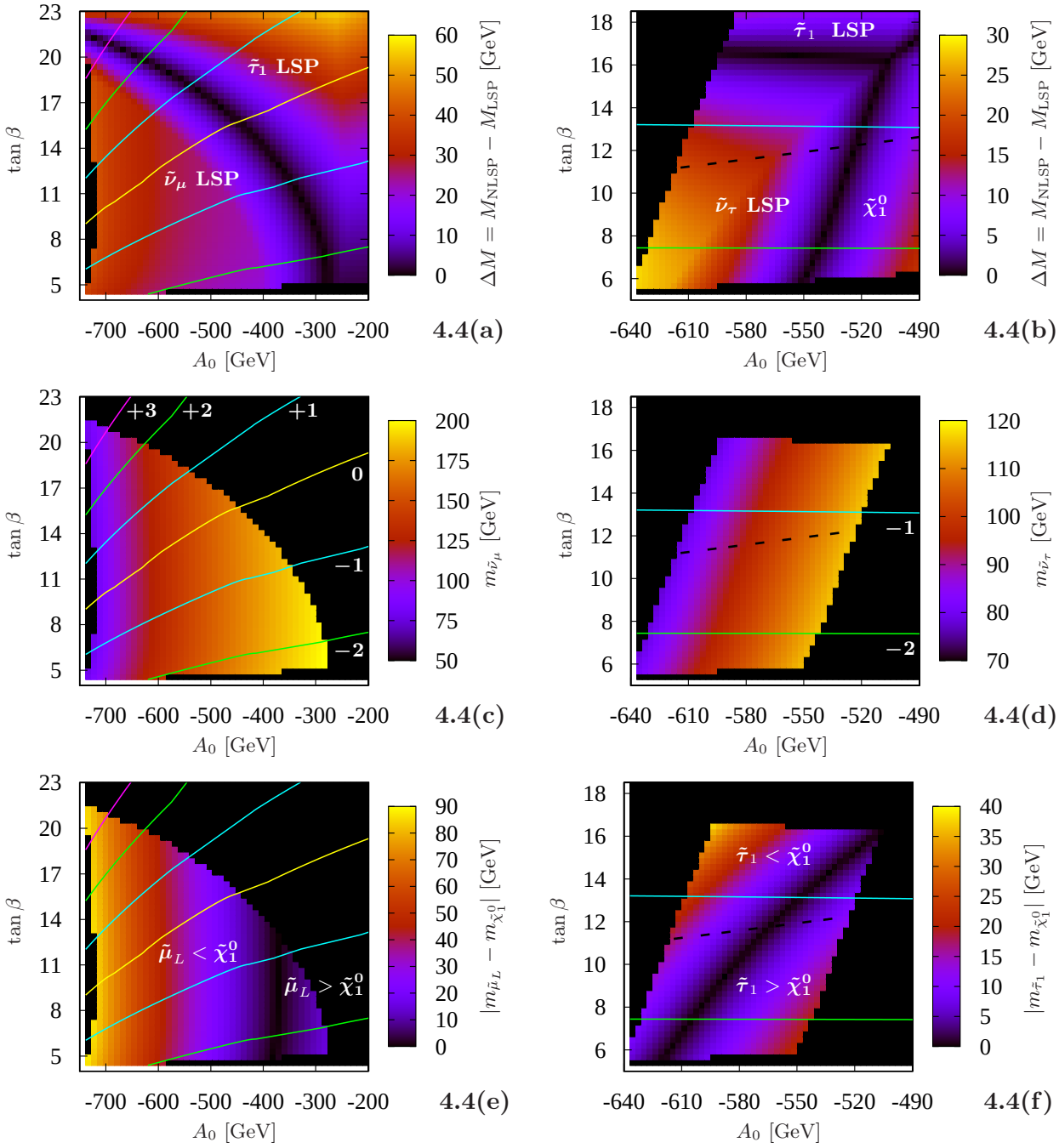

Figure 4.4.: Sneutrino LSP parameter space in the A_0–$\tan\beta$ plane. The left panel [right panel] shows the $\tilde{\nu}_\mu$ LSP [$\tilde{\nu}_\tau$ LSP] region obtained via $\lambda'_{231}|_{\rm GUT} = 0.11$, $M_0 = 50$ GeV, $M_{1/2} = 500$ GeV and $\mathrm{sgn}(\mu) = +1$ [$\lambda'_{331}|_{\rm GUT} = 0.12$, $M_0 = 200$ GeV, $M_{1/2} = 290$ GeV and $\mathrm{sgn}(\mu) = +1$]. The plots show from top to bottom the mass difference between the NLSP and LSP [Fig. 4.4(a) and Fig. 4.4(b)], the mass of the sneutrino LSP [Fig. 4.4(c) and Fig. 4.4(d)], and the mass difference between the $\tilde{\chi}_1^0$ and $\tilde{\mu}_L$ [Fig. 4.4(e)] and between the $\tilde{\chi}_1^0$ and $\tilde{\tau}_1$ [Fig. 4.4(f)]. We have in Fig. 4.4(e) and Fig. 4.4(f) $m_{\tilde{\mu}_L/\tilde{\tau}_1} > m_{\tilde{\chi}_1^0}$ (denoted by $\tilde{\mu}_L/\tilde{\tau}_1 > \tilde{\chi}_1^0$) and $m_{\tilde{\mu}_L/\tilde{\tau}_1} < m_{\tilde{\chi}_1^0}$ (denoted by $\tilde{\mu}_L/\tilde{\tau}_1 < \tilde{\chi}_1^0$). The yellow (labeled with "0"), blue (labeled with "$\pm$ 1"), green (labeled with "$\pm$ 2") and magenta (labeled with "$\pm$ 3") contours correspond to different SUSY contributions to the anomalous magnetic moment of the muon as described in Eq. (4.13). The dashed black line (right panel) corresponds to $\mathrm{BR}(b \to s\gamma) = 2.74 \times 10^{-4}$, Eq. (4.15).

We show in Fig. 4.4(b) the $\tilde{\nu}_\tau$ LSP parameter space. We observe a "smaller" $\tilde{\nu}_\tau$ LSP region compared to the $\tilde{\nu}_\mu$ LSP region, Fig. 4.4(a). We only find a $\tilde{\nu}_\tau$ LSP between $A_0 = -630$ GeV and $A_0 = -540$ GeV for $\tan\beta = 8$. In addition, the experimental 2σ windows for $\delta a_\mu^{\rm SUSY}$, Eq. (4.13), and BR($b \to s\gamma$), Eq. (4.15), restrict the allowed $\tilde{\nu}_\tau$ LSP region in Fig. 4.4(b) to lie between $\tan\beta = 7$ and $\tan\beta = 11$.

We again obtain in Fig. 4.4(b) the $\tilde{\tau}_1$ as LSP when we go to larger values of $\tan\beta$ ($\tan\beta \approx 17$). Although the $\tilde{\nu}_\tau$ mass will also be reduced by a larger tau Yukawa coupling, *cf.* Eq. (A.15), the squared mass of the right-handed stau is reduced twice as much as the $\tilde{\nu}_\tau$ mass. In addition, $\tan\beta$ increases mixing between the $\tilde{\tau}_R$ and $\tilde{\tau}_L$, Eq. (A.13). But it is not possible to find a B_3 mSUGRA point, where the mass difference between the $\tilde{\nu}_\tau$ LSP and the $\tilde{\tau}_1$ is large, because $\lambda'_{331}|_{\rm GUT}$ also reduces the mass of the $\tilde{\tau}_1$.

We also obtain in Fig. 4.4(b) a $\tilde{\chi}_1^0$ LSP instead of a $\tilde{\nu}_\tau$ or $\tilde{\tau}_1$ LSP if we increase A_0 beyond a certain value. The parameter space shown in Fig. 4.4(b) posses a $\tilde{\chi}_1^0$ LSP for vanishing $\lambda'_{331}|_{\rm GUT}$. Increasing A_0 reduces the effect of $\lambda'_{331}|_{\rm GUT}$ on the $\tilde{\nu}_\tau$ and $\tilde{\tau}_1$ mass, but leaves the (bino-like) $\tilde{\chi}_1^0$ mass unaffected. Thus, if the influence of $\lambda'_{331}|_{\rm GUT}$ on the $\tilde{\nu}_\tau$ and $\tilde{\tau}_1$ mass is getting smaller, we re-obtain the $\tilde{\chi}_1^0$ as the LSP.

Finally we want to mention in our discussion of Fig. 4.4(b) that we have a "triple-point", where the $\tilde{\nu}_\tau$, the $\tilde{\tau}_1$ and the $\tilde{\chi}_1^0$ are degenerate in mass. The existence of this "triple-point" is a general feature of the sneutrino LSP parameter space. This has important consequences for the LHC phenomenology, because close to a "triple-point", we effectively have three nearly degenerate LSPs at the same time. There are also large regions in Fig. 4.4(a) and Fig. 4.4(b), where two of the three LSP candidates are nearly degenerate in mass, *i.e.* $\Delta M \leq 5$ GeV.

We present in Fig. 4.4(c) [Fig. 4.4(d)] the mass of the $\tilde{\nu}_\mu$ [$\tilde{\nu}_\tau$] for the corresponding sneutrino LSP regions of Fig. 4.4(a) [Fig. 4.4(b)]. The lightest sneutrino LSPs have a mass of 78 GeV stemming from LEP bounds, *cf.* Sect. 4.1.3.1. The heaviest sneutrino LSPs, consistent with $a_\mu^{\rm exp}$, Eq. (4.12), and BR($b \to s\gamma$), Eq. (4.15), are found in Fig. 4.4(c) and posses a mass of roughly 200 GeV. If one wants to have a sneutrino LSP scenario consistent with the anomalous magnetic moment of the muon, than the sneutrino mass is not allowed to be much larger than 200 GeV (see also the next section).

We show in Fig. 4.4(e) [Fig. 4.4(f)] the mass difference in GeV between the $\tilde{\chi}_1^0$ and the $\tilde{\mu}_L$ [mainly left-handed $\tilde{\tau}_1$]. Whether, $m_{\tilde{\chi}_1^0} > m_{\tilde{\mu}_L}$ [$m_{\tilde{\tau}_1}$] or $m_{\tilde{\chi}_1^0} < m_{\tilde{\mu}_L}$ [$m_{\tilde{\tau}_1}$] has important consequences for collider phenomenology. For example, the $\tilde{\mu}_L$ can not decay into a μ and $\tilde{\chi}_1^0$ if $m_{\tilde{\chi}_1^0} > m_{\mu_L}$. This is the case in most of the $\tilde{\nu}_\mu$ LSP parameter space. The cascade decay, Eq. (4.10), is then forbidden and can not be explored at the Tevatron or LHC, as stated in Sect. 4.1.3.2. We discuss further phenomenological implications in Sect. 4.3.

4.2.3. $M_{1/2}$–M_0 Plane

We present in Fig. 4.5(a) [Fig. 4.5(b)] the $\tilde{\nu}_\mu$ LSP [$\tilde{\nu}_\tau$ LSP] region in the $M_{1/2}$–M_0 plane. We have chosen $\lambda'_{231}|_{\rm GUT} = 0.11$ [$\lambda'_{331}|_{\rm GUT} = 0.12$]. The figures show the mass difference in GeV between the NLSP and the LSP. The solid contour lines correspond again to SUSY scenarios, which contribute to a_μ the amount described in Eq. (4.13) and the dashed black line in Fig. 4.5(b) corresponds to BR($b \to s\gamma$) $= 2.74 \times 10^{-4}$, Eq. (4.15).

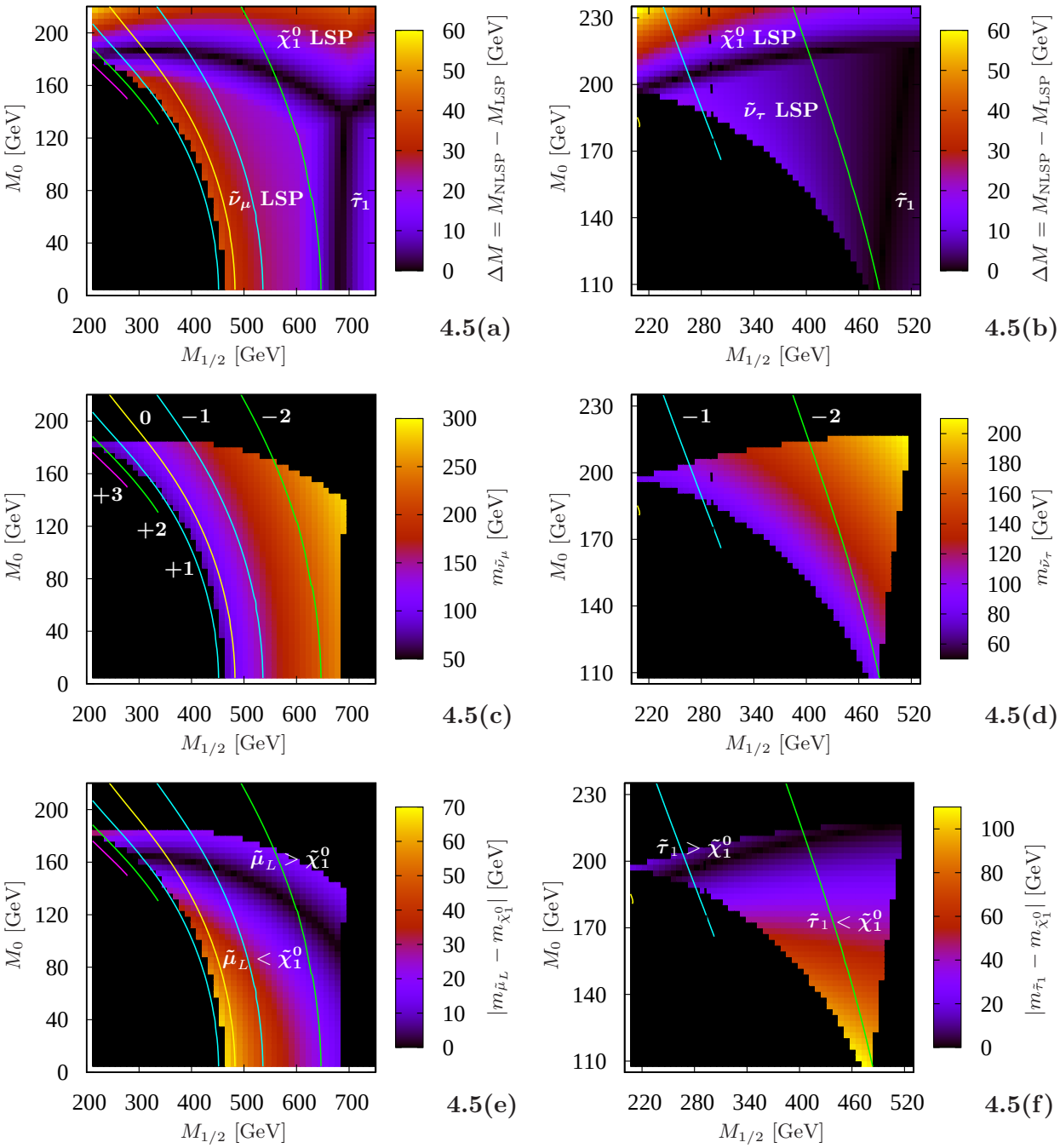

Figure 4.5.: Sneutrino LSP parameter space in the $M_{1/2}$–M_0 plane. The left panel [right panel] shows the $\tilde{\nu}_\mu$ LSP [$\tilde{\nu}_\tau$ LSP] region obtained via $\lambda'_{231}|_{\rm GUT} = 0.11$, $A_0 = -600$ GeV, $\tan\beta = 10$ and $\mathrm{sgn}(\mu) = +1$ [$\lambda'_{331}|_{\rm GUT} = 0.12$, $A_0 = -550$ GeV, $\tan\beta = 12$ and $\mathrm{sgn}(\mu) = +1$]. The plots show from top to bottom the mass difference between the NLSP and LSP [Fig. 4.5(a) and Fig. 4.5(b)], the mass of the sneutrino LSP [Fig. 4.5(c) and Fig. 4.5(d)], and the mass difference between the $\tilde{\chi}_1^0$ and $\tilde{\mu}_L$ [Fig. 4.5(e)] or between the $\tilde{\chi}_1^0$ and $\tilde{\tau}_1$ [Fig. 4.5(f)]. We have in Fig. 4.5(e) and Fig. 4.5(f) $m_{\tilde{\mu}_L/\tilde{\tau}_1} > m_{\tilde{\chi}_1^0}$ (denoted by $\tilde{\mu}_L/\tilde{\tau}_1 > \tilde{\chi}_1^0$) and $m_{\tilde{\mu}_L/\tilde{\tau}_1} < m_{\tilde{\chi}_1^0}$ (denoted by $\tilde{\mu}_L/\tilde{\tau}_1 < \tilde{\chi}_1^0$). The yellow (labeled with "0"), blue (labeled with "± 1"), green (labeled with "± 2") and magenta (labeled with "± 3") contours correspond to different SUSY contributions to the anomalous magnetic moment of the muon as described in Eq. (4.13). The dashed black line (right panel) corresponds to $\mathrm{BR}(b \to s\gamma) = 2.74 \times 10^{-4}$, Eq. (4.15).

The $\tilde{\nu}_\mu$ LSP lives in an extended region of B_3 mSUGRA parameter space. This stems from the fact, that we were able to choose a central scan point, Point I of Eq. (4.11), where the mass difference between the $\tilde{\nu}_\mu$ LSP and the other LSP candidates, $\tilde{\tau}_1$ and $\tilde{\chi}_1^0$, is large, namely 56 GeV and 75 GeV, respectively. We find a $\tilde{\nu}_\mu$ LSP between $M_{1/2} = 350$ GeV and $M_{1/2} = 600$ GeV for $M_0 = 140$ GeV, which is consistent with $a_\mu^{\rm exp}$, Eq. (4.12), and BR($b \to s\gamma$), Eq. (4.15), at 2σ. For $M_{1/2} = 500$ GeV, we obtain a consistent $\tilde{\nu}_\mu$ LSP for $M_0 < 170$ GeV.

Nearly the entire $\tilde{\nu}_\mu$ LSP region of Fig. 4.5(a) is consistent with the observed value of a_μ at the 1σ (blue lines) and 2σ (green lines) level, *cf.* Eq. (4.13). It is also consistent with BR($b \to s\gamma$) at 2σ, Eq. (4.15).

We see in Fig. 4.5(a), all three LSP candidates, the $\tilde{\nu}_\mu$, the $\tilde{\tau}_1$, and the $\tilde{\chi}_1^0$. If we increase M_0, we re-obtain at $M_0 \approx 150$ GeV the $\tilde{\chi}_1^0$ LSP instead of the $\tilde{\nu}_\mu$ or the $\tilde{\tau}_1$ LSP. This is easy to understand. M_0 increases the mass of all the sfermions, see Eq. (A.11), but leaves the mass of the (bino-like) $\tilde{\chi}_1^0$ unaffected, *cf.* Eq. (A.17).

We get a $\tilde{\tau}_1$ LSP instead of a $\tilde{\nu}_\mu$ LSP for $M_{1/2} > 650$ GeV and $M_0 < 140$ GeV. Remember that the $\tilde{\tau}_1$ is mainly right-handed for non-vanishing $\lambda'_{231}|_{\rm GUT}$ (not for large $\lambda'_{331}|_{\rm GUT}$). According to Eq. (A.15), the right-handed stau mass increases more slowly with $M_{1/2}$ than the left-handed $\tilde{\nu}_\mu$ mass, Eq. (A.11), because the right-handed sfermions couple only to the $U(1)_Y$ gaugino, whereas the left-handed sfermions couple also to the $SU(2)$ gauginos.

For M_0 between 140 GeV and 180 GeV, we obtain a $\tilde{\chi}_1^0$ LSP instead of a $\tilde{\nu}_\mu$ LSP if we increase $M_{1/2}$. In this region of parameter space, *i.e.* M_0 between 140 GeV and 180 GeV and $M_{1/2} < 700$ GeV, we have a $\tilde{\chi}_1^0$ LSP for vanishing $\lambda'_{231}|_{\rm GUT}$. With $\lambda'_{231}|_{\rm GUT}= 0.11$, we must retrieve the $\tilde{\chi}_1^0$ LSP for increasing $M_{1/2}$, because the (left-handed) $\tilde{\nu}_\mu$ couples stronger via the gauge interactions than the (bino-like) $\tilde{\chi}_1^0$; see Eq. (A.11) and Eq. (A.17) respectively.

The $M_{1/2}$–M_0 plane showing the $\tilde{\nu}_\tau$ LSP region, Fig. 4.5(b), looks similar to the $\tilde{\nu}_\mu$ LSP region, Fig. 4.5(a): We again get a $\tilde{\chi}_1^0$ LSP when we increase M_0, and a $\tilde{\tau}_1$ LSP for larger values of $M_{1/2}$. Most of the $\tilde{\nu}_\tau$ LSP region is also consistent with the observed value of a_μ at the 1σ (blue line) or 2σ (green line) level, Eq. (4.13). But we must have $M_{1/2} \gtrsim 290$ GeV [dashed black line in Fig. 4.5(b)] to be consistent with BR($b \to s\gamma$) at 2σ, *cf.* Eq. (4.15). The allowed $\tilde{\nu}_\tau$ LSP region in the $M_{1/2}$–M_0 plane is therefore "smaller" compared to the $\tilde{\nu}_\mu$ LSP region. It is worth mentioning, that one can also obtain a $\tilde{\nu}_\tau$ LSP via $\lambda'_{331}|_{\rm GUT}$ consistent with $a_\mu^{\rm exp}$, Eq. (4.12), and BR($b \to s\gamma$), Eq. (4.15), within 1σ; see an example in Ref. [106]. However the allowed $\tilde{\nu}_\tau$ LSP region in the $M_{1/2}$–M_0 [A_0–$\tan\beta$] plane is smaller in that case compared to Fig. 4.5(b) [Fig. 4.4(b)].

As explained before, $\lambda'_{331}|_{\rm GUT}$ reduces also the mass of the $\tilde{\tau}_1$, which is also a candidate for the LSP. We can see this in Fig. 4.5(b) by noting that the mass difference between the $\tilde{\nu}_\tau$ LSP and the $\tilde{\tau}_1$ NLSP is rather small, *i.e.* $\Delta M \lesssim 15$ GeV. A way to increase this mass difference is to decrease $\tan\beta$; see the discussion in Sect. 4.2.2.

Another difference between the $\tilde{\nu}_\tau$ LSP region, Fig. 4.5(b), and the $\tilde{\nu}_\mu$ LSP region, Fig. 4.5(a), is that the corresponding SUSY mass spectra for a $\tilde{\nu}_\mu$ LSP scenario are in average heavier than the SUSY mass spectra for a $\tilde{\nu}_\tau$ LSP scenario. For example, $M_0 = 100$ GeV (200 GeV) and $M_{1/2} = 500$ GeV (320 GeV) lead to squark masses of roughly 1000 GeV (700 GeV) in

the $\tilde{\nu}_\mu$ LSP ($\tilde{\nu}_\tau$ LSP) parameter space. The reason is, that we have chosen our scenarios consistent with the measured value of a_μ; see discussion after Eq. (4.13).

We have again in Fig. 4.5(a) as well as in Fig. 4.5(b) a "triple-point", where the three LSP candidates are degenerate in mass.

We give in Fig. 4.5(c) [Fig. 4.5(d)] the mass of the $\tilde{\nu}_\mu$ LSP [$\tilde{\nu}_\tau$ LSP] for the sneutrino LSP region of Fig. 4.5(a) [Fig. 4.5(b)]. The sneutrino LSP masses, which lead to SUSY scenarios in agreement with $a_\mu^{\rm exp}$ (and $b \to s\gamma$), range from 78 GeV (LEP bound, Sect. 4.1.3.1) up to roughly 250 GeV. Relaxing this bound, we claim that $a_\mu^{\rm exp}$ puts an upper bound of roughly 300 GeV at the 2σ level on the mass of a sneutrino LSP within B_3 mSUGRA. Note that BR($b \to s\gamma$) increases if we increase $M_{1/2}$, whereas $\delta a_\mu^{\rm SUSY}$ decreases, *cf.* for example Fig. 4 and Fig. 5 in Ref. [106]. The upper bound on the sneutrino LSP mass is thus due to $a_\mu^{\rm exp}$.

We finally show in Fig. 4.5(e) [Fig. 4.5(f)] the mass difference in GeV between the $\tilde{\chi}_1^0$ and the μ_L [mainly left-handed $\tilde{\tau}_1$]. We again observe that the $\tilde{\chi}_1^0$ is heavier than the $\tilde{\mu}_L$ in most regions of the $\tilde{\nu}_\mu$ LSP parameter space. The cascade decay, Eq. (4.10), is therefore not observable at the Tevatron. Further phenomenological consequences at hadron colliders will be discussed in Sect. 4.3.

4.2.4. Sneutrino LSPs with $\lambda'_{ijk}|_{\rm GUT} \neq \lambda'_{231}$ or λ'_{331}

We investigated in the last three sections in detail the $\tilde{\nu}_\mu$ LSP ($\tilde{\nu}_\tau$ LSP) parameter space with $\lambda'_{231}|_{\rm GUT}= 0.11$ ($\lambda'_{331}|_{\rm GUT}= 0.12$). We briefly consider the other couplings of Table 4.1.

For $\lambda'_{131}|_{\rm GUT}$, we obtain nearly the same parameter space as in Fig. 4.4(a) and Fig. 4.5(a), where $\lambda'_{231}|_{\rm GUT}= 0.11$. We now have a $\tilde{\nu}_e$ LSP instead of a $\tilde{\nu}_\mu$ LSP. Also the mass of the left-handed selectron, $\tilde{e}_L$, (for $\lambda'_{131}|_{\rm GUT}= 0.11$) equals the mass of the $\tilde{\mu}_L$ (for $\lambda'_{231}|_{\rm GUT}= 0.11$) and vice versa. But note, that the $\tilde{\nu}_e$ LSP parameter space is much more restricted than the $\tilde{\nu}_\mu$ LSP parameter space due to the stronger bounds on λ'_{131}, *cf.* Table 4.1. Also the LEP bound on $m_{\tilde{\nu}_e}$ is more model dependent, see Table 4.2.

We also obtain a $\tilde{\nu}_\mu$ LSP scenario via $\lambda'_{221}|_{\rm GUT}$ and $\lambda'_{212}|_{\rm GUT}$. If we choose $\lambda'_{221}|_{\rm GUT}$ or $\lambda'_{212}|_{\rm GUT}= 0.097$, we find similar regions to Fig. 4.4(a) and Fig. 4.5(a), where the $\tilde{\nu}_\mu$ is the LSP. The effect of $\lambda'_{221}|_{\rm GUT}$ and $\lambda'_{212}|_{\rm GUT}$ on $m_{\tilde{\nu}_\mu}$ is stronger, because the running of both couplings involves no loops containing the large top Yukawa coupling. In contrast, the top Yukawa coupling weakens the running of λ'_{231} (j=3!) when we go from $M_{\rm GUT}$ to M_Z [58], see also Sect. 5.2.

Analogously, similar to Fig. 4.4(b) and Fig. 4.5(b), we find parameter regions, where the $\tilde{\nu}_\tau$ is the LSP. We now have to choose $\lambda'_{321}|_{\rm GUT}$ or $\lambda'_{312}|_{\rm GUT}= 0.104$ instead of $\lambda'_{331}|_{\rm GUT}= 0.12$.

Note however, that different couplings λ'_{ijk} lead to a different collider phenomenology, because the $L_iQ_j\bar{D}_k$ operator couples to different generations of lepton and quark superfields. We discuss this topic in the next section.

4.3. Hadron Collider Phenomenology

We have shown in the last section, that a sneutrino LSP exists in an extended region of B_3 mSUGRA parameter space. We now investigate the corresponding phenomenology at hadron colliders, especially at the LHC. The main phenomenological differences between a P_6 mSUGRA scenario with a stable $\tilde{\chi}_1^0$ LSP and a B_3 mSUGRA scenario with an unstable sneutrino LSP are:

- The mass spectrum is changed. We now have a sneutrino LSP. Also some of the sleptons might be lighter than the $\tilde{\chi}_1^0$, for example the $\tilde{\mu}_L$ in the presence of $\lambda'_{231}|_{\rm GUT}$; see Fig. 4.4(e) and Fig. 4.5(e). Thus the decay chains and final state topologies are different.
- The LSP is not stable anymore and directly decays to SM particles via the B_3 coupling. In the following analysis, with $\lambda'_{231}|_{\rm GUT} \neq 0$, we have two extra jets from each $\tilde{\nu}_\mu$ LSP decay. This also results in less missing transverse momentum, $\not{p}_T$.
- We have shown, that $\lambda'_{ijk}|_{\rm GUT} = \mathcal{O}(10^{-1})$ is needed to obtain a $\tilde{\nu}_i$ LSP. This large coupling can lead to direct and dominating B_3 decays of heavy sparticles; namely of left-handed charged sleptons of generation i, of left-handed squarks of generation j and of right-handed down-type squarks of generation k. The SM decay products naturally have large momenta.
- Single sparticle production via λ'_{ijk} is possible; for example, single charged slepton and sneutrino production.

In the following, we investigate these aspects in detail. We perform a Monte Carlo simulation at the parton level using the `HERWIG` event generator [196, 197, 198, 199, 200].

4.3.1. Example Spectrum and Branching Ratios

To investigate the sneutrino LSP phenomenology at the LHC, we choose as an example a scenario with a $\tilde{\nu}_\mu$ LSP:

$$\begin{aligned} &\lambda'_{231}|_{\rm GUT}= 0.11,\ M_0 = 100\,\text{GeV},\ M_{1/2} = 450\,\text{GeV}, \\ &A_0 = -600\,\text{GeV},\ \tan\beta = 10,\ \text{sgn}(\mu) = +1\,. \end{aligned} \tag{4.18}$$

This benchmark point can be found in Fig. 4.5(a) and is consistent with $a_\mu^{\rm exp}$, Eq. (4.12), and BR($b \to s\gamma$), Eq. (4.15), at 1σ. See also Ref. [106] for a benchmark scenario with a $\tilde{\nu}_\tau$ LSP.

The resulting sparticle masses and branching ratios (BRs) are given in Table 4.4. The B_3 decays are shown in bold-face. Sparticle masses which are significantly affected by $\lambda'_{231}|_{\rm GUT}$ are also bold-face. We calculate the decay rates by piping the output of `SOFTSUSY` through `ISAWIG1.200`. This is linked to `ISAJET7.75` [201] in order to calculate the decay widths of the SUSY particles. This output is later fed into `HERWIG` to simulate events at the LHC.

We find that the decay of the $\tilde{\nu}_\mu$ LSP with a mass of 124 GeV is completely dominated by the λ'_{231} coupling. Each LSP decay leads to a bottom and a down quark and no $\not{p}_T$ [202, 203]. However, $\not{p}_T$ can be obtained from cascade decays of heavy sparticles. In principle,

	mass [GeV]	channel	BR	channel	BR
$\tilde{\nu}_\mu$	**124**	$\bar{b}d$	**100**%		
$\tilde{\mu}_L^-$	**147**	$W^-\bar{b}d$	**79.0**%	$\bar{c}d$	**21.0**%
$\tilde{\chi}_1^0$	184	$\tilde{\nu}_\mu^*\nu_\mu$	36.0%	$\tilde{\nu}_\mu\bar{\nu}_\mu$	36.0%
		$\tilde{\mu}_L^+\mu^-$	14.0%	$\tilde{\mu}_L^-\mu^+$	14.0%
$\tilde{\tau}_1^-$	188	$\tilde{\chi}_1^0\tau^-$	100%		
$\tilde{e}_R^-$ ($\tilde{\mu}_R^-$)	206	$\tilde{\chi}_1^0 e^-(\mu^-)$	100%		
$\tilde{\nu}_\tau$	316	$\tilde{\chi}_1^0\nu_\tau$	67.3%	$W^+\tilde{\tau}_1^-$	32.7%
$\tilde{\nu}_e$	319	$\tilde{\chi}_1^0\nu_e$	100%		
$\tilde{e}_L^-$	329	$\tilde{\chi}_1^0 e^-$	100%		
$\tilde{\tau}_2^-$	329	$\tilde{\chi}_1^0\tau^-$	65.1%	$h^0\tilde{\tau}_1^-$	18.2%
		$Z^0\tilde{\tau}_1^-$	16.7%		
$\tilde{\chi}_2^0$	350	$\tilde{\nu}_\mu\bar{\nu}_\mu$	23.7%	$\tilde{\nu}_\mu^*\nu_\mu$	23.7%
		$\tilde{\mu}_L^-\mu^+$	22.4%	$\tilde{\mu}_L^+\mu^-$	22.4%
		$\tilde{\nu}_\tau\bar{\nu}_\tau$	1.1%	$\tilde{\nu}_\tau^*\nu_\tau$	1.1%
$\tilde{\chi}_1^-$	350	$\tilde{\nu}_\mu^*\mu^-$	49.7%	$\tilde{\mu}_L^-\bar{\nu}_\mu$	42.6%
		$\tilde{\nu}_\tau^*\tau^-$	2.3%	$\tilde{\nu}_e^* e^-$	1.8%
		$\tilde{\tau}_1^-\bar{\nu}_\tau$	1.6%		
$\tilde{\chi}_3^0$	691	$\tilde{\chi}_1^- W^+$	29.7%	$\tilde{\chi}_1^+ W^-$	29.7%
		$\tilde{\chi}_2^0 Z^0$	26.1%	$\tilde{\chi}_1^0 Z^0$	8.3%
		$\tilde{\chi}_1^0 h^0$	1.7%	$\tilde{\chi}_2^0 h^0$	1.7%
$\tilde{t}_1$	650	$\tilde{\chi}_1^+ b$	42.1%	$\tilde{\chi}_1^0 t$	33.5%
		$\tilde{\chi}_2^0 t$	13.8%	$\mu^+ d$	**10.6**%
$\tilde{\chi}_2^-$	702	$\tilde{\chi}_2^0 W^-$	28.0%	$\tilde{\chi}_1^- Z^0$	26.6%
		$\tilde{\chi}_1^- h^0$	23.8%	$\tilde{\chi}_1^0 W^-$	7.9%
		$\tilde{t}_1^* b$	4.1%	$\tilde{\mu}_L^-\bar{\nu}_\mu$	2.5%
		$\tilde{\tau}_2^-\bar{\nu}_\tau$	2.0%	$\tilde{e}_L^-\bar{\nu}_e$	1.7%
		$\tilde{\nu}_\tau^*\tau^-$	1.3%		
$\tilde{\chi}_4^0$	702	$\tilde{\chi}_1^- W^+$	28.3%	$\tilde{\chi}_1^+ W^-$	28.3%
		$\tilde{\chi}_2^0 h^0$	22.3%	$\tilde{\chi}_1^0 h^0$	7.0%
		$\tilde{\chi}_2^0 Z^0$	2.0%	$\tilde{\chi}_1^0 Z^0$	1.8%
		$\tilde{\nu}_\mu\bar{\nu}_\mu$	1.2%	$\tilde{\nu}_\mu^*\nu_\mu$	1.2%

	mass [GeV]	channel	BR	channel	BR
$\tilde{b}_1$	**842**	$W^-\tilde{t}_1$	35.8%	$\tilde{\chi}_1^- t$	31.3%
		$\tilde{\chi}_2^0 b$	18.8%	$\bar{\nu}_\mu d$	**12.4**%
		$\tilde{\chi}_1^0 b$	1.2%		
$\tilde{d}_R$	**897**	$\nu_\mu b$	**45.3**%	$\mu^- t$	**42.1**%
		$\tilde{\chi}_1^0 d$	12.6%		
$\tilde{t}_2$	**906**	$Z^0\tilde{t}_1$	28.2%	$\tilde{\chi}_1^+ b$	23.7%
		$h^0\tilde{t}_1$	11.7%	$\tilde{\chi}_2^0 t$	10.2%
		$\mu^+ d$	**9.0**%	$\tilde{\chi}_4^0 t$	7.5%
		$\tilde{\chi}_2^+ b$	5.4%	$\tilde{\chi}_1^0 t$	2.6%
		$\tilde{\chi}_3^0 t$	1.7%		
$\tilde{b}_2$	919	$\tilde{\chi}_1^0 b$	41.3%	$W^-\tilde{t}_1$	25.3%
		$\tilde{\chi}_2^- t$	14.4%	$\tilde{\chi}_4^0 b$	5.3%
		$\tilde{\chi}_3^0 b$	5.0%	$\bar{\nu}_\mu d$	**3.4**%
		$\tilde{\chi}_1^- t$	3.2%	$\tilde{\chi}_2^0 b$	1.9%
$\tilde{s}_R$	928	$\tilde{\chi}_1^0 s$	99.8%		
$\tilde{u}_R$ ($\tilde{c}_R$)	932	$\tilde{\chi}_1^0 u(c)$	99.8%		
$\tilde{u}_L$ ($\tilde{c}_L$)	963	$\tilde{\chi}_1^+ d(s)$	65.6%	$\tilde{\chi}_2^0 u(c)$	32.6%
		$\tilde{\chi}_1^0 u(c)$	1.2%		
$\tilde{d}_L$ ($\tilde{s}_L$)	966	$\tilde{\chi}_1^- u(c)$	64.5%	$\tilde{\chi}_2^0 d(s)$	32.5%
		$\tilde{\chi}_1^0 d(s)$	1.6%	$\tilde{\chi}_2^- u(c)$	1.0%
$\tilde{g}$	1046	$\tilde{t}_1\bar{t}$	15.0%	$\tilde{t}_1^* t$	15.0%
		$\tilde{b}_1\bar{b}$	9.2%	$\tilde{b}_1^* b$	9.2%
		$\tilde{d}_R\bar{d}$	5.2%	$\tilde{d}_R^* d$	5.2%
		$\tilde{b}_2\bar{b}$	3.9%	$\tilde{b}_2^* b$	3.9%
		$\tilde{s}_R\bar{s}$	3.4%	$\tilde{s}_R^* s$	3.4%
		$\tilde{u}_R\bar{u}$ ($\tilde{c}_R\bar{c}$)	3.2%	$\tilde{u}_R^* u$ ($\tilde{c}_R^* c$)	3.2%
		$\tilde{u}_L\bar{u}$ ($\tilde{c}_L\bar{c}$)	1.7%	$\tilde{u}_L^* u$ ($\tilde{c}_L^* c$)	1.7%
		$\tilde{d}_L\bar{d}$ ($\tilde{s}_L\bar{s}$)	1.6%	$\tilde{d}_L^* d$ ($\tilde{s}_L^* s$)	1.6%

Table 4.4.: Branching ratios (BRs) and sparticle masses for the example scenario defined in Eq. (4.18). BRs smaller than 1% are neglected. B_3 decays are shown in bold-face. Masses which are reduced by more than 5 GeV (compared to the P_6 spectrum) due to $\lambda'_{231}|_{\rm GUT} = 0.11$ are also shown in bold-face.

reconstruction of the $\tilde{\nu}_\mu$ mass should be possible, although combinatorial backgrounds might complicate this task.

The $\tilde{\mu}_L$ with a mass of 147 GeV is the NLSP. This is the case in most of the $\tilde{\nu}_\mu$ LSP parameter space, *cf.* Fig. 4.4(e) and Fig. 4.5(e). The $\tilde{\mu}_L$ decays mainly via the $L_2Q_3\bar{D}_1$ operator into SM fermions, in principle to $\bar{t}d$. If this decay mode is not kinematically allowed, like for the benchmark point under study, we obtain a dominant 3-body decay into $W^-\bar{b}d$; see Appendix B for details. We thus have at least two jets, where one of the jets is a b-jet. As mentioned in Sect. 4.1.3.2, another possible 3-body decay is $\tilde{\mu}_L^- \to \mu^-\bar{\nu}_\mu\tilde{\nu}_\mu$ via a virtual neutralino. But this decay is suppressed by four orders of magnitude compared to the

3-body decay via a virtual top quark. The reasons are: small couplings (left-handed sleptons couple to a bino-like $\tilde{\chi}_1^0$), less phase space ($m_{\tilde{\mu}_L} - m_{\tilde{\nu}_\mu} = 23$ GeV), destructive interferences between diagrams with a virtual $\tilde{\chi}_1^0$ and $\tilde{\chi}_2^0$, and the decay via the virtual top is enhanced by a color factor of 3, *cf.* Appendix B. However, there is an additional 2-body decay mode, $\tilde{\mu}_L \to \bar{c}d$, in Table 4.4. This decay proceeds via a non-vanishing λ'_{221} coupling, which is generated out of $\lambda'_{231}|_{\rm GUT}$ via RGE running [58, 102].

The electroweak gauginos decay dominantly via R_6 conserving gauge interactions to 2-body final states. The lightest gaugino is the $\tilde{\chi}_1^0$, which is only the NNLSP within our benchmark scenario; $m_{\tilde{\chi}_1^0} = 184$ GeV. It decays into either the LSP or NLSP. These then undergo direct B_3 decays, as discussed before. So, the $\tilde{\chi}_1^0$ decays lead to dijet events with $\not{p}_T$ or a muon. Due to the Majorana nature of the $\tilde{\chi}_1^0$, negatively and positively charged muons are possible. Cascade decays of pair produced sparticles can therefore lead to like sign-muon events via $\tilde{\chi}_1^0$ decays; see Sect. 4.3.2. Note, that $\tilde{\nu}_\mu$ LSP scenarios exist where the $\tilde{\chi}_1^0$ is also heavier than the $\tilde{\tau}_1$ or even the right-handed smuon, $\tilde{\mu}_R$, and selectron, $\tilde{e}_R$. These scenarios can lead to multi-lepton final states. We will not consider these scenarios here, because the relevant $\tilde{\mu}_R$ and $\tilde{e}_R$ decays into the $\tilde{\nu}_\mu$ LSP and the $\tilde{\mu}_L$ NLSP are not implemented in HERWIG.

The $\tilde{\chi}_2^0$ also has a significant BR to $\tilde{\mu}_L^\pm \mu^\mp$ and $\tilde{\nu}_\mu \nu_\mu$. Similarly, the lightest chargino, $\tilde{\chi}_1^-$, decays either predominantly into $\tilde{\nu}_\mu^* \mu^-$ or $\tilde{\mu}_L^- \bar{\nu}_\mu$, leading to either a muon or missing energy in the final state. The $\tilde{\chi}_2^0$ and $\tilde{\chi}_1^-$ are wino-like in mSUGRA models. They thus decay predominantly to the left-handed $\tilde{\mu}_L$ and $\tilde{\nu}_\mu$. The decays of the heavier chargino, $\tilde{\chi}_2^-$, and neutralinos, $\tilde{\chi}_{3/4}^0$ are similar to R_6 mSUGRA scenarios.

The $\tilde{\tau}_1$ in Table 4.4 is the next-to-NNLSP (NNNLSP) with a mass of 188 GeV and almost degenerate with the $\tilde{\chi}_1^0$. The $\tilde{\tau}_1$ can in general be the NLSP, the NNLSP or NNNLSP in B_3 mSUGRA scenarios with a sneutrino LSP. Here we have $\tilde{\tau}_1^- \to \tilde{\chi}_1^0 \, \tau^-$.

The $\tilde{\mu}_R$, $\tilde{e}_R$, $\tilde{e}_L$, $\tilde{\nu}_e$, $\tilde{\nu}_\tau$ and $\tilde{\tau}_2$ in Table 4.4 decay into the $\tilde{\chi}_1^0$ or, in the case of the $\tilde{\tau}_2$ and $\tilde{\nu}_\tau$, also into the $\tilde{\tau}_1$ similar to R_6 mSUGRA scenarios. But as mentioned above, the $\tilde{\tau}_1$, the $\tilde{\mu}_R$ and the $\tilde{e}_R$ can in general be lighter than the $\tilde{\chi}_1^0$ in $\tilde{\nu}_\mu$ LSP scenarios. These particles then decay preferentially into the $\tilde{\nu}_\mu$ LSP via a 3-body decay.

The masses of the top-squarks, $\tilde{t}_{1,2}$, and the bottom-squarks, $\tilde{b}_{1,2}$, are slightly reduced due to the presence of λ'_{231} in the corresponding RGEs. The $\tilde{t}_1$ is the lightest squark with a mass of 650 GeV and has four 2-body decay modes with appreciable BRs. Three decays are via gauge interactions and one via λ'_{231}. Since the electroweak gauge couplings and λ'_{231} have the same order of magnitude, we also expect R_6 conserving and violating decays at a similar rate. The situation for the $\tilde{t}_2$, $\tilde{b}_1$ and $\tilde{b}_2$ is similar to $\tilde{t}_1$. All of these particles couple via their left-handed component to the $L_2 Q_3 \bar{D}_1$ operator and can therefore decay into two SM particles.

The masses of the left-handed and right-handed squarks of the 1st and 2nd generation are around 900 GeV. The right-handed down-squark ($m_{\tilde{d}_R} = 897$ GeV) is lighter than the right-handed strange-squark ($m_{\tilde{s}_R} = 928$ GeV). In contrast both squarks are degenerate in mass in R_6 mSUGRA. However, they are so heavy, that no problems should occur with FCNCs. $\lambda'_{231}|_{\rm GUT}$ couples only to the right-handed down squarks and not to the right-handed strange squarks. So, $m_{\tilde{d}_R}$ is reduced, keeping $m_{\tilde{s}_R}$ unchanged. For the same reason, there exist no

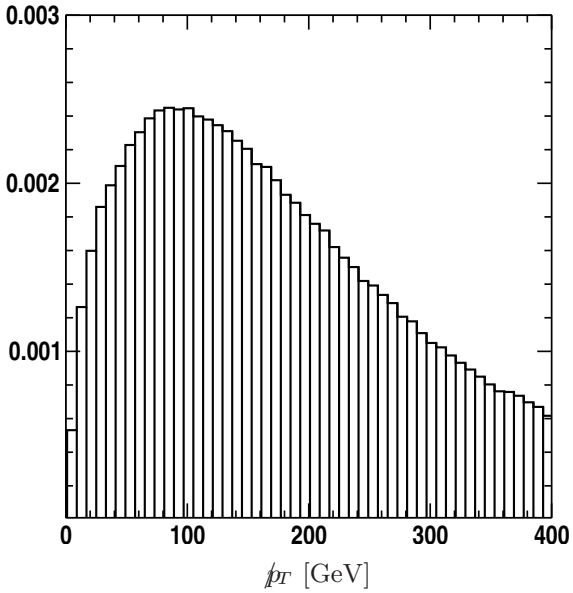

Figure 4.6.: $\not{p}_T$ distribution due to neutrinos in the final state for the example scenario Eq. (4.18). The distribution is normalized to one. Note that events with no $\not{p}_T$ in the final state are not shown.

B_3 decays of $\tilde{s}_R$ via λ'_{231} at tree-level. In contrast, $\tilde{d}_R$ has dominant direct B_3 decays to SM particles, which than have large momenta, see Sect. 4.3.2.

The heaviest sparticle is the gluino, $\tilde{g}$, with a mass of 1046 GeV. It decays only via the strong interaction. The allowed decay modes and their relative BRs depend upon the sum of the final state masses. For example, $\tilde{g} \to \tilde{t}_1 t$ has the largest BR, since the $\tilde{t}_1$ is the lightest squark.

We conclude that the heavy part of the mass spectrum looks very similar to P_6 mSUGRA scenarios with a stable $\tilde{\chi}_1^0$ LSP. However, a non-vanishing λ'_{ijk} coupling, which has the same order of magnitude as the gauge couplings, allows for additional 2-body B_3 decays of some of the squarks. Which squarks are allowed to decay via λ'_{ijk} depend on the indices j, k. The masses and compositions of the electroweak gauginos are also very similar to P_6 mSUGRA. However, the $\tilde{\chi}_1^0$ is no longer the LSP. Depending on the specific $\tilde{\nu}_i$ LSP scenario, the $\tilde{\chi}_1^0$ can decay into charged sleptons and sneutrinos of different generations. Therefore, the main difference can be found in the light part of the mass spectrum where we have the $\tilde{\nu}_i$ LSP. The $\tilde{\nu}_i$ LSP decays preferentially into two jets via λ'_{ijk}.

4.3.2. Sparticle Pair Production

We have investigated in the last section the mass spectrum and the BRs of SUSY particles for one representative B_3 mSUGRA scenario with a $\tilde{\nu}_\mu$ LSP, described by Eq. (4.18). We have pointed out the general differences compared to mSUGRA scenarios with a stable $\tilde{\chi}_1^0$ LSP. We now explore signatures at the LHC which arise from pair production of sparticles via the gauge interactions, *i.e.* mainly squark and gluino production via the strong interaction. For

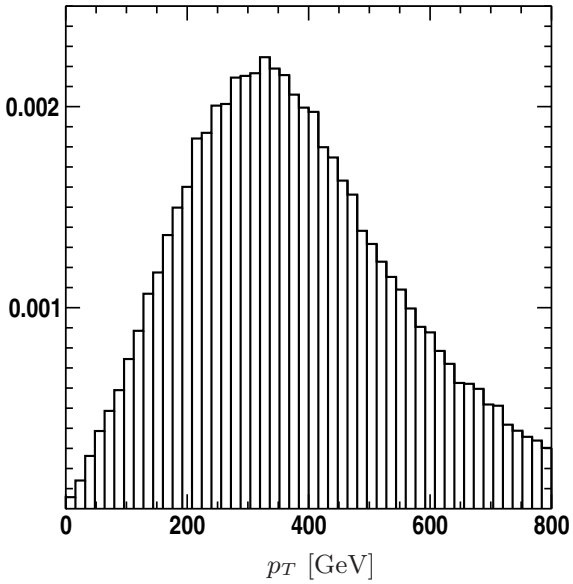

Figure 4.7.: p_T distribution of the muon from the decays $\tilde{d}_R \to \mu t$ and $\tilde{t}_{1/2} \to \mu d$ (*cf.* Table 4.4) at the LHC. The distribution is normalized to one.

this purpose we use the HERWIG event generator. We investigate single sparticle production in Sect. 4.3.3.

The masses of the strongly interacting sparticles are roughly 1 TeV. We therefore obtain from HERWIG a total sparticle pair production (leading order) cross section at the LHC of

$$\sigma_{\text{total}} = 3.0\,\text{pb}\,. \tag{4.19}$$

So, one can expect approximately 300 000 SUSY pair production events for an integrated luminosity of 100 fb^{-1}. The sparticle decays follow those in Table 4.4. The different decay chains lead to different final states. Moreover, the p_T distributions of the final state particles and the $\not{p}_T$ can be very distinctive compared to P_6 mSUGRA with a stable $\tilde{\chi}_1^0$ LSP.

We show in Fig. 4.6 the $\not{p}_T$ distribution due to neutrinos in the final state. Note, that here roughly 20% of all SUSY events posses no $\not{p}_T$ in contrast to P_6 mSUGRA scenarios. For example, if the decay chains of the pair produced sparticles into the $\tilde{\nu}_\mu$ LSP contain no neutrino than there is no $\not{p}_T$. The $\not{p}_T$ distribution in Fig. 4.6 peaks at roughly 90 GeV. Thus, $\not{p}_T$ might still be used to distinguish the SUSY signal from its SM background. Large amounts of $\not{p}_T$, *i.e.* $\not{p}_T$ of a few hundred GeV, can arise if a squark decays directly via λ'_{231} into a quark and a neutrino. For example $\tilde{d}_R \to \nu_\mu b$, *cf.* Table 4.4. This decay also leads to a high-p_T b-jet, *i.e.* p_T of $\mathcal{O}(100\,\text{GeV})$.

Instead of high-p_T neutrinos, we can also have high-p_T muons from the direct decays of $\tilde{d}_R$ and $\tilde{t}_{1/2}$ via λ'_{231}, see Table 4.4. We show in Fig. 4.7 the p_T distribution of these muons. The distribution peaks at 340 GeV. The large momenta are a consequence of the large squark masses. Nearly the entire mass of the squarks is transformed into the momenta of two SM particles. These high-p_T SM particles might also be used to reconstruct the squark mass. The muon p_T-distribution will peak at smaller values, if the squarks are lighter than in

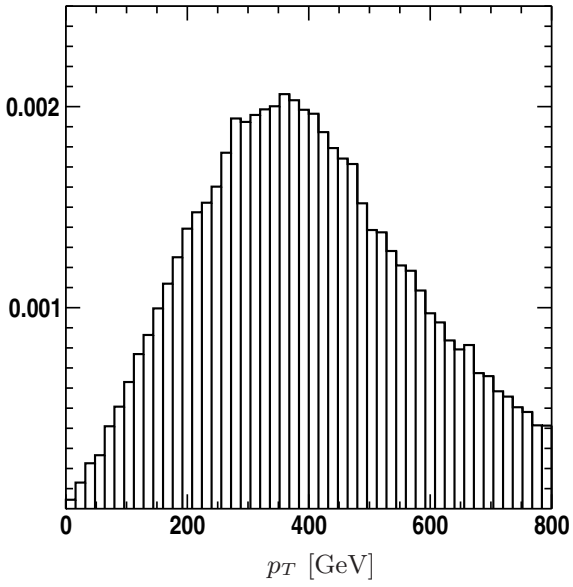

Figure 4.8.: p_T distribution of the top quark from the decay $\tilde{d}_R \to \mu t$ (*cf.* Table 4.4) at the LHC. The distribution is normalized to one.

our benchmark scenario. But at the same time we will produce more squarks and muons compared to the cross section, Eq. (4.19). If the mass spectrum is heavier compared to our example point, the cross section will be smaller. But the muon p_T-distribution will now peak at larger values. Thus stronger cuts on the muon p_T can be applied. We conclude that the high-p_T muons might be used on the one hand to distinguish the SUSY signal from the SM background and on the other hand to distinguish the B_3 mSUGRA model with a $\tilde{\nu}_\mu$ LSP from mSUGRA with a stable $\tilde{\chi}_1^0$ LSP. For our benchmark scenario Eq. (4.18), we find that 11% of all sparticle pair production events lead to at least one high-p_T muon from a squark decay. A fraction of roughly 10% is a general feature of our $\tilde{\nu}_\mu$ LSP scenarios.

The neutrino or muon from the squark decay will be accompanied by a quark with roughly the opposite p_T. These quarks lead to high-p_T jets, which might be b-jets depending on the flavor indices of λ'. For our benchmark point, we obtain high-p_T b-jets from the B_3 decay $\tilde{d}_R \to \nu_\mu b$. We also can get a top-quark, t, from the decay $\tilde{d}_R \to \mu^- t$. We show in Fig. 4.8 the p_T-distribution of this top-quark. The distribution peaks at 360 GeV. The top decay will also produce a b-jet and a W. The W might produce additional jets or leptons with $\not{p}_T$. These decay products will be boosted due to the large top momentum. Thus isolated leptons can most likely not be used to reconstruct the top quark.

Finally we want to mention an effect arising from the mass ordering in the light part of the spectrum. We have shown in Fig. 4.4(e) and Fig. 4.5(e) that the $\tilde{\mu}_L$ is lighter than the $\tilde{\chi}_1^0$ in most regions of $\tilde{\nu}_\mu$ LSP parameter space allowing for the decay $\tilde{\chi}_1^0 \to \tilde{\mu}_L^\pm \mu^\mp$. Since many decay chains in Table 4.4 involve the $\tilde{\chi}_1^0$, we expect more muons in the final state than in mSUGRA with a stable $\tilde{\chi}_1^0$ LSP[2]. For example, all right-handed squarks, which do not directly couple to the $L_2 Q_3 \bar{D}_1$ operator will predominantly decay into the $\tilde{\chi}_1^0$. Thus pair

[2]Note, that also the $\tilde{\chi}_2^0$ and $\tilde{\chi}_1^-$ decay to a muon with a BR of roughly 50%, see Table 4.4.

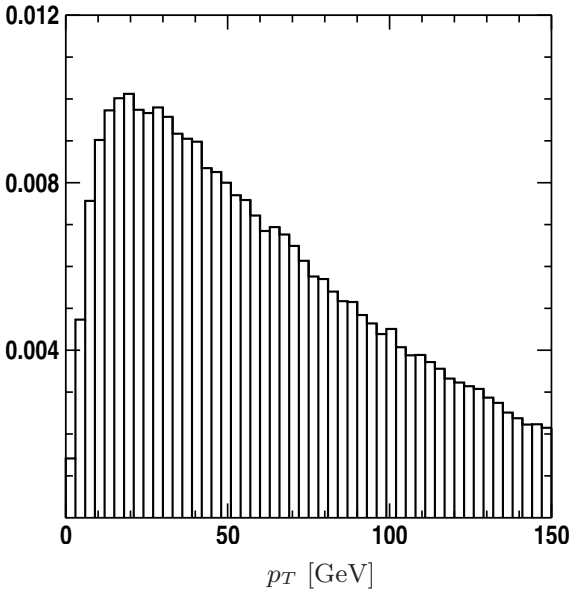

Figure 4.9.: p_T distribution of the muon from the decay $\tilde{\chi}_1^0 \to \tilde{\mu}_L \mu$ (*cf.* Table 4.4) at the LHC . The distribution is normalized to one.

production of right-handed squarks, $\tilde{q}_R$, has a large fraction of the signature

$$\tilde{q}_R \tilde{q}_R \to \mu^\pm \mu^\pm \, jjjjjj \, (WW) \,. \tag{4.20}$$

We have six jets, j, where two jets rise from the $\tilde{q}_R$ decays and four jets from the decays of the two $\tilde{\mu}_L$. If the $\tilde{\mu}_L$ decay via the 3-body decay (see Table 4.4), two jets will be b-jets and we will also have two Ws in the final state. We also find two muons from $\tilde{\chi}_1^0$ decay, where all charge combinations of the muons are possible due to the Majorana nature of the $\tilde{\chi}_1^0$. We therefore have a new source for like-sign dimuon events, which does not exist in P_6 mSUGRA scenarios with a stable $\tilde{\chi}_1^0$ LSP. In principle, it should be possible to reconstruct the full event, Eq. (4.20), although we have large combinatorial backgrounds due to the many jets in the final state.

We show in Fig. 4.9 the p_T-distribution of the muons arising from $\tilde{\chi}_1^0$ decay within our example scenario, Eq. (4.18). The distribution peaks at 20 GeV and therefore we expect that most of the muons will pass standard experimental cuts. However, the position of the peak is restricted by the mass difference of the $\tilde{\mu}_L$ and $\tilde{\chi}_1^0$. In our example the mass difference is 37 GeV. In general we find in Figs. 4.4(e), 4.5(e) mass differences of up to 90 GeV.

In a $\tilde{\nu}_i$ LSP scenario with $\lambda'_{ijk}|_{\rm GUT} \neq \lambda'_{231}|_{\rm GUT}$ we get the following differences. Now left-handed (right-handed down-type) squarks of generation j (k) will couple to the $L_i Q_j \bar{D}_k$ operator. These squarks can now decay into a quark of generation k (j) and into a lepton of generation i. In addition, the masses of these squarks will be reduced via the B_3 interaction. For $i = 1$, we have to replace the muons in the discussion above by electrons. For $i = 3$, we have taus instead of muons. We will get taus with large momenta, *i.e.* $p_\tau = \mathcal{O}(100\,\text{GeV})$, from the decays of the squarks via the B_3 interaction. These taus have a boost factor of $\gamma = \mathcal{O}(100)$ and are thus long lived leading to detached vertices of $\mathcal{O}(1\,\text{cm})$. We finally see

process	cross section
$PP \to \tilde{\nu}_\mu + X$	2.2×10^6 fb
$PP \to \tilde{\chi}_1^0 \nu_\mu + X$	4.2×10^1 fb
$PP \to \tilde{\chi}_2^0 \nu_\mu + X$	6.2×10^0 fb
$PP \to \tilde{\chi}_1^- \mu^+ + X$	1.3×10^1 fb
$PP \to \tilde{\mu}_L^- t + X$	1.3×10^4 fb

Table 4.5.: Total hadronic cross sections for single sparticle production at the LHC within the $\tilde{\nu}_\mu$ LSP scenario, Eq. (4.18), with $\lambda'_{231}|_{\rm GUT} = 0.11$. The cross sections include also the charge conjugated processes.

in Fig. 4.4(f) and Fig. 4.5(f) that also in large regions of $\tilde{\nu}_\tau$ LSP parameter space the $\tilde{\tau}_1$ is lighter than the $\tilde{\chi}_1^0$. This might lead to like-sign tau events from two decay chains involving a $\tilde{\chi}_1^0$.

4.3.3. Single Sparticle Production

Here we explore single sparticle production, which is not possible if P_6 is conserved. We expect high rates due to the large λ'_{ijk} coupling in $\tilde{\nu}_i$ LSP scenarios.

We show in Table 4.5 the hadronic cross sections for different single sparticle production processes. We again consider the example scenario, Eq. (4.18), with $\lambda'_{231}|_{\rm GUT} = 0.11$. The first four cross sections are calculated with `HERWIG` and the last cross section is taken from Sect. 6.2. The first four processes involve a real or virtual $\tilde{\nu}_\mu$, which is the LSP. The corresponding processes with the $\tilde{\mu}_L$ are not possible, because one parton in the initial state has to be a top-quark. A single $\tilde{\mu}_L$ can therefore be produced only in association with a SM particle, for example with a top-quark [184, 204, 205]; see also Sect. 6.

We indeed observe in Table 4.5 a large cross section for the resonant production of single $\tilde{\nu}_\mu$s due to the large λ'_{231} coupling, high parton luminosity (due to small Bjorken x) and large phase space. For 10 fb^{-1} integrated luminosity we will produce more than two million $\tilde{\nu}_\mu$ LSPs. However, the $\tilde{\nu}_\mu$ can only decay into two jets, *cf.* Table 4.4, where one jet is a b-jet [202, 203]. This process thus suffers from large QCD background and it will be very hard to observe an excess over the SM background at the LHC [177].

The process in Table 4.5 with the second largest cross section is single $\tilde{\mu}_L$ production in association with a top quark. This process suffers in general from the large SM $t\bar{t}$ + jet background, *cf.* Sect. 6.3. However it might be possible to see an excess over the SM in small regions of $\tilde{\nu}_\mu$ LSP parameter space, where the $\tilde{\chi}_1^0$ is lighter than the $\tilde{\mu}_L$, *cf.* Figs. 4.4(e), 4.5(e). The $\tilde{\mu}_L$ can decay in this case to $\tilde{\chi}_1^0 \mu$ and we might employ the charge asymmetry of the muons to distinguish the signal from the background, see Sect. 6.3.

The production of a $\tilde{\chi}_1^0$ [$\tilde{\chi}_2^0$] in association with a neutrino, Table 4.5, can lead to a muon with jets and $\not{p}_T$ in the final state, because 28% [44.8%] of the $\tilde{\chi}_1^0$s [$\tilde{\chi}_2^0$s] decay into a $\tilde{\mu}_L \mu$ pair. However the respective production cross sections are rather small, namely 42 fb [6.2 fb].

The production of charginos and muons, $\tilde{\chi}_1^- \mu^+$, seems more promising. Roughly 50% of the produced $\tilde{\chi}_1^-$ will decay into $\tilde{\nu}_\mu^* \mu^-$ leading to a final state with a pair of muons, and two jets, where one jet is a b-jet. But again the cross section is small, 13 fb.

In $\tilde{\nu}_i$ LSP scenarios, where $\lambda'_{ijk}|_{\rm GUT} \neq \lambda'_{231}|_{\rm GUT}$, the main difference arises if $j \neq 3$. In this case also resonant single charged slepton, $\tilde{\ell}_{Li}$, production, Eq. (4.8), is possible via an up-type quark of generation j. Therefore, if the $\tilde{\chi}_1^0$ is lighter than the $\tilde{\ell}_{Li}$, we expect a high rate of leptons from $\tilde{\ell}_{Li}$ decay to $\tilde{\chi}_1^0 \ell_i$. But this is only possible in small regions of $\tilde{\nu}_i$ LSP parameter space, see Figs. 4.4(e), 4.4(f), 4.5(e) and 4.5(f). A further bottleneck for the observation of these leptons is the small mass difference between the $\tilde{\chi}_1^0$ and $\tilde{\ell}_{Li}$ leading to small lepton momenta. The mass difference will not exceed roughly 30 GeV. Large λ'_{ijk} couplings with $j \neq 3$ are also disfavored by D_0–$\bar{D}_0$-mixing, *cf.* Sect. 4.1.2.

We conclude, that pair production of SUSY particles and their subsequent decays lead to much more promising signatures than single sparticle production. On the one hand, resonant single sneutrino production, which occurs at a high rate, lead mainly to jets in the final state and thus suffers from the large QCD background. On the other hand, processes with one or two leptons in the final state have small cross sections, *i.e.* $\lesssim \mathcal{O}(10\, fb)$.

4.4. Conclusion of Section 4

In supersymmetric models it is essential to know the nature of the LSP, since it is involved in practically all collider signals. In the MSSM the LSP is necessarily the lightest neutralino. However, in B_3 mSUGRA models this is not the case. In Sect. 4 we have analyzed in detail which B_3 mSUGRA parameter region leads to a sneutrino LSP. In particular, we have found that a coupling $\lambda'_{ijk} = \mathcal{O}(10^{-1})$ at the GUT scale will lead to a sneutrino LSP due to additional B_3 terms in the RGEs. We have shown, that such a large coupling can still be consistent with experiment, for a $\tilde{\nu}_{\mu,\tau}$ LSP. A $\tilde{\nu}_e$ LSP is disfavoured due to the strong low energy bounds on the couplings λ'_{1jk} from, for example, atomic parity violation measurements, see Table 4.1.

We have explored which conditions at the GUT scale lead to a sneutrino LSP. We have shown that a negative trilinear scalar coupling A_0 with a large magnitude enhances the negative B_3 contribution to the sneutrino mass. We have found large regions in the B_3 mSUGRA parameter space, where the sneutrino is the LSP and which are consistent with the observed anomalous magnetic moment of the muon, $a_\mu^{\rm exp}$, as well as with the experimental value for the BR($b \to s\gamma$), see Fig. 4.4 and Fig. 4.5. The allowed $\tilde{\nu}_\mu$ LSP parameter space is hereby larger than the $\tilde{\nu}_\tau$ LSP parameter space. We have also shown that $a_\mu^{\rm exp}$ puts an upper bound of roughly 300 GeV on the sneutrino LSP mass.

We have next investigated the phenomenology of sneutrino LSP models at the LHC. We have considered one benchmark scenario of supersymmetric parameters with a $\tilde{\nu}_\mu$ LSP which is obtained via $\lambda'_{231}|_{\rm GUT} = 0.11$. Within this scenario, we have found that direct decays of light as well as heavy SUSY particles lead to an excess of muons beyond the SM expectation in the final state, *cf.* Table 4.4. We also have found that signatures from pair production of SUSY particles are more promising than from single sparticle production, since the latter

mainly involve hadronic final states. Promising pair production signatures are high-p_T muons of a few hundred GeV, *cf.* Fig. 4.7, high-p_T jets, like-sign dimuon events and long-lived taus with a detached vertex of $\mathcal{O}(1\text{cm})$.

These signatures should be investigated by the experimental groups in order to find supersymmetry as well as to distinguish B_3 mSUGRA with a sneutrino LSP from "normal" mSUGRA with a stable neutralino LSP.

5. $\tilde{\tau}_1$ LSP Phenomenology: Two- versus Four-Body Decay Modes and Resonant Single Slepton Production at the LHC as an Example

If they exist, supersymmetric particles are typically much heavier than their SM partners and at colliders will mostly decay rapidly. This leads to cascade decay chains in the detector to the LSP. The nature of the LSP and its possible decay modes is thus an essential feature for all supersymmetric signatures. It is the purpose of this section to study a novel supersymmetric phenomenology, namely with the scalar tau (stau), $\tilde{\tau}_1$, as the LSP [58, 106]; see also Fig. 2.3. In particular, we analyze in detail the potential $\tilde{\tau}_1$ decays in baryon-triality, B_3, mSUGRA models[1], *cf.* Sect. 2.3 and Sect. 2.4.3. We concentrate on scenarios, where we have a dominant $L_iQ_j\bar{D}_k$ operator, Eq. (2.6), at the grand unification scale. Since the LSP is not stable, we are not restricted to the neutralino as the LSP [41]. We then study the discovery potential of a specific signature in this framework, namely resonant single slepton production at the LHC, resulting in multiple muons in the final state.

$\tilde{\tau}_1$ LSP scenarios have been studied in the literature in Refs. [58, 106, 110, 206, 207, 208, 209, 210, 211]. As we now discuss, we go beyond this work in several aspects.

5.1. New Phenomenology and Outline

The $\tilde{\tau}_1$ LSP might decay via the dominant $L_iQ_j\bar{D}_k$ operator, Eq. (2.6); for example via a 4-body decay in the presence of a non-vanishing λ'_{211}

$$\tilde{\tau}_1^- \xrightarrow{\lambda'_{211}} \tau^-\mu^- u\bar{d}\,. \tag{5.1}$$

An important feature of B_3 mSUGRA models is that additional B_3 couplings are generated via the renormalization group equation (RGE) running [58, 85, 100, 102, 103, 104, 105]. These new couplings can lead to 2-body decays of the $\tilde{\tau}_1$ LSP. For example, λ'_{211} will generate λ_{233} which allows for the decay

$$\tilde{\tau}_1^- \xrightarrow{\lambda_{233}} \mu^-\nu_\tau\,. \tag{5.2}$$

Even though $\lambda_{233} \ll \lambda'_{211}$, this might be the dominant decay mode. The decay, Eq. (5.1), is suppressed by phase space and heavy propagators.

[1] We also refer to the P_6 violating mSUGRA model as the B_3 mSUGRA model, if only lepton-number is violated.

We analyze in the following in detail the conditions for a dominance of the 2-body decay over the 4-body decay. We provide for the first time an extensive study of B_3 $\tilde{\tau}_1$ LSP decays and extend and specify thus the results of Ref. [211], where a first estimate has been performed. This is useful when studying both pair produced and singly produced SUSY particles within the B_3 mSUGRA model. Typically all heavy SUSY particle decay to the ($\tilde{\tau}_1$) LSP.

In the second half of Sect. 5, we consider the B_3 mSUGRA model with a $\tilde{\tau}_1$ LSP and focus on resonant single (left-handed) charged slepton, $\tilde{\ell}_{Li}$, and sneutrino, $\tilde{\nu}_i$, production at hadron colliders, which proceeds via a dominant $L_iQ_j\bar{D}_k$ operator:

$$\bar{u}_j d_k \xrightarrow{\lambda'_{ijk}} \tilde{\ell}^-_{Li}\,, \tag{5.3}$$

$$\bar{d}_j d_k \xrightarrow{\lambda'_{ijk}} \tilde{\nu}_i. \tag{5.4}$$

Here, u_j (d_k) is an up-type (down-type) quark of generation j (k).

Single slepton production allows us also to study two B_3 couplings at a time, depending on the scenario. The slepton is always produced via a λ' whereas the decay of the $\tilde{\tau}_1$ LSP in the decay chain of the slepton might proceed via a generated λ, *cf.* Eq (5.2).

Single slepton production within a $\tilde{\chi}^0_1$ LSP scenario leads to like-sign dileptons in the final state and has thus a very promising signature for experimental studies, see Refs. [112, 212, 213, 214, 215]. Here we show that for a $\tilde{\tau}_1$ LSP, we also obtain like-sign dilepton events and additionally events with three or four leptons in the final state. We give event rates for the LHC for two representative sets of B_3 mSUGRA parameters, see Appendix A.3. We also discuss the background, although a detailed signal over background analysis is beyond the scope of this work. This is the first study of single slepton production in $\tilde{\tau}_1$ LSP scenarios.

We assume in the following that only one non-vanishing λ'_{ijk} is present at the grand unification (GUT) scale, $M_{\rm GUT}$, similar to the dominant top Yukawa in the SM. Allowing for more than one coupling leads to stricter bounds [85, 89, 94, 148, 163, 164]. The bounds for a single λ'_{ijk} lie between $\mathcal{O}(1)$ and $\mathcal{O}(10^{-4})$ depending on the flavor indices and sparticle masses. These bounds can be up to four orders of magnitude stronger at $M_{\rm GUT}$ if one includes the generation of neutrino masses [58, 85], *cf.* Sect. 4.1.1. We therefore assume below that $\lambda'_{ijk} \lesssim \mathcal{O}(10^{-2})$ and require it to be consistent with the observed neutrino masses. However, as we have shown in Sect. 4.1.1, $\lambda'_{ijk} \gtrsim \mathcal{O}(10^{-1})$ is possible if one assumes quark mixing dominantly in the up-sector.

Resonant slepton production at hadron colliders via the $L_iQ_j\bar{D}_k$ operator was first investigated in [111, 216], using tree-level production cross sections. Three-lepton final states and like-sign dilepton events were investigated in Refs. [112, 212, 213, 214, 215]. Ref. [217] considered scenarios with a gravitino LSP. Experimental studies by the D0 collaboration at the Tevatron were performed in Refs. [218, 219] assuming a $\tilde{\chi}^0_1$ LSP and a non-vanishing λ'_{211}. The NLO QCD corrections to the cross section were computed in [114, 220, 221, 222]. The SUSY-QCD corrections were included by [114]. The latter can modify the NLO QCD prediction by up to 35%. In Refs. [184, 204, 205] single slepton production in association with a single top quark was considered; see also Sect. 6.

The outline is as follows. We derive in Sect. 5.2 approximate equations for the RGE generation of λ from λ'. In Sect. 5.3, we classify the different decay modes of the $\tilde{\tau}_1$ LSP and investigate the conditions for a dominance of the 2-body decay over the 4-body decay and *vice versa*. In Sect. 5.4, we classify all possible signatures for resonant single slepton production in B_3 mSUGRA models with a $\tilde{\tau}_1$ LSP. In Sect. 5.5 we calculate event rates for like-sign dimuon events as well as for three- and four-muon events, at the LHC. For that purpose, we define two B_3 mSUGRA scenarios with a $\tilde{\tau}_1$ LSP in Appendix A.3, as a reference for phenomenological studies. We also discuss backgrounds and cuts for like-sign dimuon events. We conclude in Sect. 5.6.

5.2. Renormalization Group Running of λ'_{ijk} and λ_{i33}

In the scenarios considered here, the dominant coupling is a λ'_{ijk}; for $i \neq 3$ it does not couple to the $\tilde{\tau}_1$ LSP. However, due to the mixing of different quark flavors, described by the CKM matrix (see Appendix A.1) the RGEs of the B_3 couplings are not independent, but highly coupled. Therefore, a single non-zero λ'_{ijk} at the GUT scale generates a set of other non-zero B_3 couplings at lower scales. Assuming a diagonal charged lepton Yukawa matrix $\mathbf{Y}_E$, Eq. (2.5), only those couplings can be generated which violate the same lepton number as λ'_{ijk}, *i.e.* λ'_{imn} and λ_{ill}. Among those, we want to focus on the λ_{i33} which do couple directly to the $\tilde{\tau}_1$ LSP. No additional source of lepton number violation is introduced.

The aim of this section is to study the RGEs of the dominant λ'_{ijk} and to quantitatively determine the generated λ_{i33}. We then use these results to predict the low energy spectrum of B_3 mSUGRA scenarios, Eq. (2.27), with $\lambda'_{ijk}|_{\rm GUT} \neq 0$. We will also derive approximate formulæ that allow for a numerical implementation of the running of the couplings.

5.2.1. Renormalization Group Equations

The full renormalization group equations for the B_3 couplings λ'_{ijk} and λ_{i33} are [58, 99, 100],

$$16\pi^2 \frac{d}{dt}\lambda'_{ijk} = \lambda'_{ijl}\,\gamma^{D_k}_{D_l} + \lambda'_{ilk}\,\gamma^{Q_j}_{Q_l} + \lambda'_{ljk}\,\gamma^{L_i}_{L_l} - \left(\mathbf{Y}_D\right)_{jk}\gamma^{L_i}_{H_1}, \tag{5.5}$$

$$16\pi^2 \frac{d}{dt}\lambda_{i33} = \lambda_{i3l}\,\gamma^{E_3}_{E_l} + \lambda_{il3}\,\gamma^{L_3}_{L_l} + \lambda_{l33}\,\gamma^{L_i}_{L_l} - \left(\mathbf{Y}_E\right)_{33}\gamma^{L_i}_{H_1} + \left(\mathbf{Y}_E\right)_{i3}\gamma^{L_3}_{H_1}, \tag{5.6}$$

with $t = \ln Q$, Q being the renormalization scale. The anomalous dimensions γ are listed in Ref. [58] at one-loop level and in Ref. [100] at two-loop level. The RGEs simplify considerably under the assumption of a single dominant B_3 coupling. Products of two or more B_3 couplings including quadratic contributions of the dominant coupling can be neglected

for $\lambda' \lesssim \mathcal{O}(10^{-2})$. In this limit, the one-loop anomalous dimensions read

$$\begin{aligned}
\gamma^{Q_i}_{Q_j} &= \big(\mathbf{Y}_D\mathbf{Y}_D^+\big)_{ij} + \big(\mathbf{Y}_U\mathbf{Y}_U^+\big)_{ij} - \delta^i_j\Big(\frac{1}{30}g_1^2 + \frac{3}{2}g_2^2 + \frac{8}{3}g_3^2\Big),\\
\gamma^{D_i}_{D_j} &= 2\big(\mathbf{Y}_D^+\mathbf{Y}_D\big)_{ji} - \delta^i_j\Big(\frac{2}{15}g_1^2 + \frac{8}{3}g_3^2\Big),\\
\gamma^{L_i}_{L_j} &= \big(\mathbf{Y}_E\mathbf{Y}_E^+\big)_{ij} - \delta^i_j\Big(\frac{3}{10}g_1^2 + \frac{3}{2}g_2^2\Big),\\
\gamma^{E_i}_{E_j} &= 2\big(\mathbf{Y}_E^+\mathbf{Y}_E\big)_{ji} - \delta^i_j\Big(\frac{6}{5}g_1^2\Big),\\
\gamma^{L_i}_{H_1} &= -3\lambda'_{iaq}\big(\mathbf{Y}_D\big)_{aq} - \lambda_{ibq}\big(\mathbf{Y}_E\big)_{bq}\,.
\end{aligned} \tag{5.7}$$

From Eq. (5.6) and Eq. (5.7), we see that the terms related to $\gamma^{L_i}_{H_1}$ allow for the dynamical generation of λ_{i33} by a non-zero λ'_{iaq} coupling [and *vice versa* for Eq. (5.5)]. All other terms in Eq. (5.6) only alter the running of λ_{i33} once it is generated. The RGEs can be further simplified. At one-loop level, all B_3 couplings but the dominant λ'_{ijk} and the generated λ_{i33} can be neglected in the RGEs since they must be generated first by λ' and thus contribute at two-loop level only.

Since we work in a diagonal charged lepton Yukawa basis, the last term in Eq. (5.6), proportional to $\big(\mathbf{Y}_E\big)_{i3}$ does not contribute to the running of λ_{i33}. It is only non-zero if $i = 3$, but owing to the ij-antisymmetry of λ_{ijk} no coupling is generated in this case ($\lambda_{333} = 0$).

Next, a general ordering of the parameters in the anomalous dimensions is[2]

$$g_3^2 > \big(\mathbf{Y}_U\big)^2_{33} > g_2^2 > g_1^2 > \big(\mathbf{Y}_D\big)^2_{33} > \big(\mathbf{Y}_E\big)^2_{33}, \tag{5.8}$$

and all other entries of the $\mathbf{Y}$ matrices are smaller by at least one order of magnitude[3]. The contributions to the RGEs are thus largest for diagonal anomalous dimensions.

As a result, the RGEs for a non-zero λ'_{ijk} at the GUT scale and a generated λ_{i33} reduce to

$$\begin{aligned}
16\pi^2\frac{d}{dt}\lambda'_{ijk} = \lambda'_{ijk}\Big[&-\frac{7}{15}g_1^2 - 3g_2^2 - \frac{16}{3}g_3^2 + \big(\mathbf{Y}_D\big)^2_{33}\big(2\delta_{k3} + \delta_{j3} + 3\delta_{j3}\delta_{k3}\big)\\
&+ \big(\mathbf{Y}_U\big)^2_{33}\delta_{j3} + \big(\mathbf{Y}_E\big)^2_{33}\delta_{i3}\Big],
\end{aligned} \tag{5.9}$$

$$16\pi^2\frac{d}{dt}\lambda_{i33} = \lambda_{i33}\Big[-\frac{9}{5}g_1^2 - 3g_2^2 + 4\big(\mathbf{Y}_E\big)^2_{33}\Big] + 3\lambda'_{ijk}\big(\mathbf{Y}_E\big)_{33}\big(\mathbf{Y}_D\big)_{jk}\,. \tag{5.10}$$

A similar analytical approximation for the generation of λ is derived in Ref. [211]. But the effect of the gauge couplings is neglected there. See also Ref. [102].

The last term in Eq. (5.10) induces the dynamical generation of λ_{i33}. Diagrammatically, this process can be understood as shown in Fig. 5.1. We see that at one-loop the lepton-doublet superfield mixes with the Higgs doublet superfield H_d via the B_3 coupling λ'_{ijk} and

[2] $\tan\beta$ will increase $\big(\mathbf{Y}_D\big)$ and $\big(\mathbf{Y}_E\big)$, *cf.* Eqs. (A.6)-(A.8). Thus for $\tan\beta \gtrsim 30$, the ordering of the parameters can change to $\big(\mathbf{Y}_D\big)^2_{33} > \big(\mathbf{Y}_E\big)^2_{33} > g_1^2$.

[3] Note that the charm Yukawa coupling $\big(\mathbf{Y}_U\big)_{22}$ is roughly equal to the tau Yukawa coupling $\big(\mathbf{Y}_E\big)_{33}$ if $\tan\beta = \mathcal{O}(1)$. We have neglected the charm Yukawa coupling, because we will assume that $\tan\beta = \mathcal{O}(10)$.

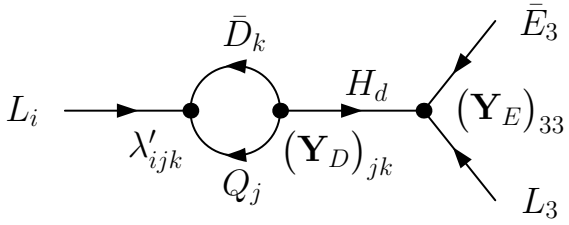

Figure 5.1.: Superfield diagram for the dynamical generation of λ_{i33} by λ'_{ijk} at one loop order, see Eq. (5.10).

the down quark Yukawa coupling $(\mathbf{Y}_D)_{jk}$. H_d then couples via the tau Yukawa coupling $(\mathbf{Y}_E)_{33}$ purely leptonically. The resulting effective interaction is of the λ_{i33}-type.

It is important to notice that the generation is related to $(\mathbf{Y}_D)_{jk}$. Whether a given λ'_{ijk} can generate λ_{i33} or not depends on whether $(\mathbf{Y}_D)_{jk} \neq 0$. For $j \neq k$ it thus depends crucially on the origin of the CKM mixing: is it dominantly down-type or up-type mixing, *cf.* Appendix A.1. In case of down-type mixing, all entries of the $\mathbf{Y}_D$ matrix are non-zero and all λ'_{ijk} can therefore generate a λ_{i33}. In contrast, if the quark mixing takes place in the up-sector, only the diagonal entries of $\mathbf{Y}_D$ are non-zero and $j = k$ is required. The flavor and size of the generated coupling depends on $\tan\beta$ and on the precise j, k configuration. A strong ordering is expected that goes along with the ordering of the entries of the $\mathbf{Y}_D$ matrix.

In order to study the running of the B_3 couplings, the RGEs for the Yukawa matrix elements $(\mathbf{Y}_D)_{jk}$, $(\mathbf{Y}_U)_{33}$, and $(\mathbf{Y}_E)_{33}$ and the gauge couplings are also needed. The full RGEs for the Yukawa couplings are given in Refs. [58, 99]. Applying the single coupling dominance hypothesis, neglecting quadratic terms in λ'_{ijk}, and considering only the dominant terms, Eq. (5.8), they read

$$16\pi^2 \frac{d}{dt}(\mathbf{Y}_U)_{33} = (\mathbf{Y}_U)_{33}\Big[-\frac{13}{15}g_1^2 - 3g_2^2 - \frac{16}{3}g_3^2 + 6(\mathbf{Y}_U)^2_{33} + (\mathbf{Y}_D)^2_{33}\Big], \tag{5.11}$$

$$16\pi^2 \frac{d}{dt}(\mathbf{Y}_E)_{33} = (\mathbf{Y}_E)_{33}\Big[-\frac{9}{5}g_1^2 - 3g_2^2 + 4(\mathbf{Y}_E)^2_{33} + 3(\mathbf{Y}_D)^2_{33}\Big], \tag{5.12}$$

$$\begin{aligned} 16\pi^2 \frac{d}{dt}(\mathbf{Y}_D)_{jk} = (\mathbf{Y}_D)_{jk}\Big[&-\frac{7}{15}g_1^2 - 3g_2^2 - \frac{16}{3}g_3^2 + (\mathbf{Y}_D)^2_{33}(3 + \delta_{j3} + 2\delta_{k3}) \\ &+ (\mathbf{Y}_U)^2_{33}\delta_{j3} + (\mathbf{Y}_E)^2_{33}\Big]. \end{aligned} \tag{5.13}$$

The one-loop order RGEs for the three gauge couplings within the SSM are given by [99]

$$16\pi^2 \frac{d}{dt} g_i = b_i\, g_i^3, \tag{5.14}$$

with $b_i = \{33/5,\, 1,\, -3\}$ for $i = 1, 2, 3$. Thus in total, a set of nine coupled differential equations, Eq. (5.9) - Eq. (5.14), has to be solved[4].

[4] In case of $j = k = 3$ only 8 equations need to be solved. But this implies that the slepton has to be produced by parton quarks of the third generation which is strongly suppressed due to their negligible parton density.

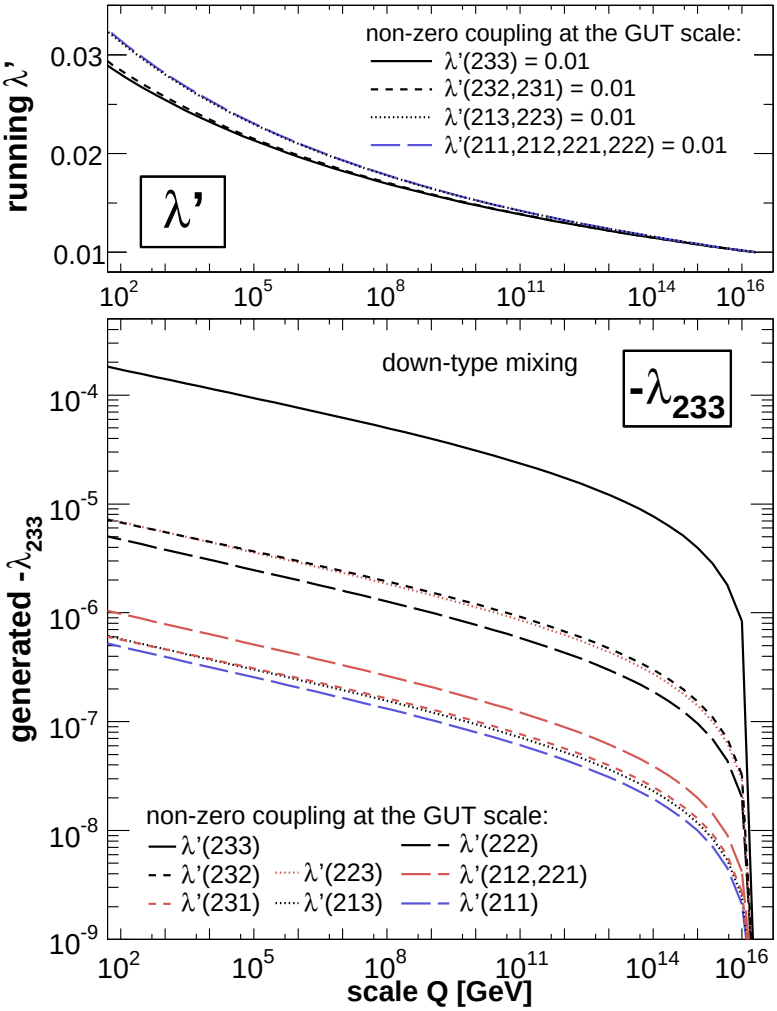

Figure 5.2.: Running of B_3 couplings assuming a single non-zero $\lambda' = 0.01$ coupling at the GUT scale (upper panel) leading to a non-zero λ_{233} coupling (lower panel) at lower scales within the B_3 mSUGRA scenario Set A (Appendix A.3) for down-type mixing.

5.2.2. Numerical Results

For the numerical implementation of the RGEs we start from the framework provided by `SOFTSUSY2.0.10` [145, 147]. First, `SOFTSUSY` evaluates all necessary parameters at the SUSY scale

$$Q_{\text{susy}} = \sqrt{m_{\tilde{t}_1}(Q_{\text{susy}})\, m_{\tilde{t}_2}(Q_{\text{susy}})}\ . \tag{5.15}$$

In a second step, we apply the (proton-hexality conserving) RGEs, Eq. (5.11)-Eq. (5.14), to run the Yukawa couplings and gauge couplings up to the GUT scale. Here we add the B_3 couplings $\lambda'_{ijk}|_{\text{GUT}} \neq 0$ and $\lambda_{i33}|_{\text{GUT}} = 0$ and evolve these couplings down to the scale Q using the above given B_3 RGEs, Eq. (5.9) and Eq. (5.10). We have implemented the RGEs using a standard Runge Kutta formalism [223].

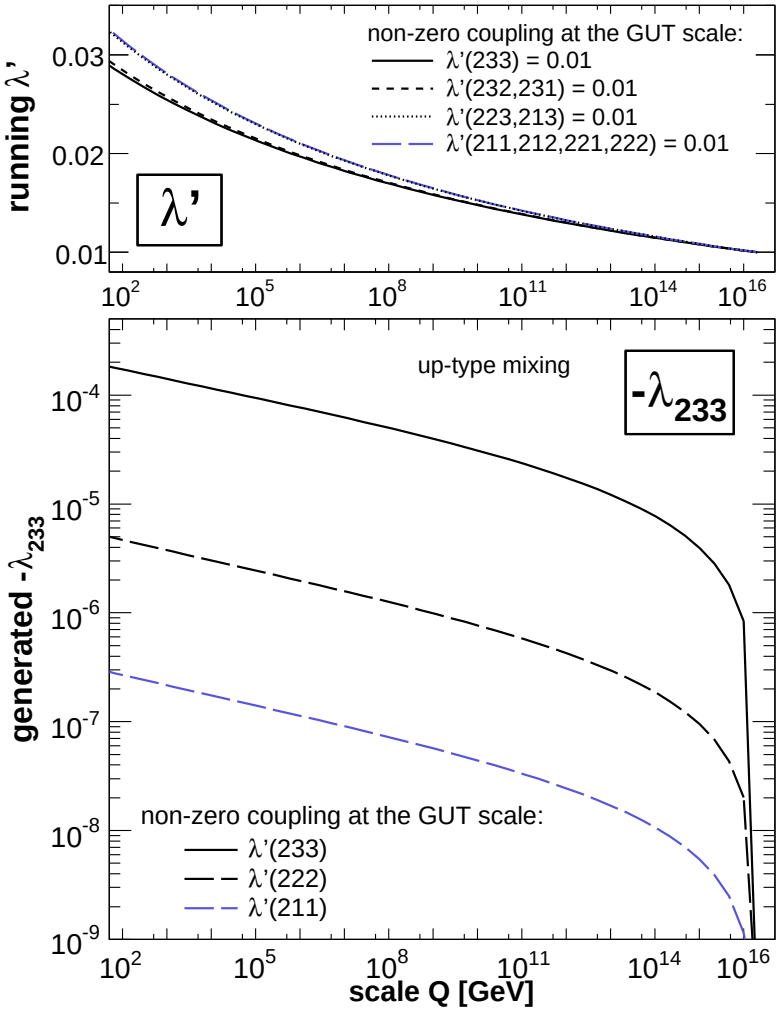

Figure 5.3.: Same as Fig. 5.2, but for quark mixing in the up-sector.

In Fig. 5.2 and Fig. 5.3, we show the running of different λ'_{2jk} couplings, starting with $\lambda'_{ijk}|_{\rm GUT} = 0.01$, for the case of down- and up-mixing respectively, *cf.* Appendix A.1. In the corresponding lower panel, we show the scale dependence of the generated $\lambda_{323} = -\lambda_{233}$ coupling. Here, we use the mSUGRA parameters of Set A ($\tan\beta = 13$), *cf.* Appendix A.3.

We see that the dominant λ'_{ijk} coupling grows by about a factor of 3, running from the GUT scale to the weak scale. This effect is mainly due to the gauge couplings, see Ref. [102], where the Yukawa couplings were omitted. Including the Yukawa couplings reduces this effect, maximally for $j = k = 3$. The generated λ_{233} coupling is at least two orders of magnitude smaller than the original λ' coupling. Furthermore it depends sensitively on the flavor structure (ijk) of the original λ' coupling. This reflects the dependence on the Yukawa matrix $\left(\mathbf{Y}_D\right)_{jk}$. In case of down-type mixing, the ordering of the corresponding entries is

$$\left(\mathbf{Y}_D\right)_{33} > \left(\mathbf{Y}_D\right)_{23,32} > \left(\mathbf{Y}_D\right)_{22} > \left(\mathbf{Y}_D\right)_{12,21} > \left(\mathbf{Y}_D\right)_{13,31} > \left(\mathbf{Y}_D\right)_{11}, \qquad (5.16)$$

Set	λ'_{ijk}		λ_{i33} (down-type mixing)		λ_{i33} (up-type mixing)	
A	Eq. (5.9)	SOFTSUSY	Eq. (5.10)	SOFTSUSY	Eq. (5.10)	SOFTSUSY
λ'_{211}	2.82×10^{-2}	2.85×10^{-2}	-3.96×10^{-7}	-3.89×10^{-7}	-2.17×10^{-7}	-2.13×10^{-7}
λ'_{231}	2.58×10^{-2}	2.61×10^{-2}	-4.65×10^{-7}	-4.80×10^{-7}	0	$+2.06 \times 10^{-12}$
λ'_{223}	2.81×10^{-2}	2.83×10^{-2}	-5.55×10^{-6}	-5.73×10^{-6}	0	-8.45×10^{-9}
λ'_{233}	2.55×10^{-2}	2.58×10^{-2}	-1.41×10^{-4}	-1.42×10^{-4}	-1.42×10^{-4}	-1.43×10^{-4}
λ'_{311}	2.81×10^{-2}	2.84×10^{-2}	0	0	0	0

Table 5.1.: Comparison between our results, Eq. (5.9) and Eq. (5.10), and the results of the B_3 version of SOFTSUSY [149, 150, 147] for λ'_{ijk} and the generated coupling λ_{i33} at the SUSY scale, Eq. (5.15). We choose different couplings $\lambda'_{ijk} = 0.01$ at the GUT scale as given in the first column of the table. The running of λ'_{ijk} is the same for down- and up-type quark mixing, *cf.* Appendix A.1. The generation of λ_{i33} depends on the quark mixing assumptions and the values at the SUSY scale are given separately. The remaining mSUGRA parameters are these of Set A, Eq. (A.18).

reflecting precisely the ordering of the generated couplings in Fig. 5.2. Small differences between the couplings generated by λ'_{i23} (λ'_{i13}) or λ'_{i32} (λ'_{i31}) are related to the different running of the respective λ'_{ijk} and $\left(\mathbf{Y}_D\right)_{jk}$ coupling, depending in turn on whether j or k equals 3.

In the case of up-type mixing, Fig. 5.3, not all λ' couplings can generate a λ. Since the down Yukawa coupling is diagonal, $j = k$ is required. Other couplings can generate λ_{i33} at higher loop levels only and are not included in our approximations.

Our results can easily be translated to other scenarios: The running of the dominant coupling λ' is mainly driven by gauge interactions, Eq. (5.9), and thus depends only weakly on the specific SUSY parameters. The dependence of the generated coupling λ on SUSY parameters is more involved but we expect $\tan\beta$ to have the largest impact. In general, the generated λ coupling scales with $\tan^2\beta$,

$$\lambda_{i33} \propto \tan^2\beta\,, \tag{5.17}$$

if $\tan^2\beta \gg 1$. This is because the down-quark Yukawa couplings, $\left(\mathbf{Y}_D\right)_{jk}$ [and the tau Yukawa coupling, $\left(\mathbf{Y}_E\right)_{33}$], are proportional to $1/\cos\beta = \sqrt{1+\tan^2\beta}$, which directly follows from Eqs. (A.6)-(A.8). Therefore the magnitude of the generated λ coupling for other scenarios can be estimated by rescaling λ of Fig. 5.2 and Fig. 5.3 according to Eq. (5.17).

5.2.3. Comparison with the Program SOFTSUSY

In this section, we compare our results for λ'_{ijk} and the generated coupling λ_{i33} at the SUSY scale, Eq. (5.15), with the B_3 version of SOFTSUSY [149, 150, 147]. This version of SOFTSUSY contains the complete one loop RGEs for λ'_{ijk}, Eq. (5.5), and λ_{i33}, Eq. (5.6), without our approximations.

We show in Table 5.1 our results and the results of SOFTSUSY for the case of down-type mixing and up-type mixing (see Appendix A.1) assuming different couplings $\lambda'_{ijk} = 0.01$ at the GUT scale. For the other parameters, we consider the Set A of Eq. (A.18).

At the SUSY scale, the differences between our results and SOFTSUSY for the case of down-type mixing, are less than 2% for all λ'_{ijk} couplings and less than 4% for the λ_{i33}, respectively. In case of up-type mixing, we find the same for the couplings λ'_{ijk} with $j = k$. However for $j \neq k$ and up-type mixing, we observe a discrepancy between our results and SOFTSUSY for the coupling λ_{233} generated by $\lambda'_{223}|_{\rm GUT} \neq 0$ and $\lambda'_{231}|_{\rm GUT} \neq 0$, respectively. This behavior can easily be understood.

The off-diagonal Yukawa matrix elements $(\mathbf{Y}_D)_{jk}$ are equal to zero at the weak scale for up-type mixing. Running from the weak scale to the GUT scale generates Yukawa couplings $(\mathbf{Y}_D)_{jk}$, $j \neq k$, at the one loop level [58, 99]. The generation of λ_{233} via Eq. (5.10) occurs therefore formally at two-loop level and has been neglected in our approximation. In SOFTSUSY this two-loop effect is taken into account and small couplings are generated also for $j \neq k$ and up-type mixing. Compared to the case of down-type mixing, see Table 5.1, the λ_{233} couplings are suppressed by five (with $\lambda'_{231}|_{\rm GUT}= 0.01$) and three (with $\lambda'_{223}|_{\rm GUT}= 0.01$) orders of magnitude. Note that the generation of $(\mathbf{Y}_D)_{jk}$ is not the only two loop effect that enters the full RGEs [58, 99, 100].

Therefore, our approximation for the generation of λ_{i33} by a non-zero λ'_{ijk} at the GUT scale, Eq. (5.10), breaks down in the case of up-type mixing and $j \neq k$. But concerning $\tilde{\tau}_1$ LSP decays, the corresponding 2-body decay branching ratio for λ_{i33} is negligible compared to the 4-body decay branching ratio via λ'_{ijk} and our approximations are applicable for such phenomenological studies. For example, the 2-body decay branching ratio for up-type mixing and $\lambda'_{231}|_{\rm GUT} = 0.01$ or $\lambda'_{223}|_{\rm GUT} = 0.01$ is less than 10^{-4} in Set A.

We conclude that our approximations are valid for the signal and decay rates that we study in this work. We also note that we have provided an independent check of the B_3 version of SOFTSUSY [149, 150]. Using a different set of mSUGRA parameters leads to a similar level of agreement.

5.3. $\tilde{\tau}_1$ LSP Decays in B_3 mSUGRA

5.3.1. General LSP Decay Modes

As we showed in Sect. 5.2, a non-vanishing coupling λ'_{ijk} at the GUT scale generates an additional coupling λ_{i33} at the weak scale which is roughly at least two orders of magnitude smaller than λ'_{ijk}, *cf.* Fig. 5.2 and Fig. 5.3. In this section, we compare the possible decay modes of the LSP via these two couplings for different B_3 scenarios.

First, let us discuss $\tilde{\chi}_1^0$ LSP scenarios. The leading order decay modes of the $\tilde{\chi}_1^0$ LSP via the dominant λ'_{ijk} and the generated λ_{i33} couplings are all three body decays[5],

$$\tilde{\chi}_1^0 \xrightarrow{\lambda'_{ijk}} \begin{cases} \ell_i^+ \, \overline{u}_j \, d_k \\ \ell_i^- \, u_j \, \overline{d}_k \end{cases} , \quad \tilde{\chi}_1^0 \xrightarrow{\lambda'_{ijk}} \begin{cases} \bar{\nu}_i \, \bar{d}_j \, d_k \\ \nu_i \, d_j \, \overline{d}_k \end{cases} , \tag{5.18}$$

[5] We have neglected the decay $\tilde{\chi}_1^0 \to \nu\gamma$ [224], which is suppressed except for very light neutralino masses [225, 226, 227].

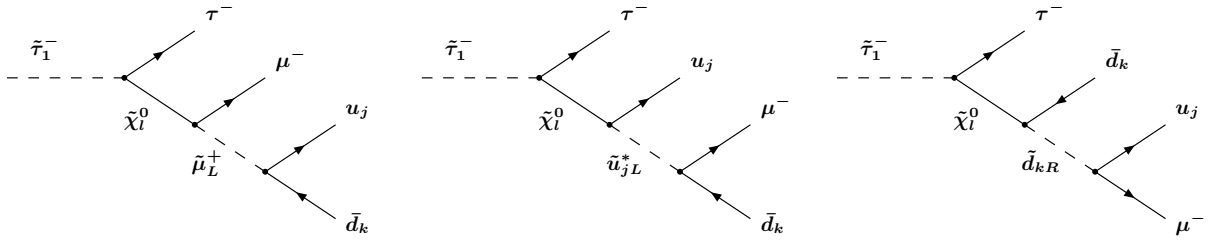

Figure 5.4.: Feynman diagrams contributing to the 4-body decay $\tilde{\tau}_1^- \to \tau^- \mu^- u_j \bar{d}_k$ of the $\tilde{\tau}_1$ LSP via λ'_{2jk}. In this example the $\tilde{\tau}_1$ decays via a virtual neutralino $\tilde{\chi}_l^0$ $(l = 1, 2, 3, 4)$ into a tau, τ^-, a muon, μ^-, an up-type quark, u_j, of generation j and a down-type anti-quark, $\bar{d}_k$, of generation k.

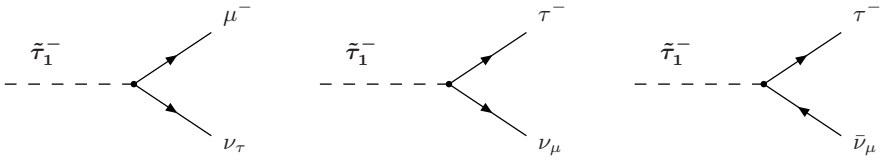

Figure 5.5.: Feynman diagrams leading to the 2-body decays of the $\tilde{\tau}_1$ LSP via the generated coupling λ_{233}. The $\tilde{\tau}_1$ decays either into a muon, μ^-, and a neutrino or into a τ^- and a neutrino.

and

$$\tilde{\chi}_1^0 \xrightarrow{\lambda_{i33}} \begin{cases} \ell_i^+ \, \bar{\nu}_\tau \, \tau^- \\ \ell_i^- \, \nu_\tau \, \tau^+ \end{cases} , \quad \tilde{\chi}_1^0 \xrightarrow{\lambda_{i33}} \begin{cases} \bar{\nu}_i \, \tau^+ \, \tau^- \\ \nu_i \, \tau^- \, \tau^+ \end{cases} . \tag{5.19}$$

The corresponding partial widths depend quadratically on λ'_{ijk} and λ_{i33}, respectively [80, 199, 228, 229, 230]. Therefore, the $\tilde{\chi}_1^0$ decay via λ_{i33} is heavily suppressed and a $\tilde{\chi}_1^0$ LSP decays predominantly via λ'_{ijk} into SM particles.

The situation changes if one considers B_3 mSUGRA scenarios with a $\tilde{\tau}_1$ LSP, where the $\tilde{\tau}_1$ couples not directly to the $L_i Q_j \bar{D}_k$ operator, *i.e.* $i = 1, 2$. In this case, the $\tilde{\tau}_1$ must first couple to a virtual gaugino. The gaugino then couples to a virtual sfermion which then decays via λ'_{ijk}, resulting in a 4-body decay of the $\tilde{\tau}_1$ LSP. The possible decay modes via a virtual neutralino are

$$\tilde{\tau}_1^- \xrightarrow{\lambda'_{ijk}} \begin{cases} \tau^- \, \ell_i^+ \, \overline{u}_j \, d_k \\ \tau^- \, \ell_i^- \, u_j \, \overline{d}_k \\ \tau^- \, \bar{\nu}_i \, \bar{d}_j \, d_k \\ \tau^- \, \nu_i \, d_j \, \overline{d}_k \end{cases} . \tag{5.20}$$

4-body decays via a virtual chargino are also possible but they are suppressed due to the higher chargino mass in comparison to the lightest neutralino mass, $m(\tilde{\chi}_1^\pm) > m(\tilde{\chi}_1^0)$. Furthermore, the (mainly right-handed) $\tilde{\tau}_1$ LSP couples stronger to the (bino-like) lightest neutralino than to the (wino-like) lightest chargino.

On the other hand, the $\tilde{\tau}_1$ can directly decay via λ_{i33} into only two SM particles

$$\tilde{\tau}_1^- \xrightarrow{\lambda_{i33}} \begin{cases} \tau^- \, \bar{\nu}_i \\ \tau^- \, \nu_i \\ \ell_i^- \, \nu_\tau \end{cases} . \tag{5.21}$$

We show in Fig. 5.4 (Fig. 5.5), example diagrams for the 4-body (2-body) decay of a $\tilde{\tau}_1$ LSP via λ'_{2jk} (λ_{233}). Although the 2-body decay suffers from the small coupling, the 4-body decay is phase space suppressed as well as by heavy propagators. Which decay mode dominates depends strongly on the parameters at the GUT scale. We will discuss in detail this topic in the next section.

As a third type of B_3 mSUGRA scenarios we want to mention $\tilde{\tau}_1$ LSP scenarios with a dominant λ'_{3jk} coupling. Here, the dominant B_3 operator couples directly to the $\tilde{\tau}_1$ LSP and allows for a 2-body decay of the $\tilde{\tau}_1$ into two jets,

$$\tilde{\tau}_1^- \xrightarrow{\lambda'_{3jk}} \bar{u}_j d_k \, . \tag{5.22}$$

λ'_{3jk} can not generate λ_{333} via the RGEs, because λ_{ijk} has to be anti-symmetric in the indices i, j. λ_{3nn} with $n \neq 3$ will be generated by the muon ($n = 2$) or electron ($n = 1$) Higgs Yukawa coupling, *cf.* Eq. (5.10). But since these Yukawa couplings are so small, the decay via λ_{3nn} is too small to be seen.

For $j = 3$, the up-type quark in Eq. (5.22) is a top quark and hence the decay Eq. (5.22) is kinematically forbidden for $m_{\tilde{\tau}_1} < m_t$. The $\tilde{\tau}_1$ LSP than decays in a 3-body decay mode via a virtual top quark into a W boson and two jets, where at least one jet is a b jet,

$$\tilde{\tau}_1^- \xrightarrow{\lambda'_{33k}} W^- \, \bar{b} \, d_k \, . \tag{5.23}$$

We present the squared matrix element and the partial width of this process in Appendix B, which to our knowledge has not been given in the literature so far.

5.3.2. Dependence of $\tilde{\tau}_1$ Decays on mSUGRA Parameters

In this section, we investigate the conditions at the GUT scale that lead to 2-body decays of the $\tilde{\tau}_1$ LSP. We assume a non-vanishing λ'_{2jk} coupling at the GUT scale. This can easily be generalized to λ'_{1jk}. We point out that the branching ratios of the $\tilde{\tau}_1$ LSP do not depend on the magnitude of λ'_{ijk}, since they cancel in the ratio. The following discussion is therefore also applicable to scenarios where the couplings are too small to produce a significant number of single slepton events at the LHC but where the $\tilde{\tau}_1$ LSP is produced in cascade decays of pair produced SUSY particles.

For the numerical implementation we use `SOFTSUSY2.0.10` [145, 147] to calculate the mass spectrum at the SUSY scale, Eq. (5.15). In addition, we use our own program to calculate λ'_{ijk} and λ_{i33} at the SUSY scale as described in Sect. 5.2.2. We than pipe the mass spectrum and the couplings through `ISAWIG1.200`, which is linked to `ISAJET7.75` [201]. `ISAJET` calculates the 2-body partial width of the SUSY particles and produces an

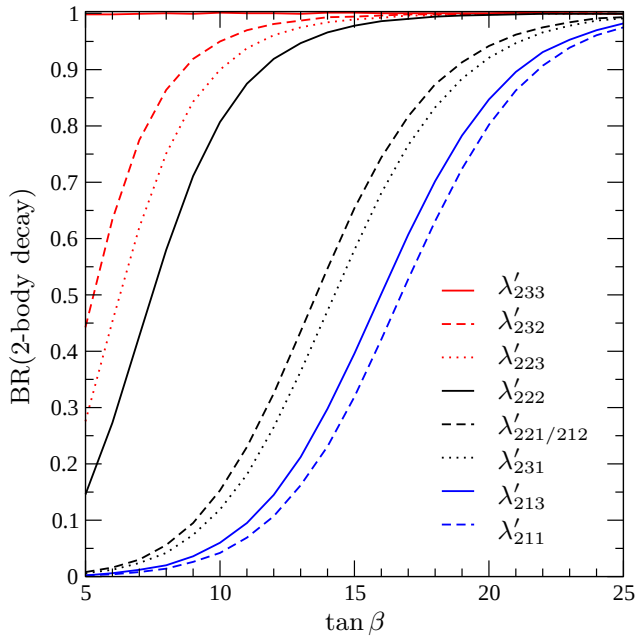

Figure 5.6.: 2-body decay branching ratio as a function of $\tan\beta$ for different dominating λ'_{2jk} couplings at the GUT scale. The quark mixing is in the down sector and the mSUGRA parameters are $M_0 = 0$ GeV, $M_{1/2} = 500$ GeV, $A_0 = 600$ GeV, $\mathrm{sgn}(\mu) = +1$.

output for `HERWIG` [196, 197, 198, 199]. We use a special version of `HERWIG6.510` which also calculates the 4-body decays of the $\tilde{\tau}_1$ LSP [200]. As an output, we consider the total 2-body decay branching ratio of the $\tilde{\tau}_1$ LSP, BR_2. It is defined as

$$\mathrm{BR}_2 = \frac{1}{1 + \Gamma_4/\Gamma_2}, \tag{5.24}$$

where Γ_2 and Γ_4 denote the sums of the partial widths for the 2- and 4-body decays, respectively.

We first show in Fig. 5.6 (Fig. 5.7) the $\tan\beta$ dependence of the 2-body decay branching ratio. We give values for different non-vanishing couplings λ'_{2jk} at the GUT scale and we assume quark mixing in the down (up) sector, *cf.* Appendix A.1.

Nearly all $\tilde{\tau}_1$ LSPs will decay via a 2-body decay for large values of $\tan\beta$, *i.e.* $\tan\beta \gtrsim 30$, and down-type mixing. In the case of up-type mixing this is also true for λ'_{211}, λ'_{222} and λ'_{233}. This behavior can be easily explained with the help of Eq. (5.24). The partial widths Γ_2, Γ_4 can be approximated by [58]

$$\Gamma_2 \;\propto\; \lambda^2_{233}\, m_{\tilde{\tau}_1}\,, \tag{5.25}$$

$$\Gamma_4 \;\propto\; \lambda'^2_{2jk}\, \frac{m^7_{\tilde{\tau}_1}}{m^2_{\tilde{\chi}} m^4_{\tilde{f}}}\,. \tag{5.26}$$

$m_{\tilde{\chi}}$ denotes the mass of the relevant gaugino and $m_{\tilde{f}}$ denotes the mass of the virtual sfermion which couples directly to $L_2 Q_j \bar{D}_k$, *cf.* Fig. 5.4.

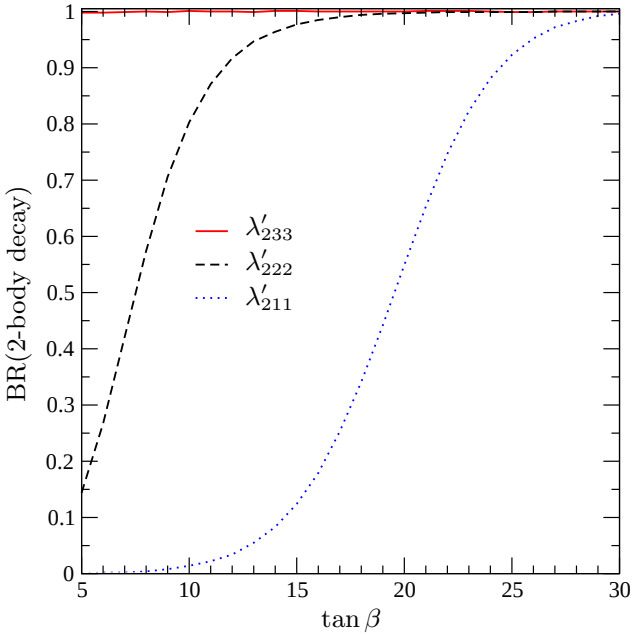

Figure 5.7.: 2-body decay branching ratio as a function of $\tan\beta$ for different dominating λ'_{2jk} couplings at the GUT scale. The quark mixing is in the up sector and the mSUGRA parameters are $M_0 = 0$ GeV, $M_{1/2} = 500$ GeV, $A_0 = 600$ GeV, $\mathrm{sgn}(\mu) = +1$. Couplings λ'_{2jk} for which the 2-body decay branching ratio nearly vanishes are not shown.

As we argued in Sect. 5.2.2, the generated coupling λ_{233} scales roughly with $\tan^2\beta$, *cf.* Eq. (5.17). Therefore, Γ_2 scales with $\tan^4\beta$. At the same time, λ'_{211} is hardly affected by $\tan\beta$. This is the main effect that enhances BR_2 for large $\tan\beta$.

Furthermore, increasing $\tan\beta$ increases the contribution from the tau Yukawa couplings to the various RGEs. This is encoded in the function X_τ, Eq. (A.15), which is proportional to $(1 + \tan^2\beta)$. As can be seen in Eq. (A.15), increasing $\tan\beta$ and X_τ reduces the mass of the right- and left-handed stau and therefore, with Eq. (A.16), the mass of the $\tilde{\tau}_1$ LSP, $m_{\tilde{\tau}_1}$. Furthermore, the off-diagonal matrix elements of the stau mass matrix, Eq. (A.13), also increase with $\tan\beta$. This leads to a stronger mixing between the right- and left-handed stau and lowers the mass of the $\tilde{\tau}_1$, *cf.* Eq. (A.16).

Note that Γ_4/Γ_2 is proportional to $m^6_{\tilde{\tau}_1}$. According to Eq. (5.24), the 2-body decay branching ratio therefore strongly increases for decreasing $m_{\tilde{\tau}_1}$.

We observe in Fig. 5.6 also a large hierarchy between the different couplings λ'_{2jk}. For example, a dominant λ'_{233} coupling leads to $\mathrm{BR}_2 \approx 100\%$ for any value of $\tan\beta$, whereas for λ'_{211} this is only the case for $\tan\beta \gtrsim 25$. This hierarchy reflects the hierarchy of the down quark Yukawa matrix elements, Eq. (5.16), which enter as the dominant term in the RGE of λ_{233}, Eq. (5.10).

For up-type quark mixing, Fig. 5.7, and $j \neq k$ the down-quark Yukawa matrix elements and therefore BR_2 are nearly vanishing.

We investigate the dependence of BR_2 on A_0 in Fig. 5.8, for a dominant coupling λ'_{211} and

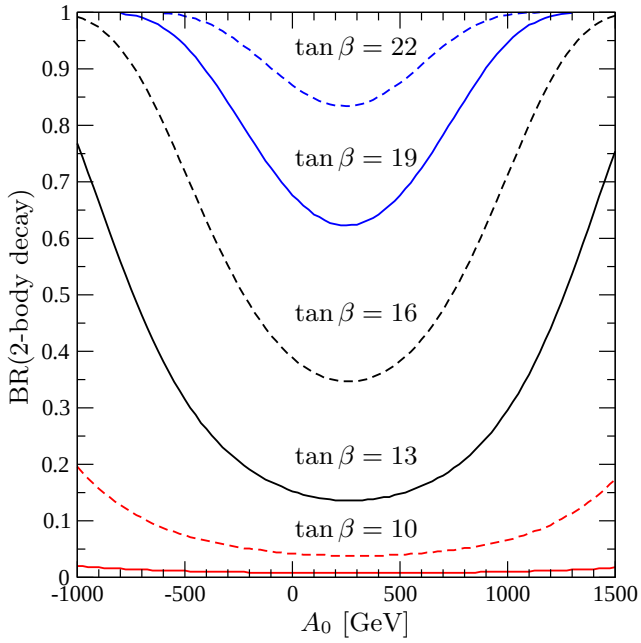

Figure 5.8.: 2-body decay branching ratio as a function of A_0 for non-vanishing λ'_{211} at the GUT scale and different $\tan\beta$. We assume down-type quark mixing. The other mSUGRA parameters are $M_0 = 0$ GeV, $M_{1/2} = 500$ GeV, $\mathrm{sgn}(\mu) = +1$. The solid red curve corresponds to $\tan\beta = 7$.

down-type mixing. We see a minimum at $A_0 \approx 250\,\mathrm{GeV}$. Here, BR_2 is reduced by up to 70% compared to $A_0 = \pm 1\,\mathrm{TeV}$. The minimum and the position of the minimum is dominated by the following two effects.

The right-handed stau couples to a left-handed stau (tau sneutrino) and a neutral Higgs (charged Higgs) via a trilinear scalar interaction $(\mathbf{h}_E)_{33}$, *cf.* Eq. (2.3). The coupling $(\mathbf{h}_E)_{33}$ has dimension one and in mSUGRA models it is equal to $A_0 \times (\mathbf{Y}_E)_{33}$ at the GUT scale. The RGE of the right-handed scalar tau mass, $m_{\tilde{\tau}_R}$, depends in the following way on $(\mathbf{h}_E)^2_{33}$ [58]:

$$\frac{dm^2_{\tilde{\tau}_R}}{dt} = +4(\mathbf{h}_E)^2_{33} + \ldots\,. \tag{5.27}$$

This term decreases $m_{\tilde{\tau}_R}$ when we go from the GUT scale to the SUSY scale, Eq. (5.15), due to the plus sign. The (negative) contribution of this term to $m^2_{\tilde{\tau}_R}$ is proportional to the integral of $(\mathbf{h}_E)^2_{33}$ from $t_{\min} = \ln(M_{\mathrm{SUSY}})$ to $t_{\max} = \ln(M_{\mathrm{GUT}})$. For the mSUGRA parameters given in Fig. 5.8, $M_0 = 0$ GeV, $M_{1/2} = 500$ GeV, $\mathrm{sgn}(\mu) = +1$, the integral of $(\mathbf{h}_E)^2_{33}$ is minimal at $A_0 \approx 180$ GeV and, therefore, $m_{\tilde{\tau}_R}$ is maximal. For $m_{\tilde{\tau}_1} = m_{\tilde{\tau}_R}$ this also leads to a maximum of $\Gamma_4/\Gamma_2 \sim m^6_{\tilde{\tau}_1}$ and hence to a minimum of BR_2; see also the discussion in Sect. 4.2.1.

But the lightest stau is an admixture of the right- and left-handed stau. The off-diagonal mass matrix elements B_{LR}, Eq (A.13), depend also on the value of $(\mathbf{h}_E)_{33}$ at the SUSY scale, Eq. (5.15), through $A_\tau = (\mathbf{h}_E)_{33}/(\mathbf{Y}_E)_{33}$. For $A_0 = 180$ GeV we find $A_\tau \approx -110$ GeV. A negative value of A_τ enhances the effect of L–R-mixing which decreases $m_{\tilde{\tau}_1}$. Therefore, the maximum of $m_{\tilde{\tau}_1}$ as a function of A_0 is shifted to $A_0 \approx 250$ GeV compared to $m_{\tilde{\tau}_R}$. Note

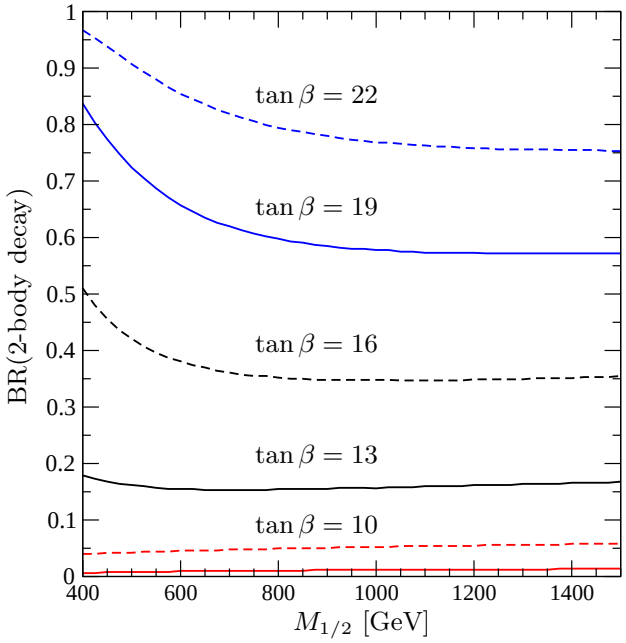

Figure 5.9.: 2-body decay branching ratio as a function of $M_{1/2}$ for non-vanishing λ'_{211} at the GUT scale and different $\tan\beta$. We assume quark mixing in the down sector. The other mSUGRA parameters are $M_0 = 0$ GeV, $A_0 = 600$ GeV, $\mathrm{sgn}(\mu) = +1$. The solid red curve corresponds to $\tan\beta = 7$.

however that the A_τ dependence of stau L–R-mixing is sub-dominant around the minimum because of $\mu \tan\beta \gg A_\tau$.

Next, we study the dependence of BR_2 on the universal gaugino mass $M_{1/2}$. We show this behavior in Fig. 5.9, again for a dominant λ'_{211} and down-type mixing. The 2-body decay branching ratios approach a constant value for increasing $M_{1/2}$. Both, the squared mass of the gauginos, *cf.* Eq. (A.17), and the squared masses of the sfermions, *cf.* Eq. (A.11) and Eq. (A.12), depend linearly on $M^2_{1/2}$. Therefore,

$$\lim_{M_{1/2}\to\infty} \Gamma_4/\Gamma_2 \propto \frac{m^6_{\tilde{\tau}_1}}{m^2_{\tilde{\chi}} m^4_{\tilde{f}}} = \text{constant}\,. \tag{5.28}$$

The dependence of BR_2 on $M_{1/2}$ for $M_{1/2} \lesssim 1$ TeV is more involved, because the ratio Γ_4/Γ_2 depends also on the other mSUGRA parameters, mainly through the running sfermion masses, *cf.* Eq. (A.11) and Eq. (A.12). For example, we observe in Fig. 5.9 that the slope of BR_2 for $M_{1/2} \lesssim 1\,\mathrm{TeV}$ strongly depends on $\tan\beta$. For $\tan\beta = 10$, the slope is small and positive whereas for $\tan\beta \gtrsim 13$ the slope is negative. The magnitude of the slope also increases when we consider larger values of $\tan\beta$. This behavior is again related to the tau Yukawa coupling $(\mathbf{Y}_E)_{33}$, Eq. (2.6), and its effects on the $\tilde{\tau}_1$ mass described by the function X_τ, Eq. (A.15). For large values of $M_{1/2}$, the influence of X_τ on the $\tilde{\tau}_1$ mass nearly vanishes. But as we go to smaller values of $M_{1/2}$ the (negative) contributions due to $(\mathbf{Y}_E)_{33}$ become more and more important. For example, for $\tan\beta = 22$ and $M_{1/2} = 1$ TeV ($M_{1/2} = 400$ GeV)

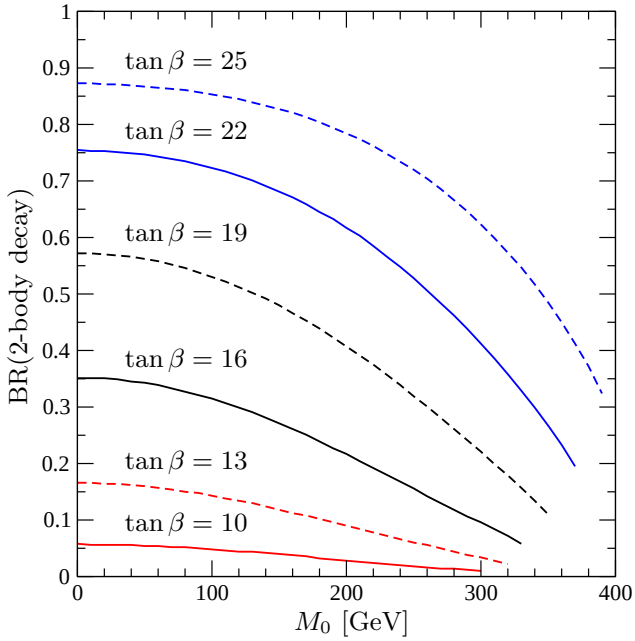

Figure 5.10.: 2-body decay branching ratio as a function of M_0 for non-vanishing λ'_{211} at the GUT scale and different $\tan\beta$. We assume quark mixing in the down sector. The other mSUGRA parameters are $M_{1/2} = 1400$ GeV, $A_0 = 600$ GeV, $\mathrm{sgn}(\mu) = +1$.

the X_τ term reduces the mass of the right-handed stau by 3% (10%) compared to vanishing $(\mathbf{Y}_E)_{33}$. This reduction of $m_{\tilde{\tau}_1}$ will also reduce Γ_4/Γ_2 resulting in an increase of BR_2. This effect is more pronounced for large $\tan\beta$ because X_τ is proportional to $(1 + \tan^2\beta)$. If we neglect the effect of $(\mathbf{Y}_E)_{33}$, the BR_2 curves in Fig. 5.9 all get a small positive slope.

Finally, we show in Fig. 5.10 the dependence of BR_2 on the universal softbreaking scalar mass M_0. Here, we have chosen a rather large value of $M_{1/2}$, $M_{1/2} = 1400$ GeV, because otherwise a $\tilde{\tau}_1$ LSP would exist only in a small interval of M_0.

The behavior of BR_2 can easily be understood. Increasing M_0 increases the mass of the sfermions, Eq. (A.11) and Eq. (A.12), but not the mass of the gauginos. Therefore, the nominator of $\Gamma_4/\Gamma_2 \propto m^6_{\tilde{\tau}_1}/(m^2_{\tilde{\chi}} m^4_{\tilde{f}})$ is a polynomial of order $\mathcal{O}(M_0^6)$, whereas the denominator is only a polynomial of order $\mathcal{O}(M_0^4)$. Therefore, the 2-body decay branching ratios fall off for increasing M_0 as shown in Fig. 5.10. The lines in the figure terminate at values of M_0 above which the $\tilde{\tau}_1$ is no longer the LSP.

5.4. Resonant Single Slepton Production in $\tilde{\tau}_1$ LSP Scenarios

We now apply the previous discussion to resonant single slepton production in B_3 mSUGRA scenarios with a $\tilde{\tau}_1$ LSP. Charged sleptons, $\tilde{\ell}_{Li}$, and sneutrinos, $\tilde{\nu}_i$, can be produced singly on resonance at the LHC via $q_k \bar{q}_j$ annihilation processes, Eq. (5.3) and Eq. (5.4). The

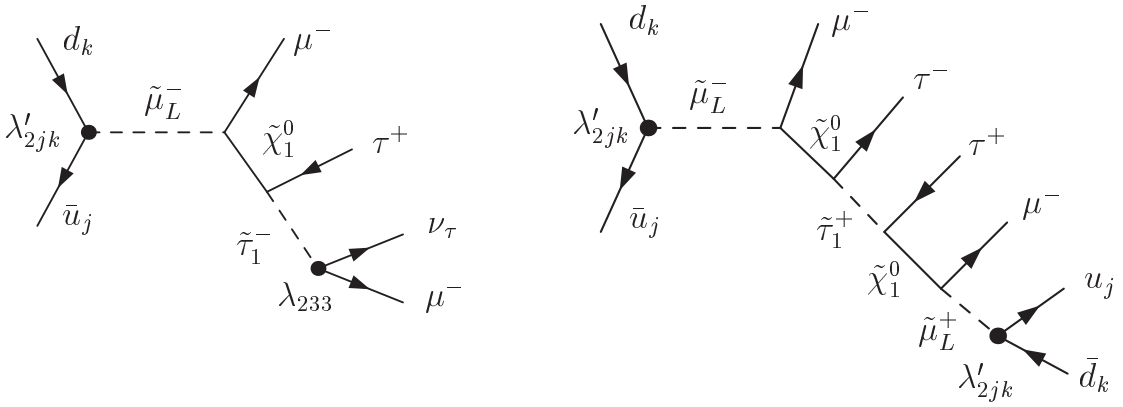

Figure 5.11.: Example Feynman graphs for single slepton production in $\tilde{\tau}_1$ LSP scenarios where the slepton decay proceeds via the generated λ_{233} coupling (2-body decay mode, left graph) and via the dominant λ'_{2jk} coupling (4-body decay mode, right graph).

production cross section is proportional to $|\lambda'_{ijk}|^2$ and therefore large slepton production rates are expected in scenarios with a dominant λ'_{ijk} coupling. The RGE generation of λ_{i33} is important for the subsequent slepton decay in $\tilde{\tau}_1$ LSP scenarios. As discussed in the previous section, a non-vanishing λ_{i33} introduces new 2-body decay channels for the $\tilde{\tau}_1$ LSP. The interplay of these 2-body decays and the 4-body decays via λ'_{ijk} determines the final state signatures. In Fig. 5.11, example Feynman graphs for single slepton production and the subsequent decay in $\tilde{\tau}_1$ LSP scenarios are shown.

It is the aim of this section to first give a general overview of the possible final states for these reactions and second to discuss the special cases $\lambda'_{2jk} \neq 0|_{\mathrm{GUT}}$ and $\lambda'_{3jk} \neq 0|_{\mathrm{GUT}}$ in more detail (Sects. 5.4.2 and 5.4.3).

5.4.1. General Signatures

In the last section, the ratio of 2- to 4-body $\tilde{\tau}_1$ LSP decay rates and its dependence on various SUSY parameters has been studied. Now, we focus on single slepton production in $\tilde{\tau}_1$ LSP scenarios and are interested in the general decay patterns, independent of the precise SUSY parameters. We first give an overview over all possible final states and signatures which could be used as the starting point for an experimental analysis.

A (left-handed) charged slepton or sneutrino can be produced directly via λ'_{ijk} and has several decay modes:

$$\bar{u}_j\, d_k \to \tilde{\ell}_{Li}^- \to \begin{cases} \bar{u}_j d_k \\ \ell_i^-\, \tilde{\chi}_m^0 \\ \nu_i\, \tilde{\chi}_n^- \end{cases} , \tag{5.29}$$

$$\bar{d}_j\, d_k \to \tilde{\nu}_i \to \begin{cases} \bar{d}_j\, d_k \\ \nu_i\, \tilde{\chi}_m^0 \\ \ell_i^-\, \tilde{\chi}_n^+ \end{cases} . \tag{5.30}$$

Both can decay via the B_3 coupling, which is the inverse production process. It is however suppressed by $|\lambda'_{ijk}|^2$. If $\lambda'_{ijk} \leq \mathcal{O}(10^{-2})$, it contributes typically at the percent level. The dominant decay channels are 2-body decays into a lepton-gaugino pair. Further 3- and more-body decays are expected to be negligible, due to phase space suppression and heavy propagators.

In case of $j = 3$, the hadronic production of a charged slepton cannot proceed via two quarks as given in Eq. (5.29), due to the vanishing top-quark parton density inside a proton. Instead, the slepton can for example be produced via a $g\bar{d}_k$ initiated Compton process in association with a single top quark, *cf.* Sect. 6. Furthermore, the decay into $t\bar{d}_k$ may be kinematically forbidden. In this case, the slepton decays via a virtual top. The corresponding decay width is given in Appendix B. Sneutrino production for $j = 3$ is possible, Eq. (5.30), but due to the low bottom-quark density small cross sections are expected. We do not consider $j = 3$ any further here and refer the reader to [184, 204, 205] and Sect. 6 for a detailed investigation of this topic.

For the following discussion, we assume that the produced slepton predominantly decays into a lepton and the lightest neutralino. This assumption is motivated by the fact that we consider $\tilde{\tau}_1$ LSP scenarios. In these scenarios, sleptons are light compared to gauginos and decays into heavier neutralinos or charginos will be kinematically excluded or strongly suppressed. See also the computed branching ratios in explicit SUSY models in Ref. [106] and in Appendix C.

The produced $\tilde{\chi}_1^0$ is not the lightest SUSY particle and will decay further into the $\tilde{\tau}_1$ LSP,

$$\tilde{\chi}_1^0 \to \tau^{\mp}\, \tilde{\tau}_1^{\pm}. \tag{5.31}$$

Since the neutralino is a Majorana fermion, both charge conjugated decays are possible. In most $\tilde{\tau}_1$ LSP scenarios this is the only possible decay mode of the neutralino. However, in some scenarios, the right-handed sleptons $\tilde{\mu}_R$ and $\tilde{e}_R$ are lighter than the $\tilde{\chi}_1^0$ and the additional channels $\tilde{\chi}_1^0 \to \tilde{\ell}_R^{\pm}\ell^{\mp}$ are open (for $\ell = \mu, e$). The $\tilde{\ell}_R$ subsequently decays into the $\tilde{\tau}_1$ LSP, a τ, and a lepton via a virtual neutralino

$$\tilde{\chi}_1^0 \to \ell^{\mp}\, \tilde{\ell}_R^{\pm}, \quad \tilde{\ell}_R^{\pm} \to \begin{cases} \ell^{\pm}\, \tau^{\mp}\, \tilde{\tau}_1^{\pm} \\ \ell^{\pm}\, \tau^{\pm}\, \tilde{\tau}_1^{\mp} \end{cases} . \tag{5.32}$$

These decay chains have smaller BRs than the decays in Eq. (5.31). However, they lead to an additional lepton pair in the final state and could be, therefore, of special interest for experimental analyses.

5.4.2. $\lambda'_{2jk}|_{\rm GUT} \neq 0$, $\lambda_{233} \ll \lambda'_{2jk}$

Let us now study more detailed the final state signatures in a scenario with $\lambda'_{2jk}|_{\rm GUT} \neq 0$ and a generated λ_{233} coupling which is small but non-zero at lower scales. In these scenarios, resonant single $\tilde{\mu}_L$ production and resonant single $\tilde{\nu}_\mu$ production at hadron colliders is possible,

$$\begin{aligned} \bar{u}_j\, d_k &\to \tilde{\mu}_L^- \to \bar{u}_j\, d_k / \mu^-\, \tilde{\chi}_1^0, \\ \bar{d}_j\, d_k &\to \tilde{\nu}_\mu \to \bar{d}_j\, d_k / \nu_\mu\, \tilde{\chi}_1^0. \end{aligned} \tag{5.33}$$

	$\bar{u}_j\, d_k \xrightarrow{\lambda'} \tilde{\mu}_L^- \longrightarrow \bar{u}_j\, d_k / \mu^- \tilde{\chi}_1^0$ or $\bar{d}_j\, d_k \xrightarrow{\lambda'} \tilde{\nu}_\mu \longrightarrow \bar{d}_j\, d_k / \nu_\mu \tilde{\chi}_1^0$	
	$\tilde{\chi}_1^0 \to \tau^+ \tilde{\tau}_1^-$ $\left[\tilde{\chi}_1^0 \to \tau^+ \tilde{\tau}_1^- \ell^+ \ell^-\right]$	$\tilde{\chi}_1^0 \to \tau^- \tilde{\tau}_1^+$ $\left[\tilde{\chi}_1^0 \to \tau^- \tilde{\tau}_1^+ \ell^- \ell^+\right]$
λ'_{2jk}	$\tilde{\tau}_1^- \to \tau^- \mu^- u_j\, d_k$ $\tilde{\tau}_1^- \to \tau^- \mu^+ \bar{u}_j d_k$ $\tilde{\tau}_1^- \to \tau^- \nu_\mu\, d_j\, \bar{d}_k$ $\tilde{\tau}_1^- \to \tau^- \bar{\nu}_\mu\, \bar{d}_j\, d_k$	$\tilde{\tau}_1^+ \to \tau^+ \mu^+ \bar{u}_j\, d_k$ $\tilde{\tau}_1^+ \to \tau^+ \mu^-\, u_j\, \bar{d}_k$ $\tilde{\tau}_1^+ \to \tau^+ \bar{\nu}_\mu\, \bar{d}_j\, d_k$ $\tilde{\tau}_1^+ \to \tau^+ \nu_\mu\, d_j\, \bar{d}_k$
λ_{233}	$\tilde{\tau}_1^- \to \tau^- \nu_\mu$ $\tilde{\tau}_1^- \to \tau^- \bar{\nu}_\mu$ $\tilde{\tau}_1^- \to \mu^- \nu_\tau$	$\tilde{\tau}_1^+ \to \tau^+ \bar{\nu}_\mu$ $\tilde{\tau}_1^+ \to \tau^+ \nu_\mu$ $\tilde{\tau}_1^+ \to \mu^+ \bar{\nu}_\tau$

Table 5.2.: Slepton decay chains with all possible final states for single $\tilde{\mu}_L^-$ and single $\tilde{\nu}_\mu$ production via λ'_{2jk}, respectively. The charge conjugated processes are not shown explicitly. Slepton decays into heavier neutralinos or charginos are neglected. The $\tilde{\chi}_1^0$ decays predominantly into a $\tilde{\tau}_1$ LSP and a τ. In some scenarios, decays as in Eq. (5.32) are possible, they are cited in brackets. Owing to the Majorana type nature of the $\tilde{\chi}_1^0$ two charge conjugated decays of the $\tilde{\chi}_1^0$ are possible (second and third column). In the first column the B_3 coupling involved in the subsequent 4- or 2-body $\tilde{\tau}_1$ decays are given.

As explained above, a small fraction of the sleptons decay via the inverse production process. Predominantly they decay into a lepton and the lightest neutralino, $\tilde{\chi}_1^0$. The decays involving heavier neutralinos or charginos are typically not accessible.

The difference between $\tilde{\mu}_L$ and $\tilde{\nu}_\mu$ production concerns the flavor of the initial quarks involved (which is related to different parton density functions and is thus important for the hadronic cross sections), and the nature of the lepton resulting from the slepton decay. In both processes a neutralino is produced in the predominant decay, which in turn decays into the $\tilde{\tau}_1$ LSP, as given in Eq. (5.31) and Eq. (5.32). Finally, the $\tilde{\tau}_1$ decays either via the dominant λ'_{2jk} coupling (4-body decay) or via the generated λ_{233} coupling (2-body decay). For the 4-body decays, only the decays via virtual neutralinos have to be considered. Decay modes via virtual charginos are suppressed due to the larger mass and their weaker couplings to the predominantly right-handed $\tilde{\tau}_1$ LSP. The complete cascade decay chains are listed in Table 5.2.

A classification of all possible final state signatures is given in Table 5.3, for $\tilde{\mu}_L$ and for $\tilde{\nu}_\mu$ production. For completeness, we include here the direct B_3 decays via λ'_{2jk}, which usually contribute at the percent level for couplings at the order of $\mathcal{O}(10^{-2})$. Neutrinos do not give a signal in a detector and are denoted as missing transverse energy, $\not{E}_T$. Final state quarks are treated as indistinguishable jets, j.

The 4-body decays via λ'_{2jk} and the 2-body decays via the inverse production process lead to two jets in the final state. In contrast, the 2-body decays via λ_{233} are purely leptonic.

	$\tilde{\mu}_L^-$ production				
λ'_{2jk}	$\tau^+\tau^-$	$\mu^-\,\mu^\pm$			jj
	$\tau^+\tau^-$	μ^-		$\not{E}_T$	jj
	$[\,\tau^+\tau^-$	$\mu^-\,\mu^-\,\mu^\pm\,\mu^+$			$jj\,]$
	$[\,\tau^+\tau^-$	$\mu^-\,\mu^-\,\mu^+$		$\not{E}_T$	$jj\,]$
	$[\,\tau^+\tau^-$	$\mu^-\,\mu^\pm$	e^+e^-		$jj\,]$
	$[\,\tau^+\tau^-$	μ^-	$e^+\,e^-$	$\not{E}_T$	$jj\,]$
λ_{233}	$\tau^\pm$	$\mu^-\,\mu^\mp$		$\not{E}_T$	
	$\tau^+\tau^-$	μ^-		$\not{E}_T$	
	$[\,\tau^\pm$	$\mu^-\,\mu^-\,\mu^\mp\,\mu^+$		$\not{E}_T$	$\,]$
	$[\,\tau^+\tau^-$	$\mu^-\,\mu^-\mu^+$		$\not{E}_T$	$\,]$
	$[\,\tau^\pm$	$\mu^-\,\mu^\mp$	$e^+\,e^-$	$\not{E}_T$	$\,]$
	$[\,\tau^+\tau^-$	μ^-	$e^+\,e^-$	$\not{E}_T$	$\,]$
inv. prod.					jj
	$\tilde{\nu}_\mu$ production				
λ'_{2jk}	$\tau^+\tau^-$	$\mu^\pm$		$\not{E}_T$	jj
	$\tau^+\tau^-$			$\not{E}_T$	jj
	$[\,\tau^+\tau^-$	$\mu^-\,\mu^\pm\,\mu^+$		$\not{E}_T$	$jj\,]$
	$[\,\tau^+\tau^-$	$\mu^-\,\mu^+$		$\not{E}_T$	$jj\,]$
	$[\,\tau^+\tau^-$	$\mu^\pm$	$e^+\,e^-$	$\not{E}_T$	$jj\,]$
	$[\,\tau^+\tau^-$		$e^+\,e^-$	$\not{E}_T$	$jj\,]$
λ_{233}	$\tau^\pm$	$\mu^\mp$		$\not{E}_T$	
	$\tau^+\tau^-$			$\not{E}_T$	
	$[\,\tau^\pm$	$\mu^-\,\mu^\mp\,\mu^+$		$\not{E}_T$	$\,]$
	$[\,\tau^+\tau^-$	$\mu^-\,\mu^+$		$\not{E}_T$	$\,]$
	$[\,\tau^\pm$	$\mu^\mp$	$e^+\,e^-$	$\not{E}_T$	$\,]$
	$[\,\tau^+\tau^-$		$e^+\,e^-$	$\not{E}_T$	$\,]$
inv. prod.					jj

Table 5.3.: Summary of all possible final states for single slepton production via λ'_{2jk}. Decays involving the dominant λ'_{2jk} coupling and involving the generated λ_{233} coupling are listed separately, *cf.* Tab. 5.2. If kinematically allowed, the $\tilde{\chi}_1^0$ may also decay into a light-flavor lepton-slepton pair which gives rise to an additional $\mu^+\mu^-$ or e^+e^- pair in the final state. The corresponding signatures are given in brackets. The decay via the inverse production process is also listed.

Many cascade decay chains provide missing transverse energy. Furthermore, since we are considering $\tilde{\tau}_1$ LSP scenarios, there is always at least one τ among the final state particles. The experimentally most promising signatures are most likely those involving a large number of muons, for example like-sign dimuons and three or four final state muons. If the $\tilde{\chi}_1^0$ decays only into $\tilde{\tau}_1\tau$, there are two signatures including like-sign dimuons for $\tilde{\mu}_L$ production. For $\tilde{\nu}_\mu$ production, muons can be produced singly only. But if the decays, Eq. (5.32), are open, both slepton production processes allow for dimuon and trimuon production. In case of $\tilde{\mu}_L$ production, even four final state muons are possible. Additionally, depending on how

easily taus will be identified, an analysis could be based on like-sign $\mu\tau$-pairs.

The final state signatures depend sensitively on which particle is the LSP. Compared to slepton production in the $\tilde{\chi}_1^0$ LSP scenarios [111, 112, 212, 213, 214, 215, 216, 218, 219], there are three main differences here. First, for a $\tilde{\tau}_1$ LSP we have always one or two taus in the final state, which in $\tilde{\chi}_1^0$ LSP scenarios is only possible for smuon production if heavier neutralinos are involved in the decay chain. These heavy neutralinos then decay into the lightest neutralino and possibly taus. Second, the generation of a λ coupling can be neglected in $\tilde{\chi}_1^0$ LSP scenarios. As argued above, λ only allows for additional 3-body decays which are thus not phase-space enhanced compared to the 3-body decays via the dominant λ' coupling. As a consequence, purely leptonic final state signatures are absent in $\tilde{\chi}_1^0$ LSP scenarios. Third, due to the modified spectra in $\tilde{\chi}_1^0$ LSP scenarios, also $\tilde{\nu}_\mu$ production can provide like-sign dimuon events. In this case, $\tilde{\nu}_\mu$ can often decay into a μ and a chargino. Like-sign dimuons arise either if the chargino directly decays via λ' into a μ and two quarks, or if the chargino first decays into the $\tilde{\chi}_1^0$ LSP and then the $\tilde{\chi}_1^0$ LSP decays via λ' into a μ and two quarks.

This discussion can easily be translated to scenarios with $\lambda'_{1jk} \neq 0$ by replacing the muons by electrons (and *vice versa*). Since there is typically no difference in mass between sleptons of the first and second generation, respectively, the kinematics are the same. Note however that the bounds on the B_3 couplings are stronger for λ'_{1jk} than for λ'_{2jk} for example due to the non-observation of neutrinoless double beta decays [85, 89, 94, 148].

5.4.3. $\lambda'_{3jk}|_{\rm GUT} \neq 0$

Some additional remarks are in order for a dominant λ'_{3jk} B_3 coupling. These couplings allow for resonant single $\tilde{\nu}_\tau$ production and, owing to the L-R-mixing in the stau-sector, also both resonant $\tilde{\tau}_1$ and $\tilde{\tau}_2$ production ($j \neq 3$).

For $\tilde{\tau}_1$ production, we refer to the discussion of LSP decay modes in Sect. 5.3.1. Here the LSP couples directly to the B_3 operator and the inverse production process dominates the decay rate,

$$\bar{u}_j\, d_k \to \tilde{\tau}_1^- \to \bar{u}_j\, d_k\,. \tag{5.34}$$

This decay is kinematically accessible if $j \neq 3$. For $j = 3$ the stau decays via a virtual top-quark, *cf.* Eq. (5.23), for $m_{\tilde{\tau}_1} < m_t$. Note that $j = 3$ requires associated production, *e.g.* $g\, d_k \to \tilde{\tau}\, t$, due to the absence of top quarks inside the proton, *cf.* Refs. [184, 204, 205] and Sect. 6.

For $\tilde{\tau}_2$ and $\tilde{\nu}_\tau$ production, there are the following 2-body decay modes:

$$\bar{u}_j\, d_k \to \tilde{\tau}_2^- \to \left\{ \begin{array}{l} \bar{u}_j\, d_k, \\ \tau^-\, \tilde{\chi}_1^0 \\ \tilde{\tau}_1^-\, h^0/Z^0 \end{array} \right. , \tag{5.35}$$

$$\bar{d}_j\, d_k \to \tilde{\nu}_\tau \to \left\{ \begin{array}{l} \bar{d}_j\, d_k, \\ \nu_\tau\, \tilde{\chi}_1^0 \\ \tilde{\tau}_1^-\, W \end{array} \right. . \tag{5.36}$$

The inverse production process contributes and leads to a jj final state. The decay into a lepton and a neutralino often dominates for small $\tan\beta$ ($\tan\beta \lesssim 10$). The neutralino decays further into the $\tilde{\tau}_1$ LSP which directly decays into two quarks:

$$\tilde{\chi}_1^0 \to \tau^\pm \tilde{\tau}_1^\mp, \quad \tilde{\tau}_1^- \to \bar{u}_j d_k \,, \tag{5.37}$$

where we have included the two charge conjugated decays of the neutralino. The final states of these decay modes are $\tau^-\tau^\pm jj$, and there is the possibility of like-sign tau events. If the $\tilde{\chi}_1^0$ decay, Eq. (5.32), is kinematically allowed, we can have an additional pair of electrons or muons in the final state.

The singly produced slepton can also decay into the $\tilde{\tau}_1$ LSP and a SM particle, Z^0, h^0, or W, respectively (final states: $h^0/Z^0/W\,jj$). This decay mode is special for singly produced sleptons of the third generation because they are L-R mixed eigenstates. It can be the dominant decay mode of the $\tilde{\tau}_2$ and $\tilde{\nu}_\tau$, depending on the parameters.

The branching ratios for all B_3 conserving $\tilde{\tau}_2$ and $\tilde{\nu}_\tau$ 2-body decay modes are given in Table C.3 in Appendix C, for the SUSY parameter sets A and B.

5.5. Single Smuon Production: An Explicit Numerical Example

In this section, we present explicit calculations of promising signal rates for resonant slepton production at the LHC in the B_3 mSUGRA model with a $\tilde{\tau}_1$ LSP, focussing on parameter sets A and B, *cf.* Eq. (A.18). First, we consider in Sect. 5.5.1 (exclusive) like-sign dimuon events, *i.e.* events with exactly two muons of the same charge in the final state. An analysis of SM and SUSY backgrounds for the like-sign dimuon signature is given in Sect. 5.5.2. Second, in Sect. 5.5.3, we present event rates for single smuon production leading to three or four muons in the final states, which are kinematically accessible within sets A and B.

5.5.1. Like-Sign Dimuon Events

Following Refs. [112, 212], we first concentrate on events with exclusive like-sign dimuons. Here events with more than two muons are rejected. In this sense, in $\tilde{\tau}_1$ LSP scenarios, only single smuon production leads to exclusive like-sign dimuon pairs, *cf.* Table 5.3. It has been shown in Refs. [112, 212] that this selection criterion enhances the signal to background ratio considerably. In Refs. [112, 212] it was shown that using a set of cuts, the SM background rate at the LHC, $\Gamma_B|_{\rm SM}$, can be reduced to

$$\Gamma_B|_{\rm SM} = 4.9 \pm 1.6 \text{ events}/10 \text{ fb}^{-1}. \tag{5.38}$$

At the same time the cut efficiency, *i.e.* the number of signal events which pass the cuts, lies roughly between 20% and 30%. Note that Refs. [112, 212] assume a $\tilde{\chi}_1^0$ LSP. As we will argue in Sect. 5.5.2, similar cuts are also applicable in $\tilde{\tau}_1$ LSP scenarios. For the numbers presented in this section, however, no cuts are applied and full cross sections and event rates are given.

The total cross section for like-sign dimuon events is given by the resonant $\tilde{\mu}_L^+$ or $\tilde{\mu}_L^-$ production cross section multiplied by the respective branching ratios leading to like-sign dimuon final states. Both decays via the dominant λ'_{2jk} coupling and a generated λ_{233} coupling contribute. For a negatively charged smuon they are:

$$\begin{aligned}
\bar{u}_j\, d_k \xrightarrow{\lambda'} \tilde{\mu}_L^- \to \mu^- \tilde{\chi}_1^0, & \\
& \hookrightarrow \tau^+ \tilde{\tau}_1^- \\
& \qquad \overset{\lambda'}{\hookrightarrow} \tau^- \mu^- u_j\, \bar{d}_k\,, \\
& \qquad \overset{\lambda}{\hookrightarrow} \nu_\tau\, \mu^-\,, \\
& \hookrightarrow \tau^- \tilde{\tau}_1^+ \\
& \qquad \overset{\lambda'}{\hookrightarrow} \tau^+ \mu^- u_j\, \bar{d}_k\,,
\end{aligned} \tag{5.39}$$

plus the analogous decay chains where the neutralino decays first into an $\tilde{e}_R^{\pm}$-$e^{\mp}$ pair, *cf.* Eq. (5.32). The couplings depicted on the arrows indicate the employed B_3 coupling. The decay chain for a positively charged smuon can be obtained by charge conjugation. However, one should keep in mind that the production cross sections for $\tilde{\mu}_L^+$ and $\tilde{\mu}_L^-$ differ at pp colliders, since charge conjugated quarks (and corresponding parton densities) are involved.

The cross sections for the exclusive like-sign dimuon final states are presented in Table 5.4 for Set A and in Table 5.5 for Set B. The smuon production cross sections, $\sigma_{\text{prod.}}(\tilde{\mu}_L^{\mp})$ (see also Table C.1 and Table C.2), include NLO QCD and SUSY-QCD corrections [114]. For the numerical analysis, we only consider couplings λ'_{2jk} that involve partons of the first generation leading to large production cross sections at the LHC.

As already discussed, the $\tilde{\tau}_1$ LSP can either decay via λ' (4-body decay) or via λ (2-body decay). A list of the respective branching ratios is given in Appendix C, Tables C.4 and C.5, for sets A and B and for several λ'_{2jk} couplings. Here we show the resulting cross section times branching ratio, $\sigma_{\text{prod.}} \times \text{BR}_{\lambda'}$ and $\sigma_{\text{prod.}} \times \text{BR}_{\lambda}$, for like-sign dimuon events involving $\tilde{\tau}_1$ decays via λ' and λ, respectively, as described in Eq. (5.39).

The total number of exclusive like-sign dimuon events is given by the integrated luminosity multiplied by the total cross section. In Set A with up-type (down-type) quark mixing (Appendix A.1), we obtain per $10\,\text{fb}^{-1}$

$$\begin{aligned}
N(\mu^-\mu^- + \mu^+\mu^+)/10\,\text{fb}^{-1} &= \Big[\sigma_{\text{prod.}}(\tilde{\mu}_L^-) + \sigma_{\text{prod.}}(\tilde{\mu}_L^+)\Big] \times \Big[\text{BR}_{\lambda'} + \text{BR}_{\lambda}\Big] \times 10 \\
&= \begin{cases} 325 \;\; (330) \\ 110 \;\; (115) \\ 195 \;\; (210) \\ 110 \;\; (115) \end{cases} /10\,\text{fb}^{-1} \quad \text{for} \quad \begin{cases} \lambda'_{211}|_{\text{GUT}} \\ \lambda'_{221}|_{\text{GUT}} \\ \lambda'_{212}|_{\text{GUT}} \\ \lambda'_{213}|_{\text{GUT}} \end{cases} = 0.002.
\end{aligned} \tag{5.40}$$

Note that for up-type mixing, some larger couplings may be considered. From the neutrino mass bounds, also $\lambda'_{211,\,221,\,212,\,213}|_{\text{GUT}} = 0.01$ (and even larger) are allowed. The cross sections are proportional to $|\lambda'|^2$ and thus a five times larger coupling implies cross sections and event numbers multiplied by a factor of 25 compared to those of Table 5.4.

Set A			up-type mixing		down-type mixing	
		$\sigma_{\text{prod.}}(\tilde{\mu}_L^{\mp})$ [fb]	$\sigma_{\text{prod.}} \times \text{BR}_{\lambda'}$	$\sigma_{\text{prod.}} \times \text{BR}_{\lambda}$	$\sigma_{\text{prod.}} \times \text{BR}_{\lambda'}$	$\sigma_{\text{prod.}} \times \text{BR}_{\lambda}$
$\lambda'_{211}\|_{\text{GUT}} = 2 \times 10^{-3}$	$\mu^-\,\mu^-$	61.6	11.1	0.71	9.81	2.09
	$\mu^+\,\mu^+$	108	19.4	1.25	17.2	3.66
$\lambda'_{221}\|_{\text{GUT}} = 2 \times 10^{-3}$	$\mu^-\,\mu^-$	42.0	7.84	–	4.51	3.88
	$\mu^+\,\mu^+$	16.2	3.03	–	1.74	1.50
$\lambda'_{212}\|_{\text{GUT}} = 2 \times 10^{-3}$	$\mu^-\,\mu^-$	18.6	3.46	–	1.99	1.71
	$\mu^+\,\mu^+$	86.0	16.1	–	9.23	7.94
$\lambda'_{213}\|_{\text{GUT}} = 2 \times 10^{-3}$	$\mu^-\,\mu^-$	8.80	1.67	–	1.32	0.40
	$\mu^+\,\mu^+$	49.8	9.43	–	7.43	2.24

Table 5.4.: Cross sections for exclusive like-sign dimuon ($\mu^-\mu^-$ or $\mu^+\mu^+$) final states at the LHC within Set A. In the left column, we present the single-smuon production cross sections, $\sigma_{\text{prod.}}(\tilde{\mu}_L^{\mp})$, see also Tables C.1 and C.2. In the right column, we have folded in the relevant decay branching ratios, in order to obtain like-sign dimuons. All cross sections are given in fb. Where they exist, we have assumed always a cascade of 2-body decays. We consider in turn quark mixing in the up- and down-sector (Appendix A.1), when determining the dominant $\tilde{\tau}_1$ decay mode. The $\tilde{\tau}_1$ LSP can either decay via λ' (4-body decay) or via λ (2-body decay), *cf.* Table 5.2, which leads to different like-sign dimuon cross sections, $\sigma_{\text{prod.}} \times \text{BR}_{\lambda'}$ and $\sigma_{\text{prod.}} \times \text{BR}_{\lambda}$, respectively. The λ'_{2jk} couplings are in accordance with neutrino mass bounds [58]. In case of up-type mixing, larger values of λ'_{2jk} for the four considered couplings are allowed by the neutrino mass bounds. The cross sections scale with $|\lambda'|^2$ and the corresponding rescaling can easily be performed.

Set B			up-type mixing		down-type mixing	
		$\sigma_{\text{prod.}}(\tilde{\mu}_L^{\mp})$ [fb]	$\sigma_{\text{prod.}} \times \text{BR}_{\lambda'}$	$\sigma_{\text{prod.}} \times \text{BR}_{\lambda}$	$\sigma_{\text{prod.}} \times \text{BR}_{\lambda'}$	$\sigma_{\text{prod.}} \times \text{BR}_{\lambda}$
$\lambda'_{211}\|_{\text{GUT}} = 1 \times 10^{-2}$	$\mu^-\,\mu^-$	476	1.04	101	0.21	102
	$\mu^+\,\mu^+$	885	1.93	188	0.39	189
$\lambda'_{221}\|_{\text{GUT}} = 1 \times 10^{-2}$	$\mu^-\,\mu^-$	309	62.8	–	–	66.2
	$\mu^+\,\mu^+$	105	21.4	–	–	22.5
$\lambda'_{212}\|_{\text{GUT}} = 1 \times 10^{-2}$	$\mu^-\,\mu^-$	123	25.1	–	–	26.3
	$\mu^+\,\mu^+$	681	139	–	–	146
$\lambda'_{213}\|_{\text{GUT}} = 1 \times 10^{-2}$	$\mu^-\,\mu^-$	54.6	11.2	–	0.02	11.7
	$\mu^+\,\mu^+$	370	75.6	–	0.16	79.4

Table 5.5.: Same as Table 5.4 but for single slepton production within Set B. The neutrino mass bounds are less restrictive in the case of Set B and $\lambda'_{2jk}|_{\text{GUT}} = 0.01$ are considered for both up- and down-type quark mixing. All cross sections are given in fb.

For Set B, $\lambda'_{2jk}|_{\rm GUT} = 0.01$ is allowed for both up- and down-type mixing. The numbers of like-sign dimuon events are,

$$N(\mu^-\mu^- + \mu^+\mu^+)/10\,\text{fb}^{-1} = \begin{cases} 2920\,(2920) \\ 840\ \ (890) \\ 1640\,(1720) \\ 870\ \ (910) \end{cases} /10\,\text{fb}^{-1} \quad \text{for} \quad \begin{cases} \lambda'_{211}|_{\rm GUT} \\ \lambda'_{221}|_{\rm GUT} \\ \lambda'_{212}|_{\rm GUT} \\ \lambda'_{213}|_{\rm GUT} \end{cases} = 0.01, \qquad (5.41)$$

for up-type (down-type) quark mixing, respectively.

As can be seen in Eq. (5.40) and Eq. (5.41), for each non-zero λ' coupling the total event numbers for up- and down-mixing are of the same order. But as Table 5.4 and Table 5.5 show, the parts contributing to the event rate can be quite different. In case of up-type mixing and $j \neq k$, the 4-body decays via λ' dominate and the contributions of the 2-body decay are negligible [since the size of the necessary λ coupling is proportional to $\left(\mathbf{Y}_D\right)_{jk}$, Eq. (2.5)]. In contrast, for down-type mixing all four considered couplings can generate a relatively large λ_{233}, *cf.* Fig. 5.2, and the 2-body decay modes contribute considerably. In Set B, where $\tan\beta$ is large and where thus the fraction of 2-body decays is especially high (see discussion of Fig. 5.6), reliable event numbers are only obtained if the generation of λ_{233} is included in the theoretical framework. Moreover, a measurement of the ratio of 2-body to 4-body $\tilde{\tau}_1$ decays can reveal information about where the quark mixing takes place.

For $j = k$, the generation of a λ coupling is also possible in case of up-type mixing. In Set A, the generated λ_{233} is not large enough to allow for large 2-body decay rates. However in Set B, due to the large $\tan\beta$ value, the 2-body decays dominate over the 4-body decays. Thus, the different $\tilde{\tau}_1$ decay modes contain also information about $\tan\beta$.

We present in Table 5.4 and Table 5.5 also the total hadronic cross sections for single smuon production, $\sigma_{\text{prod.}}(\tilde{\mu}_L^{\mp})$. Within one parameter set, the cross sections vary strongly for different λ'_{2jk}. This is of course related to corresponding required parton density functions. The largest cross section is obtained for $\lambda'_{211} \neq 0$, *i.e.* for the processes $\bar{u}\,d \to \tilde{\mu}_L^-$ and $u\,\bar{d} \to \tilde{\mu}_L^+$. Smaller cross sections are obtained for $\lambda'_{212} \neq 0$ (involving an up quark and a strange quark) and the smallest cross section for $\lambda'_{221} \neq 0$ (charm quark and down quark) and $\lambda'_{213} \neq 0$ (up quark together with bottom quark).

Since the LHC is a *pp* collider, there is an asymmetry between the $\tilde{\mu}_L^+$ and $\tilde{\mu}_L^-$ production cross sections. If experimentally a distinction between $\mu^+\mu^+$ and $\mu^-\mu^-$ event rates is found, the ratio can be used to constrain the indices of the non-zero λ'_{2jk} coupling. For example, a non-vanishing coupling λ'_{211} leads to a ratio of $N(\mu^+\mu^+) : N(\mu^-\mu^-) \sim 2 : 1$ in sets A and B, whereas for non-vanishing λ'_{221} the ratio is $1 : 2.5$ in Set A and $1 : 3$ in Set B. The highest event rates are obtained for processes that involve the valence quarks u and d. The charge conjugated processes, involving $\bar{u}$ or $\bar{d}$, are suppressed in comparison. Thus, a larger fraction of $\mu^+\mu^+$ events goes along with $j = 1$ (where the production process is $u\,\bar{d}_k \to \tilde{\mu}_L^+$) and a larger fraction of $\mu^-\mu^-$ events is related to $k = 1$ and $j \neq 1$ (production process $\bar{u}_j\,d \to \tilde{\mu}_L^-$).

5.5.2. Discussion of Background and Cuts for Like-Sign Dimuon Final States

In this section, we discuss the background for like-sign dimuon events from the SM and from SUSY particle pair production via gauge interactions. We follow Refs. [112, 212] closely. There, single smuon production via λ'_{211} was investigated assuming a $\tilde{\chi}_1^0$ LSP. A detailed signal over background analysis was performed based on like-sign dimuon events. We argue that a similar or even the same set of cuts might be used to suppress the background in our case and we compare background and signal rates to determine the discovery potential of our analysis.

The main SM background sources are $t\bar{t}$ production, $b\bar{b}$ production, single top production, and gauge boson pair production, *i.e.* WW, WZ and ZZ production. In Refs. [112, 212], the dominant signature from single smuon production including like-sign dimuon events is

$$\tilde{\mu}_L^- \to \mu^- \tilde{\chi}_1^0 \to \mu^- (\mu^- u \bar{d}), \tag{5.42}$$

The two muons of the signal, Eq. (5.42), are isolated because they stem from different decays of SUSY particles. In addition, the muons carry large momenta since they originate from the decay of (heavy) SUSY particles. The following cuts were proposed to improve the signal over SM background ratio at the LHC:

- The muon rapidity $|\eta| < 2.0$, thus requiring all the leptons in the central region of the detector,
- a cut on the transverse momentum on each muon: $p_T|_\mu \geq 40$ GeV,
- an isolation cut on each of the muons,
- a cut on the transverse mass of each of the muons, 60 GeV $< M_T <$ 85 GeV,
- a veto on the presence of a muon with the opposite charge as the like-sign dimuons,
- a cut on the missing transverse energy, $\not{E}_T \leq 20\,\text{GeV}$.

These cuts reduce the SM background to 4.9 ± 1.6 events per 10 fb^{-1} at the LHC , *cf.* Eq. (5.38). Among the above cuts, the isolation and p_T cut lead to the strongest suppression of the SM background.

We now investigate the case of a $\tilde{\tau}_1$ LSP. If the 4-body decays, Eq. (5.20), of the $\tilde{\tau}_1$ LSP dominate, the leading signature of resonant single smuon production including like-sign dimuon events can be written as

$$\tilde{\mu}_L^- \to \mu^- \tilde{\chi}_1^0 \to \mu^- \tau^\mp \tilde{\tau}_1^\pm \to \mu^- \tau^\mp (\tau^\pm \mu^- u \bar{d}), \tag{5.43}$$

As above, the muons originate from the decay of heavy particles ($\tilde{\tau}_1$ and $\tilde{\mu}_L$), are in general well isolated, and carry large momenta. Thus, for both signals, Eq (5.42) and Eq. (5.43), the same cuts should allow to discriminate between the signal and the SM background. Furthermore, the additional pair of taus in Eq. (5.43) allows to require one or two isolated taus. This might additionally improve the signal to background ratio.

If the $\tilde{\tau}_1$ LSP predominantly decays via 2-body decay modes, Eq. (5.21), the situation is a bit different. The like-sign dimuon signature is now

$$\tilde{\mu}_L^- \to \mu^- \tilde{\chi}_1^0 \to \mu^- \tau^+ \tilde{\tau}_1^- \to \mu^- \tau^+ (\mu^- \nu_\tau), \tag{5.44}$$

Set A	$\sigma(--+)$	$\sigma(++-)$	$\sigma(--++)$	$\sigma(+++-)$	$\sigma(---+)$	$\sum\sigma(--\dots)$	$\sum\sigma(++\dots)$
$\lambda'_{211}=2\times10^{-3}$	9.38 (9.39)	12.9 (13.0)	5.32 (5.26)	3.39 (3.35)	1.93 (1.91)	16.6 (16.6)	21.7 (21.6)
$\lambda'_{221}=2\times10^{-3}$	5.77 (5.77)	3.84 (3.74)	1.89 (1.77)	0.53 (0.49)	1.36 (1.27)	9.02 (8.81)	6.26 (6.00)
$\lambda'_{212}=2\times10^{-3}$	4.02 (3.93)	9.05 (9.24)	3.39 (3.17)	2.79 (2.61)	0.60 (0.56)	8.01 (7.66)	15.2 (15.0)
$\lambda'_{213}=2\times10^{-3}$	2.04 (2.02)	5.14 (5.19)	1.85 (1.80)	1.57 (1.53)	0.28 (0.27)	4.17 (4.09)	8.56 (8.52)

Table 5.6.: Cross sections for signals with three or four final state muons within parameter Set A, assuming down-type (up-type) quark mixing. The couplings λ'_{2jk} are given at $M_{\rm GUT}$. We show the cross sections as defined in Eqs. (5.45)-(5.48) and the sums for two negatively or positively charged muons, $\sum\sigma(--\dots)$ or $\sum\sigma(++\dots)$, respectively. All cross sections are given in fb.

We again have two isolated muons with large momenta and the same isolation and $p_T|_\mu$ cuts as before should be useful to suppress the SM background. But the neutrino of the $\tilde\tau_1$ decay leads to high missing transverse energy $\not{E}_T$ in the signal and an upper bound on $\not{E}_T$ is not appropriate anymore. Alternatively we propose a cut that requires a minimum missing energy, *e.g.* $\not{E}_T \geq 60$ GeV. This would also reduce the SM background where the main source of $\not{E}_T$ are low-energetic neutrinos from W decays. Furthermore, we can again require an additional tau in the final state. Finally, one can exploit the fact that the 2-body decays lead to a pure leptonic final state and a jet veto can be applied.

In Refs. [112, 212], the SUSY background on like-sign dimuon events is suppressed by vetoing all events with more than two jets of $p_T|_{\rm jet} > 50$ GeV. This cut will also work if the 4-body decay mode of the $\tilde\tau_1$ LSP, Eq. (5.20), dominates. The 2-body decay modes lead to purely leptonic final states and even no high-p_T jet may be required.

We conclude that for $\tilde\tau_1$ LSP scenarios, the background for like-sign dimuon events can be suppressed similarly as it has been proposed for $\tilde\chi_1^0$ LSP scenarios in Refs. [112, 212].

We thus compare our signal, as given in Eq. (5.40) and Eq. (5.41) for sets A and B respectively, to the background, assuming that cuts as discussed above reduce the SM background to less than 5 events per 10 fb^{-1}, *cf.* Eq. (5.38). For the signal efficiency, we assume 20%, *i.e.* 20% of signal events pass the cuts. We neglect systematic errors, at this stage of the analysis.

For Set A a more than 5σ excess over the SM background can be obtained for an integrated luminosity of 10 fb^{-1} for all couplings given in Eq. (5.40). For Set B, a cut efficiency of 20% for the signal corresponds to an excess between $100\,\sigma$ and $300\,\sigma$ for the number of like-sign muon events over the SM background! Therefore, within Set B, couplings can be tested at the LHC down to $\lambda'_{2jk}|_{\rm GUT}\sim\mathcal{O}(10^{-3})$. But a detailed Monte-Carlo based signal over background analysis remains to be done.

5.5.3. Final States with 3 and 4 Muons

To round off our studies, we consider in this section final states with more than two muons. For example, for parameter sets A and B, the $\tilde\chi_1^0$ cannot only decay into a $\tilde\tau_1$-τ pair but

Set B	$\sigma(--+)$	$\sigma(++-)$	$\sigma(--++)$	$\sigma(+++-)$	$\sigma(---+)$	$\sum\sigma(--\dots)$	$\sum\sigma(++\dots)$
$\lambda'_{211}=1\times10^{-2}$	20.8 (20.8)	29.1 (29.1)	13.4 (13.4)	8.73 (8.73)	4.69 (4.69)	38.9 (38.9)	51.3 (51.3)
$\lambda'_{221}=1\times10^{-2}$	11.9 (12.0)	7.77 (7.59)	4.08 (3.88)	1.04 (0.98)	3.05 (2.89)	19.1 (18.7)	12.9 (12.4)
$\lambda'_{212}=1\times10^{-2}$	8.14 (7.98)	19.5 (19.9)	7.93 (7.53)	6.72 (6.39)	1.21 (1.15)	17.3 (16.7)	34.2 (33.8)
$\lambda'_{213}=1\times10^{-2}$	3.94 (3.85)	10.4 (10.6)	4.20 (4.00)	3.66 (3.48)	0.54 (0.51)	8.68 (8.36)	18.3 (18.1)

Table 5.7.: Same as Table 5.6 but for single slepton production within Set B. All cross sections are given in fb.

also into a $\tilde{\mu}_R$-μ or $\tilde{e}_R$-e pair. These are kinematically accessible and have non-negligible branching ratios (Set A: 7.0%, Set B: 2.2%; see Table C.3). As we have shown in Table 5.3, these decays lead to three or even four muons of mixed signs in the final state. Each of the muons stems from the decay of a different SUSY particle. Especially the four-muon final state cannot be found at a high rate in $\tilde{\chi}_1^0$ LSP scenarios and its observation could be a hint for a $\tilde{\tau}_1$ LSP. Therefore, we analyze the three- and four-muon final states in this section. All necessary branching ratios and production cross sections are given in Appendix C.

The four–muon events may be classified into $\mu^-\mu^-\mu^-\mu^+$, $\mu^-\mu^-\mu^+\mu^+$, and $\mu^-\mu^+\mu^+\mu^+$ signatures and we introduce the notations $\sigma(---+)$, $\sigma(--++)$, and $\sigma(+++-)$, for the respective cross sections. The four-muon final states require a long decay chain and many different decays contribute at various stages. For smuon production, summing up all contributions, the cross sections can be written in the following compact form

$$\begin{aligned}
\sigma_{\tilde{\mu}}(---+) &= \sigma_{\text{prod.}}(\tilde{\mu}_L^-) \times \text{BR}(\tilde{\mu}_L^- \to \tilde{\chi}_1^0\,\mu^-) \times \text{BR}(\tilde{\chi}_1^0 \to \tilde{\mu}_R^+\,\mu^-) \times P_{\tilde{\tau}_1}(1\mu)\,, \\
\sigma_{\tilde{\mu}}(+++-) &= \sigma_{\tilde{\mu}}(---+) \times \sigma_{\text{prod.}}(\tilde{\mu}_L^+)/\sigma_{\text{prod.}}(\tilde{\mu}_L^-)\,, \\
\sigma_{\tilde{\mu}}(--++) &= \sigma_{\tilde{\mu}}(---+) + \sigma_{\tilde{\mu}}(+++-),
\end{aligned} \tag{5.45}$$

where $P_{\tilde{\tau}_1}(1\mu) = \text{BR}(\tilde{\tau}_1^- \to \mu^- \dots) + \text{BR}(\tilde{\tau}_1^+ \to \mu^- \dots)$ denotes the probability of a negatively charged final state muon in a $\tilde{\tau}_1$ decay. The difference between $\sigma_{\tilde{\mu}}(---+)$ and $\sigma_{\tilde{\mu}}(+++-)$ stems from the different partons and parton densities involved in the production cross sections.

Smuon production can also lead to exactly three final state charged muons, $\mu^-\mu^-\mu^+$ or $\mu^+\mu^+\mu^-$. The corresponding cross sections now involve the probability $P_{\tilde{\tau}_1}(0\mu)$ for a $\tilde{\tau}_1$ decay without a final state muon,

$$\begin{aligned}
\sigma_{\tilde{\mu}}(--+) &= \sigma_{\text{prod.}}(\tilde{\mu}_L^-) \times \text{BR}(\tilde{\mu}_L^- \to \tilde{\chi}_1^0\,\mu^-) \times \text{BR}(\tilde{\chi}_1^0 \to \tilde{\mu}_R^+\,\mu^-) \times 2P_{\tilde{\tau}_1}(0\mu)\,, \\
\sigma_{\tilde{\mu}}(++-) &= \sigma_{\tilde{\mu}}(--+) \times \sigma_{\text{prod.}}(\tilde{\mu}_L^+)/\sigma_{\text{prod.}}(\tilde{\mu}_L^-)\,.
\end{aligned} \tag{5.46}$$

There are 16 different decay chains of the $\tilde{\mu}_L^-$ leading to a $\mu^-\mu^-\mu^+$ final state. The factor of 2 in Eq. (5.46) is a consequence of summing over all these decay chains.

The same final state signatures (exactly three muons) can be obtained via $\tilde{\nu}_\mu$ production. The decay chain is similar to that of a produced smuon. The missing muon from the slepton

decay is here replaced by demanding a muon in the final $\tilde{\tau}_1$ decay,

$$\begin{aligned}\sigma_{\tilde{\nu}}(--+) = &\left[\sigma_{\text{prod.}}(\tilde{\nu}_\mu) + \sigma_{\text{prod.}}(\tilde{\nu}_\mu^*)\right] \\ &\times \text{BR}(\tilde{\nu}_\mu \to \tilde{\chi}_1^0 \nu_\mu) \times \text{BR}(\tilde{\chi}_1^0 \to \tilde{\mu}_R^+ \mu^-) \times P_{\tilde{\tau}_1}(1\mu)\,, \\ \sigma_{\tilde{\nu}}(++-) = &\sigma_{\tilde{\nu}}(--+)\,.\end{aligned} \tag{5.47}$$

The total cross sections for (exactly) three final state muons are then given by

$$\sigma(\mp\mp\pm) = \sigma_{\tilde{\mu}}(\mp\mp\pm) + \sigma_{\tilde{\nu}}(\mp\mp\pm). \tag{5.48}$$

Table 5.6 and Table 5.7 give an overview over the numerical results. The same λ' couplings as in the previous Table 5.4 and Table 5.5 are considered. The generation of λ_{233} has been taken into account for the $\tilde{\tau}_1$ decays and the cross sections give total numbers, including both 4- and 2-body $\tilde{\tau}_1$ decays.

We see that the sum of three– and four-muon events is in the same order of magnitude as the results for purely like-sign dimuons. For Set A, where $\text{BR}(\tilde{\chi}_1^0 \to \tilde{\mu}_R\,\mu) = 7\%$, the event numbers are even larger. In Set B, with $\text{BR}(\tilde{\chi}_1^0 \to \tilde{\mu}_R\,\mu) = 2\%$, the total contributions are smaller by a factor of about three. Depending on the experimental goals, these channels thus give important contributions and should be included in an analysis. On the other hand, these events also suggest to use three or four final state muons as a signal for slepton production since the background is expected to be very low.

5.6. Conclusion of Section 5

B_3 interactions allow for LSP decays and thus reopen large regions in the SUSY parameter space, where the LSP is charged. We have investigated for the first time in detail the phenomenology of B_3 mSUGRA models with a $\tilde{\tau}_1$ LSP. We have hereby assumed only one non-vanishing B_3 coupling λ'_{ijk} at the GUT scale.

An essential feature of the B_3 mSUGRA signatures is the decay of the $\tilde{\tau}_1$ LSP. Given only one B_3 coupling at M_{GUT}, we would expect either a 4-body or 2-body decay of the $\tilde{\tau}_1$ LSP depending on whether it couples directly to the dominant B_3 operator or not. However, in B_3 mSUGRA models the RGEs are highly coupled and further couplings are generated at the weak scale. These are of course suppressed relative to the dominant coupling but may lead to 2-body decays, which have larger phase space and do not involve heavy propagators.

We have here numerically investigated the generation of λ_{i33} couplings via dominant λ'_{ijk} couplings. The generated couplings are typically smaller by at least two orders of magnitude; see Fig. 5.2 and Fig. 5.3. We have then performed a first detailed analysis of the parameter dependence of the $\tilde{\tau}_1$ LSP decay modes. It turned out that in large regions of parameter space the 2-body decay dominates over the 4-body decay, see Figs. 5.6-5.10.

In the second part of Sect. 5, we applied our results to resonant single slepton production at the LHC, which is possible in B_3 scenarios with a non-zero λ'_{ijk} coupling. We first studied the general decay signatures. From the experimental point of view, the final states with two

like-sign or even more charged leptons are of special interest. Each event is also accompanied by at least one tau.

We further investigated numerically single smuon production for $\lambda'_{2jk} \neq 0$ within two representative $\tilde{\tau}_1$ LSP scenarios, *i.e.* for two sets of B_3 mSUGRA parameters. We include the 2-body $\tilde{\tau}_1$ LSP decays via the generated λ_{233} couplings in our analysis. The cross sections for like-sign dimuon final states are given in Table 5.4 and Table 5.5 and those for final states with three or four muons in Table 5.6 and Table 5.7. For example, we found resulting cross sections for exclusive like-sign dimuon events of $\mathcal{O}(100\,\text{fb})$ for $\lambda'_{2jk}|_{\text{GUT}} = 0.01$. Additional three- and four-muon events can occur with the same rate. This is a novel supersymmetry discovery mechanism for the LHC and should be investigated in more detail, also by the LHC experimental groups.

6. Single Slepton Production in Association with a Single Top Quark at the Tevatron and LHC

We have seen in Sect. 5 that a non-vanishing $L_iQ_j\bar{D}_k$ operator, Eq. (2.6), allows for resonant single charged slepton and sneutrino production, Eq. (5.3) and Eq. (5.4), at hadron colliders. As pointed out in Sect. 5, the case $j = 3$ in Eq. (5.3) is special, as there are no top quarks in the incoming proton. Instead, one must consider the production of a single slepton in association with a SM particle.

In this section, we calculate the total cross section for single charged slepton production in association with a top quark at hadron colliders via a non-vanishing $L_iQ_3\bar{D}_k$ operator, Eq. (2.6), in the baryon-triality, B_3, supersymmetric standard model, *cf.* Sect. 2.2 and Sect. 2.3. We compute event rates for the Tevatron and LHC. We study the signatures for different supersymmetric scenarios including neutralino and stau LSPs. We perform a detailed analysis with basic cuts for the B_3 operator λ'_{231} using Monte Carlo simulations to show that the signal can be distinguished from the background at the LHC. In particular we employ the resulting lepton charge asymmetry.

6.1. Introduction and Outline

Several mechanisms for associated single supersymmetry production, *e.g.* $d_j\bar{d}_k \to \tilde{\chi}_1^+\ell_i^-$, have been studied in the literature, see for example Refs. [113, 204, 215, 231, 232]. In the following, we investigate in detail the case of the operator $L_iQ_3\bar{D}_k$. Here, single charged slepton production is only possible in association with a top quark. Before studying the phenomenological details, we first recall the strongest experimental bounds on the couplings λ'_{i3k} at the 2σ level. They are shown in Table 6.1 [85, 89, 94, 148, 163]. We neglect bounds, which assume a specific (SM) quark mixing between the three generations [164] (see also Appendix A.1) or bounds using the renormalization group running of λ'_{i3k} [58, 85, 100].

At leading order there are two production mechanisms for slepton production in association with a top quark. The first mechanism includes the Compton-like processes

$$g + d_k \;\to\; \tilde{\ell}_i^- + t\,, \tag{6.1a}$$
$$g + \bar{d}_k \;\to\; \tilde{\ell}_i^+ + \bar{t}\,. \tag{6.1b}$$

The relevant leading-order diagrams are given in Fig. 6.1. Here, g denotes an incoming gluon in the proton and t a final-state top quark.

λ'_{131}	$0.019 \times (m_{\tilde{t}_L}/100\ \text{GeV})$	λ'_{132}	$0.28 \times (m_{\tilde{t}_L}/100\ \text{GeV})$
λ'_{231}	$0.18 \times (m_{\tilde{b}_L}/100\ \text{GeV})$	λ'_{232}	$0.45\,(m_{\tilde{s}_R} = 100\,\text{GeV})$
λ'_{331}	$0.45\ (m_{\tilde{q}} = 100\,\text{GeV})$	λ'_{332}	$0.45\ (m_{\tilde{q}} = 100\,\text{GeV})$
λ'_{i33}	$\mathcal{O}(10^{-4})$		

Table 6.1.: Upper 2σ bounds on λ'_{i3k}. The strong bounds on λ'_{i33} stem from neutrino masses m_ν, assuming $m_\nu < 1\,\text{eV}$ and left right mixing in the sbottom sector. The limits depend on the squark masses; $m_{\tilde{q}_{L(R)}}$ is the mass of the left- (right-) handed squark $\tilde{q}_{L(R)}$.

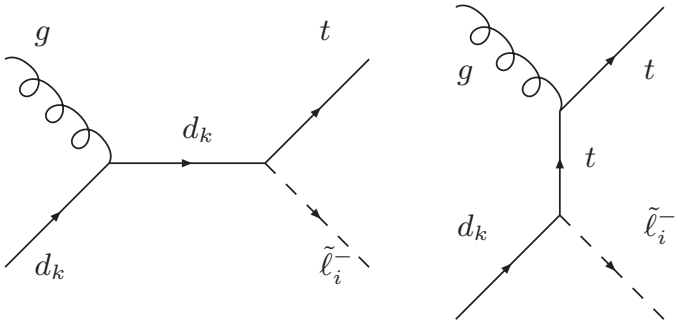

Figure 6.1.: Feynman diagrams contributing to the partonic process $g + d_k \to t + \tilde{\ell}_i^-$.

The second slepton production mechanism is $t\bar{t}$ pair production followed by the t or $\bar{t}$ decaying into $\tilde{\ell}_i^+$ or $\tilde{\ell}_i^-$, respectively. The main production mechanisms for $t\bar{t}$ production, at $O(\alpha_s^2)$, are

$$\left.\begin{array}{rcl} q + \bar{q} & \to & t + \bar{t} \\ g + g & \to & t + \bar{t} \end{array}\right\}, \qquad t \to \tilde{\ell}_i^+ + d_k \tag{6.2}$$

where q ($\bar{q}$) is a (anti-)quark. This is only kinematically allowed if

$$m_t > m_{\tilde{\ell}_i} + m_{d_k}\,. \tag{6.3}$$

Since, as we shall see, the branching fraction for the B_3 top quark decay is small, we only consider one B_3 decay, for either the top or the anti-top quark.

In Ref. [204], single slepton production was considered for the specific case of $\lambda'_{333} \neq 0$. This process is however disfavored due to the strict bound on the relevant coupling from neutrino masses, *cf.* Table 6.1[1]. Thus the work was extended to the couplings λ'_{331} and λ'_{332} [205]. We go beyond this work to include a signal over background analysis. We also present the analytic formula for the cross section, Eq. (6.6), for the first time, and analyze the resulting signatures. We give a detailed phenomenological analysis for the special case λ'_{231} which can be generalized to λ'_{131}.

In Ref. [184], top quark pair production and subsequent top decay via λ'_{i3k} was considered. Off-shell top quark effects were also taken into account. A signal over background analysis

[1]Even if one assumes that the one-loop contributions to the neutrino mass are suppressed, two loop contributions lead to a bound on λ'_{333} of 10^{-2} [233], which still leads to a suppressed cross section.

was performed for two scenarios. The first scenario assumed maximal stop-scharm mixing. It was pointed out that associated slepton production with slepton masses 150 GeV and 200 GeV can be measured, depending on the magnitude of λ'_{i3k}. The second scenario assumed no flavor violation in the squark sector. Ref. [184] claimed that in this regime sleptons with mass 200 GeV can not be measured. We go beyond the work of [184]. We show that it is possible to detect associated slepton production even for slepton masses larger than 300 GeV, if λ'_{231} or λ'_{131} is of $\mathcal{O}(0.1)$. We will achieve this with the help of the Compton-like process, Eq. (6.1).

The outline of Sect. 6 is as follows. In Sect. 6.2 we calculate the cross section for the production of a charged slepton in association with a top quark, at leading order. In Sect. 6.3 we systematically present the possible resulting signatures at the LHC. In Sect. 6.4 we discuss in detail a case study for the operator $\lambda'_{231}L_2Q_3\bar{D}_1$. We study the dominant $t\bar{t}$ and $W^\pm$ backgrounds. Using the HERWIG Monte Carlo program [196, 197, 198, 199, 200], we devise a set of cuts in order to distinguish the two. We do not include a simulation of the detector. Our conclusions are presented in Sect. 6.5.

6.2. Single Slepton Production via λ'_{i3k}

6.2.1. Partonic Cross Sections

The spin and color averaged matrix element squared for the Compton-like process, Eq. (6.1), is given at leading order by

$$|\overline{M}|^2 = \frac{\pi\lambda'^2_{i3k}\alpha_s C_F |L^{\ell_i}_{1\alpha}|^2}{4}\left\{\frac{m_t^2-\hat{t}}{\hat{s}} + \frac{2[m_t^2\hat{s}+(\hat{t}-m^2_{\tilde{\ell}_i})(m^2_{\ell_i}-m_t^2-\hat{s})]}{\hat{s}(\hat{t}-m_t^2)} + \frac{(m^2_{\tilde{\ell}_i}-m_t^2)(m^2_{\tilde{\ell}_i}-\hat{s}-\hat{t})-(3m_t^2-m^2_{\tilde{\ell}_i}+\hat{s})(\hat{t}-m^2_{\tilde{\ell}_i})}{(\hat{t}-m_t^2)^2}\right\}, \tag{6.4}$$

where α_s is the QCD coupling constant, $C_F = 4/3$ is the quadratic Casimir of $SU(3)_C$, $m_{\tilde{\ell}_i}$ is the mass of the slepton and $L^{\ell_i}_{1\alpha}$ is the relevant matrix element of the left-right slepton mixing matrix. The explicit form as a function of the mixing angle is given, for example, in Refs. [80, 199]. In accordance with the parton model, we have neglected the mass of d_k. We have made use of the partonic Mandelstam variables

$$\hat{s} = (d_k+g)^2 = (t+\tilde{\ell}_i)^2\,, \tag{6.5a}$$

$$\hat{t} = (d_k-\tilde{\ell}_i)^2 = (g-t)^2\,, \tag{6.5b}$$

where we denote the particle four momenta by the particle letter. Integrating over phase space, we obtain the total partonic cross section:

$$\begin{aligned}\hat{\sigma} =& \frac{\lambda'^2_{i3k}\alpha_s C_F |L^{\ell_i}_{1\alpha}|^2}{64\hat{s}^2}\Bigg\{\frac{1}{2\hat{s}}\left[2m_t^2(\hat{t}_+ - \hat{t}_-) - (\hat{t}_+^2 - \hat{t}_-^2)\right] + (\hat{s}+2m_t^2)\ln\left(\frac{\rho_-}{\rho_+}\right) \\ &+ \frac{2m_t^2(m^2_{\tilde{\ell}_i} - m_t^2)(\hat{t}_+ - \hat{t}_-)}{\rho_+\rho_-} + \frac{2(m^4_{\tilde{\ell}_i} + m_t^4 - 2m_t^2 m^2_{\tilde{\ell}_i} - m^2_{\tilde{\ell}_i}\hat{s})}{\hat{s}}\ln\left(\frac{\rho_-}{\rho_+}\right) \\ &+ \frac{2(\hat{t}_+ - \hat{t}_-)(m^2_{\tilde{\ell}_i} - m_t^2 - \hat{s})}{\hat{s}}\Bigg\}, \end{aligned} \tag{6.6}$$

where

$$\rho_\pm = m_t^2 - \hat{t}_\pm, \tag{6.7}$$

$$\hat{t}_\pm = m^2_{\tilde{\ell}_i} - \frac{1}{2}[\hat{s} + m^2_{\tilde{\ell}_i} - m_t^2 \mp \lambda^{\frac{1}{2}}(\hat{s}, m^2_{\tilde{\ell}_i}, m_t^2)], \tag{6.8}$$

with the phase-space function given by $\lambda(x,y,z) = x^2 + y^2 + z^2 - 2xy - 2xz - 2yz$.

The tree-level partonic matrix element squared for top quark pair production is given for example in Ref. [234]. We shall only consider on-shell top quark pair production. The slepton then arises through the decay of a real top quark. In order to obtain the signal rate, we thus also require the partial decay width of the top quark, via the $L_i Q_3 \bar{D}_k$ operator. It is given by

$$\Gamma_{t\to d_k \tilde{\ell}_i^+} = \frac{\lambda'^2_{i3k}|L^{\ell_i}_{1\alpha}|^2}{32\pi m_t}\left(1 + \frac{m_{d_k}^2}{m_t^2} - \frac{m^2_{\tilde{\ell}_i}}{m_t^2}\right)\lambda^{1/2}(m_t^2, m_{d_k}^2, m^2_{\tilde{\ell}_i})\ . \tag{6.9}$$

See also Refs. [164, 183, 184, 204, 235]. We obtain a branching ratio of 8.2×10^{-4} for the B_3 top decay, Eq. (6.9), for $\lambda'_{i3k} = 0.1$, $m_t = 175\,\text{GeV}$, top width $\Gamma_t = 1.5\,\text{GeV}$ and $m_{\tilde{\ell}_i} = 150\,\text{GeV}$. We neglect the mass of d_k and set $L^{\ell_i}_{1\alpha} = 1$.

6.2.2. Total Hadronic Cross Section

In Fig. 6.2 (Fig. 6.3), we show the hadron level cross section at the Tevatron (LHC) for single slepton production in association with a top quark, as a function of the slepton mass including both production mechanisms. We set $\lambda'_{i3k} = 0.1$ and assume it is the only non-vanishing B_3 coupling. We vary the index k and the charge of the final state slepton, which correspond to different parton density functions (PDFs). Here we use the CTEQ6L1 PDFs [236], corresponding to $\Lambda_5^{LO} = 165$ MeV at the one-loop level of the strong coupling $\alpha_s(\mu_R)$ using $\alpha_s(M_Z) = 0.130$. We use the same running α_s to calculate the cross section Eq. (6.6). The renormalization, μ_R, and factorization, μ_F, scales are taken to be equal, $\mu_R = \mu_F = m$, where $m \equiv 2m_t$ [$\equiv m_{\tilde{\ell}_i} + m_t$] in the case of slepton production via a $t\bar{t}$ pair, Eq. (6.2) [via the Compton-like process, Eq. (6.1)]. Furthermore, we set the L-R slepton mixing matrix element $L^{\ell_i}_{1\alpha}$ equal to one. Results for other values of λ'_{i3k} and mixing matrix elements $L^{\ell_i}_{1\alpha}$ are easily obtained by rescaling according to Eq. (6.6) and Eq. (6.9). The top mass is

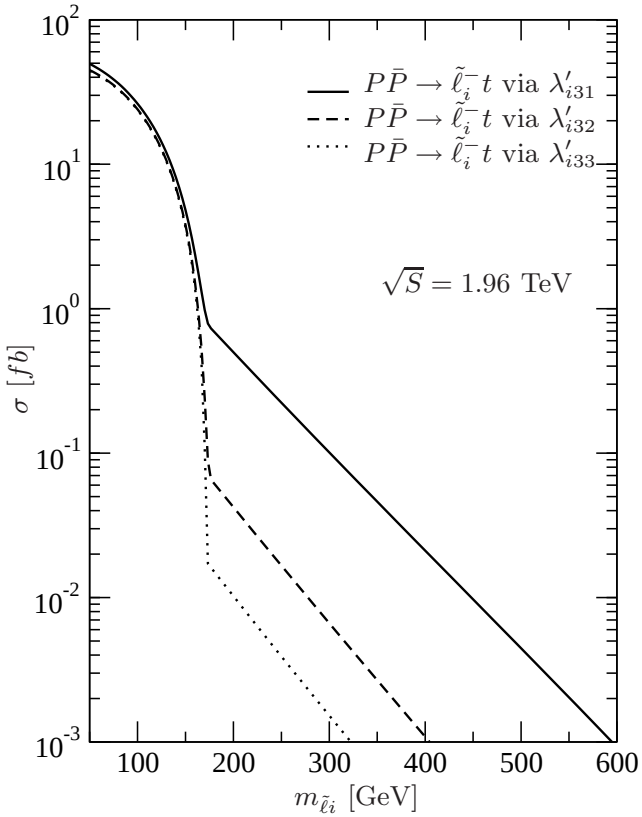

Figure 6.2.: Single slepton production in association with a top at the Tevatron. The cross sections for $\tilde{\ell}_i^+ \bar{t}$ production are equal to the cross sections for $\tilde{\ell}_i^- t$ production.

taken to be 175 GeV and the total (SM) top quark decay width to be 1.5 GeV. We take $m_{d_3} = m_b = 4.5\,\text{GeV}$, if we have a b quark in the final state and neglect the masses of the d and s quarks.

In both figures, we see a kink in the cross section when $m_{\tilde{\ell}_i} = m_t - m_{d_k}$. For smaller slepton masses the top quark pair production mechanism dominates; for larger masses the Compton-like processes dominate, since the slepton can no longer be produced on-shell in top decay.

For comparative discussions later, Fig. 6.4 (Fig. 6.5) shows the NLO hadronic cross section for resonant sneutrino production, *cf.* Eq. (5.3), at the Tevatron (LHC) via $\lambda'_{i3k} = 0.1$, including NLO QCD corrections [114, 220, 221, 222][2]. We employ the $\overline{\text{MS}}$ renormalization scheme and the (NLO) CTEQ6M PDFs [236], corresponding to $\Lambda_5^{\overline{MS}} = 226$ MeV at the two-loop level of $\alpha_s(\mu_R)$ with $\alpha_s(M_Z) = 0.118$. The renormalization and factorization scales are taken to be the sneutrino mass, $\mu_R = \mu_F = m_{\tilde{\nu}_i}$.

In Fig. 6.2, we see that at the Tevatron, even for small slepton masses, $m_{\tilde{\ell}_i} = 100\,\text{GeV}$, we expect only 25 (25) charged slepton events with negative (positive) charge, *i.e.* $\tilde{\ell}_i^-$ ($\tilde{\ell}_i^+$), for

[2]For simplicity, we do not include the supersymmetric QCD corrections given in Ref. [114], since we must then include a discussion of the dependence on the soft supersymmetry breaking parameters.

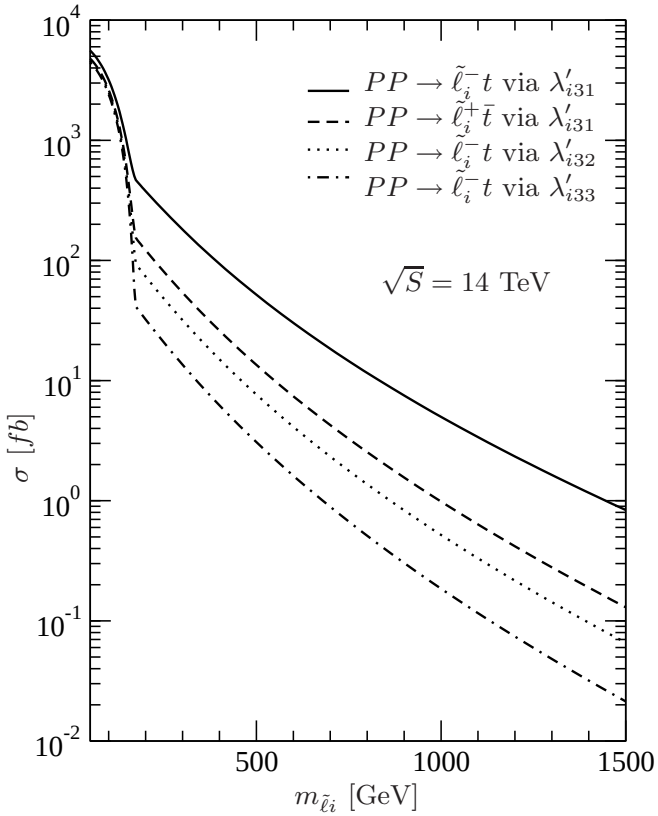

Figure 6.3.: Same as Fig. 6.2, but for the LHC. The cross section for $\tilde{\ell}_i^+ \bar{t}$ production via λ'_{i32} (λ'_{i33}) is equal to the cross section for $\tilde{\ell}_i^- t$ production via λ'_{i32} (λ'_{i33}), as it always involves incoming sea quarks.

an integrated luminosity of $1\,\mathrm{fb}^{-1}$ and the (relatively large) coupling $\lambda'_{i31} = 0.1$. The cross section is dominated by the $t\bar{t}$ pair production, Eq. (6.2). Only 10% of the above sleptons at the Tevatron are produced by the Compton-like process, Eq. (6.1). At the Tevatron, the cross section is symmetric in the slepton charge due to the charge symmetry of the incoming state.

As we can see in Fig. 6.3, we have a significantly larger hadronic cross section at the LHC for a given slepton mass. In particular, for $m_{\tilde{\ell}_i} = 100\,\mathrm{GeV}$ and $\lambda'_{i31} = 0.1$ the LHC will produce more than 31 000 (26 000) sleptons $\tilde{\ell}_i^-$ ($\tilde{\ell}_i^+$) for an integrated luminosity of $10\,\mathrm{fb}^{-1}$. Of these sleptons, 27% (11%) are produced via the Compton-like process. For the same coupling and for $m_{\tilde{\nu}_i} = 100\,\mathrm{GeV}$, we will produce approximately 14 000 sneutrinos at the Tevatron (Fig. 6.4) for $1\,\mathrm{fb}^{-1}$ and 3 800 000 at the LHC (Fig. 6.5) for $10\,\mathrm{fb}^{-1}$, via the partonic process Eq. (5.3). Thus, depending on the decays, we might expect this to be the discovery mode, for equal supersymmetric masses. Here we focus on the potential of the charged slepton production cross section.

For heavier charged sleptons, $m_{\tilde{\ell}_i} = 800$ GeV, we expect no events at the Tevatron and more than 110 (25) $\tilde{\ell}_i^-$ ($\tilde{\ell}_i^+$) events at the LHC with $10\,\mathrm{fb}^{-1}$. Above the threshold of $m_{\tilde{\ell}_i} = m_t - m_{d_k}$, practically all slepton events are produced via the Compton-like process, since the

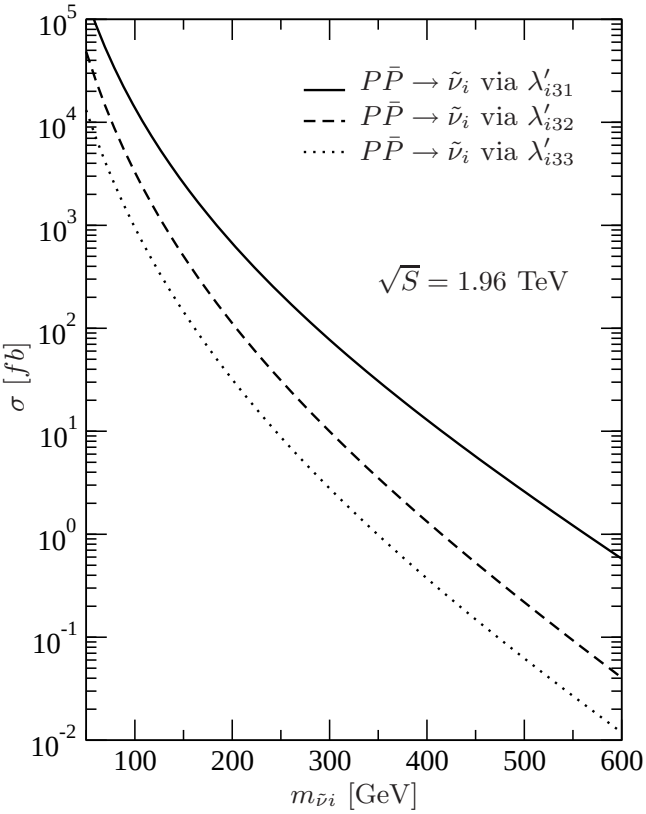

Figure 6.4.: Single sneutrino production cross section at the Tevatron. The cross sections for $\tilde{\nu}_i^*$ production are equal to the cross sections for $\tilde{\nu}_i$ production.

other process only proceeds via off-shell top quarks. The cross section is so small because the parton luminosity is too small at the required high values of the proton/anti-proton fractional momenta, $x \gtrsim 0.1$. This situation changes at the LHC, where we probe significantly smaller values, $x < 0.1$, for the same slepton mass. Furthermore, the Tevatron will produce no sneutrinos, for $\lambda'_{i31} = 0.1$, and $m_{\tilde{\nu}_i} = 800\,\text{GeV}$. For the same set of B_3 parameters, the LHC will produce about 3 200 sneutrinos for $10\,\text{fb}^{-1}$.

At the LHC, there is an asymmetry between the hadronic cross sections for $\tilde{\ell}_i^-$ and $\tilde{\ell}_i^+$ production via the $L_iQ_3\bar{D}_1$ operator ($k = 1$!). This is perhaps not surprising, as the initial state is asymmetric under charge reversal. In the case of the Compton-like process, Eq. (6.1), the asymmetry is due to the negatively charged slepton being produced by an incoming valence d-quark, while the positively charged slepton is produced by a $\bar{d}$ sea quark. The latter has a lower luminosity in the proton. In Sect. 6.4 we will use this asymmetry to separate the B_3 process from the SM background.

In order to estimate the influence of higher order corrections on the production cross section, we vary the renormalization and factorization scales independently between $m/2$ and $2m$. At the Tevatron, Fig. 6.6 (left figure), the hadronic cross section for $\tilde{\ell}_i^- t$ production via λ'_{i31} changes by up to 40%. At the LHC, Fig. 6.6 (right figure), the scale uncertainties are reduced to approximately 25%. In the domain where $m_{\tilde{\ell}_i} < m_t - m_{d_k}$, we have a

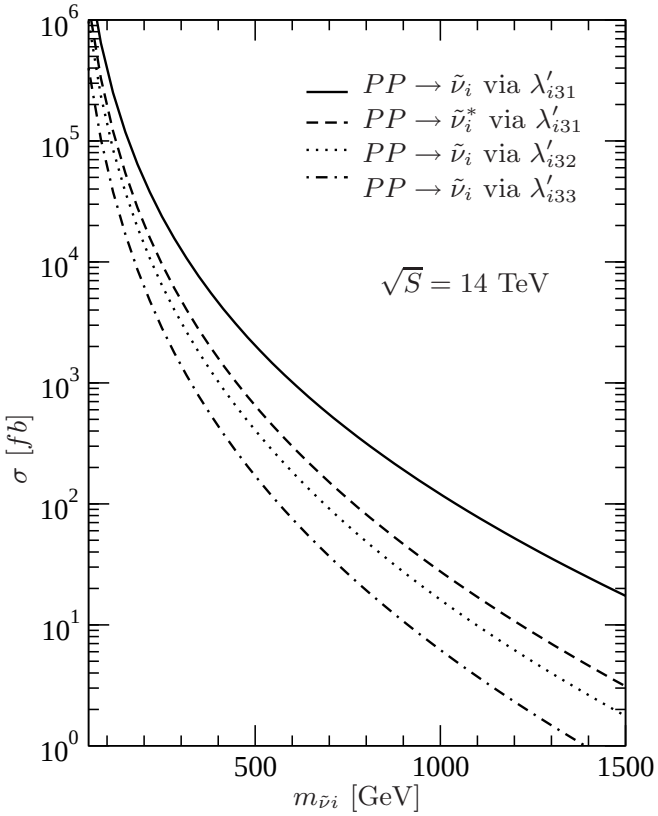

Figure 6.5.: Same as Fig. 6.4, but for the LHC. The cross section for $\tilde{\nu}_i^*$ production via λ'_{i32} (λ'_{i33}) is equal to the cross section for $\tilde{\nu}_i$ production via λ'_{i32} (λ'_{i33}), since only initial-state sea quarks are involved.

stronger dependence on the renormalization scale compared to $m_{\tilde{\ell}_i} > m_t - m_{d_k}$, because $t\bar{t}$ production is $\mathcal{O}(\alpha_s^2(\mu_r))$. According to Refs. [237, 238], NLO-QCD corrections, including a NLL resummation, increase the $t\bar{t}$ production cross section by approximately 40% (80%) at the Tevatron (LHC).

Due to the large scale uncertainties a NLO calculation is called for. In the case of non-vanishing λ'_{i33} the Compton-like process, Eq. (6.1a), is similar to associated charged Higgs production [204] via the partonic process

$$g + b \;\; \to \;\; H^- + t\,, \tag{6.10}$$

with the replacement $\tilde{\ell}_i^- \to H^-$. This process has first been calculated at NLO in QCD in Refs. [239, 240]. It was shown that the NLO contributions enhance the total hadronic cross section between 30% and 80%. It was also shown that the perturbative behavior is well under control and that the higher order contributions reduce the scale uncertainties significantly. However, for $\lambda'_{i31(2)}$, the correspondence to the Higgs production process, Eq. (6.10), at the hadron level no longer holds due to the light quark, *i.e.* d-quark (s-quark), instead of the heavy b-quark in the initial state. The parton-level calculation for different couplings λ'_{i3k} is the same. We conclude that, particularly for the case of non-vanishing λ'_{i31}, where the

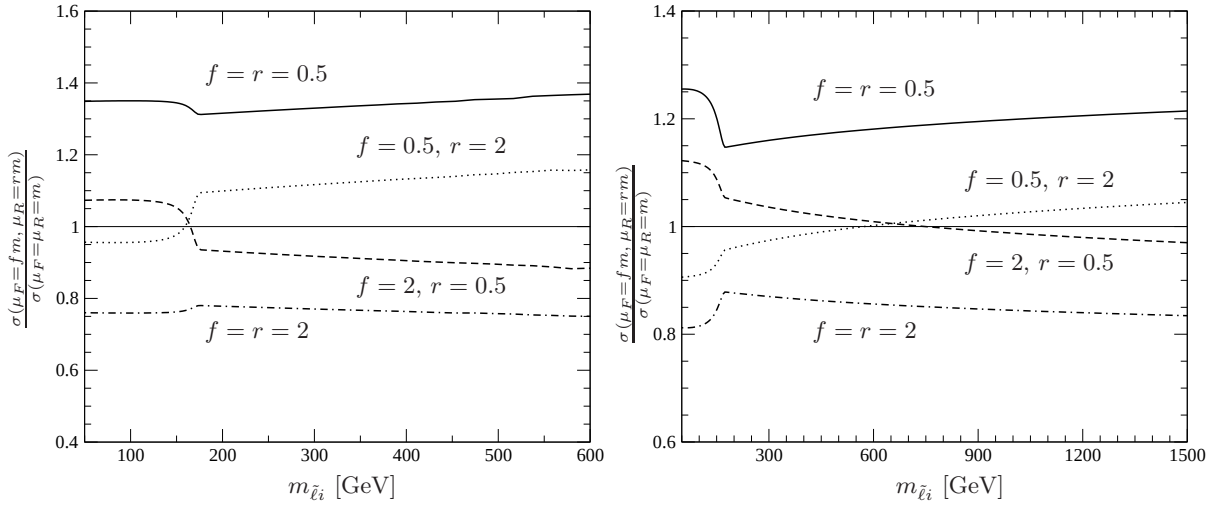

Figure 6.6.: Factorization scale $\mu_F = f \cdot m$ and renormalization scale $\mu_R = r \cdot m$ dependence of the hadronic $\tilde{\ell}_i^- t$ production cross section via λ'_{i31} at the Tevatron (left figure) and LHC (right figure). μ_F and μ_R are independently taken equal to 2 and 0.5 times m, where $m \equiv 2m_t$ [$\equiv m_{\tilde{\ell}_i} + m_t$] in the case of slepton production via a $t\bar{t}$ pair, Eq. (6.2) [via the Compton-like process, Eq. (6.1)].

lepton charge asymmetry can be observed at the LHC, a NLO calculation has to be done. It is, however, beyond the scope of this work.

The hadronic cross section for single stau, $\tilde{\tau}$, production via a non-vanishing λ'_{333} coupling, was also considered by Borzumati *et. al.* [204]. There, the $2 \to 2$ processes, Eq. (6.1), were included, together with the (tree-level) $2 \to 3$ slepton-strahlung processes

$$\left.\begin{array}{l} g + g \\ q + \bar{q} \end{array}\right\} \to t + \bar{b} + \tilde{\tau}^- \,, \tag{6.11}$$

which are shown, for $m_{\tilde{\tau}} < m_t - m_b$, to be equivalent to the $2 \to 2$ processes, Eqs. (6.2). The $\bar{b}$ and $\tilde{\tau}^-$ are produced via a virtual top. They employed the CTEQ4L [241] PDFs and all matrix elements were multiplied by the CKM factor V_{tb}. We have calculated the hadronic cross sections using the same PDFs and the same parameter set [242]. We agree exactly, where single slepton production is dominated by the $t\bar{t}$ process, *i.e* for $m_{\tilde{\tau}} < m_t - m_b$. For $m_{\tilde{\tau}} > m_t - m_b$, we underestimate the total cross section at the Tevatron by 20% for $m_{\tilde{\tau}} = 300\,\text{GeV}$ and by a factor of roughly two for $m_{\tilde{\tau}} = 200$ GeV, compared to Ref. [204]. In this region the above $2 \to 3$ processes, where the slepton is produced by a quark-antiquark pair, can give the main contribution compared to the $gb \to \tilde{\tau} t$ partonic process, where a gluon and/or sea-quark is needed with large Bjorken x. However, in this region where there are large discrepancies, practically no sleptons are produced at the Tevatron. Our prediction for the LHC differs by +30% for $m_{\tilde{\tau}} > m_t - m_b$.

Borzumati *et. al.* extended their analysis to the λ'_{332} and λ'_{331} couplings [205]. They presented the results for the $2 \to 2$ process, Eq. (6.1), and the $2 \to 3$ process, Eq. (6.11), separately. For $m_{\tilde{\tau}} < m_t - m_{d_k}$, we agree exactly at the Tevatron as well as at the LHC. For $m_{\tilde{\tau}} > m_t - m_{d_k}$, our predictions coïncide exactly with their cross section predictions for the $2 \to 2$ process. Furthermore, it is shown in Ref. [205] that for $m_{\tilde{\tau}} > m_t - m_{d_k}$, the $2 \to 3$

	Tevatron	LHC
$m_{\tilde{\ell}_i} = 100\,\text{GeV}$	25.5 fb	3180 (2620) fb
$m_{\tilde{\ell}_i} = 250\,\text{GeV}$	2.10×10^{-1} fb	259 (80.0) fb
$m_{\tilde{\ell}_i} = 800\,\text{GeV}$	2.86×10^{-5} fb	11.6 (2.54) fb

Table 6.2.: Hadronic cross section predictions for $\tilde{\ell}_i^- t$ ($\tilde{\ell}_i^+ t$) production via $\lambda'_{i31} = 0.1$ at the Tevatron ($\sqrt{S} = 1.96$ TeV) and the LHC ($\sqrt{S} = 14$ TeV). Results are presented for the CTEQ6L1 [236] PDF parametrization.

contributions are small or even negligible. At the Tevatron, the $2 \to 3$ process contributes roughly 35% (5%) to the total hadronic cross section for $\lambda'_{332} \neq 0$ ($\lambda'_{331} \neq 0$). At the LHC these contributions are 25% (5%). The reason is that the cross sections induced by the $2 \to 3$ process have similar sizes for any value of k. But the $2 \to 2$ process for $\lambda'_{332} \neq 0$ ($\lambda'_{331} \neq 0$) is enhanced by a factor of 5 ($\gtrsim 10$) due to a s-quark (valence d-quark) in the initial state.

We conclude, that our LO approximation is valid in the phenomenologically relevant region, where one is able to produce a single slepton in association with a top quark. We have not included the $2 \to 3$ processes as they are formally higher order. Furthermore, the essential ingredient in our phenomenological analysis below is the lepton charge asymmetry due to a non-vanishing λ'_{i31} coupling. The $2 \to 3$ processes do not contribute, as their initial states are charge symmetric and their contributions to the hadronic cross section are only 5%.

We end this section by presenting in Table 6.2 selected cross section predictions for slepton production with $m_{\tilde{\ell}_i} = 100$ GeV, $m_{\tilde{\ell}_i} = 250$ GeV and $m_{\tilde{\ell}_i} = 800$ GeV at the Tevatron and the LHC via $\lambda'_{i31} = 0.1$.

6.3. Possible LHC Signatures

Apart from the B_3 process, the sleptons and sneutrinos can decay through gauge interactions. Neglecting mixing between left- and right-handed sleptons the possible tree-level decays are [see also Eq. (5.29) and Eq. (5.30)]:

$$\tilde{\ell}_i^- \to \begin{cases} \bar{t}\, d_k \\ \ell_i^- \tilde{\chi}_m^0 \\ \nu_i \tilde{\chi}_n^- \end{cases}, \qquad \tilde{\nu}_i \to \begin{cases} \bar{b}\, d_k \\ \nu_i \tilde{\chi}_m^0 \\ \ell_i^- \tilde{\chi}_n^+ \end{cases}. \tag{6.12}$$

The branching ratios depend on the masses of the sparticles, the admixtures of the gauginos and on the size of the λ'_{i3k} coupling. We shall first assume, that the lightest neutralino, $\tilde{\chi}_1^0$, is the LSP. Possible decay modes via the λ'_{i3k} interaction are:

$$\tilde{\chi}_1^0 \xrightarrow{\lambda'} \begin{cases} \ell_i^+ \bar{t}\, d_k \\ \ell_i^- t\, \overline{d}_k \end{cases}, \qquad \tilde{\chi}_1^0 \xrightarrow{\lambda'} \begin{cases} \bar{\nu}_i \bar{b}\, d_k \\ \nu_i b\, \overline{d}_k \end{cases}; \tag{6.13}$$

cf. Eq. (5.18). Here the branching ratios depend mainly on the admixture of the lightest neutralino. The heavier neutralinos $\tilde{\chi}^0_{2,3,4}$ and the charginos $\tilde{\chi}^+_{1,2}$ dominantly decay into lighter gauginos via gauge interactions, as in the P_6-MSSM.

In SUSY scenarios, where the slepton (sneutrino) mass is of the order of a few hundred GeV, the slepton (sneutrino) will decay dominantly into the lightest neutralino and a lepton (neutrino). However, significant chargino decay modes are also possible, if they are kinematically accessible. Furthermore, decay chains involving a top quark in the final state are either phase-space suppressed or kinematically forbidden, unless the slepton is very heavy. This affects the neutralino decays, Eq. (6.13), involving charged leptons. Therefore, the dominant hadron collider signatures of single slepton production in association with a top quark are

$$g d_k \to \tilde{\ell}_i^- t \to \ell_i^- \tilde{\chi}_1^0 \, t \to \begin{cases} \ell_i^- \, (\bar{\nu}_i \bar{b} d_k) \, [b W^+] \\ \ell_i^- \, (\nu_i b \bar{d}_k) \, [b W^+] \end{cases} . \tag{6.14}$$

In parentheses are the neutralino LSP decay products, Eq. (6.13); the particles in brackets arise from the top quark decay. As mentioned before, for $k = 1$ there is an asymmetry between the number of positively and negatively charged leptons $\ell_i^\pm$ at the LHC.

The dominant signatures for a resonantly produced single sneutrino are

$$\bar{b} \, d_k \to \tilde{\nu}_i \to \begin{cases} \bar{b} \, d_k \\ \nu_i \, (\bar{\nu}_i \bar{b} \, d_k) \\ \nu_i \, (\nu_i b \, \bar{d}_k) \end{cases} , \tag{6.15}$$

again the neutralino decay products are in parentheses. Although the sneutrino production cross section at the LHC (Fig. 6.5) is up to two orders of magnitude larger than the slepton plus top quark cross section (Fig. 6.3), the event signature, Eq. (6.15), is much harder to extract above the SM background. It involves only two jets and possibly some missing transverse energy. It therefore suffers from a large QCD background. However, if the sneutrino decays into charginos and heavier neutralinos are possible, Eq. (6.12), we can have (additional) charged leptons in the final state.

We now consider SUSY scenarios, where the stau, $\tilde{\tau}_1$, is the LSP instead of the lightest neutralino, *cf.* Fig. 2.3 and Sect. 5. In this scenario the lightest neutralino dominantly decays into a tau and the stau LSP, $\tilde{\chi}_1^0 \to \tilde{\tau}_1^\pm \tau^\mp$. For $i = 1, 2$, the stau will dominantly decay into a tau and a virtual neutralino [see also Eq. (5.20)], leading to a four-body decay of the stau LSP. The signatures for a stau LSP are

$$g d_k \to \tilde{\ell}_i^- t \to \begin{cases} \ell_i^- \tau^\pm \, (\tau^\mp \bar{\nu}_i \bar{b} d_k) \, [b W^+] \\ \ell_i^- \tau^\pm \, (\tau^\mp \nu_i b \bar{d}_k) \, [b W^+] \end{cases} . \tag{6.16}$$

The particles in parentheses are now the stau LSP decay products and the particles in brackets are from the top quark decay. The difference between the final states in Eq. (6.16) and Eq. (6.14) is, that for a stau LSP, the event is accompanied by an additional pair of taus compared to scenarios with a neutralino LSP. We find the same behavior for the sneutrino decay chains. It is therefore easier to distinguish the signal from the background in stau LSP scenarios as long as one is able to reconstruct the tau pair in the final state.

Note that for $i = 3$ the two-body stau decay is kinematically suppressed, or forbidden, due to the large top quark mass. The stau LSP will in this case decay via a virtual top quark; see Appendix B for details. Furthermore, we can produce heavy staus, $\tilde{\tau}_2$, as well as light staus, $\tilde{\tau}_1$, due to L-R mixing in the stau sector. In this case the signatures are

$$gd_k \to \tilde{\tau}_2^- t \to \begin{cases} \tau^-\tau^+ \, (\bar{b}d_k W^-) \, [bW^+] \\ \tau^-\tau^- \, (b\bar{d}_k W^+) \, [bW^+] \\ Z^0/h^0 \, (\bar{b}d_k W^-) \, [bW^+] \end{cases} , \tag{6.17}$$

and

$$gd_k \to \tilde{\tau}_1^- t \to (\bar{b}d_k W^-) \, [bW^+] \, . \tag{6.18}$$

The particles in parentheses are the stau LSP decay products and those in brackets are from the top quark decay. We see in Eq. (6.17) that one of the $\tilde{\tau}_2$ decay chains involves like-sign tau events. This can help to distinguish signal from background although poor tau identification could limit this possibility.

6.4. Numerical Study for $\lambda'_{231} \neq 0$ and a $\tilde{\chi}_1^0$ LSP

6.4.1. The Scenario and Basic Cuts

We now perform an explicit numerical study of single associated slepton production. We focus on the more difficult case of a neutralino LSP and restrict ourselves to $\lambda'_{231} \neq 0$, as the dominant B_3 coupling. We assume that similar results can be obtained for $\lambda'_{131} \neq 0$. A central analysis criterion will be the lepton charge asymmetry of the final state.

According to Eq. (6.14), the final-state signature to examine is

$$\tilde{\ell}_L^{\mp} + t \;\longrightarrow\; \ell^{\mp} + (b + d + \nu) + [b + W^{\pm}] \, , \tag{6.19}$$

with the $W^{\pm}$ decaying hadronically. We thus have one charged lepton, some missing p_T, and five jets, where two are b-quark jets. In our specific scenario, the charged lepton is a muon.

The main background for this process is $t\bar{t} + j$ production (which has been calculated at NLO in Ref. [243]) followed by the semi-leptonic decay of one of the top quarks. The second background we examine is $b\bar{b} + W^{\pm} +$ jets production followed by the leptonic decay of the W boson.

For our simulation, we assume an SPS1a′ similar scenario [244]. We take the SPS1a′ spectrum and couplings and add one B_3 coupling, λ'_{231}. The relevant SPS1a′ masses are:

$$m_{\tilde{\ell}_L^{\pm}} = 190 \text{ GeV}; \quad m_{\tilde{\nu}_\mu} = 173 \text{ GeV}; \tag{6.20a}$$

$$m_{\tilde{\chi}_1^0} = 98 \text{ GeV}; \quad m_{\tilde{\chi}_2^0} = 184 \text{ GeV}; \tag{6.20b}$$

$$m_{\tilde{\chi}_1^{\pm}} = 183 \text{ GeV}. \tag{6.20c}$$

λ'_{231}	0	0.1	0.2	0.3	0.4
$\mathrm{Br}(\tilde{\mu}_L^- \to \bar{t} + d)$	0.0%	2.2%	8.4%	17.1%	26.8%
$\mathrm{Br}(\tilde{\mu}_L^- \to \mu^- + \tilde{\chi}_1^0)$	90.9%	88.9%	83.3%	75.4%	66.5%
$\mathrm{Br}(\tilde{\mu}_L^- \to \mu^- + \tilde{\chi}_2^0)$	3.2%	3.1%	2.9%	2.6%	2.3%
$\mathrm{Br}(\tilde{\mu}_L^- \to \nu_\mu + \tilde{\chi}_1^-)$	5.9%	5.8%	5.4%	4.9%	4.3%

Table 6.3.: Relevant branching ratios for SPS1a′ for different couplings λ'_{231}.

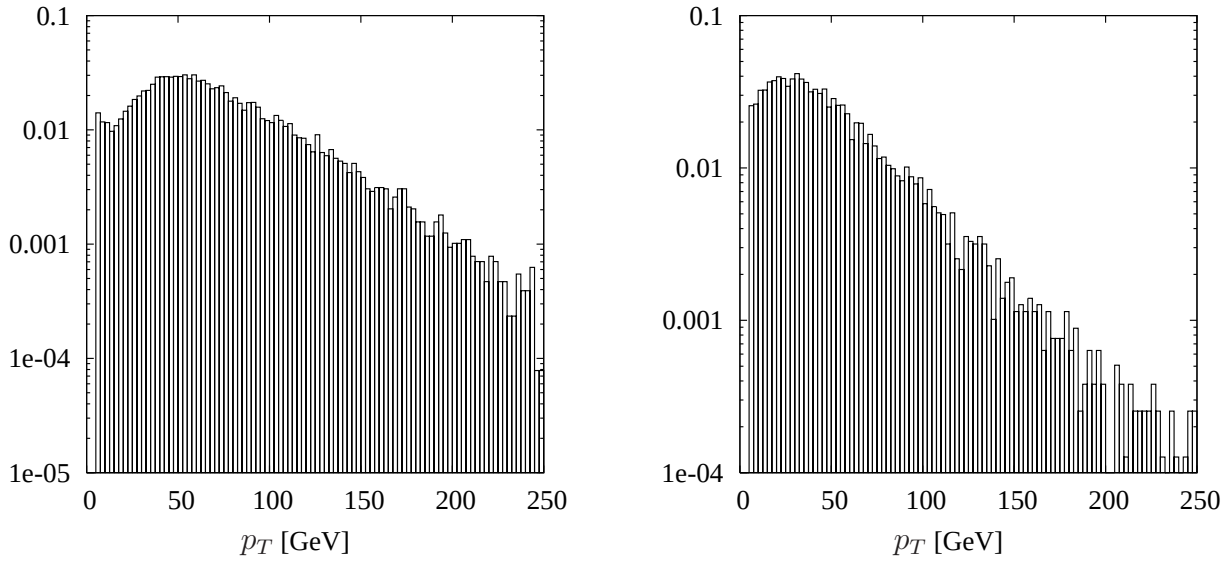

Figure 6.7.: Relative p_T distribution of the final-state signal $\ell^\pm$ for SPS1a′ (left figure) and the final-state $\ell^\pm$ from $t\bar{t} + j$ background (right figure) at the LHC. We employ only the isolation cut on the lepton.

All the charged slepton decays of Eq. (6.12) are therefore kinematically possible. The corresponding branching ratios are given in Table 6.3 for various couplings λ'_{231}. Note that kinematically the sneutrino can only decay via the neutralino or via the λ'_{231} coupling. The potential signature would then be two jets possibly with some missing energy, *cf.* Eq. (6.15).

For the simulation of the single slepton plus top quark signal we have written our own Monte Carlo program using the Les Houches accord [245] and linked this to `HERWIG6.5` [196, 197, 198, 199, 200]. The averaging of the color flow in the s- and t-channel single slepton production diagrams is implemented by the method developed in Ref. [246]. The supersymmetric particle spectra are produced with `SOFTSUSY` [145]. The $t\bar{t}$-background is simulated using the `MC@NLO` program [247, 248]. The $b\bar{b} + W^\pm +$ jets background is simulated by using `MadEvent` [249] to generate a sample of $b\bar{b} + W^\pm + 2$ jet events which are then showered and hadronized using `HERWIG6.5`. We use the CTEQ61 parton distribution functions [236]. The top quark mass is set to $m_t = 175$ GeV.

Since our signature is very similar to the final state and distributions of $t\bar{t} + j$ production followed by the semi-leptonic decay, we use the standard set of CMS cuts for $t\bar{t}$ production followed by the semi-leptonic decay, given in Ref. [250] and require an additional jet. This

	simulated	ℓ^- events after cuts	ℓ^+ events after cuts	Events $\times$ pb^{-1}
signal	99 900	5 042	1 664	0.0108
$W^- + b\bar{b} +$ jets bg	994 000	28 600	0	0.0431
$W^+ + b\bar{b} +$ jets bg	993 500	0	29 700	0.0625
$t\bar{t} + 1$ j bg	9 990 500	135 330	136 360	22.00

Table 6.4.: Results of simulating SPS1a$'$ with cuts given in the text. The number of leptons and the expected event rates are after cuts.

set of cuts leaves the large semi-leptonic $t\bar{t} + j$ production, for which the cuts are designed, and fewer $b\bar{b} + W^{\pm} +$ jets events as backgrounds for the signal process. The precise cuts are summarized below.

The main difference between the semi-leptonically decaying top pair and our signal is the p_T distribution of the lepton stemming from the slepton compared to the one from the $W^{\pm}$ from one of the top decays. We therefore compare in Figs. 6.7 the p_T distributions of the leptons arising from the signal and the $t\bar{t} + j$ background processes, respectively. We see, that the p_T of the signal leptons has a peak around 50 GeV. This peak corresponds to the mass difference between the slepton and the neutralino with the energy carried away by the lepton subtracted. The background lepton distribution peaks at 25 GeV and then falls more steeply than the signal distribution for increasing p_T. We thus harden the CMS semi-leptonic $t\bar{t}$ cut for the isolated observed lepton from $p_T \geq 20$ GeV to $p_T \geq 35$ GeV.

In addition to the charged lepton in the final state, we require two tagged b-jets, as well as two further jets. Thus, the employed cuts are

- 1 isolated lepton with pseudo-rapidity $\eta < 2.4$, $p_T > 35$ GeV. The isolation cut required less than 2 GeV of transverse energy in a cone of radius 0.4 around the lepton direction.
- 2 isolated b jets and 2 non-b jets, pseudo-rapidity $\eta < 2.4$, $p_T > 30$ GeV.

The jets are defined using `PXCONE` [251] which uses the mid-point between two particles as a seed in addition to the particles themselves to improve the infrared behavior of the algorithm. A cone radius of 0.5 was used to define the jets. For the bottom and charm quarks produced in the perturbative stage of the event the nearest jet in (η, ϕ) is considered to have been produced by that quark if the distance in (η, ϕ) was less than 0.2. We employ a b-tagging probability of 0.6 and the probability for mistagging a c-quark or light quark as a b-quark of 0.05 and 0.02, respectively.

For the signal, we simulated 10^5 events. Employing all cuts, including $p_T(\ell^{\pm}) \geq 35$ GeV, we have 5×10^3 surviving ℓ^- events and 1.7×10^3 surviving ℓ^+ events. For the $b\bar{b} + W^{\pm} +$ jets background we simulated 10^6 events for both W^- and W^+ production. After all cuts we are left with 2.9×10^4 ℓ^- and 3.0×10^4 ℓ^+ events, respectively. 10^7 $t\bar{t} + j$ events were simulated resulting in 1.35×10^5 events for ℓ^- production and 1.36×10^5 events for ℓ^+production. This is summarized in Table 6.4.

For the simulated signal, we set $\lambda'_{231} = 0.053$. In the following we will estimate the signal

for other values of λ'_{231} by taking into account the λ'^2_{231} dependence of the cross section. We also employ the λ'_{231} dependence of the the $\tilde{\mu}^-_L \to \mu^- \tilde{\chi}^0_1$ branching ratio.

6.4.2. Lepton Charge Asymmetry

In order to distinguish the signal from the background at the LHC after these cuts, we propose as the decisive observable the lepton charge asymmetry

$$\mathcal{A}_{\ell\pm} \equiv \frac{N_{\ell+} - N_{\ell-}}{N_{\ell+} + N_{\ell-}} \,. \tag{6.21}$$

Here $N_{\ell+}$ and $N_{\ell-}$ are the number of events with a positively or negatively charged lepton, respectively. In Fig. 6.3, we can see the separate signal cross sections for ℓ^+ and ℓ^- production at the LHC. For $m_{\tilde{\ell}^\pm_L} > m_t - m_d$, the ℓ^- cross section is significantly larger. This is due to the fact that the d-quark PDF luminosity is significantly larger than that of the $\bar{d}$-quark for $x \gtrsim 10^{-2}$.

We would expect the lepton charge asymmetry to be zero for the $t\bar{t} + j$ background, as we have an equal number of top quarks and anti-top quarks. For the background process $b\bar{b} + W^\pm +$ jets, we expect a positive asymmetry, since the (valence) u-quark luminosity is significantly larger than the (valence) d-quark luminosity in the proton. For the signal, as we have seen, we expect a negative asymmetry.

However, in general, inclusive $t\bar{t}$ production has a charge asymmetry in the final state at the LHC. It has been shown to be in the range $[-0.025\%; 0]$, if the detector has a symmetric acceptance in the rapidity range $[-y_0; y_0]$. For $y_0 \to \infty$ (0) the asymmetry goes to 0 (-0.025%) [252, 253, 254]. This stems from the asymmetry in $q\bar{q}$ induced $t\bar{t}$ production, which in turn is due to the interference of C-odd and C-even modes, where C is the charge conjugation operator. In the following, we will neglect this small asymmetry because the statistical fluctuations lead to an even larger asymmetry. The number of $\ell^\pm$ events in Table 6.4 for the $t\bar{t} + j$ background are consistent with a lepton charge asymmetry of zero within two sigma.

In Fig. 6.8, we show the significance, Σ, of the signal for the SPS1a′ spectrum as a function of λ'_{231}, where

$$\Sigma \equiv \frac{(A_{SM} - A_{SM+S})}{\Delta A_{SM}} \,. \tag{6.22}$$

Here A_{SM} is the SM lepton charge asymmetry. A_{SM+S} is the asymmetry for the signal and the SM background combined. ΔA_{SM} is the error of the SM asymmetry prediction assuming purely statistical errors for the number of positive and negative charged leptons for each process separately, *i.e.* $\sqrt{N_{\ell+}}$ and $\sqrt{N_{\ell-}}$. The significance is shown for integrated luminosities at the LHC of $30\,\text{fb}^{-1}$ (lower curves), $100\,\text{fb}^{-1}$, $300\,\text{fb}^{-1}$, and $1000\,\text{fb}^{-1}$, respectively. We vary the cross section by $\pm 20\%$ (grey region) to show possible effects due to higher order corrections for the signal, *cf.* Fig. 6.6.

In Fig. 6.8, we see that for $30\,\text{fb}^{-1}$ we can probe couplings down to about 0.3 for the SPS1a′ spectrum. In the SPS1a′ spectrum the squark mass is 544 GeV, thus the experimental bound

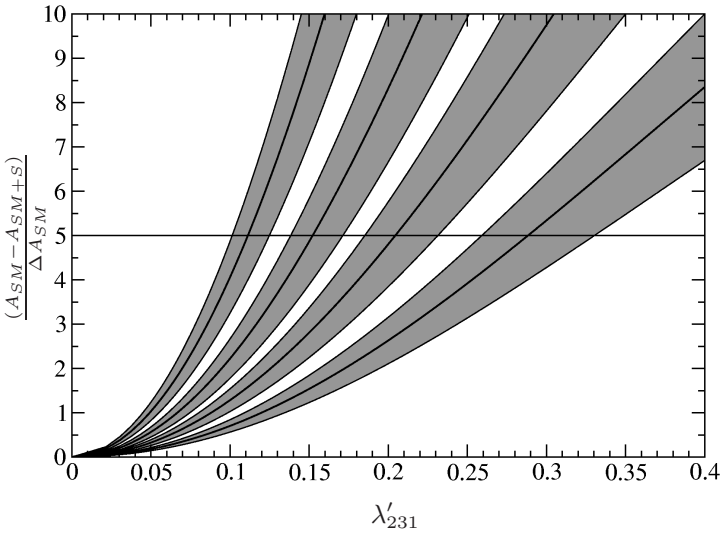

Figure 6.8.: Significance at the LHC as a function of λ'_{231} for SPS1a′ with lepton $p_T \geq 35$ GeV. We show the significance for an integrated luminosity of $30\,\text{fb}^{-1}$ (lower curve), $100\,\text{fb}^{-1}$, $300\,\text{fb}^{-1}$, and $1000\,\text{fb}^{-1}$, respectively. Furthermore, we varied the signal cross section by ±20% (gray region).

λ'_{231}	0	0.1	0.2	0.3	0.4
$\text{Br}(\tilde{\mu}_L^- \to \bar{t} + d)$	0.0%	22.0%	53.0%	71.8%	81.9%
$\text{Br}(\tilde{\mu}_L^- \to \mu^- + \tilde{\chi}_1^0)$	60.9%	47.5%	28.6%	17.2%	11.0%
$\text{Br}(\tilde{\mu}_L^- \to \mu^- + \tilde{\chi}_2^0)$	13.8%	10.8%	6.5%	3.9%	2.5%
$\text{Br}(\tilde{\mu}_L^- \to \nu_\mu + \tilde{\chi_1}^-)$	25.3%	19.7%	11.9%	7.1%	4.6%

Table 6.5.: Relevant branching ratios for SPS1b for different couplings λ'_{231}.

is $\lambda'_{231} < 1.0$, *cf.* Table 6.1. For 300 fb^{-1} we can probe couplings down to about 0.15. In the extreme case of 1000 fb^{-1} this improves to about $\lambda'_{231} = 0.1$.

We have repeated the above analysis for the parameter set SPS1b [146]. Here we have the following masses:

$$m_{\tilde{\mu}_L} = 342 \text{ GeV}; \quad m_{\tilde{\nu}_\mu} = 333 \text{ GeV}; \tag{6.23a}$$

$$m_{\tilde{\chi}_1^0} = 163 \text{ GeV}; \quad m_{\tilde{\chi}_2^0} = 306 \text{ GeV}; \tag{6.23b}$$

$$m_{\tilde{\chi}_1^\pm} = 306 \text{ GeV}. \tag{6.23c}$$

We show the branching ratios for different λ'_{231} in Table 6.5. We see, that the B_3 decay into a d quark and a top quark is the dominant decay for large λ'_{231}, *i.e.* $\lambda'_{231} > 0.19$. One might thus consider an analysis based on this decay mode. However the signature is $t\bar{t} + j$, which has a very large background. We thus continue to consider the neutralino decay mode. The significance will then approach a constant value for a constant luminosity and large λ'_{231}, because the cross section and the B_3 decay both scale with λ'^2_{231}. Furthermore the slepton mass is now significantly larger, but so is the lightest neutralino mass. The mass difference

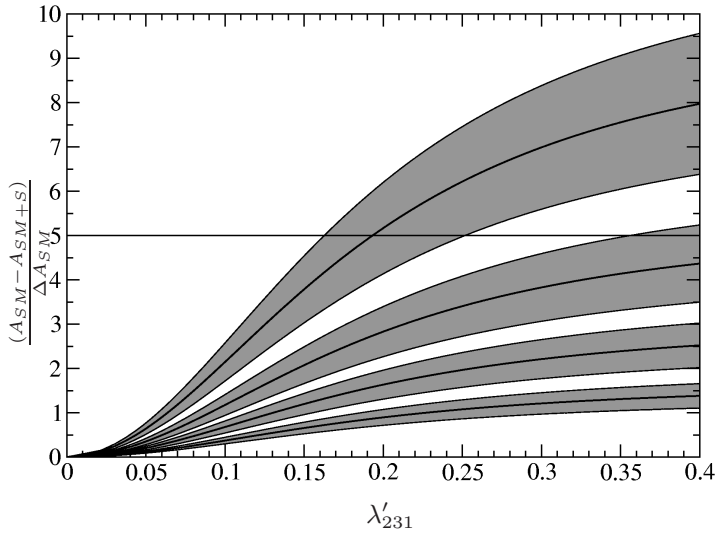

Figure 6.9.: Same as for Fig. 6.8, but for the parameter set SPS1b with lepton $p_T \geq 70$ GeV.

λ'_{231}	0	0.1	0.2	0.3	0.4
$\mathrm{Br}(\tilde{\mu}_L^- \to \bar{t} + d)$	0.0%	23.7%	55.4%	73.6%	83.2%
$\mathrm{Br}(\tilde{\mu}_L^- \to \mu^- + \tilde{\chi}_1^0)$	100%	76.3%	44.6%	26.4%	16.8%

Table 6.6.: Relevant branching ratios for the high p_T scenario for different couplings λ'_{231}. The scenario is described in the text.

however has grown, leading to significantly higher charged lepton p_T's compared to SPS1a$'$, *cf.* Fig. 6.7. We thus impose the stricter cut on the lepton transverse momentum

$$p_T(\ell^\pm) \geq 70 \text{ GeV}\,. \tag{6.24}$$

The results are shown in Fig. 6.9. In this case, for the relatively low integrated luminosity of 30 fb^{-1} we have no chance of observing the signal via the lepton asymmetry; the neutralino branching fraction is too small to have enough events. In fact, it is only for the extremely high integrated luminosity of 1000 fb^{-1} that we have a significant sensitivity range, down to about $\lambda'_{231} = 0.2$.

In order to see what can be probed at the LHC, we have chosen as a third example a mass spectrum which optimizes our signal. For this we considered a modified SPS1b spectrum, where we first lowered the mass of the lightest neutralino to

$$m_{\tilde{\chi}^0_1} \;=\; 80 \text{ GeV}\,, \tag{6.25}$$

in order to obtain a larger mass difference between the smuon and the lightest neutralino. We can then harden the p_T cut to

$$p_T(\ell^\pm) \geq 120 \text{ GeV}\,. \tag{6.26}$$

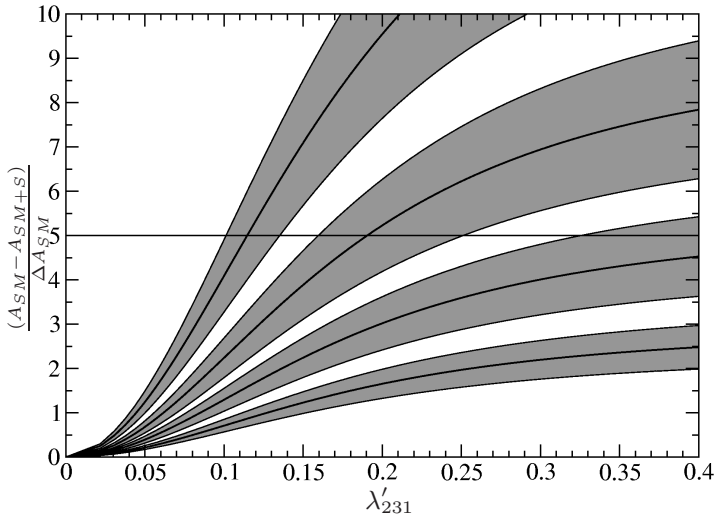

Figure 6.10.: Same as for Fig. 6.8, but for the high-p_T scenario and with lepton $p_T \geq 120$ GeV. The scenario is described in the text.

This leads to a better signal to background ratio compared to SPS1b. Second, we increased the masses of $\tilde{\chi}_2^0$ and $\tilde{\chi}_1^\pm$ to

$$m_{\tilde{\chi}_2^0} = m_{\tilde{\chi}_1^\pm} \quad = \quad 450 \text{ GeV}\,. \tag{6.27}$$

This increases the $\tilde{\mu}_L^- \to \mu^- + \tilde{\chi}_1^0$ branching ratio compared to SPS1b, because decays into heavier neutralinos and into charginos are now kinematically forbidden. We show the relevant branching ratios for different λ'_{231} in Table 6.6. We refer to this scenario as the high-p_T scenario. The resulting significance for the high-p_T scenario is shown in Fig. 6.10.

As can be seen, for an integrated luminosity of 30 fb^{-1} we still have no sensitivity in λ'_{231}. But now for an integrated luminosity of 300 fb^{-1}, we can probe couplings down to 0.19, well below the experimental bound of 1.5, *cf.* Table 6.1 where now $m_{\tilde{b}_L} = 830$ GeV in SPS1b. For an integrated luminosity of 1000 fb^{-1} we can probe couplings down to 0.11.

The influence of systematic errors in the background cross section on our sensitivity are small. Varying the $t\bar{t}+j$ cross section by $+10\%$ (-10%) changes the asymmetry by roughly -9% ($+11\%$). Varying the $b\bar{b}+W^\pm+$jets cross section by $\pm 10\%$ only effects the asymmetry by $\mp 1.6\%$ for SPS1a$'$ with $\lambda'_{231} = 0.3$ and by $\mp 1.2\%$ for the high-p_T scenario with $\lambda'_{231} = 0.3$. Yet, detector effects resulting in an error on the observed charge asymmetry are a problem. Misalignment in the detector can lead to a difference in p_T measurement of positive and negative leptons, respectively. This will lead to an observed, effective charge asymmetry after a cut on the lepton p_T [255]. An analysis of this must be performed by the experimentalists and is well beyond the scope of this work.

For SPS1a$'$ with $\lambda'_{231} = 0.3$, a simulated detector based charge asymmetry of 0.66% leads to an asymmetry of the $t\bar{t}$ background of the same size as that of the signal. For the special case chosen with high p_T leptons in the final state, *i.e.* the high-p_T scenario with $\lambda'_{231} = 0.3$,

a simulated asymmetry of 0.89% would lead to the same effect. Therefore, a higher p_T cut is less sensitive to systematic errors, due to the high p_T cut effecting the $t\bar{t}$ background.

6.5. Conclusion of Section 6

In Sect. 6, we have investigated single charged slepton production due to the B_3 couplings λ'_{i3k}. These couplings are special, because for resonant charged slepton production they require an incoming top quark, which is not available. Instead single charged slepton production must proceed via associated production with a final state top quark. In Sect. 6.2, we have computed the cross section for the Tevatron and the LHC assuming $\lambda'_{i3k} = 0.1$. At the Tevatron we obtain a sizeable cross section only for slepton masses below about 200 GeV. At the LHC we have a sizeable cross section, greater than about 10 fb, up to about 800 GeV in slepton mass, *cf.* Fig. 6.3. It should be kept in mind that the resonant sneutrino production via the same coupling is substantially larger, see Fig. 6.4, and Fig. 6.5. However the signature is not necessarily as promising (because of a lack of charged leptons), depending on the nature of the LSP and the dominant sneutrino decay mode. We furthermore showed that the QCD scale uncertainties in the predictions for the associated charged slepton production cross sections are quite large, see Fig. 6.6, and therefore a NLO calculation is called for in the future.

Next we classified the possible signatures of associated slepton production with a top quark at the LHC for a neutralino or a stau LSP. We found several promising cases. In Sect. 6.4, we then analyzed the specific case of a dominant λ'_{231} or λ'_{131} coupling and a neutralino LSP. As the decisive observable, we propose the lepton charge asymmetry at the LHC, which stems from the different parton luminosities involved. We then analyzed the SM background in detail, which stems mainly from $t\bar{t} + j$ production, followed by the leptonic decays of one of the top quarks. We proposed a set of cuts and showed that slepton masses up to 350 GeV can be explored at the LHC depending on the scenario, see Figs. 6.8-6.10.

7. Summary and Conclusions

Supersymmetry (SUSY) is a potential solution of the hierarchy problem and is thus one of the most promising extensions of the standard model (SM) of particle physics. Its simplest form, the supersymmetric standard model (SSM) is also consistent with several phenomenological observations, like unification of gauge couplings or precision fits to electroweak data. However, the SSM has more than two hundred free parameters and is thus intractable for detailed phenomenological studies.

A well motivated and restricted framework for the SSM is provided by the proton-hexality, P_6, violating mSUGRA model. It reduces the number of free parameters to six. In supersymmetric models it is essential to know the nature of the lightest supersymmetric particle (LSP), since it is involved in practically all SUSY collider signals. In this thesis, we have investigated all possible LSP candidates of the P_6 violating mSUGRA model and their signatures at hadron colliders.

We have found that a non-vanishing $L_iL_j\bar{E}_k$ operator at the grand unification (GUT) scale can lead to a right-handed selectron, $\tilde{e}_R$, $(i = 1)$ or right-handed smuon, $\tilde{\mu}_R$, $(i = 2)$ LSP; *cf.* Fig. 3.1. A non-vanishing $L_iQ_j\bar{D}_k$ operator can lead to a sneutrino, $\tilde{\nu}_i$, LSP; *cf.* Figs. 4.2-4.5. We can also obtain squark LSPs, namely the $\tilde{s}_R$, $\tilde{d}_R$, $\tilde{b}_1$ and $\tilde{t}_1$ via a non-vanishing $\bar{U}_i\bar{U}_j\bar{D}_k$ operator; see Fig. 3.2, Fig. 3.3 and Fig. 3.4 respectively. We have found $\tilde{\mu}_R$, $\tilde{\nu}_i$, $\tilde{b}_1$ and $\tilde{t}_1$ LSP scenarios consistent with the observed anomalous magnetic moment of the muon and $b \to s\gamma$ as well as consistent with collider constraints from LEP and the Tevatron.

We have also analyzed the phenomenology of $\tilde{\nu}_i$ LSP models at the LHC. We have considered one benchmark scenario with a $\tilde{\nu}_\mu$ LSP. Within this scenario, we have found that direct decays of light as well as heavy SUSY particles lead to an excess of muons in the final state compared to SM rates, see Table 4.4. In general, promising pair production signatures are high-p_T muons of a few hundred GeV, *cf.* Fig. 4.7, high-p_T jets, like-sign muon events and long-lived taus with a detached vertex of the order of 1 cm. These signatures can be used to discover SUSY as well as to distinguish P_6 violating from P_6 conserving models.

In addition, we have investigated for the first time in detail the phenomenology of baryontriality, B_3, mSUGRA models with a stau, $\tilde{\tau}_1$, LSP. We have hereby assumed only one non-vanishing B_3 coupling λ'_{ijk} at the GUT scale. We would expect either a four-body or two-body decay of the $\tilde{\tau}_1$ LSP depending on whether it couples directly to the dominant B_3 operator or not. However, in B_3 mSUGRA models the renormalization group equations are highly coupled and further couplings are generated at the weak scale.

We have numerically investigated the generation of λ_{i33} couplings via dominant λ'_{ijk} couplings. λ_{i33} will always lead to a two-body decay of the $\tilde{\tau}_1$ LSP whereas λ'_{ijk} for $i = 1, 2$ leads to a four-body decay. We have found that the generated λ_{i33} couplings are typically

at least two orders of magnitude smaller than the dominant λ'_{ijk} coupling, *cf.* Fig. 5.2 and Fig. 5.3. However, it turned out that in large regions of parameter space the two-body decay dominates over the four-body decay; see Figs. 5.6-5.10.

We have applied our results to resonant single slepton production at the LHC. We have investigated numerically single smuon production for $\lambda'_{2jk} \neq 0$ within two representative $\tilde{\tau}_1$ LSP scenarios. We have included the two-body $\tilde{\tau}_1$ LSP decays via the generated λ_{233} couplings in our analysis. We have found as promising signatures like-sign dimuon events and three- and four-muon final states, *cf.* Table 5.3. Within our example scenarios the respective cross sections are of the order of 100 fb; see Tables 5.4-5.7.

For the special case of dominant B_3 couplings λ'_{i3k}, resonant single charged slepton production is not possible at hadron colliders, as there are no incoming top quarks in the proton. Instead we have to consider the associated production with a top quark. We have analyzed this difficult signature in detail. As the decisive observable for λ'_{131} and λ'_{231} we have proposed the lepton charge asymmetry. We have shown that the signal can be distinguished from the SM background for slepton masses up to 350 GeV depending on the scenario; see Figs. 6.8-6.10

We want to encourage the experimental groups to look for the new LHC signatures which we have found in this thesis. Especially the signatures which involve muons in the final state might be explored with early LHC data, *i.e.* high-p_T and like-sign dimuon events in $\tilde{\nu}_\mu$ LSP scenarios and like-sign dimuon and three- and four-muon final states for single slepton production with a $\tilde{\tau}_1$ LSP.

A. The Low Energy Spectrum of mSUGRA

A.1. Fermion Mixing

All parameters in the superpotential, Eq. (2.4), are given in the weak-current eigenstate basis. This includes the quark and lepton Yukawa coupling matrices $\mathbf{Y}_U$, $\mathbf{Y}_D$, $\mathbf{Y}_E$ and the corresponding mass matrices $\mathbf{m_u}$, $\mathbf{m_d}$, $\mathbf{m_e}$. Since, in general, these matrices are not diagonal, we need to rotate the (charged) lepton and quark fields from the weak into the mass eigenstate basis,

$$f_{L,R}^{\text{mass}} = \mathbf{V_{fL,R}}\, f_{L,R}^{\text{weak}}\,, \tag{A.1}$$

with $f_{L,R}$ denoting the left- and right-handed fermion fields, respectively and $\mathbf{V_{fL,R}}$ denoting the corresponding rotation matrices. The mass matrices in the mass eigenstate basis are then given by

$$\begin{aligned} \mathbf{V_{uL}}\,\mathbf{m_u}\,\mathbf{V_{uR}^{+}} &= \text{diag}(m_u, m_c, m_t), \\ \mathbf{V_{dL}}\,\mathbf{m_d}\,\mathbf{V_{dR}^{+}} &= \text{diag}(m_d, m_s, m_b), \\ \mathbf{V_{eL}}\,\mathbf{m_e}\,\mathbf{V_{eR}^{+}} &= \text{diag}(m_e, m_\mu, m_\tau), \end{aligned} \tag{A.2}$$

defined at the weak scale M_Z. The rotation matrices $\mathbf{V_{fL,R}}$ are not directly experimentally accessible but only the CKM matrix $\mathbf{V}_{\text{CKM}}$,

$$\mathbf{V}_{\text{CKM}} = \mathbf{V_{uL}}\mathbf{V_{dL}^{+}}. \tag{A.3}$$

In general, the rotation matrices for the left-handed fields differ from those for the right-handed fields. However, we can simplify the structure of the Yukawa couplings, if we assume real and symmetric Yukawa coupling matrices, thus $\mathbf{V_{fL}} = \mathbf{V_{fR}}$. Furthermore we neglect neutrino masses in this context and assume that $\mathbf{Y}_E$ is diagonal in the weak-current basis. Correspondingly, $\mathbf{V_{eL,R}} = \mathbb{1}_{3\times3}$.

To further constrain the quark Yukawa couplings, we can restrict ourselves to the extreme cases of quark mixing taking place completely in the up- or the down-quark sector, respectively. We will refer to it as "up-type mixing" if

$$\mathbf{V_{uL,R}} = \mathbf{V}_{\text{CKM}}, \quad \mathbf{V_{dL,R}} = \mathbb{1}_{3\times3}, \tag{A.4}$$

at the weak scale M_Z and as "down-type mixing" if

$$\mathbf{V_{uL,R}} = \mathbb{1}_{3\times3}, \quad \mathbf{V_{dL,R}} = \mathbf{V}_{\text{CKM}}^{+} \tag{A.5}$$

at the weak scale. Therefore, in up-type mixing scenarios, the Yukawa matrices are

$$\begin{aligned}\mathbf{Y}_U(M_Z) \times v_u &= \mathbf{V}_{\rm CKM}^{+} \cdot \mathrm{diag}(m_u, m_c, m_t) \cdot \mathbf{V}_{\rm CKM}, \\ \mathbf{Y}_D(M_Z) \times v_d &= \mathrm{diag}(m_d, m_s, m_b),\end{aligned} \tag{A.6}$$

and in down-type mixing scenarios, the Yukawa matrices are

$$\begin{aligned}\mathbf{Y}_U(M_Z) \times v_u &= \mathrm{diag}(m_u, m_c, m_t), \\ \mathbf{Y}_D(M_Z) \times v_d &= \mathbf{V}_{\rm CKM} \cdot \mathrm{diag}(m_d, m_s, m_b) \cdot \mathbf{V}_{\rm CKM}^{+},\end{aligned} \tag{A.7}$$

respectively. In Sect. 4 and Sect. 5, we will consider these two extreme cases. v_u (v_d) is the vacuum expectation value of the up-type (down-type) neutral CP-even Higgs with

$$v_u = v \sin\beta\,, \qquad v_d = v \cos\beta\,, \tag{A.8}$$

where $v = 174$ GeV is the SM vacuum expectation value[1].

As a consequence of the non-trivial quark rotation matrices, the λ'_{ijk} coupling in Eq. (2.6) also has to be rotated from the weak basis into the quark mass basis for a comparison with experimental data. In case of up-type mixing, the $L_i Q_j \bar{D}_k$ interactions of the superpotential, Eq. (2.6), in the quark mass basis are in terms of $SU(2)$ component superfields

$$\lambda'_{ijk}[N_i D_j^m - E_i (\mathbf{V}_{\rm CKM}^{+})_{jl} U_l^m] \bar{D}_k^m\,. \tag{A.9}$$

In the case of down-mixing they are

$$\lambda'_{ijk}[N_i (\mathbf{V}_{\rm CKM})_{jl} D_l^m - E_i U_j^m] (\mathbf{V}_{\rm CKM}^{+})_{nk} \bar{D}_n^m\,. \tag{A.10}$$

See also Ref. [164]. However for the slepton production cross sections, we do not take into account these CKM effects. If needed, the corresponding rescaling of the λ' coupling can be done easily. Furthermore the sub-dominant interactions, which include non-diagonal matrix elements of $\mathbf{V}_{\rm CKM}$, do not allow for large production cross sections since λ' enters only quadratically.

A.2. Sparticle Spectra

We cite here approximate expressions for the relevant SUSY particle masses in terms of the P_6 mSUGRA parameters, Eq. (2.17), as given in Ref. [256], *cf.* also the original work in Ref. [257]. The masses of the sleptons and squarks of the first and second generation are

$$\begin{aligned} m^2_{\tilde{\ell}_R} &= M_0^2 + 0.15 M_{1/2}^2 - \sin^2\theta_W M_{Z^0}^2 \cos 2\beta, \\ m^2_{\tilde{\ell}_L} &= M_0^2 + 0.52 M_{1/2}^2 - \left(\frac{1}{2} - \sin^2\theta_W\right) M_{Z^0}^2 \cos 2\beta, \\ m^2_{\tilde{\nu}} &= M_0^2 + 0.52 M_{1/2}^2 + \frac{1}{2} M_{Z^0}^2 \cos 2\beta, \end{aligned} \tag{A.11}$$

[1] In B_3 SUSY models, (A.8) is in general modified by additional sneutrino vacuum expectation values v_i. But $v_i \ll v$ in order to be consistent with neutrino masses [58]. We therefore neglect v_i in Eq. (A.8).

$$
\begin{aligned}
m^2_{\tilde{u}_R} &= M_0^2 + (0.07 + c_{\tilde{g}})M^2_{1/2} + \frac{2}{3}\sin^2\theta_W M^2_{Z^0}\cos 2\beta, \\
m^2_{\tilde{d}_R} &= M_0^2 + (0.02 + c_{\tilde{g}})M^2_{1/2} - \frac{1}{3}\sin^2\theta_W M^2_{Z^0}\cos 2\beta, \\
m^2_{\tilde{u}_L} &= M_0^2 + (0.47 + c_{\tilde{g}})M^2_{1/2} + \left(\frac{1}{2} - \frac{2}{3}\sin^2\theta_W\right) M^2_{Z^0}\cos 2\beta, \\
m^2_{\tilde{d}_L} &= M_0^2 + (0.47 + c_{\tilde{g}})M^2_{1/2} - \left(\frac{1}{2} - \frac{1}{3}\sin^2\theta_W\right) M^2_{Z^0}\cos 2\beta,
\end{aligned}
\tag{A.12}
$$

where θ_W denotes the electroweak mixing angle and M_{Z^0} is the mass of the Z boson. The third terms in Eq. (A.11) and Eq. (A.12) originate from the D-term quartic interactions. The coefficient $c_{\tilde{g}}$ varies between approximately 4.5 and 6 for squark masses between 100 GeV and 1 TeV.

For sfermions of the third generation, the mixing between left- and right-handed gauge-current eigenstates has to be taken into account. The stau mass matrix squared $\mathfrak{M}^2_{\tilde{\tau}}$ is given by [79]

$$
\mathfrak{M}^2_{\tilde{\tau}} = \begin{pmatrix} m_\tau^2 + A_{LL} & m_\tau B_{LR} \\ m_\tau B_{LR} & m_\tau^2 + C_{RR} \end{pmatrix}, \tag{A.13}
$$

with m_τ denoting the tau lepton mass and, expressed in terms of left- and right-handed third generation softbreaking parameters $(\mathbf{m}^2_{\tilde{\mathbf{L}}})_{33}$ and $(\mathbf{m}^2_{\tilde{\mathbf{E}}})_{33}$, Eq. (2.3), respectively,

$$
\begin{aligned}
A_{LL} &= (\mathbf{m}^2_{\tilde{\mathbf{L}}})_{33} - (0.5 - \sin^2\theta_W)M^2_{Z^0}\cos 2\beta\,, \\
B_{LR} &= A_\tau - \mu\tan\beta\,, \\
C_{RR} &= (\mathbf{m}^2_{\tilde{\mathbf{E}}})_{33} - \sin^2\theta_W M^2_{Z^0}\cos 2\beta,
\end{aligned}
\tag{A.14}
$$

where A_τ is the trilinear coupling of the left- and right-handed stau to the Higgs. In mSUGRA, $A_\tau = A_0$ at the GUT scale. The softbreaking parameters depend on the mSUGRA parameters as follows [256],

$$
\begin{aligned}
(\mathbf{m}^2_{\tilde{\mathbf{E}}})_{33} &= M_0^2 + 0.15M^2_{1/2} - \frac{2}{3}X_\tau, \\
(\mathbf{m}^2_{\tilde{\mathbf{L}}})_{33} &= M_0^2 + 0.52M^2_{1/2} - \frac{1}{3}X_\tau, \\
X_\tau &\equiv 10^{-4}(1 + \tan^2\beta)\left(M_0^2 + 0.15M^2_{1/2} + 0.33A_0^2\right),
\end{aligned}
\tag{A.15}
$$

where X_τ parameterizes the influence of the tau Yukawa coupling. Note, that X_τ can have a strong impact on the stau masses due to its $\tan^2\beta$ dependence, even though X_τ is suppressed by a factor 10^{-4}.

The stau mass eigenstates $\tilde{\tau}_{1,2}$ are obtained from the gauge eigenstates by a unitary rotation U such that U diagonalizes the mass matrix, $U\mathfrak{M}^2_{\tilde{\tau}}U^\dagger = \mathrm{diag}\left(m^2_{\tilde{\tau}_1}, m^2_{\tilde{\tau}_2}\right)$, yielding for the masses $m_{\tilde{\tau}_{1,2}}$

$$
m^2_{\tilde{\tau}_{1,2}} = m_\tau^2 + \frac{1}{2}(A_{LL} + C_{RR}) \mp \frac{1}{2}\sqrt{(A_{LL} - C_{RR})^2 + 4m_\tau^2 B^2_{LR}}\,. \tag{A.16}
$$

The gaugino masses can be approximated in terms of the universal gaugino mass $M_{1/2}$ [256],

$$\begin{aligned} m_{\tilde{\chi}_1^0} &\simeq M_1 = 0.41 M_{1/2}, \\ m_{\tilde{\chi}_2^0} &\simeq M_2 = 0.84 M_{1/2}. \end{aligned} \tag{A.17}$$

Here it has been used that the lightest neutralino, $\tilde{\chi}_1^0$, is bino-like in many mSUGRA models and that its mass can be approximated by the bino mass parameter M_1 at the weak scale. Accordingly, the second lightest neutralino, $\tilde{\chi}_2^0$, is mainly wino-like and its mass governed by the wino mass parameter M_2.

A.3. Reference Scenarios with a $\tilde{\tau}_1$ LSP

For the purpose of numerical studies and as future reference points, we define two specific sets of B_3 mSUGRA scenarios with a $\tilde{\tau}_1$ LSP:

$$\begin{aligned} \textbf{Set A:}\ & M_0 = 0\,\text{GeV},\ M_{1/2} = 500\,\text{GeV}, \\ & A_0 = 600\,\text{GeV},\ \tan\beta = 13, \text{sgn}(\mu) = +1, \\ & \text{a single } \lambda'_{ijk}|_{\text{GUT}} \neq 0, \\ \textbf{Set B:}\ & M_0 = 0\,\text{GeV},\ M_{1/2} = 700\,\text{GeV}, \\ & A_0 = 1150\,\text{GeV}\,, \tan\beta = 26, \text{sgn}(\mu) = +1, \\ & \text{a single } \lambda'_{ijk}|_{\text{GUT}} \neq 0. \end{aligned} \tag{A.18}$$

They are chosen in accordance with the following bounds (see also Sect. 4.2 and Sect. 4.1.1 for more details)[2]:

- $\text{BR}(B_s \to \mu^+\mu^-) < 4.7 \times 10^{-8}$ at the 95% C.L. [151].
- $2.74 \times 10^{-4} < \text{BR}(b \to s\gamma) < 4.30 \times 10^{-4}$ [151, 193, 194].
- The discrepancy between experiment and the SM prediction of the anomalous magnetic moment of the muon is $\delta a_\mu = a_\mu^{\text{exp}} - a_\mu^{\text{SM}} = (29.5 \pm 8.8) \times 10^{-10}$, *i.e.* 3.4σ [4, 5, 6]. The sets Eq. (A.18) are chosen such that $\delta a_\mu^{\text{SUSY}} = a_\mu^{\text{MSSM}} - a_\mu^{\text{SM}}$ agrees with δa_μ within 2σ.
- Higgs mass $m_{h^0} \geq 114.4$ GeV [152] which we reduce by 3 GeV to account for numerical uncertainties [40, 106, 153, 154].
- All couplings λ'_{ijk} in the following are chosen such that the tree-level neutrino mass is smaller than 0.71 eV [161, 162]. A corresponding comprehensive set of bounds for the mSUGRA parameter set SPS1a [146] with one non-vanishing coupling λ'_{ijk} is given in Ref. [58]. Note, that the generated tree-level neutrino mass depends on all mSUGRA parameters, Eq. (2.27). The neutrino mass bounds on λ'_{ijk} for Set A and Set B are weaker compared to those for SPS1a.

We use `micrOMEGAs1.3.7` [195] to calculate $\text{BR}(B_s \to \mu^+\mu^-)$, $\text{BR}(b \to s\gamma)$, and $\delta a_\mu^{\text{SUSY}}$. This program does not include the B_3 couplings. But the corresponding effects are negligible for

	masses [GeV]			masses [GeV]	
	Set A	Set B		Set A	Set B
$\tilde{\tau}_1$	179	146	$\tilde{\chi}_1^0$	203	290
$\tilde{e}_R$	193	266	$\tilde{\chi}_2^0$	380	544
$\tilde{\tau}_2$	340	453	$\tilde{\chi}_3^0$	571	754
$\tilde{e}_L$	340	471	$\tilde{\chi}_4^0$	587	765
$\tilde{\nu}_\tau$	326	437	$\tilde{\chi}_1^\pm$	383	549
$\tilde{\nu}_e$	329	461	$\tilde{\chi}_2^\pm$	583	761
$\tilde{t}_1$	841	1160	h^0	113	115
$\tilde{b}_1$	970	1300	H^0	643	795
$\tilde{u}_R$	1010	1370	A^0	642	795
$\tilde{t}_2$	1010	1340	H^+	648	799
$\tilde{b}_2$	995	1340			
$\tilde{u}_L$	1040	1410	$\tilde{g}$	1150	1560

Table A.1.: Sparticle masses for the B_3 mSUGRA sets A and B as defined in Eq. (A.18), evaluated for a renormalization scale $Q_{\rm susy} = \sqrt{m_{\tilde{t}_1}(Q_{\rm susy})\, m_{\tilde{t}_2}(Q_{\rm susy})}$ using `SOFTSUSY2.0.10` [145, 147]. The variation due to different $\lambda'_{ijk}|_{\rm GUT} \neq 0$ and quark mixing (see Sect. A.1) is below the percent level. The masses in the second generation coincide with those in the first generation.

only one dominant $\lambda'_{ijk} \lesssim \mathcal{O}(10^{-2})$ [106].

We show in Table A.1 the supersymmetric mass spectra of the parameter sets A and B, Eq. (A.18). We have neglected the mass dependence on the different non-zero B_3 couplings which is valid if $\lambda'_{ijk} \lesssim \mathcal{O}(10^{-2})$ [106], *cf.* Fig. 2.4. The main B_3 effect on the spectrum is that we allow for a $\tilde{\tau}_1$ LSP.

One naturally obtains a $\tilde{\tau}_1$ LSP spectrum for $M_{1/2} \gg M_0$. The large $M_{1/2}$ raises the lightest neutralino mass, Eq. (A.17), faster than the right-handed slepton masses, Eq. (A.11). It also drives the gluino and indirectly via the RGEs the squark masses up, *cf.* Fig. 2.2. We thus see in Table A.1 squark and gluino masses $\gtrsim 1\,\text{TeV}$, while the slepton masses are below 500 GeV. Another general feature of a $\tilde{\tau}_1$ LSP scenario is that the second lightest neutralino and the lightest chargino are also heavier than the sleptons. Therefore the only conventional supersymmetric decays of the left-handed sleptons are via the lightest neutralino. Depending on the dominant B_3 coupling and its size, the left-handed sleptons can also decay into two jets.

Nearly all sparticles in Set B ($M_{1/2} = 700$ GeV) are heavier than in Set A ($M_{1/2} = 500$ GeV). The most important difference for the phenomenology at colliders arises from the different values of $\tan\beta$ ($\tan\beta = 13$ in Set A, $\tan\beta = 26$ in Set B). According to Eq. (A.15), the soft breaking parameters of the stau decrease for increasing $\tan\beta$ and thus both stau

[2] In Ref. [106], specific benchmark scenarios with a $\tilde{\tau}_1$ LSP where proposed. We do not consider them here because even the weakest bounds on λ' assuming down-type quark mixing, Eq. (A.5), are at the order of $\mathcal{O}(10^{-3})$ for which the rate of resonant slepton production is suppressed.

mass eigenstates are reduced for large values of $\tan\beta$. Furthermore, the mass of the lighter stau is reduced due to the larger L–R-mixing, *cf.* Eq. (A.13). This effect can be seen in Table A.1, where the mass of the $\tilde{\tau}_1$ LSP is 179 GeV in Set A but only 146 GeV in Set B. The $\tilde{\tau}_1$ mass and $\tan\beta$ strongly influence the possible 2- and 4-body $\tilde{\tau}_1$ LSP branching ratios. We investigate this topic in detail in Sect. 5.3.

B. The B_3 Slepton Decay $\tilde{\ell}_i^- \to W^- \bar{b} d_k$

A non-vanishing $L_i Q_3 \bar{D}_k$ operator, Eq. (2.5), allows for slepton decay into a top quark, t, and a down-type quark, d_k, of generation k,

$$\tilde{\ell}_i^- \to \bar{t} d_k \,. \tag{B.1}$$

However, this decay mode is kinematically only allowed if $m_{\tilde{\ell}_i} > m_t + m_{d_k}$. For $m_{\tilde{\ell}_i} < m_t + m_{d_k}$, the slepton decays via a virtual top quark,

$$\tilde{\ell}_i^- \to W^- \bar{b} d_k. \tag{B.2}$$

This 3-body decay has not been considered in the literature yet and is not implemented in the P_6 violating version of `Herwig` [196, 197, 198, 199, 200], either. We complete the picture by calculating the 3-body decay, Eq. (B.2), in the following.

The relevant parts of the supersymmetric Lagrangian are [80]

$$\begin{aligned} \mathcal{L}_{L_i Q_3 \bar{D}_k} &= \lambda'_{i3k} L_{1\beta} \tilde{\ell}^-_{i\beta}\, \bar{d}_k \, P_L \, t + h.c. \,, \\ \mathcal{L}_{bWt} &= -\frac{g}{\sqrt{2}} \, W^+_\mu \, \bar{t} \, \gamma^\mu \, P_L \, b + h.c. \,, \end{aligned} \tag{B.3}$$

where $L_{\alpha\beta}$ is the slepton mixing matrix, α labels the left/right current eigenstate, and β labels the mass eigenstate. From Eq. (B.3), the squared matrix element (summed over final state polarizations and colors) can be derived,

$$\begin{aligned} \left| \overline{\mathcal{M}}\big(\tilde{\ell}^-_{i\beta} \to W^- \bar{b} d_k\big) \right|^2 = \frac{3}{2} \frac{\lambda'^2_{i3k} L^2_{1\beta} g^2}{[(W+b)^2 - m_t^2]^2 + m_t^2 \Gamma_t^2} \Bigg\{ & 4 (d_k \cdot W) \left[m_b^2 + 2 (W \cdot b) - m_b^2 \, \frac{(W \cdot b)}{m_W^2} \right] \\ & + 2 (d_k \cdot b) \left[m_b^2 - m_W^2 + 4 (W \cdot b) + \frac{4 (W \cdot b)^2}{m_W^2} \right] \Bigg\}. \end{aligned} \tag{B.4}$$

We denote the particle four-momenta by the particle letter, and m_t, m_b, and m_W, are the top, bottom and W mass, respectively. Γ_t is the total width of the top quark.

From the squared matrix element, Eq. (B.4), we obtain easily the partial width for the 3-body decay, Eq. (B.2), see *e.g.* [80, 199]. We show in Fig. B.1 the partial width $\Gamma(\tilde{e}_L \to W^- \bar{b} d)$ as a function of the left-handed selectron mass, $m_{\tilde{e}_L}$. Here we take $\lambda'_{131} = 0.01$ and $L_{11} = 1$, in Eq. (B.4).

In comparison to the 3-body decay, Eq. (B.2), the possible 4-body decays via λ'_{i3k} are negligible. For example for the parameter Set B (see Appendix A.3) with non-vanishing λ'_{331}, the branching ratio of the 3-body $\tilde{\tau}_1$ LSP decay is larger by five orders of magnitude than the branching ratio of the 4-body $\tilde{\tau}_1$ LSP decays.

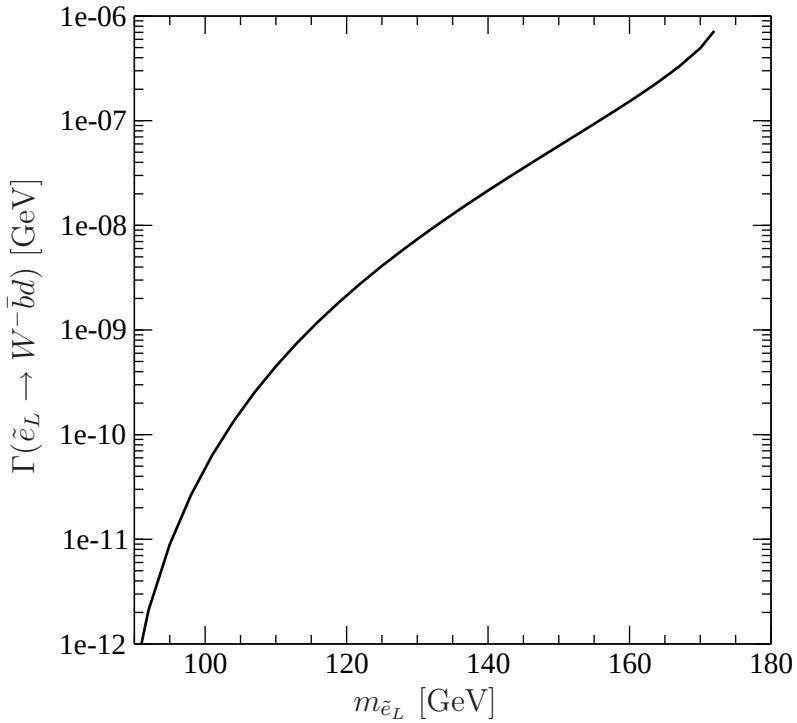

Figure B.1.: Partial width in GeV for the 3-body decay $\tilde{e}_L \to W^- \bar{b} d$ as a function of the selectron mass, $m_{\tilde{e}_L}$. We take $\lambda'_{131} = 0.01$ and $L_{11} = 1$, in Eq. (B.4).

C. Cross Sections and Branching Ratios for Slepton Production and Decay

In this Appendix we give the necessary cross sections and branching ratios to calculate rates of all possible decay signatures for single slepton production at the LHC, within the B_3 sets A and B with a $\tilde{\tau}_1$ LSP, *cf.* Eq. (A.18).

In Table C.1 and Table C.2, all hadronic production cross sections of resonant single sleptons within parameter Set A and Set B, respectively, are given. We consider here $\lambda'_{ijk}|_{\rm GUT} = 0.01$, but the cross section scales with $|\lambda'_{ijk}|^2$. The running of λ'_{ijk} is taken into account according to Eq. (5.9), leading to the following values at the SUSY scale, $Q_{\rm susy}$, *cf.* Eq. (5.15):

$$\begin{aligned} \text{Set A:}\quad & \lambda'_{2jk} = 0.0282, \quad \lambda'_{3jk} = 0.0282, \\ & \lambda'_{23k} = 0.0258, \quad \lambda'_{33k} = 0.0257, \\ & \lambda'_{2j3} = 0.0281, \quad \lambda'_{3j3} = 0.0280, \\ & \lambda'_{233} = 0.0255, \quad \lambda'_{333} = 0.0254; \end{aligned} \tag{C.1}$$

$$\begin{aligned} \text{Set B:}\quad & \lambda'_{2jk} = 0.0274, \quad \lambda'_{3jk} = 0.0271, \\ & \lambda'_{23k} = 0.0249, \quad \lambda'_{33k} = 0.0247, \\ & \lambda'_{2j3} = 0.0269, \quad \lambda'_{3j3} = 0.0266, \\ & \lambda'_{233} = 0.0238, \quad \lambda'_{333} = 0.0236, \end{aligned} \tag{C.2}$$

where $j, k = 1, 2$ and $Q_{\rm susy} = 893$ GeV for Set A and $Q_{\rm susy} = 1209$ GeV for Set B.

The production cross sections include NLO SUSY-QCD corrections [114]. The latter depend on the trilinear quark-squark-slepton coupling, $(\mathbf{h}_{D^k})_{ij}$, defined in Eq. (2.11). Numerically, it is $(\mathbf{h}_{D^k})_{ij} = -23.4$ GeV (-21.2 GeV) within Set A (Set B) at the SUSY scale. We incorporated the running of $(\mathbf{h}_{D^k})_{ij}$ by using the one-loop contributions from gauge interactions, Eq. (4.17).

Second, for the calculation of the rate for a given signature of resonant single slepton production, the branching ratios for the slepton decay and for the subsequent decay chains down to the $\tilde{\tau}_1$ LSP are needed. For all dominant λ'_{ijk} couplings these branching ratios are universal within parameter Set A and Set B, respectively, and are given in Tab. C.3.

Finally, we show in Table C.4 (Table C.5) all branching ratios of $\tilde{\tau}_1$ LSP decays for different couplings λ'_{2jk} at the GUT scale. Branching ratios within scenarios with $\lambda'_{1jk} \neq 0$

Set A	$\sigma_{\text{prod.}}$ [fb]									
	$\tilde{e}_L^+/\tilde{\mu}_L^+$	$\tilde{e}_L^-/\tilde{\mu}_L^-$	$\tilde{\nu}_{e/\mu}^*$	$\tilde{\nu}_{e/\mu}$	$\tilde{\tau}_2^+$	$\tilde{\tau}_2^-$	$\tilde{\tau}_1^+$	$\tilde{\tau}_1^-$	$\tilde{\nu}_\tau^*$	$\tilde{\nu}_\tau$
$\lambda'_{i11}\|_{\text{GUT}}= 0.01$	2700	1540	1860	1860	2620	1500	434	272	190	190
$\lambda'_{i22}\|_{\text{GUT}}= 0.01$	268	268	410	410	2600	2600	64.5	64.5	421	421
$\lambda'_{i12}\|_{\text{GUT}}= 0.01$	2150	464	1430	602	2090	451	360	103	1460	616
$\lambda'_{i21}\|_{\text{GUT}}= 0.01$	405	1050	602	1430	393	1020	91.9	197	616	1460
$\lambda'_{i13}\|_{\text{GUT}}= 0.01$	1240	220	788	292	1210	214	216	51.3	806	299
$\lambda'_{i23}\|_{\text{GUT}}= 0.01$	119	119	191	191	116	116	30.0	30.0	196	196
$\lambda'_{i31}\|_{\text{GUT}}= 0.01$	–	–	247	666	–	–	–	–	253	681
$\lambda'_{i32}\|_{\text{GUT}}= 0.01$	–	–	161	161	–	–	–	–	166	166
$\lambda'_{i33}\|_{\text{GUT}}= 0.01$	–	–	69.3	69.3	–	–	–	–	71.1	71.1

Table C.1.: Complete list of hadronic cross sections for resonant single slepton/sneutrino production via $\lambda'_{ijk}|_{\text{GUT}}= 0.01$ at the pp collider LHC ($\sqrt{S} = 14$ TeV) within the parameter Set A. The cross sections include QCD and SUSY-QCD corrections at NLO [114]. For λ'_{i3k}, sleptons cannot be produced because of the vanishing top-quark density in the proton.

Set B	$\sigma_{\text{prod.}}$ [fb]									
	$\tilde{e}_L^+/\tilde{\mu}_L^+$	$\tilde{e}_L^-/\tilde{\mu}_L^-$	$\tilde{\nu}_{e/\mu}^*$	$\tilde{\nu}_{e/\mu}$	$\tilde{\tau}_2^+$	$\tilde{\tau}_2^-$	$\tilde{\tau}_1^+$	$\tilde{\tau}_1^-$	$\tilde{\nu}_\tau^*$	$\tilde{\nu}_\tau$
$\lambda'_{i11}\|_{\text{GUT}}= 0.01$	885	476	559	559	949	515	1168	750	657	657
$\lambda'_{i22}\|_{\text{GUT}}= 0.01$	67.3	67.3	102	102	74.7	74.7	192	192	124	124
$\lambda'_{i12}\|_{\text{GUT}}= 0.01$	681	123	414	155	735	136	976	301	490	187
$\lambda'_{i21}\|_{\text{GUT}}= 0.01$	105	309	155	414	117	337	269	548	187	490
$\lambda'_{i13}\|_{\text{GUT}}= 0.01$	370	54.6	214	70.2	401	60.6	572	146	255	85.4
$\lambda'_{i23}\|_{\text{GUT}}= 0.01$	28.2	28.2	44.4	44.4	31.4	31.4	87.2	87.2	54.3	54.3
$\lambda'_{i31}\|_{\text{GUT}}= 0.01$	–	–	60.4	184	–	–	–	–	73.5	219
$\lambda'_{i32}\|_{\text{GUT}}= 0.01$	–	–	38.2	38.2	–	–	–	–	46.7	46.7
$\lambda'_{i33}\|_{\text{GUT}}= 0.01$	–	–	14.8	14.8	–	–	–	–	18.2	18.2

Table C.2.: Same as Tab. C.1 but for parameter Set B.

	BRs [%]			
	$\lambda'_{2jk}\|_{\rm GUT} = 0.01$		$\lambda'_{3jk}\|_{\rm GUT} = 0.01$	
	Set A	Set B	Set A	Set B
$\tilde{\mu}_L^- \to \tilde{\chi}_1^0\,\mu^-$	91.1	91.3	100	100
$\tilde{\mu}_L^- \to \bar{u}_j\,d_k$	8.9	8.7	–	–
$\tilde{\nu}_\mu \to \tilde{\chi}_1^0\,\nu_\mu$	91.7	91.5	100	100
$\tilde{\nu}_\mu \to \bar{d}_j\,d_k$	9.3	8.4	–	–
$\tilde{\chi}_1^0 \to \tilde{\tau}_1^\pm\,\tau^\mp$	36.0	45.7	36.0	45.7
$\tilde{\chi}_1^0 \to \tilde{\mu}_R^\pm\,\mu^\mp$	7.0	2.2	7.0	2.2
$\tilde{\chi}_1^0 \to \tilde{e}_R^\pm\,e^\mp$	7.0	2.1	7.0	2.1
$\tilde{\mu}_R^- \to \tilde{\tau}_1^+\,\mu^-\,\tau^-$	54.3	64.1	54.3	64.1
$\tilde{\mu}_R^- \to \tilde{\tau}_1^-\,\mu^-\,\tau^+$	45.7	35.9	45.7	35.9
$\tilde{\tau}_2^- \to \tilde{\chi}_1^0\,\tau^-$	58.4	14.7	55.5	14.5
$\tilde{\tau}_2^- \to \tilde{\tau}_1^-\,h^0$	22.5	41.8	21.4	41.2
$\tilde{\tau}_2^- \to \tilde{\tau}_1^-\,Z^0$	19.1	43.5	18.1	42.9
$\tilde{\tau}_2^- \to \bar{u}_j\,d_k$	–	–	5.0	1.3
$\tilde{\nu}_\tau \to \tilde{\chi}_1^0\,\nu_\tau$	62.2	13.6	58.8	13.4
$\tilde{\nu}_\tau \to \tilde{\tau}_1^-\,W^+$	37.8	86.4	35.8	85.2
$\tilde{\nu}_\tau \to \bar{d}_j\,d_k$	–	–	5.4	1.4

Table C.3.: Table of branching ratios, BRs, that are relevant for single slepton production and decays within the B_3 mSUGRA scenarios Set A and Set B. Two different non-zero B_3 couplings are considered, $\lambda'_{2jk}|_{\rm GUT} = 0.01$ for columns 2 and 3 and $\lambda'_{3jk}|_{\rm GUT} = 0.01$ for columns 4 and 5. The branching ratios for $\lambda'_{1jk} \neq 0$ can be obtained from those for $\lambda'_{2jk} \neq 0$ by interchanging muon and electron flavor in the first four decay channels. The branching ratios for $\tilde{e}_L$ ($\tilde{\nu}_e$, $\tilde{e}_R$) in scenarios with $\lambda'_{ijk} \neq 0$, $i \neq 1$ are equal to those of $\tilde{\mu}_L$ ($\tilde{\nu}_\mu$, $\tilde{\mu}_R$) with $\lambda'_{3jk} \neq 0$. The branching ratios for $\tilde{\tau}_1$ LSP decays are listed separately in Table. C.4 and Table C.5.

are analogous and can be obtained from the tables by replacing μ by e in the final state signatures.

In the case of a non-vanishing λ'_{3jk}, the $\tilde{\tau}_1$ LSP directly couples to the dominant $L_3 Q_j \bar{D}_k$ operator and decays predominantly via the inverse production process, see also the discussion in Sect. 5.3.1. For the special case of $\lambda'_{33k} \neq 0$ and $m_{\tilde{\tau}_1} < m_t$, however, the $\tilde{\tau}_1$ decays into a W boson and two jets, *cf.* Eq. (5.23). The corresponding matrix element and partial width are calculated in Appendix B.

Set A	$\tilde{\tau}_1^- \xrightarrow{\lambda} \nu_\mu \tau^-$ $[= \tilde{\tau}_1^- \xrightarrow{\lambda} \nu_\tau \mu^-]$		$\tilde{\tau}_1^- \xrightarrow{\lambda} \bar{\nu}_\mu \tau^-$		$\tilde{\tau}_1^- \xrightarrow{\lambda'} \tau^- \mu^- u_j \bar{d}_k$		$\tilde{\tau}_1^- \xrightarrow{\lambda'} \tau^- \mu^+ \bar{u}_j d_k$		$\tilde{\tau}_1^- \xrightarrow{\lambda'} \tau^- \nu_\mu d_j \bar{d}_k$		$\tilde{\tau}_1^- \xrightarrow{\lambda'} \tau^- \bar{\nu}_\mu \bar{d}_j d_k$	
λ'_{211}	7.9%	(2.7%)	0.2%	(0.1%)	11.8%	(13.3%)	25.3%	(28.5%)	15.2%	(17.1%)	31.6%	(35.6%)
λ'_{212}	21.5%	(−)	0.5%	(−)	7.9%	(14.2%)	17.1%	(29.3%)	10.2%	(18.1%)	21.3%	(38.4%)
λ'_{213}	10.5%	(−)	0.2%	(−)	11.1%	(14.1%)	23.8%	(30.2%)	14.3%	(18.1%)	29.6%	(37.6%)
λ'_{221}	21.5%	(−)	0.5%	(−)	7.9%	(14.2%)	17.1%	(29.3%)	10.2%	(18.1%)	21.3%	(38.4%)
λ'_{222}	46.8%	(46.8%)	1.1%	(1.1%)	0.7%	(0.8%)	1.6%	(1.6%)	1.0%	(1.0%)	2.0%	(2.0%
λ'_{223}	48.2%	(−)	1.1%	(−)	0.4%	(14.2%)	0.8%	(29.3%)	0.5%	(18.2%)	1.0%	(38.4%)
λ'_{231}	17.9%	(−)	0.4%	(−)	–	(−)	–	(−)	20.7%	(32.1%)	43.0%	(67.9%)
λ'_{232}	48.8%	(−)	1.1%	(−)	–	(−)	–	(−)	0.4%	(32.5%)	0.8%	(67.5%)
λ'_{233}	49.4%	(49.4%)	1.1%	(1.1%)	–	(−)	–	(−)	–	(−)	–	(−)

Table C.4.: Branching ratios of the $\tilde{\tau}_1$ LSP for different non-zero λ'_{2jk} couplings at the GUT scale. The branching ratios are calculated within the mSUGRA parameter Set A for the SUSY breaking scale $Q_{\text{susy}} = 893$ GeV. We assume down-type (up-type) quark mixing. Branching ratios for non-vanishing λ'_{1jk} are analogous, with μ replaced by e.

Set B	$\tilde{\tau}_1^- \xrightarrow{\lambda} \nu_\mu \tau^-$ $[= \tilde{\tau}_1^- \xrightarrow{\lambda} \nu_\tau \mu^-]$		$\tilde{\tau}_1^- \xrightarrow{\lambda} \bar{\nu}_\mu \tau^-$		$\tilde{\tau}_1^- \xrightarrow{\lambda'} \tau^- \mu^- u_j \bar{d}_k$		$\tilde{\tau}_1^- \xrightarrow{\lambda'} \tau^- \mu^+ \bar{u}_j d_k$		$\tilde{\tau}_1^- \xrightarrow{\lambda'} \tau^- \nu_\mu d_j \bar{d}_k$		$\tilde{\tau}_1^- \xrightarrow{\lambda'} \tau^- \bar{\nu}_\mu \bar{d}_j d_k$	
λ'_{211}	49.0%	(48.6%)	1.7%	(1.7%)	–	(0.1%)	0.1%	(0.4%)	–	(0.1%)	0.1%	(0.5%)
λ'_{212}	49.1%	(−)	1.7%	(−)	–	(5.6%)	–	(41.1%)	–	(6.3%)	–	(46.9%)
λ'_{213}	49.0%	(−)	1.7%	(−)	–	(5.7%)	0.1%	(41.0%)	–	(6.4%)	0.1%	(46.9%)
λ'_{221}	49.1%	(−)	1.7%	(−)	–	(5.6%)	–	(41.0%)	–	(6.3%)	–	(47.0%)
λ'_{222}	49.1%	(49.1%)	1.7%	(1.7%)	–	(−)	–	(−)	–	(−)	–	(−)
λ'_{223}	49.1%	(−)	1.7%	(−)	–	(5.7%)	–	(41.0%)	–	(6.4%)	–	(47.0%)
λ'_{231}	49.1%	(−)	1.7%	(−)	–	(−)	–	(−)	–	(12.0%)	0.1%	(88.0%)
λ'_{232}	49.1%	(−)	1.7%	(−)	–	(−)	–	(−)	–	(12.0%)	–	(88.0%)
λ'_{233}	49.1%	(49.1%)	1.7%	(1.7%)	–	(−)	–	(−)	–	(−)	–	(−)

Table C.5.: Branching ratios of the $\tilde{\tau}_1$ LSP for different non-zero λ'_{2jk} couplings at the GUT scale. The branching ratios are calculated within the mSUGRA parameter Set B for the SUSY breaking scale $Q_{\text{susy}} = 1209$ GeV. We assume down-type (up-type) quark mixing. Branching ratios for non-vanishing λ'_{1jk} are analogous, with μ replaced by e.

Bibliography

[1] S. L. Glashow, Nucl. Phys. **22**, 579 (1961).

[2] S. Weinberg, Phys. Rev. Lett. **19**, 1264 (1967).

[3] Particle Data Group, C. Amsler *et al.*, Phys. Lett. **B667**, 1 (2008).

[4] Muon G-2 Collaboration, G. W. Bennett *et al.*, Phys. Rev. **D73**, 072003 (2006), hep-ex/0602035.

[5] J. P. Miller, E. de Rafael, and B. L. Roberts, Rept. Prog. Phys. **70**, 795 (2007), hep-ph/0703049.

[6] D. Stöckinger, (2007), arXiv:0710.2429 [hep-ph].

[7] D. Stöckinger, J. Phys. **G34**, R45 (2007), hep-ph/0609168.

[8] M. Drees, (1996), hep-ph/9611409.

[9] E. Gildener, Phys. Rev. **D14**, 1667 (1976).

[10] M. J. G. Veltman, Acta Phys. Polon. **B12**, 437 (1981).

[11] N. Sakai, Zeit. Phys. **C11**, 153 (1981).

[12] E. Witten, Nucl. Phys. **B188**, 513 (1981).

[13] S. P. Martin, (1997), hep-ph/9709356.

[14] D. A. Dicus and V. S. Mathur, Phys. Rev. **D7**, 3111 (1973).

[15] B. W. Lee, C. Quigg, and H. B. Thacker, Phys. Rev. **D16**, 1519 (1977).

[16] I. J. R. Aitchison and A. J. G. Hey, *Gauge theories in particle physics: A practical introduction. Vol. 2: Non-Abelian gauge theories: QCD and the electroweak theory* , Bristol, UK: IOP (2004) 454 p.

[17] S. R. Coleman and J. Mandula, Phys. Rev. **159**, 1251 (1967).

[18] R. Haag, J. T. Lopuszanski, and M. Sohnius, Nucl. Phys. **B88**, 257 (1975).

[19] P. Nath and R. L. Arnowitt, Phys. Lett. **B56**, 177 (1975).

[20] R. L. Arnowitt, P. Nath, and B. Zumino, Phys. Lett. **B56**, 81 (1975).

[21] D. Z. Freedman, P. van Nieuwenhuizen, and S. Ferrara, Phys. Rev. **D13**, 3214 (1976).

[22] S. Deser and B. Zumino, Phys. Lett. **B62**, 335 (1976).

[23] D. Z. Freedman and P. van Nieuwenhuizen, Phys. Rev. **D14**, 912 (1976).

[24] E. Cremmer *et al.*, Nucl. Phys. **B147**, 105 (1979).

[25] E. Cremmer, S. Ferrara, L. Girardello, and A. Van Proeyen, Nucl. Phys. **B212**, 413 (1983).

[26] M. B. Green, J. H. Schwarz, and E. Witten, *Superstring theory. Vol. 1: Introduction* , Cambridge, UK: Univ. Pr. (1987) 469 p. (Cambridge Monographs On Mathematical Physics).

[27] M. B. Green, J. H. Schwarz, and E. Witten, *Superstring theory. Vol. 2: Loop amplitudes, anomalies and phenomenology* , Cambridge, UK: Univ. Pr. (1987) 596 p. (Cambridge Monographs On Mathematical Physics).

[28] D. Bailin and A. Love, *Supersymmetric gauge field theory and string theory* , Bristol, UK: IOP (1994) 322 p. (Graduate student series in physics).

[29] J. Polchinski, *String theory. Vol. 1: An introduction to the bosonic string* , Cambridge, UK: Univ. Pr. (1998) 402 p.

[30] J. Polchinski, *String theory. Vol. 2: Superstring theory and beyond* , Cambridge, UK: Univ. Pr. (1998) 531 p.

[31] J. R. Ellis, S. Kelley, and D. V. Nanopoulos, Phys. Lett. **B260**, 131 (1991).

[32] U. Amaldi, W. de Boer, and H. Furstenau, Phys. Lett. **B260**, 447 (1991).

[33] P. Langacker and M.-x. Luo, Phys. Rev. **D44**, 817 (1991).

[34] P. Langacker and N. Polonsky, Phys. Rev. **D47**, 4028 (1993), hep-ph/9210235.

[35] G. G. Ross and R. G. Roberts, Nucl. Phys. **B377**, 571 (1992).

[36] L. E. Ibanez and G. G. Ross, Phys. Lett. **B110**, 215 (1982).

[37] LEP Electroweak Working Group, M. Grünewald *et al.*, http://lepewwg.web.cern.ch/LEPEWWG/ .

[38] Tevatron New Phenomena, Higgs working group, (2009), arXiv:0903.4001 [hep-ex].

[39] S. Heinemeyer, W. Hollik, and G. Weiglein, Eur. Phys. J. **C9**, 343 (1999), hep-ph/9812472.

[40] G. Degrassi, S. Heinemeyer, W. Hollik, P. Slavich, and G. Weiglein, Eur. Phys. J. **C28**, 133 (2003), hep-ph/0212020.

[41] J. R. Ellis, J. S. Hagelin, D. V. Nanopoulos, K. A. Olive, and M. Srednicki, Nucl. Phys. **B238**, 453 (1984).

[42] K. Rajagopal, M. S. Turner, and F. Wilczek, Nucl. Phys. **B358**, 447 (1991).

[43] E. J. Chun and H. B. Kim, Phys. Rev. **D60**, 095006 (1999), hep-ph/9906392.

[44] E. J. Chun and H. B. Kim, JHEP **10**, 082 (2006), hep-ph/0607076.

[45] L. J. Hall and M. Suzuki, Nucl. Phys. **B231**, 419 (1984).

[46] Y. Grossman and H. E. Haber, Phys. Rev. **D59**, 093008 (1999), hep-ph/9810536.

[47] Y. Grossman and H. E. Haber, (1999), hep-ph/9906310.

[48] F. Borzumati, Y. Grossman, E. Nardi, and Y. Nir, Phys. Lett. **B384**, 123 (1996), hep-ph/9606251.

[49] S. Davidson and M. Losada, Phys. Rev. **D65**, 075025 (2002), hep-ph/0010325.

[50] P. Minkowski, Phys. Lett. **B67**, 421 (1977).

[51] T. Yanagida, In Proceedings of the Workshop on the Baryon Number of the Universe and Unified Theories, Tsukuba, Japan, 13-14 Feb 1979.

[52] R. N. Mohapatra and G. Senjanovic, Phys. Rev. Lett. **44**, 912 (1980).

[53] M. Gell-Mann, P. Ramond, and R. Slansky, Print-80-0576 (CERN).

[54] R. N. Mohapatra and G. Senjanovic, Phys. Rev. **D23**, 165 (1981).

[55] CDF Collaboration, T. Adams, (2008), arXiv:0808.0728 [hep-ex].

[56] ATLAS Collaboration, CERN-LHCC-99-15.

[57] CMS Collaboration, G. L. Bayatian *et al.*, J. Phys. **G34**, 995 (2007).

[58] B. C. Allanach, A. Dedes, and H. K. Dreiner, Phys. Rev. **D69**, 115002 (2004), hep-ph/0309196.

[59] H. K. Dreiner and S. Grab, (2008), arXiv:0811.0200 [hep-ph].

[60] M. A. Bernhardt, S. P. Das, H. K. Dreiner, and S. Grab, Phys. Rev. **D79**, 039905 (2008), arXiv:0810.3423 [hep-ph].

[61] M. A. Bernhardt, S. Prasad Das, H. K. Dreiner, and S. Grab, AIP Conf. Proc. **1078**, 306 (2009), arXiv:0809.3176 [hep-ph].

[62] H. K. Dreiner, S. Grab, and M. K. Trenkel, Phys. Rev. **D79**, 016002 (2009), arXiv:0808.3079 [hep-ph].

[63] M. A. Bernhardt, H. K. Dreiner, S. Grab, and P. Richardson, Phys. Rev. **D78**, 015016 (2008), arXiv:0802.1482 [hep-ph].

[64] P. P. Srivastava, *Supersymmetry, superfields and supergravity: An introduction* , Bristol, UK: Hilger (1986) 162 P. (Graduate Student Series In Physics).

[65] H. E. Haber and G. L. Kane, Phys. Rept. **117**, 75 (1985).

[66] I. J. R. Aitchison, *Supersymmetry in particle physics: An elementary introduction* .

[67] H. Baer and X. Tata, *Weak scale supersymmetry: From superfields to scattering events* , Cambridge, UK: Univ. Pr. (2006) 537 p.

[68] P. C. West, *Introduction to supersymmetry and supergravity* , Singapore, Singapore: World Scientific (1990) 425 p.

[69] H. K. Dreiner, H. E. Haber, and S. P. Martin, (2008), arXiv:0812.1594 [hep-ph].

[70] H. P. Nilles, Phys. Rept. **110**, 1 (1984).

[71] H. Kalka and G. Soff, *Supersymmetry. (In German)* , Stuttgart, Germany: Teubner (1997) 444 p.

[72] H. E. Haber, (1993), hep-ph/9306207.

[73] S. Y. Choi *et al.*, (2008), arXiv:0812.3586 [hep-ph].

[74] L. Alvarez-Gaume and S. F. Hassan, Fortsch. Phys. **45**, 159 (1997), hep-th/9701069.

[75] S. Y. Choi, M. Drees, A. Freitas, and P. M. Zerwas, (2008), arXiv:0808.2410 [hep-ph].

[76] M. M. Nojiri *et al.*, (2008), arXiv:0802.3672 [hep-ph].

[77] H. E. Haber, Nucl. Phys. Proc. Suppl. **62**, 469 (1998), hep-ph/9709450.

[78] L. Girardello and M. T. Grisaru, Nucl. Phys. **B194**, 65 (1982).

[79] J. F. Gunion and H. E. Haber, Nucl. Phys. **B272**, 1 (1986).

[80] P. Richardson, (2000), hep-ph/0101105.

[81] F. Gabbiani, E. Gabrielli, A. Masiero, and L. Silvestrini, Nucl. Phys. **B477**, 321 (1996), hep-ph/9604387.

[82] S. Jager, Eur. Phys. J. **C59**, 497 (2009), arXiv:0808.2044 [hep-ph].

[83] N. Sakai and T. Yanagida, Nucl. Phys. **B197**, 533 (1982).

[84] S. Weinberg, Phys. Rev. **D26**, 287 (1982).

[85] B. C. Allanach, A. Dedes, and H. K. Dreiner, Phys. Rev. **D60**, 075014 (1999), hep-ph/9906209.

[86] S. Dimopoulos, S. Raby, and F. Wilczek, Phys. Lett. **B112**, 133 (1982).

[87] A. Y. Smirnov and F. Vissani, Phys. Lett. **B380**, 317 (1996), hep-ph/9601387.

[88] G. Bhattacharyya and P. B. Pal, Phys. Rev. **D59**, 097701 (1999), hep-ph/9809493.

[89] R. Barbier *et al.*, Phys. Rept. **420**, 1 (2005), hep-ph/0406039.

[90] Super-Kamiokande Collaboration, M. Shiozawa *et al.*, Phys. Rev. Lett. **81**, 3319 (1998), hep-ex/9806014.

[91] H. K. Dreiner, C. Luhn, and M. Thormeier, Phys. Rev. **D73**, 075007 (2006), hep-ph/0512163.

[92] L. E. Ibanez and G. G. Ross, Phys. Lett. **B260**, 291 (1991).

[93] L. E. Ibanez and G. G. Ross, Nucl. Phys. **B368**, 3 (1992).

[94] H. K. Dreiner, (1997), hep-ph/9707435.

[95] L. M. Krauss and F. Wilczek, Phys. Rev. Lett. **62**, 1221 (1989).

[96] T. Banks, Nucl. Phys. **B323**, 90 (1989).

[97] H. K. Dreiner and G. G. Ross, Nucl. Phys. **B365**, 597 (1991).

[98] R parity Working Group, B. Allanach *et al.*, (1999), hep-ph/9906224.

[99] S. P. Martin and M. T. Vaughn, Phys. Rev. **D50**, 2282 (1994), hep-ph/9311340.

[100] B. C. Allanach, A. Dedes, and H. K. Dreiner, Phys. Rev. **D60**, 056002 (1999), hep-ph/9902251.

[101] I. Jack, D. R. T. Jones, and A. F. Kord, Phys. Lett. **B632**, 703 (2006), hep-ph/0505238.

[102] B. de Carlos and P. L. White, Phys. Rev. **D54**, 3427 (1996), hep-ph/9602381.

[103] H. K. Dreiner and H. Pois, (1995), hep-ph/9511444.

[104] V. D. Barger, M. S. Berger, R. J. N. Phillips, and T. Wohrmann, Phys. Rev. **D53**, 6407 (1996), hep-ph/9511473.

[105] E. Nardi, Phys. Rev. **D55**, 5772 (1997), hep-ph/9610540.

[106] B. C. Allanach, M. A. Bernhardt, H. K. Dreiner, C. H. Kom, and P. Richardson, Phys. Rev. **D75**, 035002 (2007), hep-ph/0609263.

[107] R. Hempfling, Nucl. Phys. **B478**, 3 (1996), hep-ph/9511288.

[108] M. Hirsch, M. A. Diaz, W. Porod, J. C. Romao, and J. W. F. Valle, Phys. Rev. **D62**, 113008 (2000), hep-ph/0004115.

[109] B. C. Allanach and C. H. Kom, JHEP **04**, 081 (2008), arXiv:0712.0852 [hep-ph].

[110] H. K. Dreiner, J. Soo Kim, and M. Thormeier, (2007), arXiv:0711.4315 [hep-ph].

[111] S. Dimopoulos and L. J. Hall, Phys. Lett. **B207**, 210 (1988).

[112] H. K. Dreiner, P. Richardson, and M. H. Seymour, Phys. Rev. **D63**, 055008 (2001), hep-ph/0007228.

[113] B. C. Allanach, H. K. Dreiner, P. Morawitz, and M. D. Williams, Phys. Lett. **B420**, 307 (1998), hep-ph/9708495.

[114] H. K. Dreiner, S. Grab, M. Krämer, and M. K. Trenkel, Phys. Rev. **D75**, 035003 (2007), hep-ph/0611195.

[115] F. Gabbiani and A. Masiero, Nucl. Phys. **B322**, 235 (1989).

[116] MEGA Collaboration, M. L. Brooks *et al.*, Phys. Rev. Lett. **83**, 1521 (1999), hep-ex/9905013.

[117] M. Ciuchini *et al.*, JHEP **10**, 008 (1998), hep-ph/9808328.

[118] D. Becirevic *et al.*, Nucl. Phys. **B634**, 105 (2002), hep-ph/0112303.

[119] J. Foster, K.-i. Okumura, and L. Roszkowski, Phys. Lett. **B641**, 452 (2006), hep-ph/0604121.

[120] L. Silvestrini, Ann. Rev. Nucl. Part. Sci. **57**, 405 (2007), arXiv:0705.1624 [hep-ph].

[121] A. G. Cohen, D. B. Kaplan, and A. E. Nelson, Phys. Lett. **B388**, 588 (1996), hep-ph/9607394.

[122] J. D. Wells, (2003), hep-ph/0306127.

[123] N. Arkani-Hamed and S. Dimopoulos, JHEP **06**, 073 (2005), hep-th/0405159.

[124] Y. Nir and N. Seiberg, Phys. Lett. **B309**, 337 (1993), hep-ph/9304307.

[125] G. D. Kribs, E. Poppitz, and N. Weiner, Phys. Rev. **D78**, 055010 (2008), arXiv:0712.2039 [hep-ph].

[126] A. E. Blechman and S.-P. Ng, JHEP **06**, 043 (2008), arXiv:0803.3811 [hep-ph].

[127] S. Dimopoulos and H. Georgi, Nucl. Phys. **B193**, 150 (1981).

[128] H. Fritzsch and P. Minkowski, Ann. Phys. **93**, 193 (1975).

[129] R. N. Mohapatra, (1999), hep-ph/9911272.

[130] G. G. Ross, *Gand unified theories* , Reading, USA: Benjamin/cummings (1984) 497 p. (Frontiers In Physics, 60).

[131] P. H. Chankowski, O. Lebedev, and S. Pokorski, Nucl. Phys. **B717**, 190 (2005), hep-ph/0502076.

[132] A. Dedes and P. Slavich, Nucl. Phys. **B657**, 333 (2003), hep-ph/0212132.

[133] S. Dimopoulos and D. W. Sutter, Nucl. Phys. **B452**, 496 (1995), hep-ph/9504415.

[134] J. R. Ellis, S. Ferrara, and D. V. Nanopoulos, Phys. Lett. **B114**, 231 (1982).

[135] W. Buchmuller and D. Wyler, Phys. Lett. **B121**, 321 (1983).

[136] J. Polchinski and M. B. Wise, Phys. Lett. **B125**, 393 (1983).

[137] F. del Aguila, M. B. Gavela, J. A. Grifols, and A. Mendez, Phys. Lett. **B126**, 71 (1983).

[138] D. V. Nanopoulos and M. Srednicki, Phys. Lett. **B128**, 61 (1983).

[139] T. Ibrahim and P. Nath, Rev. Mod. Phys. **80**, 577 (2008), arXiv:0705.2008 [hep-ph], and references therein.

[140] T. Falk, K. A. Olive, M. Pospelov, and R. Roiban, Nucl. Phys. **B560**, 3 (1999), hep-ph/9904393.

[141] A. H. Chamseddine, R. L. Arnowitt, and P. Nath, Phys. Rev. Lett. **49**, 970 (1982).

[142] R. Barbieri, S. Ferrara, and C. A. Savoy, Phys. Lett. **B119**, 343 (1982).

[143] L. J. Hall, J. D. Lykken, and S. Weinberg, Phys. Rev. **D27**, 2359 (1983).

[144] S. K. Soni and H. A. Weldon, Phys. Lett. **B126**, 215 (1983).

[145] B. C. Allanach, Comput. Phys. Commun. **143**, 305 (2002), hep-ph/0104145.

[146] B. C. Allanach *et al.*, Eur. Phys. J. **C25**, 113 (2002), hep-ph/0202233.

[147] We use as SM inputs for `SOFTSUSY` the following parameters: $M_Z = 91.1876$ GeV ($m_t = 172.5$ GeV) for the pole mass of the Z boson (top quark); $\alpha^{-1}(M_Z) = 127.918$ and $\alpha_s(M_Z) = 0.1187$ for the gauge couplings in the $\overline{MS}$ scheme; $m_b(m_b) = 4.25$ GeV, $m_u(2\text{GeV}) = 0.003$ GeV, $m_d(2\text{GeV}) = 0.00675$ GeV, $m_s(2\text{GeV}) = 0.1175$ GeV and $m_c(m_c) = 1.2$ GeV for the light quark masses in the $\overline{MS}$ scheme.

[148] M. Chemtob, Prog. Part. Nucl. Phys. **54**, 71 (2005), hep-ph/0406029.

[149] B. C. Allanach and M. A. Bernhardt, (2009), arXiv:0903.1805 [hep-ph].

[150] The proton-hexality violating version of `SOFTSUSY` was published in Ref. [149] after the research for this thesis had been concluded.

[151] Heavy Flavor Averaging Group, E. Barberio *et al.*, (2008), arXiv:0808.1297 [hep-ex].

[152] LEP Working Group for Higgs boson searches, R. Barate *et al.*, Phys. Lett. **B565**, 61 (2003), hep-ex/0306033.

[153] B. C. Allanach, S. Kraml, and W. Porod, JHEP **03**, 016 (2003), hep-ph/0302102.

[154] B. C. Allanach, A. Djouadi, J. L. Kneur, W. Porod, and P. Slavich, JHEP **09**, 044 (2004), hep-ph/0406166.

[155] J. A. Grifols and A. Mendez, Phys. Rev. **D26**, 1809 (1982).

[156] CDF Collaboration, CDF note 9246 .

[157] ALEPH Collaboration, A. Heister *et al.*, Eur. Phys. J. **C31**, 1 (2003), hep-ex/0210014.

[158] D. Choudhury, M. Datta, and M. Maity, Phys. Rev. **D73**, 055013 (2006), hep-ph/0508009.

[159] J. R. Ellis, G. Gelmini, C. Jarlskog, G. G. Ross, and J. W. F. Valle, Phys. Lett. **B150**, 142 (1985).

[160] T. Banks, Y. Grossman, E. Nardi, and Y. Nir, Phys. Rev. **D52**, 5319 (1995), hep-ph/9505248.

[161] WMAP Collaboration, D. N. Spergel *et al.*, Astrophys. J. Suppl. **148**, 175 (2003), astro-ph/0302209.

[162] M. Colless *et al.*, (2003), astro-ph/0306581.

[163] H. K. Dreiner, M. Krämer, and B. O'Leary, Phys. Rev. **D75**, 114016 (2007), hep-ph/0612278.

[164] K. Agashe and M. Graesser, Phys. Rev. **D54**, 4445 (1996), hep-ph/9510439.

[165] A. A. Petrov and G. K. Yeghiyan, Phys. Rev. **D77**, 034018 (2008), arXiv:0710.4939 [hep-ph].

[166] E. Golowich, J. Hewett, S. Pakvasa, and A. A. Petrov, Phys. Rev. **D76**, 095009 (2007), arXiv:0705.3650 [hep-ph].

[167] BABAR Collaboration, B. Aubert *et al.*, Phys. Rev. **D76**, 014018 (2007), arXiv:0705.0704 [hep-ex].

[168] BABAR Collaboration, B. Aubert *et al.*, Phys. Rev. Lett. **98**, 211802 (2007), hep-ex/0703020.

[169] BELLE Collaboration, K. Abe *et al.*, Phys. Rev. Lett. **99**, 131803 (2007), arXiv:0704.1000 [hep-ex].

[170] Belle Collaboration, M. Staric *et al.*, Phys. Rev. Lett. **98**, 211803 (2007), hep-ex/0703036.

[171] CDF Collaboration, T. Aaltonen *et al.*, Phys. Rev. Lett. **100**, 121802 (2008), arXiv:0712.1567 [hep-ex].

[172] A. J. Schwartz, Chin. Phys. **C32**, 477 (2008), arXiv:0803.0082 [hep-ex].

[173] L. Wolfenstein, Phys. Rev. Lett. **51**, 1945 (1983).

[174] CKMfitter Group, J. Charles *et al.*, Eur. Phys. J. **C41**, 1 (2005), hep-ph/0406184.

[175] OPAL Collaboration, G. Abbiendi *et al.*, Eur. Phys. J. **C33**, 149 (2004), hep-ex/0310054.

[176] M. Wendel and H. Fraas, Phys. Rev. **D44**, 60 (1991).

[177] J. L. Hewett and T. G. Rizzo, (1998), hep-ph/9809525.

[178] D0 Collaboration, V. M. Abazov *et al.*, Phys. Rev. **D69**, 111101 (2004), hep-ex/0308033.

[179] CDF Collaboration, F. Abe *et al.*, Phys. Rev. Lett. **74**, 3538 (1995), hep-ex/9501001.

[180] CDF Collaboration, F. Abe *et al.*, Phys. Rev. **D55**, 5263 (1997), hep-ex/9702004.

[181] DØ Collaboration, DØ note 4403-CONF .

[182] Particle Data Group, W. M. Yao *et al.*, J. Phys. **G33**, 1 (2006).

[183] H. K. Dreiner and R. J. N. Phillips, Nucl. Phys. **B367**, 591 (1991).

[184] A. Belyaev, M.-H. Genest, C. Leroy, and R. R. Mehdiyev, JHEP **09**, 012 (2004), hep-ph/0401065.

[185] G. Eilam, A. Gemintern, T. Han, J. M. Yang, and X. Zhang, Phys. Lett. **B510**, 227 (2001), hep-ph/0102037.

[186] K. J. Abraham, K. Whisnant, J. M. Yang, and B.-L. Young, Phys. Rev. **D63**, 034011 (2001), hep-ph/0007280.

[187] D. K. Ghosh, S. Raychaudhuri, and K. Sridhar, Phys. Lett. **B396**, 177 (1997), hep-ph/9608352.

[188] K.-i. Hikasa, J. M. Yang, and B.-L. Young, Phys. Rev. **D60**, 114041 (1999), hep-ph/9908231.

[189] P.-Y. Li, G.-R. Lu, J. M. Yang, and H. Zhang, Eur. Phys. J. **C51**, 163 (2007), hep-ph/0608223.

[190] UA2 Collaboration, J. Alitti *et al.*, Z. Phys. **C49**, 17 (1991).

[191] UA2 Collaboration, J. Alitti *et al.*, Nucl. Phys. **B400**, 3 (1993).

[192] J. E. Kim, B. Kyae, and H. M. Lee, Phys. Lett. **B520**, 298 (2001), hep-ph/0103054.

[193] P. Gambino and M. Misiak, Nucl. Phys. **B611**, 338 (2001), hep-ph/0104034.

[194] A. J. Buras, A. Czarnecki, M. Misiak, and J. Urban, Nucl. Phys. **B631**, 219 (2002), hep-ph/0203135.

[195] G. Belanger, F. Boudjema, A. Pukhov, and A. Semenov, Comput. Phys. Commun. **149**, 103 (2002), hep-ph/0112278.

[196] G. Corcella *et al.*, JHEP **01**, 010 (2001), hep-ph/0011363.

[197] G. Corcella *et al.*, (2002), hep-ph/0210213.

[198] S. Moretti, K. Odagiri, P. Richardson, M. H. Seymour, and B. R. Webber, JHEP **04**, 028 (2002), hep-ph/0204123.

[199] H. K. Dreiner, P. Richardson, and M. H. Seymour, JHEP **04**, 008 (2000), hep-ph/9912407.

[200] The version of `HERWIG` used in this work includes modifications to simulate the four-body decays of the stau LSP and is available on request from Peter Richardson.

[201] F. E. Paige, S. D. Protopopescu, H. Baer, and X. Tata, (2003), hep-ph/0312045.

[202] The $\tilde{\nu}_\mu$ LSP might also decay via a 4-body decay, *e.g.* $\tilde{\nu}_\mu \to \nu_\mu \bar{\nu}_\mu d\bar{b}$, via a virtual neutralino and sneutrino. However, we estimate that the 4-body decay rates are suppressed by eight orders of magnitude compared to the 2-body decay. We employed the analytical formulæ of Ref. [58].

[203] The $\tilde{\nu}_\mu$ can in principle also decay via a RGE generated λ_{121} (λ_{323}) coupling into a $e\nu_e$ ($\tau\nu_\tau$) pair. However the generated λ's are at least ten orders of magnitude smaller than the λ'_{231} coupling. The relevant RGEs to generate the λs involve off-diagonal down-Yukawa matrix elements, which vanish at $M_{\rm Z}$, see Sect. 4.1.1.

[204] F. Borzumati, J.-L. Kneur, and N. Polonsky, Phys. Rev. **D60**, 115011 (1999), hep-ph/9905443.

[205] E. Accomando *et al.*, (2006), hep-ph/0608079.

[206] A. G. Akeroyd, M. A. Diaz, J. Ferrandis, M. A. Garcia-Jareno, and J. W. F. Valle, Nucl. Phys. **B529**, 3 (1998), hep-ph/9707395.

[207] A. de Gouvea, A. Friedland, and H. Murayama, Phys. Rev. **D59**, 095008 (1999), hep-ph/9803481.

[208] A. G. Akeroyd, C. Liu, and J.-H. Song, Phys. Rev. **D65**, 015008 (2002), hep-ph/0107218.

[209] A. Bartl, M. Hirsch, T. Kernreiter, W. Porod, and J. W. F. Valle, JHEP **11**, 005 (2003), hep-ph/0306071.

[210] B. C. Allanach *et al.*, (2007), arXiv:0710.2034 [hep-ph].

[211] Kom, C. H., Cambridge, Ph.D. Thesis.

[212] H. K. Dreiner, P. Richardson, and M. H. Seymour, (2000), hep-ph/0001224.

[213] H. K. Dreiner, P. Richardson, and M. H. Seymour, (1998), hep-ph/9903419.

[214] G. Moreau, E. Perez, and G. Polesello, Nucl. Phys. **B604**, 3 (2001), hep-ph/0003012.

[215] F. Deliot, G. Moreau, and C. Royon, Eur. Phys. J. **C19**, 155 (2001), hep-ph/0007288.

[216] S. Dimopoulos, R. Esmailzadeh, L. J. Hall, and G. D. Starkman, Phys. Rev. **D41**, 2099 (1990).

[217] B. C. Allanach, M. Guchait, and K. Sridhar, Phys. Lett. **B586**, 373 (2004), hep-ph/0311254.

[218] D0 Collaboration, V. M. Abazov *et al.*, Phys. Rev. Lett. **89**, 261801 (2002), hep-ex/0207100.

[219] D0 Collaboration, V. M. Abazov *et al.*, Phys. Rev. Lett. **97**, 111801 (2006), hep-ex/0605010.

[220] D. Choudhury, S. Majhi, and V. Ravindran, Nucl. Phys. **B660**, 343 (2003), hep-ph/0207247.

[221] L. L. Yang, C. S. Li, J. J. Liu, and Q. Li, Phys. Rev. **D72**, 074026 (2005), hep-ph/0507331.

[222] Y.-Q. Chen, T. Han, and Z.-G. Si, JHEP **05**, 068 (2007), hep-ph/0612076.

[223] W. H. Press *et al.*, editors, *Numerical Recipes in C++* (Cambridge University Press, 2002, Second Edition).

[224] S. Dawson, Nucl. Phys. **B261**, 297 (1985).

[225] H. K. Dreiner *et al.*, (2009), arXiv:0901.3485 [hep-ph].

[226] H. K. Dreiner, C. Hanhart, U. Langenfeld, and D. R. Phillips, Phys. Rev. **D68**, 055004 (2003), hep-ph/0304289.

[227] D. Choudhury, H. K. Dreiner, P. Richardson, and S. Sarkar, Phys. Rev. **D61**, 095009 (2000), hep-ph/9911365.

[228] J. Butterworth and H. K. Dreiner, Nucl. Phys. **B397**, 3 (1993), hep-ph/9211204.

[229] H. K. Dreiner and P. Morawitz, Nucl. Phys. **B428**, 31 (1994), hep-ph/9405253.

[230] E. A. Baltz and P. Gondolo, Phys. Rev. **D57**, 2969 (1998), hep-ph/9709445.

[231] G. Moreau, M. Chemtob, F. Deliot, C. Royon, and E. Perez, Phys. Lett. **B475**, 184 (2000), hep-ph/9910341.

[232] M. Chaichian, A. Datta, K. Huitu, S. Roy, and Z.-h. Yu, Phys. Lett. **B594**, 355 (2004), hep-ph/0311327.

[233] F. Borzumati and J. S. Lee, Phys. Rev. **D66**, 115012 (2002), hep-ph/0207184.

[234] B. L. Combridge, Nucl. Phys. **B151**, 429 (1979).

[235] T. Han and M. B. Magro, Phys. Lett. **B476**, 79 (2000), hep-ph/9911442.

[236] J. Pumplin, A. Belyaev, J. Huston, D. Stump, and W. K. Tung, JHEP **02**, 032 (2006), hep-ph/0512167.

[237] R. Bonciani, S. Catani, M. L. Mangano, and P. Nason, Nucl. Phys. **B529**, 424 (1998), hep-ph/9801375.

[238] M. Cacciari, S. Frixione, M. L. Mangano, P. Nason, and G. Ridolfi, JHEP **04**, 068 (2004), hep-ph/0303085.

[239] S.-h. Zhu, Phys. Rev. **D67**, 075006 (2003), hep-ph/0112109.

[240] T. Plehn, Phys. Rev. **D67**, 014018 (2003), hep-ph/0206121.

[241] H. L. Lai *et al.*, Phys. Rev. **D55**, 1280 (1997), hep-ph/9606399.

[242] We thank Jean-Loic Kneur for private discussions on the parameters used in Ref. [204].

[243] S. Dittmaier, P. Uwer, and S. Weinzierl, Phys. Rev. Lett. **98**, 262002 (2007), hep-ph/0703120.

[244] J. A. Aguilar-Saavedra *et al.*, Eur. Phys. J. **C46**, 43 (2006), hep-ph/0511344.

[245] E. Boos *et al.*, (2001), hep-ph/0109068.

[246] K. Odagiri, JHEP **10**, 006 (1998), hep-ph/9806531.

[247] S. Frixione and B. R. Webber, (2006), hep-ph/0612272.

[248] S. Frixione, P. Nason, and B. R. Webber, JHEP **08**, 007 (2003), hep-ph/0305252.

[249] F. Maltoni and T. Stelzer, JHEP **02**, 027 (2003), hep-ph/0208156.

[250] CMS Collaboration, CERN-LHCC-2006-021 .

[251] The `PXCONE algorithm` by L. Del Pozo and M. H. Seymour is publically available as part of the FastJet package available from http://www.lpthe.jussieu.fr/∼salam/fastjet/.

[252] J. H. Kuhn and G. Rodrigo, Phys. Rev. **D59**, 054017 (1999), hep-ph/9807420.

[253] M. T. Bowen, Phys. Rev. **D73**, 097501 (2006), hep-ph/0503110.

[254] L. G. Almeida, G. Sterman, and W. Vogelsang, Phys. Rev. **D78**, 014008 (2008), arXiv:0805.1885 [hep-ph].

[255] S. Blusk *et al.*, 1st LHC Detection Alignment Workshop 4-6 Sep 2006, Geneva, Switzerland.

[256] M. Drees and S. P. Martin, (1995), hep-ph/9504324.

[257] L. E. Ibanez, C. Lopez, and C. Munoz, Nucl. Phys. **B256**, 218 (1985).